Heat Transfer Correlation in Nuclear Reactor Safety Calculations

Abel-Larsen, H.; Olsen, Aksel Aage; Miettinen, J.; Siikonen, T.; Rasmussen, J.; Sjöberg, A.; Becker, K.

Publication date:
1985

Document Version
Publisher's PDF, also known as Version of record

DK8600012

[redacted]

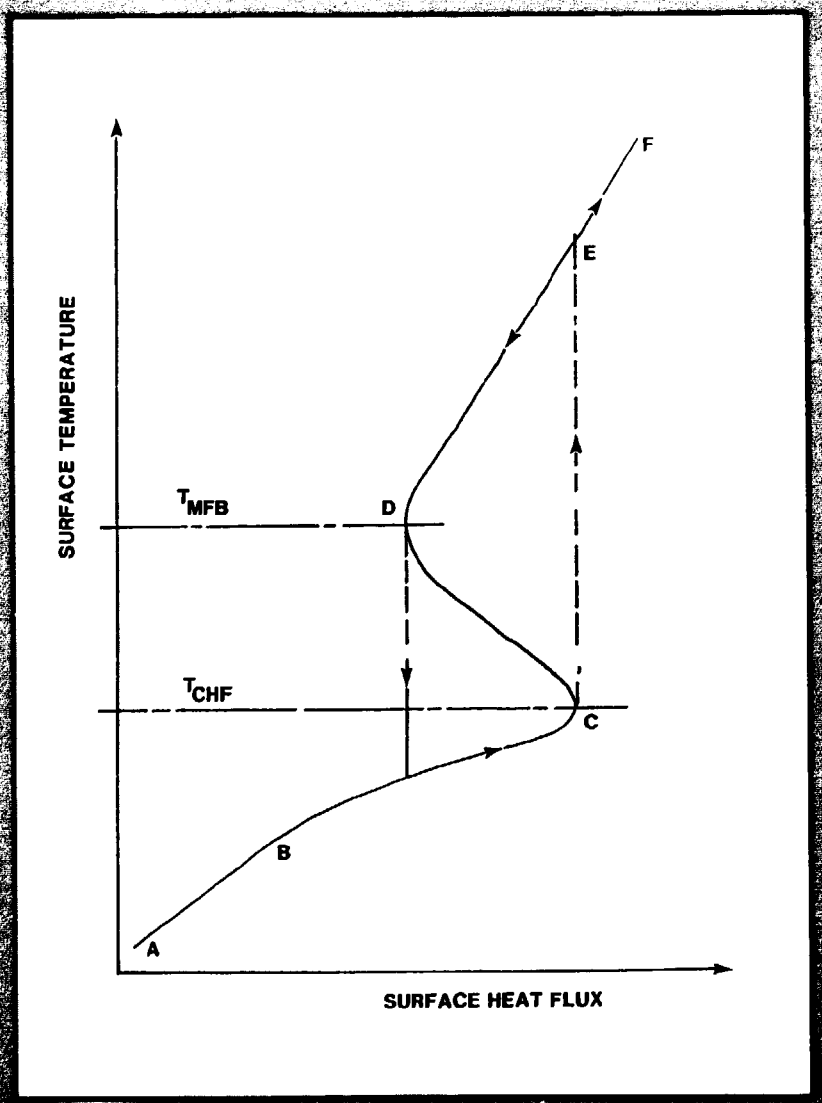

nka

Nordisk kontaktorgan for atomenergispørgsmål | Nordiska kontaktorganet för atomenergifrågor | Pohjoismainen atomienergia-yhdyselin | Nordic liaison committee for atomic energy

RISØ-M-2504

(Vol. 1)

HEAT TRANSFER CORRELATIONS IN NUCLEAR REACTOR SAFETY CALCULATIONS SÄK-5

H. Abel-Larsen, Risø
A. Olsen, Risø
J. Miettinen, VTT
T. Siikonen, VTT
J. Rasmussen, IFE
A. Sjöberg, Studsvik
K. Becker, KTH

June 1985

Risø: Risø National Laboratory, Denmark
VTT: Technical Research Centre of Finland
IFE: Institute for Energy Technology, Norway
Studsvik: Studsvik Energiteknik AB, Sweden
KTH: Royal Institute of Technology, Stockholm, Sweden

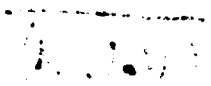

ISBN 87-550-1109-8
ISSN 0418-6435
minab/gotab Stockholm 1985

ABSTRACT

Heat transfer correlations, most of them incorporated in the heat transfer packages of the nuclear reactor safety computer programmes RELAP-5, TRAC (PF1) and NORA have been tested against a relevant set of transient and steady-state experiments. In addition to usually measured parameters the calculations provided information on other physical parameters. Results are presented and discussed.

The report consists of a main report (Vol.I) and appendices (Vol.II). Chapters 3,4 and 5 of the main report are primarily intended for computer programme users. Chapter 6 is recommended for those looking for main results rather than details. The appendices will be useful for computer programme developers.

INIS descriptors:

CRITICAL HEAT FLUX - COMPARATIVE EVALUATIONS - CORRELATIONS - COORDINATED RESEARCH PROGRAMS - DENMARK - DROPLETS - EVAPORATION - FINLAND - FAILURES - FUEL ELEMENTS - FILM BOILING-FORCED CONVECTION - HEAT TRANSFER - LOSS OF COOLANT - NORWAY - N CODES - NUCLEATE BOILING - NATURAL CONVECTION - R CODES - REACTOR SAFETY - SWEDEN - T CODES - TRANSIENT - TRANSITION BOILING - THERMAL RADIATION

This report is part of the safety programme sponsored by NKA, the Nordic Liaison Committee for Atomic Energy, 1981-85. The project work has been partly financed by the Nordic Council of Ministers.

LIST OF CONTENTS

VOLUME I:

VOLUME II : Page

FIGURES. Page

VOLUME I:

VOLUME II:

Page

Page

TABLES

Steering committee for the NKA/SÄK reactor safety programme, SÄK-5 1981 - 1985:

C. Gräslund (Chairman)	Swedish Nuclear Power Inspectorate, SKI Stockholm
T. Eurola	Finish Centre for Radiation and Nuclear Safety, Helsingfors
E. Hellstrand	Studsvik Energiteknik AB, Nyköping, Sweden
D. Malnes	Institute for Energy Technology, Norway
F. Marcus	NKA, Roskilde, Denmark
B. Micheelsen	Risø National Laboratory, Roskilde, Denmark
E. Sokolowski	Nuclear Safety Board of the Swedish Utilities, Sverige

SUMMARY

Knowledge about temperatures on the surface of nuclear fuel rods plays an important role in nuclear reactor safety analysis. There is a need to calculate surface temperatures during operational transients and postulated accidents under the assumption that the engineered safety features of the reactor are activated and working. A typical sequence to be calculated is a loss-of-coolant accident (LOCA).

The purpose of the calculations is to examine whether the integrity of the fuel rod cladding, the first of three engineered barriers against radiological release, may be threatened by the rise in surface temperature that may occur.

The integrity of the cladding depends on several individual phenomena, primarily metallurgical, all very sensitive to the cladding temperature.

For this purpose thermo-hydraulic computer programmes have been developed e.g. the American programmes TRAC and RELAP-5 and the Norwegian programme NORA, all used in the present project.

In order to calculate realistic temperature differences between the cladding surface and the coolant, reliable heat transfer correlations are needed for the different heat transfer regions occuring during a transient (cf. the front page figure).

The heat transfer correlations actually used in the computer programmes are empirical to a high degree. They have been found from the results of independent steady-state experiments, using boundary conditions, that coincide with boundary conditions in safety calculations only partly.

A comprehensive test program is therefore necessary to show whether the computer programmes can provide reasonable simulations of well-defined experiments that are selected so that their conditions may be comparable with those occurring in the fuel element channels of a nuclear reactor.

During the project, 16 experiments, (3 of them transient and 13 steady state) were chosen, and their results were compared with calculations with the computer programmes TRAC (PF1), RELAP-5 and NORA.

Not all relevant parameters for the evaluation of a correlation can be measured in an experiment. Those missing will be calculated by the computer programmes according to their inherent logics and models.

Using the transient experiments it turned out that the heat transfer packages in the computer programmes did not give an adequate picture. This may be due to the influence of other transport phenomena (subcooled void, slip, thermodynamic non-equilibrium) just as different empirical correlations apart from the heat transfer correlations may dominate the calculation. More simplified experiments appeared to be needed, preferably steady state experiments with well-defined boundary conditions. These experiments would need to cover the complete spectrum of heat transfer modes in each flow region with the critical heat flux (CHF) exceeded. CHF is characterized by the loss of contact between the liquid coolant and the cladding surface, when the heat flux applied to the surface is monotonously increased to this point.

CHF is an important parameter, since, with an appropriate safety margin, it separates normal and abnormal operation of a nuclear reactor.

The heat transfer correlations used in pre-CHF flow regions were found to be adequate. The heat transfer in these regions is very efficient and will not be a limiting factor for the fuel and cladding during an operational transient or a postulated loss of coolant accident.

The CHF correlations used in the computer programmes (Biasi, CISE-4) are, however, not adequate. The correlations cannot predict the locus of CHF with sufficient accuracy.

As a consequence, it was decided to start an independent examination of four relevant CHF correlations: Barnett, Becker, Biasi and CISE-4, using results from six full-scale rod bundle experiments (table B4.1.I), and using a separately developed computer programme.

The conclusion from these calculations is that the Biasi and CISE-4 correlations cannot predict the CHF-conditions with adequate accuracy. An explanation may be that these two correlations are developed from single tube data and have no provisions to incorporate the influence of unheated surfaces and internal rod-to-rod power distribution.

The two other correlations, developed in the late 1960's for rod bundle geometries, correlate the experimental data better.

The post-CHF heat transfer conditions strongly depend on the locus of CHF. As the locus could not be calculated with sufficient accuracy it was fixed in the calculations as measured in the continuous examinations of the 13 steady state experiments.

After this the surface temperatures were recalculated. They were too low in RELAP-5 and TRAC, too high in NORA. These deviations were referred back to erroneous predictions of the thermodynamic nonequilibrium.

The thermodynamic nonequilibrium is governed primarily by mass transfer between droplets and vapour due to interfacial heat transfer. A decrease in the vapour generation rate will increase the vapour temperature (superheating) under equal conditions thus allowing the thermodynamic nonequilibrium to be more pronounced. Based on this it must be concluded that the interfacial heat transfer coefficients are too high in RELAP-5 and TRAC too low in NORA.

A recently developed semi-empirical vapour generation model was therefore implemented in the programmes. Hereafter, the results were substantially improved, and a better agreement was obtained between measured and calculated post-CHF surface temperatures.

It is obvious even from these last few calculations, together with the examinations of transition boiling heat transfer using a separately developed programme, that more realistic and phenomenological heat transfer models have to be developed for the post-CHF regions. It is recognized that the degree of thermodynamic nonequilibrium at any axial level will depend on the upstream competition between the heat transfer mechanisms wall-to-vapour by convection, wall-to-droplet by droplet impingment on the surface and vapour-to-droplet by interfacial heat transfer.

The present project has been limited to application of the heat correlations in nuclear reactors. However, the same basic technical questions concerning heat transfer in fluids with droplets or particles and the correlations used to descibe the heat transfer find wide application in a number of fields such as chemical processes, fluidized bed combustion, spray cooling, heat and mass transfer in evaporators, once-through steam generators to name a few.

The problems described in this report are an example of how advanced methods developed for the nuclear area can contribute to other technical areas of current interest.

SAMMENFATNING

Uranbrændslet i en kernekraftreaktor er stærkt radioaktivt. Det er vigtigt, at brændslet indesluttes effektivt, så ingen radioaktive stoffer kan frigøres til omgivelserne. Tre konstruerede barrierer tjener dette formål. De tre barrierer er først indkapslingen, der indeslutter det nukleare brændsel, dernæst reaktortanken, der omslutter reaktorkernen og det primære kølesystem og endelig den tryktætte reaktorbygning, der indslutter reaktoranlæggets primære systemer.

Et vigtigt led i sikkerhedsanalysen af kernekraftreaktorer er at eftervise, at temperaturerne på overfladen af indkapslingen under unormale driftsforstyrrelser og påstulerede uheld, som f.eks. tab-af-kølemiddel-uheld, ikke overstiger en fastsat værdi, når reaktoranlæggets beskyttelsessystemer virker.

Overstiger indkapslingstemperaturen den fastsatte grænseværdi kan indkapslingen revne. Årsagen hertil er flere metallurgiske fænomener alle følsomme overfor temperaturen.

Den absolutte størrelse af temperaturen afhænger af dels, hvor godt man kan bestemme de metallurgiske fænomeners temperaturafhængighed og dels, hvor godt man kan bestemme indkapslingens overfladetemperatur.

Projektet har beskæftiget sig med een side af sidstnævnte punkt.

Beregning af realistiske temperaturforskelle mellem indkapslingens overflade og kølemidlet forudsætter pålidelige varmeovergangskorrelationer. Ved en korrelation skal her forstås et matematisk udtryk, der nok støtter sig til fysiske principper, men primært er baseret på statistisk behandling af forsøgsdata.

Det primære formål med nærværende projekt var at undersøge pålideligheden af nogle udvalgte korrelationer for varmetransporten med henblik på deres anvendelse i datamaskine-programmer, der modellerer forholdene i reaktorkernen under et uheldsforløb.

Et eksempel på en brændelsestavs overfladetemperatur undet såvel normal drift som under et uheldsforløb er givet på forsiden af denne rapport. Kølemidlet er kogende vand, d.v.s. der er både damp og vand tilstede (to-fase køling).

Ved normal drift af en kernekraftreaktor skal overfladetemperaturen af indkapslingen holdes under den temperatur, der svarer til den kritiske varmestrøm (punkt C på forsidefiguren).

Undersøgelsen af de korrelationer, som anvendes ved bestemmelsen af varmetransporten <u>før</u> kritisk varmestrøm, bekræftede, at de er tilstrækkelig pålidelige. Varmetransporten her er meget effektiv og vil ikke være en begrænsende faktor for indkapslingen.

Kritisk varmestrøm er karakteriseret ved tabet af kontakt mellem indkapslingens overflade og kølevand på grund af dannelsen af et overhedet lag af damp.

De korrelationer, som blev benyttet til bestemmelse af værdien af og stedet for kritisk varmestrøm i de anvendte datamaskine-programmer var ikke tilstrækkelig pålidelige. En uafhængig undersøgelse med et separat udviklet program blev derfor udført på dels de to anvendte korrelationer og dels to andre, ældre korrelationer. Resultatet var, at de to ældre korrelationer bedre kunne forudsige forsøgsdata fra 6 forsøg med elektrisk opvarmede brændselselementer i fuld-skala.

Undersøgelsen af korrelationer for varmetransporten <u>efter</u> kritisk varmestrøm viser, at de tilstrækkelig pålideligt kan eftervise målte overfladetemperaturer i de forsøg, som er benyttet ved sammenligningen, når der tages nødvendigt hensyn til to fysiske fænomener:

1. termodynamisk uligevægt
2. dråbekøling.

Ved den termodynamiske uligevægt skal forstås, at damptemperaturen, efter at den kritiske varmestrøm er passeret, kan blive højere end vandtemperaturen, idet varmetransporten primært vil ske til dampen og herfra videre til vanddråber i dampen. Dampen overhedes d.v.s. varmetransporten til dråber er ikke i ligevægt med varmetransporten til dampen. Ved at tage hensyn til denne overhedning kunne en væsentlig bedre overensstemmelse mellem forsøgsdata og beregnede overfladetemperaturer opnås.

Resultaterne fra undersøgelsen af termodynamisk uligevægt og resultater fra undersøgelsen af den såkaldte transition-kogning (området mellem punkterne C og D på forsidefiguren) viser, at dråbekølingen er et særdeles vigtigt led i varmetransporten.

Ved transitionkogning er varmetransporten bedre end i området for filmkogning (området mellem D og E på forsidefiguren), fordi dråber, som rammer indkapslingens overflade, kan væde overfladen. Kølingen forstærkes ved direkte fordampning af dråberne.

De to nævnte fænomener afhænger stærkt af hinanden, idet graden af den termodynamiske uligevægt vil afhænge af konkurrencen mellem varmetransporten: indkapslingsoverflade til damp ved konvektion, indkapslingsoverflade til dråber ved fordampning og endelig damp til dråber ved såkaldt interfase varmeovergang.

Undersøgelserne i SAK-5 projektet har klarlagt dråbernes betydning for varmetransporten i områderne efter kritisk varmestrøm. Man har vist, at om man vil forbedre pålideligheden er det nødvendigt at inddrage de fysiske fænomener mere d.v.s., der bør udvikles mere realistiske modeller, som i højere grad baseres på de fysiske fænomener end korrelationerne er. Det skal dog bemærkes, at fænomenologiske modeller, der kan bestå af flere matematiske udtryk, kan øge kompleksiteten af beregningsprogrammet og beregningstiden. Et valg mellem den detaljerede fænomenologiske model og den statistiske korrelation kan derfor blive

nødvendig.

Undersøgelserne har været begrænset til varmetransport i kernekraftreaktorer, men de grundlæggende fysiske og tekniske spørgsmål er de samme for varmetransport indenfor store områder af den moderne teknik, der således også kan drage nytte af undersøgelserne.

1. INTRODUCTION

1.1. The aim of the project

The aim is to establish a set of reliable heat transfer correlations primarily for application in best-estimate computer programmes for nuclear reactor safety calculations.

Correlations in this sense are sets of mathematical expressions, based on physical principles and experimental data, but resting primarily on experimental data.

A best estimate is the most favourable with respect to reality. Favourable is in this context according to use and best knowledge.

Reality refers to those transients that have to be evaluated to assure the authorities that the safety of the system is acceptable. The transients are all expected operational transients and postulated accidents such as a break in the pressure boundary integrity resulting in a loss of core cooling water (Loss-of-Coolant-Accident, LOCA).

1.2. Organization of the report

This report contains a main report (VOL.I) and appendices (VOL.II) The main report covers the examined area from a more general point of view. It provides a natural introduction to the appendices, which describe the work done in detail.

The participating organizations and the actual distribution of the work are dealt with in Chapter 2.

The project was initiated with a literature search. The general considerations and results are discussed in Chapter 3 and Appendix A.

The comparison of selected heat transfer correlations with experimental data using the American computer programmes RELAP-5, TRAC(PF1), the Norwegian computer programme NORA, and separate programmes developed especially for this project is described in Chapter 4 and Appendix B.

Discussions and recommendations based on the results attained are given in Chapter 5.

Chapter 6 contains the conclusion of the report.

1.3. Heat transfer regions

The heat transfer correlations are closely connected with the actual flow region. The expressions flow region and heat transfer region may therefore be interchangeable.

The heat transfer regions and their occurrence in light water reactors may be demonstrated by considering the temperature course that a local spot on a heat transfer surface may experience during a LOCA.

An example of such a temperature course as function of surface heat flux is shown in Fig. 1, the so-called boiling curve. The course from A to B represents the single-phase liquid flow region. In the succeeding boiling region two different modes of flow can occur. In one mode, the nucleate boiling mode, the liquid is the continuous fluid; vapour is generated at specific nucleation sites on the heating surface and vapour bubbles are discretely distributed through the continuous, saturated liquid phase (liquid continuous). The other mode, the forced convective boiling mode, is characterized by the vapour as being the continuous fluid with the liquid distributed partly as a film on the heating surface and partly as droplets in the vapour (vapour continuous).

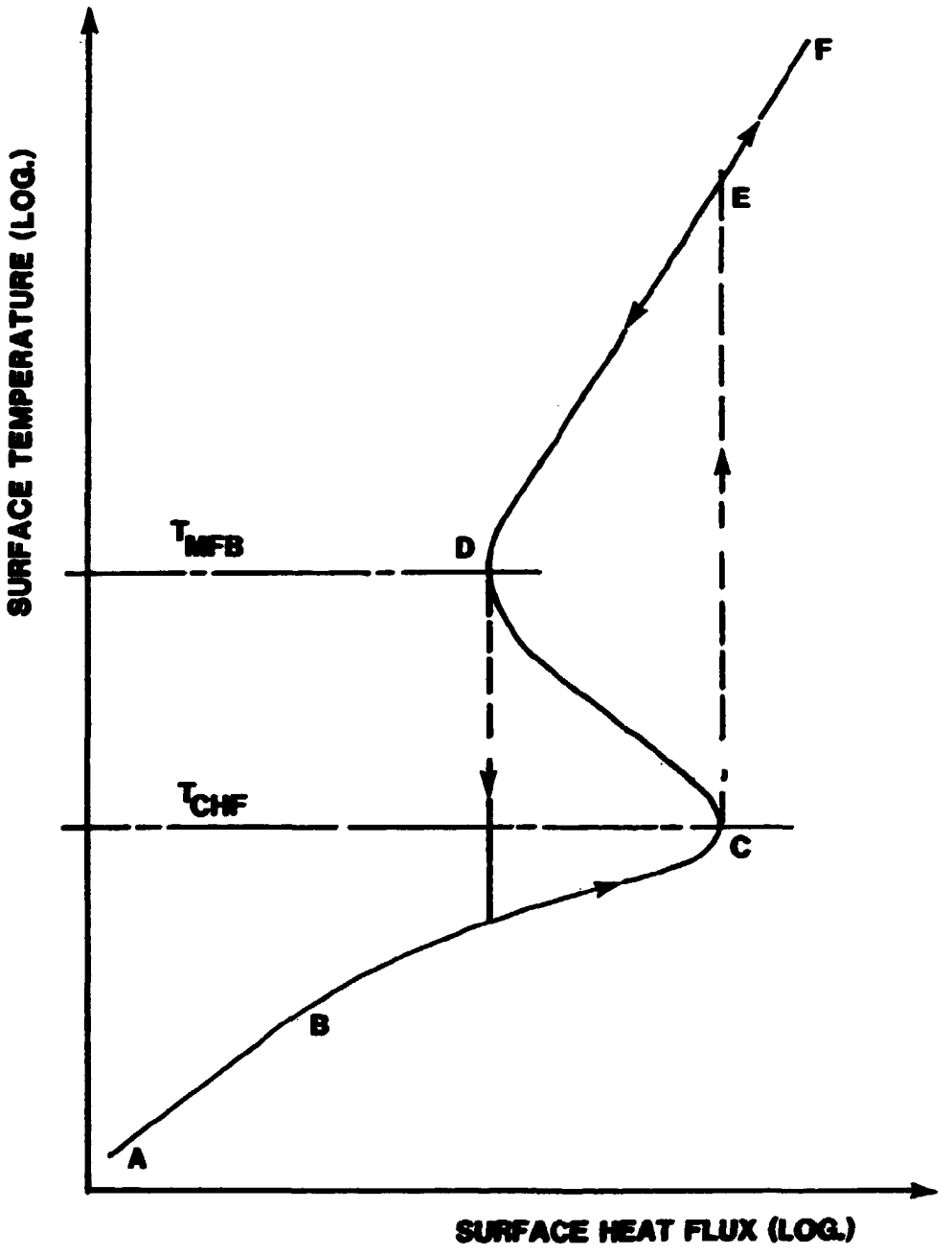

BOILING CURVE (Heat Flux Controlled)

FIGURE 1

When the heat flux applied to the surface in contact with the liquid is progressively increased, a point is reached at which the continuous contact between the surface and the liquid is lost and the critical heat flux (CHF) is attained.

The temperature course in Fig. 1 is shown for a heat flux-controlled surface, i.e. the heat flux is the independent variable as in electric and nuclear-heated systems.

When the surface heat flux in a heat flux-controlled system is further increased the temperature will jump to point E. This temperature increase may cause a burnout in the real sense of the word and a certain safety margin to the CHF point has to be secured during normal operation of a nuclear reactor.

The surface temperature may go from F to E and further to D by decreasing the heat flux. The temperature at D is the so-called minimum film boiling temperature. From here the temperature may jump to the nucleate boiling, i.e. a form of hysteresis effect may exist.

During a strong transient, such as a LOCA, the fuel rods may behave as a temperature-controlled system due to their thermal capacities. The temperature course can then move into the transition boiling flow region (from C to D), where the heat transfer is much better than in the film boiling flow region (from D to E and F).

The transition boiling flow region is active between the temperature at CHF and the minimum film boiling temperature and can be realized only in temperature-controlled systems.

The flow regions as they may occur in emergency core cooling by reflood is shown in Fig. 2.

In general the logic in the selection of the heat transfer corlations may appear from these thoughts. Figures 3 and 4 show the main features of the selection.

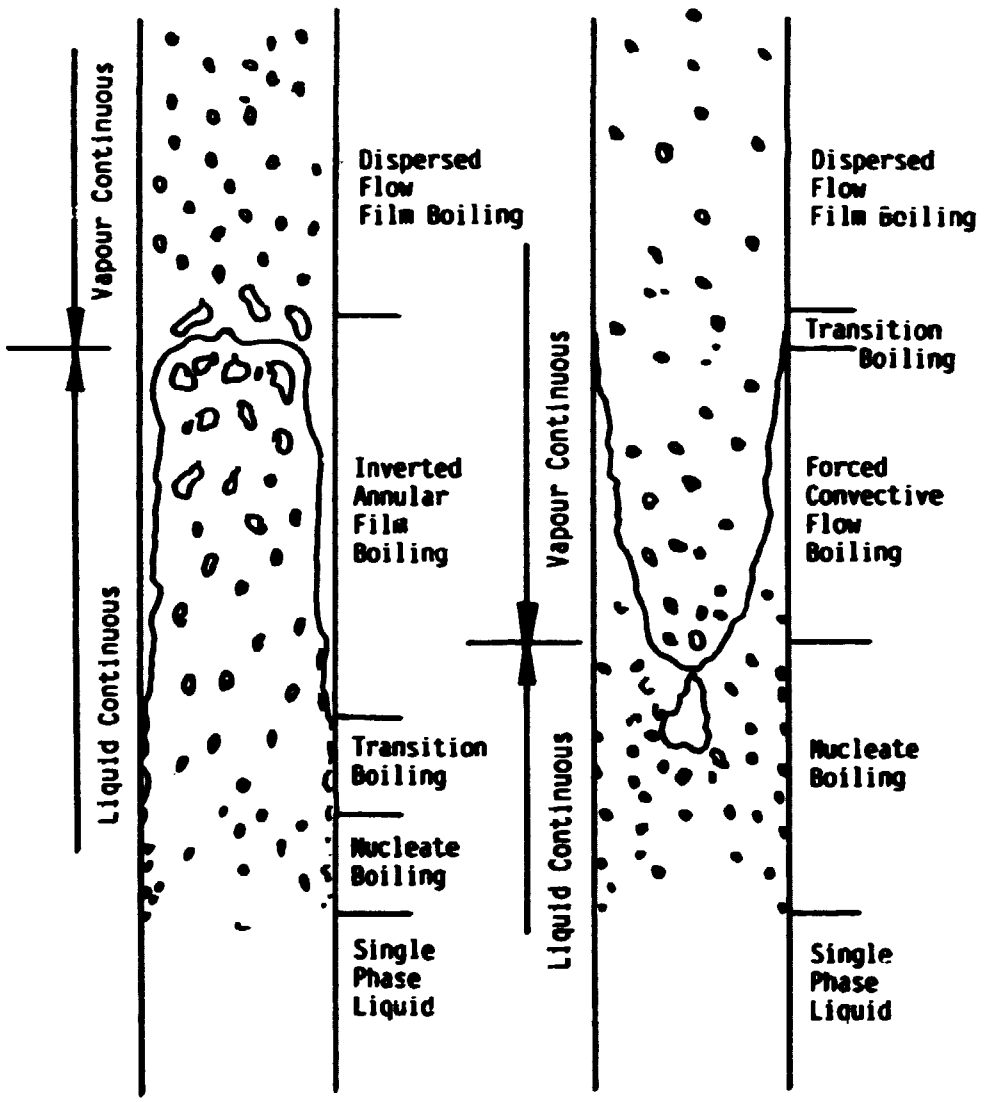

HEAT TRANSFER REGIONS

FIGURE 2

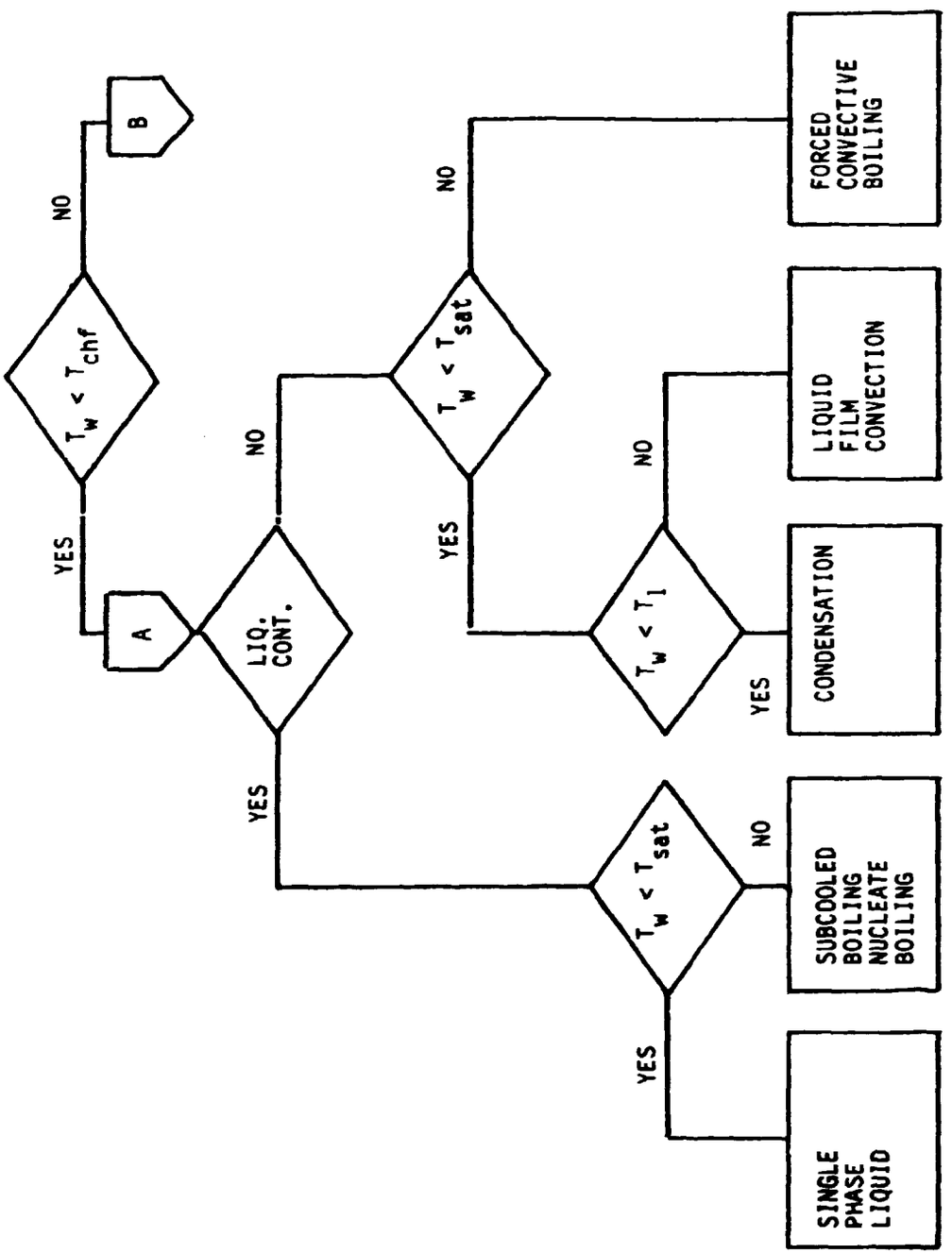

HEAT TRANSFER REGIONS

FIGURE 3

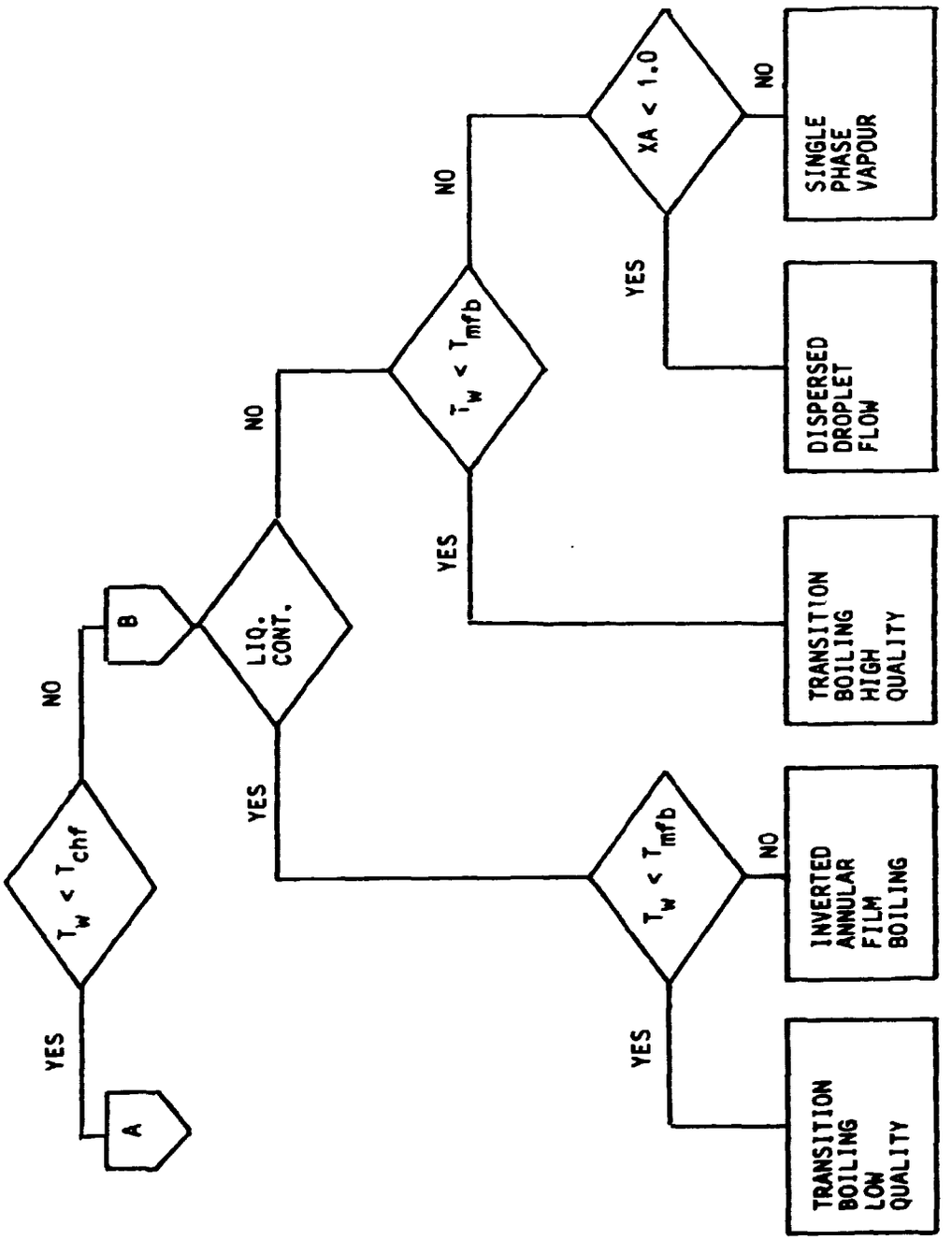

HEAT TRANSFER REGIONS

FIGURE 4.

From what is stated above, the heat transfer during the whole temperature course can be traced to be dependent primarily on the surface temperature and secondarily on whether the flow is liquid continuous or vapour continuous.

The transport equation of heat, first set up by Newton in 1701, is written:

$$Q = h \cdot A \cdot \Delta T \ ,$$

where Q is the heat flow rate, A a characteristic surface area, ΔT a characteristic temperature difference, and the proportionality factor h is defined as the heat transfer coefficient.

The heat transfer coefficient depends on the physical properties of the fluid, mass flux, pressure, absolute vapour quality and the geometry of the system.

2. ORGANIZATION OF THE PROJECT

The project is part of the safety programme of NKA, the Nordic Liaison Committee for Atomic Energy and is in part financed by funds from the Nordic Council of Ministers.

2.1. Participating organizations

The participants have been:

Risø National Laboratory, Denmark
H. Abel-Larsen
A. Olsen (project leader),

Technical Research Centre of Finland, VTT,
J. Miettinen,
T. Siikonen,

Institute for Energy Technology, IFE, Norway,
J. Rasmussen,

Studsvik Energiteknik AB, Studsvik, Sweden,
A. Sjöberg,

Royal Institute of Technology, KTH, Sweden,
Department of Nuclear Energy,
K.M. Becker.

2.2. Distribution of work

The logic classification of the boiling curve has been used as a base for the initial distribution of work in the literature search.

IFE has examined the single phase liquid and the nucleate boiling and forced convective boiling flow region including the critical heat flux.

Risø has examined the transition boiling flow region.

Studsvik examined the film boiling and single phase vapour flow region.

VTT examined the quenching phenomena during the emergency core cooling through top-spray and bottom-reflooding and the interfacial heat transfer.

Professor Becker has taken part in the project since January 1983 as a consultant.

3. PRESENT KNOWLEDGE

The result of a literature search is given in Appendix A. Below is given a general view of the transport phenomena of heat for the physical understanding of the heat transfer and its correlation.

3.1. General considerations

Some basic criteria and general requirements for the selection of heat transfer correlation may be set up as follows (1):

a. The range of the experimental data base on which the correlation is based must coincide with the range of interest.

b. The deviation of the predicted results with the correlation from the experimental data should be low, i.e. a correlation with a lower standard deviation should be selected over another correlation with higher standard deviation.

c. If a. and b. are satisfied, the correlation based on phenomenological or mechanistic considerations should be preferred to the purely statistical correlation.

The phenomenological correlation may offer the possibility of extrapolation outside the range of the data it is tested against and further it may be possible to gain a better understanding of the physical processes involved.

Phenomenological correlations often consist of various mathematical expressions based on primarily physical principles. The phenomenological model may, however, increase the complexity of the computer programme management and increase the use of

computer time. A compromise between the detailed phenomenological model and the statistical correlation may therefore be necessary. This depends primarily on the sensitivity of the surface temperature to the selected correlation. If the sensitivity is low, it may be justifyable to lower the complexity.

A key feature of a well-made computer programme is a high degree of modularity so that correlations and models can be easily changed.

3.2. Heat transfer in different flow regions

Heat transfer coefficients in single-phase fluids, liquids or gases, are determined from dimensional analysis and experiments.

Heat transfer coefficients are calculated from correlations determined in this way:

$$\frac{h \cdot D}{k} = C1 \cdot \left(\frac{G \cdot D}{\mu} \right)^{C2} \cdot \left(\frac{C_p \cdot \mu}{k} \right)^{C3} \cdot F$$

where the dimensionless term on the left side is the Nusselt number and the two dimensionless numbers on the right side are the Reynold and Prandtl numbers, respectively. C1, C2 and C3 are constants that are to be determined from experiments under similarity conditions. F is a correction factor, which e.g. may take the length-to-diameter ratio into account.

The other parameters are defined in the nomenclature list.

Heat transfer in two-phase flow is much more complicated due to the interacting interfaces between the two phases, liquid and vapour. There are four types of liquid-vapour interfaces:

1. bubbles in liquid continuous flow
2. droplets in vapour continuous flow,
3. vapour film in liquid continuous flow, and
4. liquid film in vapour continuous flow.

Further, the three different types of heat transfer have to be considered:

a. convection
b. conduction, and
c. radiation.

Figure 5 gives schematically an impression of the highly complex mechanisms involved in the two-phase flow heat transfer.

It is understandable that it is not possible to obtain a single heat transfer correlation that may cover all the flow regions shown in Fig. 1 and schematically in Figs. 3 and 4.

Not all the heat transfer mechanisms occur at the same time and they differ radically in the various flow regions. In most cases the thermal radiation is negligible.

To a great extent, the physical considerations from structuring single-phase heat transfer correlations have been transferred to two-phase flow with appropriate additions even for interfacial heat transfer.

Superposition of the different heat transfer mechanisms is assumed. Nucleate boiling heat transfer, e.g., is correlated as the sum of the heat transfer by liquid-vapour exchange caused by bubble agitation in the boundary layer (microconvection) and the heat transfer by the single-phase liquid convection between patches of bubbles (macroconvection). Appropriately determined weighing factors are assigned to each term.

In the post-CHF regions with vapour continuous flow the heat transfer is very much dependent on the droplet concentration and the surface temperature. At relatively low temperatures the droplets will be able to wet the heating surface when striking it and thus can be evaporated by direct contact with the surface. The heat transfer may be assumed to be a weighted sum of

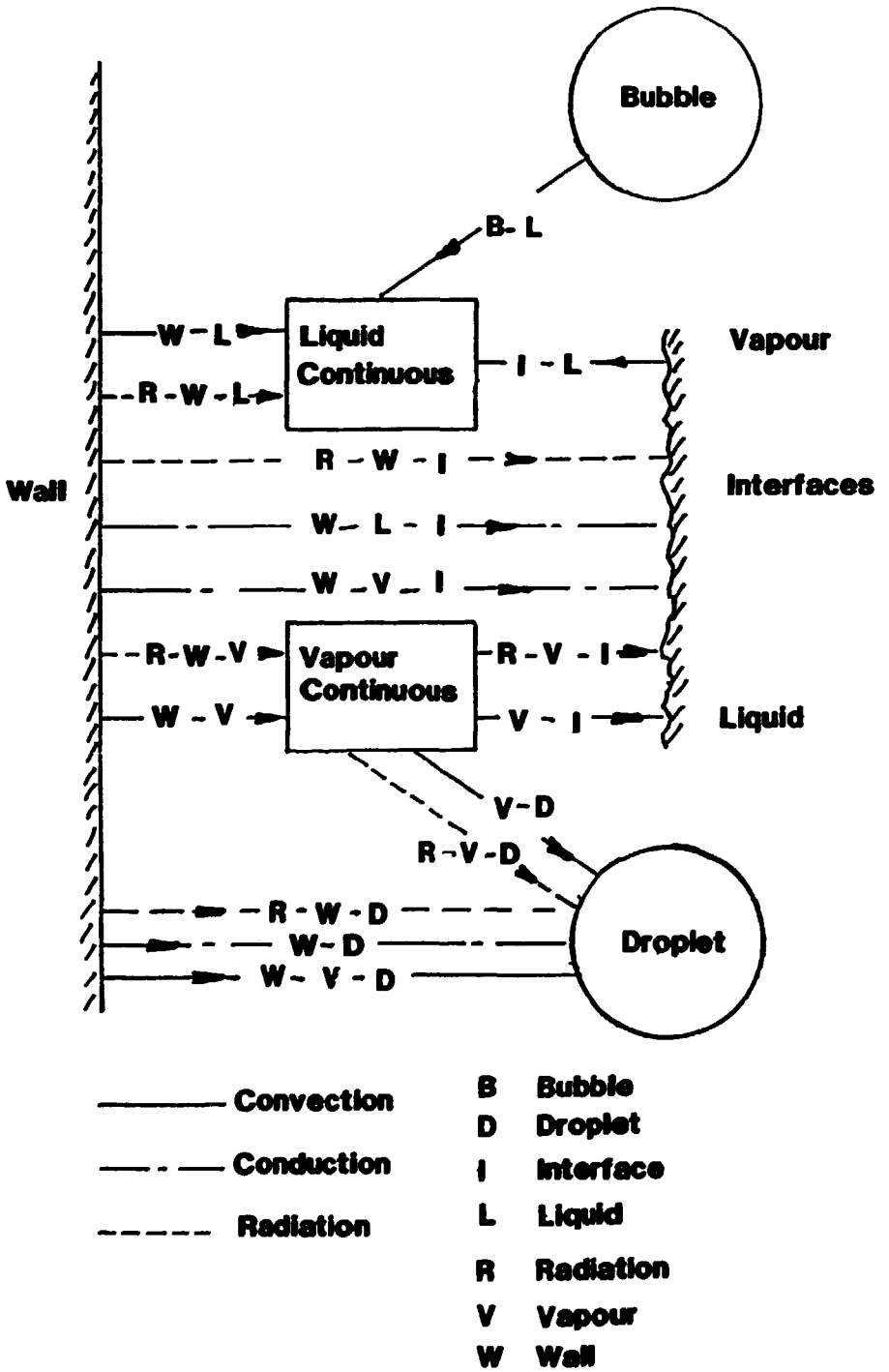
Bubble
B-L
W-L
R-W-L
Liquid Continuous
I-L
Vapour
Wall
R-W-I
Interfaces
W-L-I
W-V-I
R-W-V
Vapour Continuous
R-V-I
W-V
V-I
Liquid
V-D
R-V-D
R-W-D
W-D
W-V-D
Droplet
Convection
Conduction
Radiation
B Bubble
D Droplet
I Interface
L Liquid
R Radiation
V Vapour
W Wall

FIGURE 5.

wall-to-droplet heat transfer and vapour convection heat transfer (transition boiling heat transfer). With a relatively high surface temperature the droplets are no longer able to wet the surface. The heat transfer is decreased, but the presence of droplets in superheated vapour will lower the bulk temperature of the vapour towards saturation temperature due to interfacial heat transfer, thus increasing the heat transfer. Further the temperature profile of the vapour will be changed causing a steeper temperature gradient close to the heating surface, which will also enhance the heat transfer.

Two important points on the boiling curve with their corresponding temperatures are very decisive for the flow region and thus the heat transfer:

1. critical heat flux, and
2. minimum film boiling heat flux.

The critical heat flux (CHF) is by far the most important as it, separates normal and abnormal operation with an appropriate safety margin.

Two mechanisms of CHF are postulated, departure from nucleate boiling (DNB) in liquid continuous flow and dryout (DO) in vapour continuous flow (Fig. 6).

DNB occurs on a heating surface under subcooled or saturated nucleate boiling. Bubbles become crowded in the vicinity of the heating surface and form a moving bubble layer as shown in Fig. 6a. When the bubble layer becomes thick enough to impede cooling liquid contacting the hot surface the bubbles will merge into a vapour film changing the boiling in heat flux controlled systems from the efficient nucleate boiling to the highly inefficient film boiling. Surface temperature excursion is high and fast. Earlier DNB was therefore called fast burnout.

Dryout occurs on a heating surface under forced convective boiling. CHF occurs when liquid film becomes too thin and breaks

down into dry patches as shown in Fig. 6b. Surface temperature excursion is low and slow. Dryout was therefore called slow burnout in the past.

It is obvious that the two CHF mechanisms cannot be expressed by the same correlation.

The minimum film boiling heat flux and the corresponding minimum film boiling temperature is an important parameter in temperature-controlled systems as it separates the high temperature region, where the inefficient film boiling takes place, from the lower temperature region, where the more efficient transition boiling occurs. It thus provides a limit to the initiating rewetting by emergency core cooling. The heat transfer coefficient on either side of the minimum film boiling temperature can differ by two orders of magnitude.

As the starting point, more recent studies do not take the minimum film boiling heat flux but rather whether the droplet can wet the surface or not. The surface can, in fact be rewetted even if the minimum film boiling temperature has already been passed, if the kinetic energy of the droplets perpendicular to the surface can overcome the repulsive forces. This is discussed in Appendix C.

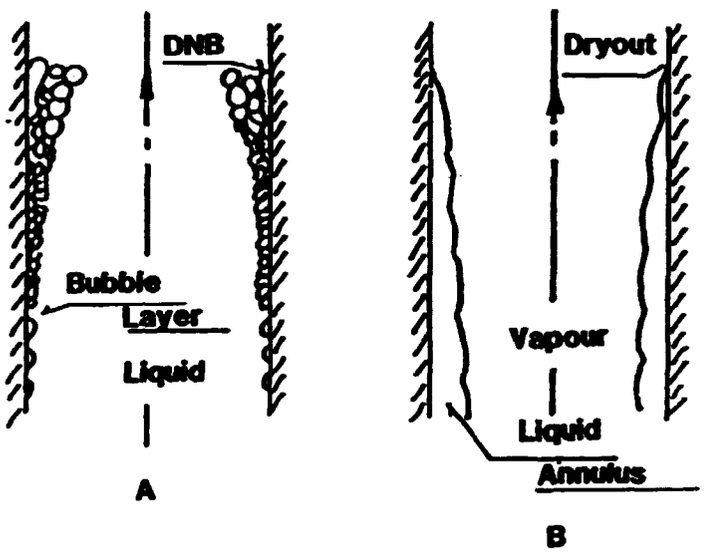

Two postulated Mechanisms of CHF

A: Departure from Nucleate Boiling (DNB)

B: Departure from Forced Convective Boiling (DFCB) or Dryout.

FIGURE 6.

4. COMPARISON OF CORRELATIONS WITH DATA

4.1. Computer programmes used

Another task (SAK-3) under the SAK-project has been to provide one or more computer programmes suitable for small break LOCA analysis.

The SAK-3 work has mainly been concentrated on the American computer programmes RELAP-5 and TRAC(PF1). It is therefore natural to use the heat transfer correlations and the programme selection logic in these programmes as the starting point for the comparison. The Norwegian programme NORA has also been used in the work.

The programme heat transfer packages are described in Appendix B1.

It cannot be expected that all necessary input data are measured in relevant experiments. It is therefore obvious to let the programme in which the correlation is used calculate these unknown parameters. This has been done in some of the comparisons.

However, using large computer programmes like RELAP-5 and TRAC(PF1) in the comparison, especially in transient calculations, include influences from so many physical phenomena and empirical correlations that it cannot be excluded that other transport phenomena apart from the heat transport may be dominant and thus impede the actual aim of assessing heat transfer correlations.

Separate developed programmes have been used in comparisons of the transition boiling heat transfer and to a certain degree also in the comparison of CHF-correlations in rod bundles.

4.2. Comparisons with data

Several sets of experimental data have been used for the assessment of the heat transfer correlations. In all the experiments the basic measured parameter was the wall temperature of the heater surface. Very minor amounts of information were supplied about the local prevailing two-phase conditions of the system. For this reason some reliance had to be placed in the two-phase flow models of the computer programmes that were used. These two-phase flow models provided the necessary input parameters to the heat transfer correlations; thus, it was obvious that the wall temperature calculations were strongly dependent on the adequacy of the two-phase models as well as the heat transfer correlations. It was an early suggestion in the project that test sections with simple tubular geometry should preferably be used in order to have a possibility to track the two-phase flow calculations. In these experiments the boundary conditions for the test section should be well defined by adequate measurements.

The different experiments selected as test cases are summarized in Table 4.2.I. In all the cases the test section was vertically oriented and the power distributions were axially and in the rod bundle cases also radially uniform. (For details of the different experiments and of the comparisons, refer to Appendix B2.)

In what follows there will be only a summary of the results obtained from the comparison between calculated and measured parameters.

The three first test cases in Table 4.2.I were different types of transients. As pointed out in Appendix B2 it was very difficult to assess the adequacy of the heat transfer package in the computer programmes from the results of these test cases.

The basic reason for this was that in transient calculations the results are influenced by a number of models and empirical correlations describing different kinds of transport phenomena

and it is a delicate task to separate the influences from the heat transfer correlations alone. Hence, in the selection of experiments it was decided to switch from transient to steady-state experiments concentrating on the Becker cases.

The Becker cases were conducted at the Royal Institute of Technology in Stockholm and reported in (2), and were kindly placed at the projects disposal by Prof. Becker. The test section was a vertical circular tube directly heated in the tube wall and insulated on the outer surface. The heated length was 7 meters with an uniform power distribution. The inner wall surface temperatures were determined from thermocouple measurements at the outer surface and the calculations with RELAP-5, TRAC and NORA were aimed at simulating the axial temperature distributions when measured inlet and outlet conditions were applied as boundary conditions.

As there were no options in RELAP-5 nor in TRAC to calculate the steady state this had to be done by calculating a transient with time invariant boundary conditions until the solution was stable. With 20 to 35 axial nodes the CPU-time on a CDC CYBER 170-835 for obtaining the steady state in these cases ended up in the range 10 to 20 minutes while the NORAS programme (steady-state version of NORA) required only a few seconds.

From the comparisons between measured and predicted wall surface temperatures, it was obvious that the pre-CHF heat transfer calculations were quite accurate. For single phase forced convection the heat transfer coefficient was calculated from an ordinary Dittus-Boelter type correlation and in saturated boiling region from Chen's correlation (3) in all three of the programmes.

The DO-predictions were not satisfactory in any of the computer programmes. In RELAP-5 the W-3 correlation (4) or the Biasi correlation (5) was used, but an upper void limit 0.96 was also used, and CHF was assumed to have occurred if this value was

TABLE 4.2.I.

Test case	Type of experiment	Geometry	Initial conditions			
			Pressure (MPa)	Mass flux ($kg/m^2/sec$)	Subcooling (^oC)	Heat rate (MW/m^2)
Roumy Case 1	Flow transient	Single tube	14.00	1532	178.1	2.267
Roumy Case 2	Flow/power transient	Single tube	14.00	1527	93.6	2.010
CE/EPRI Case 11	Blowdown	Single tube	15.86	3526	50.5	0.459
Becker Case 1	Steady-state post-DO	Single tube	5.02	1476	9.8	1.015
Becker Case 2	Steady-state post-DO	Single tube	10.01	502	12.1	0.457
Becker Case 3	Steady-state post-DO	Single tube	2.98	498	8.9	0.562
Becker Case 4	Steady-state post-DO	Single tube	7.02	1000	11.7	0.815
Becker Case 5	Steady-state post-DO	Single tube	3.00	1487	9.7	0.869
Becker Case 6	Steady-state post-DO	Single tube	3.01	1005	10.2	0.765
Becker Case 7	Steady-state post-DO	Single tube	13.99	500	9.5	0.405
ORNL Case B	Steady-state Post-DO	Rod bundle	12.76	713	19.1	0.910
ORNL Case C	Steady-state post-DO	Rod bundle	12.46	334	34.8	0.560
ORNL Case H	Steady-state post-DO	Rod bundle	8.89	256	38.0	0.417
ORNL Case K	Steady-state Post-DO	Rod bundle	4.38	226	45.8	0.440
ORNL Case N	Steady-state post-DO	Rod bundle	8.52	806	14.3	0.940
ORNL Case O	Steady-state post-DO	Rod bundle	5.98	307	22.2	0.530

exceeded. In TRAC the Biasi correlation or a void limit of 0.97 was used. In both RELAP-5 and TRAC calculations the DO was generally predicted to occur too far upstream. In the RELAP-5 case the DO predictions were also subjected to some flow oscillations during the course to steady state, which were influencing the results. For that reason a separate examination and assessment of CHF-correlations was made and the results from these efforts are summarized in Chapter 5.2 and Appendix B4.1.

In order to make it possible to examine the post-CHF heat transfer, both RELAP-5 and TRAC were modified so that the DO position could be specified through the input. In NORAS another approach was used: The CHF-value from the correlation was adjusted by a factor to obtain the measured DO position. From these cases, so recalculated it was obvious that the predicted post-DO wall temperatures were significantly lower than the measured ones and also that the calculation of the nonequilibrium effects typical for the post-DO region was inadequate.

Both NORAS and RELAP-5 were modified in order to have the post-DO calculations improved. As the nonequilibrium effects are basically governed by the mass transfer rates between the phases it is obvious that a decrease of the vapour generation rate will increase the vapour temperature thus allowing for the nonequilibrium conditions to be more pronounced. For that reason a new vapour generation model (6) was implemented for the post-DO region in these programmes. In RELAP-5 also the heat transfer models were modified so that the heat was transferred from the wall to the vapour phase and then from the vapour phase to the droplets. The calculated results after these modifications were substantially improved and a satisfactory agreement between the measured and calculated post-DO wall temperatures was obtained.

4.3. Experiences using the computer programmes

During the work a number of difficulties have been encountered with the programmes. The main ones have been concerned with

the numerical methods used in RELAP-5 and TRAC. These programmes turned out to be inefficient in the calculation of steady state tests. The implicit methods used have been more effective by a factor of 10...100 in the present test cases.

Another group of difficulties has been caused by the constitutive models. Because RELAP-5 and TRAC are primarily intended for transient calculations, the constitutive models have not been suitable for steady-state situations. An example is the way the critical heat flux is calculated in RELAP-5. Furthermore, many set of correlations contain discontinuities, which may cause troubles for the numerical method. In some cases it is possible that no steady-state solution can be found by RELAP-5.

The most important experiences using the computer programmes are, however, concerned with the accuracy of the correlation packages used. The main emphasis has been paid to wall heat transfer correlations. During the SAR-5 project it appeared that also the friction correlations and especially the interfacial heat transfer correlations used in the system programmes were poorly tested. The interfacial heat transfer correlations are closely connected with wall heat transfer correlations and have a strong effect on wall surface temperatures in the post-dryout region. The experiences using computer programmes are described in more detail in Appendix B3.

4.4. Comparisons using separate programmes

The test section in the vast majority of experiments is made as direct resistance heated tubes with no filler material in the tubes. The thermal capacity of such a test section is much smaller than in nuclear reactor fuel rods. The transient behaviour, e.g. in a simulation of a LOCA will not be correctly reproduced, the velocity of the rewetting front will be too high and the transition boiling region is hardly reproduced. It is possible to make electrical resistance heaters that can

simulate the stored heat, but the costs of such heaters are high, at least 50 times higher than a simple resistance heater tube.

Further, compared to the other flow regions, the transition boiling flow region is short both in extent and time for run-through and difficult to measure in a larger integral post-CHF experiment.

Rewetting and transition boiling heat transfer are therefore examined in experiments made for this special purpose, i.e. special considerations are taken to make the experiment temperature controlled, e.g. use of thermal storage block in connection with the test section or the water is boiled by indirectly heating by another fluid, e.g. hot mercury as in the EPRI-experiment.

Recalculation of such experiments calls for separately developed smaller computer programmes.

An advantage of such programmes is that several heat transfer correlations may be compared with experimental data. It is then necessary, however, to assume that the correlations used in the prediction depend only on local parameters, i.e. rather than on the upstream history. It must be foreseen that should more realistic models be developed, the degree of nonequilibrium at any axial location must be the result of a historically developed state dependent on the upstream competition between the heat transfer mechanisms wall-to-vapour, wall-to-droplet and vapour-to-droplet.

5. DISCUSSIONS AND RECOMMENDATIONS

5.1. Nucleate and forced convective boiling

Highly accurate heat transfer correlations in the nucleate boiling and forced convective boiling flow regions are not required in order to calculate heat transfer during a LOCA (7). The reason for this is that heat transfer in these regions is very efficient and should not be a limiting factor concerning the behaviour of fuel and cladding during a LOCA. For using heat transfer correlations in steam generators in PWR systems, the situation is somewhat more restrictive.
During a LOCA the heat flow in the steam generators may change direction and cause steam generation in the recirculation loops - which strongly influences the flow of coolant through the loops.

In single-phase forced convection any well-known heat transfer correlation may be used, e.g. Dittus-Boelter.

In the nucleate boiling flow region, most heat transfer correlations can be written in the following form:

$$h_{NcB} = B1(P) \cdot (T_W - T_{SAT})^{B2}$$

$$\dot{q}_{NcB} = h_{NcB} \cdot (T_W - T_{SAT}).$$

The heat transfer correlations that seem to give the best fit to experimental data have a value close to 2.0 for B2. The correlation by Stephan and Auracher (Table A1. II) has this value and is recommended to be used for both the reactor core and steam generators. For the reactor core, a somewhat simplified

version of the Chen correlation is considered accurate enough.

5.2. Critical heat flux

The results of the literature search are given in Appendix A2 and the outcome of some recent assessments of CHF correlations in rod bundle geometries is summarized in Appendix B4.1.

Leung(22) has demonstrated that an appropriate steady state CHF correlation was adequate for the prediction of CHF onset during a wide range of transients. He also indicated that the local condition hypothesis can be used for CHF predictions. This method is most advantageous in transient analyses. It is very difficult to define an adequate boiling length at each instance during the course of a transient, which is a requirement when other methods are employed.

In Appendix A2 it is recommended to use Griffith-Zuber correlation for the low mass flux range:

$$-240 < G < 100 \text{ kg/m}^2\text{s}.$$

Outside this mass flux range the Biasi and CISE-4 correlations were found to be equally good possibilities. However, it has to be emphasized that this outcome was based on the comparison between the measured and predicted time to CHF during different kinds of transient in round-tube or scaled-rod bundle test sections. When Biasi and CISE-4 correlations were used for prediction of the CHF in full-scale rod bundle steady-state experiments they were found to be very non-conservative (cf. Appendix B4.1). This was attributed to the development of these two correlations from single-tube data. There were no provisions for incorporating the effects of unheated wall surfaces and internal rod-to-rod power distributions. As would be expected, the rod bundle CHF correlations were found to be much more accurate when predicting the CHF in this type of geometry, and it was recommended that the Becker rod bundle CHF correlation

be used within the following parameter ranges:

Pressure 3.0 - 9.0 MPa

Mass flux 400 - 3000 kg/m^{2}s

Heat flux 0.5 - 3.0 MW/m^2

For mass fluxes between 100 and 400 kg/m^{2}s an interpolation of the Becker and the Griffith-Zuber correlations has to be made.

Above 9.0 MPa it is not clear which correlation to use. No testing of CHF correlations in this pressure range has been performed within the project, and no firm recommendation can be given. In the literature several possible correlations are reported, e.g. the correlation proposed by EPRI (8) and the one by Bezrukov et al. (9), but these have to be more thoroughly tested and validated before drawing any conclusions.

Also, the situation in the low-pressure range (P < 3.0 MPa) is not very well examined. Due to the lack of rod bundle experimental CHF data for these low pressures no assessments of CHF correlations have been made and thus no recommendations can be given. It is obvious that there is a strong need for more experimental data and analysis in this low-pressure range.

5.3. Transition boiling

The experimental data used in this comparison are primarily in the vapour continuous flow region and only very few in the transition flow between vapour and liquid continuous (churn/slug flow).

The correlations selected for comparison (except the correlation by Hsu) were developed primarily for the dispersed flow region in vapour continuous flow. It cannot be expected that the correlations can be used in the inverted annular flow region, i.e.

liquid continuous flow.

The comparison shows the necessity of taking thermodynamic non-equilibrium into account.

The comparison also shows that the direct liquid-wall contact heat transfer is important and has to be accounted for especially in regions near the CHF location. This is in contradiction to the widely used assumption that the contact heat transfer is negligible.

Much more work is needed, however, before transport phenomena in transition boiling can be described.

It is the purely empirical and simple heat transfer correlation by Bjornard and Griffith (11) that relates the test data best; therefore, it must be recommended for use until better phenomenological correlations or models are developed.

The inverted annular flow region in liquid continuous flow has not been examined.

5.4. Rewetting

The rewetting process means a reversal from film boiling conditions after DO or DNB back to nucleate boiling and the main interest concerning the phenomena is connected with large LOCA reflooding or spray cooling.

Two possible methods may be seen for the modelling of the rewetting front:

The two-dimensional heat conduction equation may be solved numerically and the moving mesh techniques are used to split the heat structure around the rewetting front into finer meshes. The numerical inaccuracy is avoided if the finest meshes in axial direction are shorter than 0.001 mm. In moving-mesh techniques the heat transfer correlations are used for the nucleate boiling,

critical heat flux and transition boiling. The moving-mesh techniques should not be used if the computing time consumption is limited.

The second possibility is to apply a mathematical correlation for the rewetting velocity. Then the formula of Dua and Tien is recommended:

$$Pe = \left[\frac{Bi}{\theta_w \cdot (\theta_w - 1)} \cdot \left(1 + 0.40 \cdot \frac{Bi}{\theta_w \cdot (\theta_w - 1)} \right) \right]^{0.5}$$

$$Pe = \frac{\delta \cdot \rho \cdot c \cdot u}{k}; Bi = \frac{h \cdot \delta}{k}; \theta = \frac{T - T_{SAT}}{T_O - T_{SAT}}; \theta_w = \theta(T_w).$$

The fitting parameters of the mathematical formula are the heat transfer coefficient h in the Biot, number Bi and the rewetting temperature T_O in the nondimensional temperature. The recommended heat transfer coefficient is the critical heat flux of Zuber correlation divided by the temperature difference ($\Delta T_{SAT} = T_{CHF} - T_{SAT}$); this difference is calculated from the wall temperature during nucleate boiling determined by the Chen correlation. The slowing down of the rewetting due to void fraction is taken into account by the factor $(1-\alpha)$ proposed by Griffith. Two possibilities are recommended for the rewetting temperature: the use of minimum film boiling temperature or a simpler formula like: $T_O = T_{SAT} + 160 + 6 \cdot \Delta T_{sub}$.

5.5. Film boiling

The film boiling region can be divided into basically two flow sub-regions: inverted annular flow and dispersed droplet flow. The development of these sub-regions is strongly influenced by the prevailing pre-CHF region which can be determined from a flow region map.

For the inverted annular flow the heat transfer mechanisms are as yet not very well understood. Until more research sheds light on these issues a simplified approach using a modified Bromley correlation is recommended to calculate the wall heat transfer:

$$q'' = h_{FB} \cdot (T_w - T_{SAT})$$

$$h_{FB} = 0.62 \cdot \left[\frac{k_v^3 \cdot \rho_v \cdot (\rho_l - \rho_v) \cdot H_{lg}^{l} \cdot g}{\lambda_c \cdot \mu_v \cdot \Delta T_{SAT}} \right]^{1/4}$$

$$\lambda_c = 2\pi \cdot \left[\frac{\sigma}{g(\rho_l - \rho_v)} \right]^{1/2}$$

The parameter range for this correlation is

Pressure	0.1 - 0.7 MPa
Wall heat flux	30 - 130 kW/m^2
Subcooling	< 78 K
Velocity	< 0.3 m/s
Void	< 0.4

The transition of inverted annular flow to dispersed droplet flow may be related to a critical Weber number. When this Weber number is exceeded the liquid core in the inverted annular flow will break down into slugs and droplets. The Weber number is defined as

$$We_{tr} = \frac{\rho_v \cdot (V_g - V_l)^2 \cdot D}{\sigma}$$

and the critical We-number according to this definition has the range 10-20.

For the dispersed droplet flow different approaches have been adopted when calculating the wall heat transfer. The most promising seems to be the phenomenological approach in conjunction with a separate fluid model. Different heat transfer modes are then identified and described as well as the interfacial transport phenomena. This approach is also very well suited for thermohydraulic programmes like RELAP-5 and TRAC.

In the film boiling region it is usually assumed that the radiation and wall-to-liquid heat transfer terms are negligible compared with the wall-to-vapour terms. This latter heat transfer can be calculated according to the revised version of the modified CSO (Chen-Sundaram-Ozkaynak) correlation:

$$q'' = h \cdot (T_W - T_V)$$

$$h = h_{mod\ CSO}\ (1+F_S)(1+0.8/(L/D))$$

$$F_S = 250 \left[\frac{P}{P_C}\right]^{0.69} \left[\frac{1-XA}{XA}\right]^{0.49} Re_V^{-0.55}$$

$$h_{mod\ CSO} = \frac{f}{2} \cdot C_{pvf} \cdot G \cdot XA \cdot Pr_{vf}^{-2/3}$$

$$f = f_O \cdot \left(\frac{T_W}{T_V}\right)^{-0.1}$$

$$\frac{1}{\sqrt{f_O}} = 3.48 - 4 \cdot \log_{10}\left[\frac{2\varepsilon}{D} + \frac{9.35}{Re_V \sqrt{f_O}}\right]$$

The basic interfacial processes are dealt with in Chapter 5.6.

When the flow region is single-phase steam flow, where the steam may be superheated, the well-proven correlations of Dittus-Boelter's type can be used to calculate the heat transfer coefficient. The Sieder-Tate correlation is one example of this type:

$$q'' = h \cdot (T_W - T_V)$$

$$h = \frac{k_V}{D} \cdot Re_V^{0.8} \cdot Pr_V^{1/3} \cdot \left(\frac{\mu_V}{\mu_W}\right)^{0.14}$$

The revised version of the modified CSO correlation seems to have a smooth transition to this correlation when XA approaches unity.

For very low flows natural convection may become a significant contributor to the total heat transfer. For turbulent natural convection heat transfer to single-phase vapour the following correlation can be used:

$$q'' = h \cdot (T_w - T_v)$$

$$h = 0.13 \cdot k_{vf} \frac{\rho_{vf}^2 \cdot g \cdot \beta_{vf} \cdot (T_w - T_v)}{\mu_{vf}^2}^{1/3} \cdot Pr_{vf}^{1/3}$$

where the properties are evaluated at film temperature.

5.6. Interfacial heat transfer

When thermodynamic nonequilibrium between the phases is assumed, a constitutive model is needed for the interfacial heat transfer. The way in which the constitutive model is applied depends on the assumptions made in the hydraulic model. When a two-fluid model is applied two constitutive equations are needed, one for the heat transfer from the interface-to-vapour phase (Q_{ig}) and another from the interface-to-liquid phase (Q_{il}). These are related to the interfacial mass transfer as

$$\Gamma = - \frac{Q_{ig} + Q_{il}}{H_{fg}}$$

where H_{fg} is the latent heat of evaporation.

If simplifying assumptions have been made in the hydraulics the number of interfacial constitutive equations decreases. The usual assumption is that one of the phases is saturated while the other phase is in thermodynamic nonequilibrium. In that case only one equation for the interfacial energy transfer must be specified. Usually the model is applied for Γ. Because there is a lack of experimental correlations the same approach is very often used also with the two-fluid model. The interfacial heat transfer rates are expressed as:

$$Q_{ik} = h_{ik} \cdot (T_{SAT} - T_k)$$

where T is temperature, h_{ik} is a kind of heat transfer coefficient (Joule/$m^3 \cdot s \cdot {}^oC$) and the subscript k is either g or ℓ. When this equation is used the phase can be forced to be saturated by applying a large interfacial heat transfer coefficient h_{ik}. In some cases the interfacial heat transfer is closely related to the wall heat transfer. One example is subcooled boiling. In this case a separate wall boiling model must be applied, because when the average fluid is subcooled, no evaporation is predicted through the above equations. If Γ_w is the amount of wall flashing, the total flashing rate is expressed as:

$$\Gamma_{tot} = \Gamma_w + \Gamma$$

where Γ is calculated from the above mentioned equation. Γ is negative (condensation) in the case of subcooled boiling. In practice it is very difficult to model Γ_w so that the total flashing rate is correct. For example, the TRAC(PF1)-programme was unable to predict any subcooled boiling in the test cases analyzed in the SÄK-5 project.

Another case where the interfacial heat transfer rate has a strong effect on the wall heat transfer is post-dryout heat transfer. In the post-dryout flow region the interfacial area between the phases is small and the heat transfer coefficient h_{ig} is low. Consequently, the vapour temperature is increasing in that region, which results in higher wall surface temperatures if the wall heat transfer coefficient remains constant. Encouraging results have been obtained in the SÄK-5 project by applying interfacial heat transfer models in the post-dryout region. Another approach in the post-dryout region would be the modification of the wall heat transfer coefficient so that better agreement with experimental surface temperature is obtained. In fact, this is the only way if equilibrium between the phases is assumed. The use of a nonequilibrium assumption enables the more realistic prediction of the wall temperature distributions.

Although the interfacial heat transfer has an important role in two-phase flow predictions, relatively few empirical correlations exist at present. In the SÄK-5 project only two areas have been studied and only preliminary results have been obtained. These results cover the area of flashing and post-dryout flow region.

The flashing rate is important in the prediction of the pressure recovery following a rapid depressurization and in the prediction of the liquid superheat in quasi-steady flow. The latter is important in the calculation of critical flow. Several flashing correlations have been tested (14). According to the test cases performed the experimental correlation of Bauer et al. (15) gave the best agreement with experimental data. This correlation can be expressed for h_{il} as

$$h_{il} = \frac{(1-\alpha)\cdot\rho_l\cdot C_{pl}}{\tau}$$

where α is void fraction, C_p is specific heat and ρ_l is liquid density. The time constant τ is defined as

$$\tau = \frac{660}{(\alpha+\alpha_o)(u+u_o)^2\sqrt{P}}$$

where u is liquid velocity and P is pressure in Pa. This correlation is valid in the range of $0.01 < \alpha < 0.96$ and 5 m/s $< u < 54$ m/s, when $\alpha_o = u_o = 0$. However, because there are no other suitable correlations, it is suggested that this correlation is extrapolated outside its validity limits. For this purpose the constants α_o and u_o have been determined to be 0.003 and 4 m/s. In this form the correlation predicts critical flow data with good agreement. In the prediction of the pressure recovery following a rapid depressurization, the agreement seems to depend on the flow area. Relatively good pressure history is predicted with medium-size pipes. In the case of Edward's pipe test, the predicted pressure recovery is too slow and in the case of a large vessel it is too fast. However, this kind of uncertainty has not such a vital importance as has the uncertainty in the calculated critical flow.

Another area that has been studied in the SAK project is the post-dryout flow region. Calculations have been performed using NORAS and RELAP-5 programmes, which both gave good results. The correlation used for Γ has been developed by Webb et al. (6)

$$\Gamma = 1.32 \left[\frac{P}{P_c}\right]^{-1.1} \left[\frac{GXA}{\alpha}\right]^2 \frac{(1-\alpha)^{2/3} \cdot k_v \cdot (T_v - T_{SAT})}{\rho_v \cdot D \cdot \sigma \cdot H_{fg}}$$

where P_c is critical pressure, G is mass flux, XA is actual quality, k_v is thermal conductivity of superheated vapour, D is hydraulic diameter, and σ is surface tension. This correlation has been used only for the post-dryout region. In that region $Q_{ig} >> Q_{il}$, which makes it possible to express the correlation for h_{ig} as

$$h_{ig} = 1.32 \cdot \left[\frac{P}{P_c}\right]^{-1.1} \cdot \left[\frac{G \cdot XA}{\alpha}\right]^2 \cdot \frac{(1-\alpha)^{2/3} \cdot k_v}{\rho_v \cdot \sigma \cdot D}$$

This correlation has been extensively compared with experimental data elsewhere (16). According to the recent studies the correlation gives a mass transfer rate just after the DO position that is too low. Because of this a modified version of it has been developed (17). The increased vapour generation rate in this "near-field region" is referred to some sputtering effects when the wall liquid film is driven violently off (or reformed by droplet-wall contact) at the CHF-location, i.e. this is not really an interfacial heat transfer. At present, a final evaluation of the correlation as yet has not been made.

In calculating the interfacial heat transfer one possibility is to use the above equations for h_{il} and h_{ig} whenever evaporation occurs. This is justified by the simple fact that there are no better correlations. Furthermore, usually either Q_{ig} or Q_{il} is dominant in the calculation and the extrapolations of the other correlations outside its range are not so harmful. It is obvious that a lot of work must be performed in the future with the interfacial heat transfer mechanism. In this context only two recommendations can be made. However, the correlations recommended are not yet thoroughly tested; their use with a wall boiling model especially remains to be studied in the future.

6. CONCLUSION

It is both natural and rather obvious to test heat transfer correlations in the environment in which they are to be used, i.e. the computer programmes TRAC, RELAP-5 and NORA. The advantage is that parameters not measured in the experiment are calculated under conditions in the programme which ought to correspond to reality in the experiment.

It was, however, not possible in the transient calculations to assess the adequacy of the heat transfer package in the individual programmes. It can not be excluded that other transport phenomena (subcooled void, slip, thermodynamic nonequilibrium) and empirical correlations veil the actual aim, viz. to assess the heat transfer correlations.

The general idea, to use the computer programmes in the comparison, was retained, but it was decided to make a switch in the selection of experiments from transient to steady state, simple experiments.

The accuracy of heat transfer correlations in pre-CHF regions i.e. the nucleate boiling region and the forced convective boiling region does not have to be very high for the purpose of calculating heat transfer during a LOCA The heat transfer in these regions is very efficient and should not be a limiting factor for the fuel and cladding during a LOCA.

The critical heat flux (CHF) calculations were carried out with the W-3 correlation (4) (primarily a DNB correlation) in RELAP-5 as well as the Biasi correlation (5). The predicted dryout locations were too far upstream (up to ~ 3 m at low pressure). The CHF were in some cases determined by a cutoff void limit of 0.96 when the Biasi correlation was used.

The results from TRAC were fairly accurate except at low pressure. TRAC makes use of the Biasi correlation, but in none of the cases did the correlation determine the locus of dryout. An arbitrarily chosen cutoff void limit of 0.97 caused dryout.

The NORAS calculations used three different CHF-correlations, Biasi, CISE-4 (24) and Becker (64). Biasi and Becker correlations predicted dryout too far downstream while CISE-4 correlation predicted dryout too far upstream at high quality and too far downstream at low quality.

It was therefore necessary to freeze the locus of CHF at the measured location in order to compare the surface temperatures. This comparison was not good in any of the programmes used. The calculated surface temperatures were too low in RELAP-5 and TRAC indicated an interfacial heat transfer that was too high. NORAS gave too high surface temperatures, i.e. too low interfacial heat transfer.

This can be seen from a single calculation using NORAS and 5 calculations using RELAP-5 in Figs. B2.21-B2.27. In two of the RELAP-5 cases the interfacial heat transfer was so high that no vapour superheat was calculated (the liquid and vapour post-dryout temperatures were about the same).

The test section was an electrically heated tube with a very low thermal capacity i.e. a typically heat flux controlled experiment. The thermodynamic nonequilibrium effects are therefore primarily governed by mass transfer between droplets and vapour due to interfacial heat transfer. A decrease in the vapour generation rate will increase the vapour temperature under equal conditions, thus allowing the thermodynamic nonequilibrium to be more pronounced.

The programmes were modified by implementing a recently developed vapour-generation model by Chen (6). Recalculated results were substantially improved and a satisfactory agreement between measured and calculated post-dryout surface temperatures was obtained.

From these examinations, together with the examinations of the transition boiling heat transfer with a separate computer programme, it is obvious that more realistic and phenomenological heat transfer models have to be developed. It must be recognized that the degree of thermodymamic nonequilibrium at any axial location is dependent not only on local conditions but especially on the upstream competition between the heat transfer mechanisms wall-to-vapour, wall-to-droplet and vapour-to-droplet.

Up to now this report treated the post-CHF region in more independent chapters, transition boiling heat transfer, rewetting, interfacial heat transfer and film boiling with and without droplets. To get realistic models the transport phenomena have to be considered in more detail and the post-dryout region may be treated as one region where the dividing point between transition boiling and film boiling is not the minimum film boiling temperature, but rather the point where the droplet can wet the surface or not. The surface can, in fact, be rewetted even if the minimum film boiling temperature has been passed, if the momentum of the droplets perpendicular to the surface can prevail over the repulsive forces due to evaporation at the wall. The project decided to touch upon these phenomena in a somewhat more detail and the results are discussed in Appendix C.

With respect to the discouraging results of critical heat flux calculations, the project decided to make a closer elaboration of 4 relevant CHF-correlations: Barnett, Becker, CISE-4 and Biasi using results from full-scale rod bundle experiments. The results indicate that Biasi and CISE-4 correlations, which are used in computer programmes like RELAP-5 and TRAC, cannot predict the CHF-conditions with adequate accuracy. An explanation is believed to be that these two correlations are developed from single tube data and have no provisions to incorporate the influence of unheated surfaces and internal rod-to-rod power distribution. The two other CHF-correlations are developed for rod bundle geometries and correlate the experimental data more accurately. It is therefore recommended that these correlations instead of Biasi and CISE be used.

NOMENCLATURE LIST

A	Area	m^2
C_p	Specific heat capacity	joule/kg^oC
C_o	Distribution parameter	
d	Diameter droplet	m
D	Diameter	m
E	Entrainment	
e	Internal energy	joule/kg
f	Friction coefficient	
G	Mass flux	$kg/m^2 \cdot s$
g	Gravitational constant	m/s^2
h	Heat transfer coefficient	$W/m^{2o}C$
H	Enthalpy	joule/kg
H_{fg}	Latent heat of evaporation	joule/kg
j	Volumetric flux (superficial velocity)	m^3/m^2s
k	Thermal conductivity	W/m^oC
L	Length	m
L_C	Characteristic length	m
M_{ik}	Generalized interfacial drag force	N/m^3
n	Normal vector	
P	Pressure	Pa
P_c	Critical pressure	Pa
q"	Heat flux	W/m^2
Q	Heat flow rate	Watt
r	Radius droplet	m
R	Gas constant	joule/kg^oC
T	Temperature	^oC
t	Time	s
u	Velocity	m/s
v	Velocity	m/s
V	Volume	m^3
XA	Quality (nonequilibrium)	
XE	Quality (equilibrium)	
y	Distance normal to wall and positive towards centre of channel	m

Greeks

α	Void fraction	
β	Volumetric expansion coefficient $(- 1/\rho\ (\partial\rho/\partial T)_p)$	$1/^oC$
δ	Wall thickness or boundary layer thickness	m
Γ	Vapour generation rate	kg/m^3s
ε	Surface roughness	m
κ	Thermal diffusivity	m^2/s
μ	Dynamic viscosity	kg/m•s
ξ	Integral variable	S
ρ	Density	kg/m^3
σ	Surface tension	N/m
τ_z	Shear stress	N/m^3
τ_{zz}	Viscous or turbulent stresses	N/m^3

Subscripts

b	Boiling
CHF	At critical heat flux
d	Droplet
e	Equivalent
f	Fluid (liquid)
FB	Film boiling
FF	Far field region
g	Vapour (saturated)
i	Interface
k	Generalized phase index
ℓ	Liquid
LC	Liquid contact
MFB	At minimum film boiling
NF	Near field region
NcB	Nucleate boiling
NU	Nonuniform
SAT	At saturation
TB	Transition boiling
T	Total
V	Vapour (superheated)

Dimensional groups

Bi	Biot number	$\frac{h \cdot \delta}{k_w}$
Pr	Proude number	$\frac{v^2}{g \cdot D}$
Gr	Grashof number	$\frac{\rho^2 \beta \cdot g(T_w - T) D^3}{\mu^2}$
Nu	Nusselt number	$\frac{h \cdot D}{k}$
Pe	Peclet number	$Re \cdot Pr$
Pr	Prandtl number	$\frac{C_p \cdot \mu}{k}$
Re	Reynold number	$\frac{G \cdot D}{\mu}$

REFERENCES.

1. Y. Y. HSU
Best-Estimate Recommendations for Blowdown Heat Transfer.
LOCA Research Highlights, 1975 (NRC).

2. K. M. BECKER et al.
An Experimental Investigation of Post Dryout Heat Transfer
KTH-NEL-33
Department of Nuclear Reactor Engineering, Royal Institute of Technology, Stockholm, May 1983

3. J. C. CHEN
Correlation for Boiling Heat Transfer to Saturated Fluids in Convective Flow
I&EC Process Design and Development.
Vol 5, No 3
July 1966

4. L. S. TONG
Prediction of Departure from Nucleate Boiling for an Axially Non-uniform Heat Flux Distribution.
Journal of Nuclear Energy, 21, pp 241-248

5. L. BIASI et al.
Studies on Burnout Part 3
Energia Nucleare 14, 1967

6. S. W. WEBB, J. C. CHEN, R. K. SUNDARAM.
Vapour Generation Rate in Non-equilibrium Convective Film Boiling.
7th Int Heat Transfer Conference, Munich, Sept 1982

7. J. RASMUSSEN
Correlations for Heat Transfer in Forced Convection and Nucleate Boiling and Critical Heat Flux.
SAK-5-N (81)-2.

8. D. G. REDDY, C. F. FIGHETTI.
Parametric Study of CHF-data, vol. 2
A Generalized Subchannel CHF-correlation for PWR and BWR Fuel Assemblies.
EPRI NP-2609. Jan. 1983.

9. YU. A. BEZRUKOV et al.
Experimental Investigation and Statistical Analysis of Data on Burnout in Rod Bundles for Water-Moderated Water-Cooled Reactors.
Teploenegetika, 1976, 23(2) 80-82.

10. J. G. M. ANDERSEN et al.
BWR Refill-Reflood Program
Basic Models for the BWR
Version of TRAC
NUREC/CR 2573 (GEAP-22051)
September 1983.

11. T. A. BJORNARD and P. GRIFFITH
PWR Blowdown Heat Transfer.
Thermal and Hydraulic Aspects of
Nuclear Reactor Safety. Vol. I LWR.
ASME Winter Annual Meeting Atlanta,
Georgia, 1977

12. A. SJÖBERG
"Heat Transfer in the Post Critical
Heat Flux Regime"
Studsvik Technical Report NR-82/77
SÄK-5-S(82)1
Jan 1982

13. K. MISHIMA, M. ISHII "Flow Regime Transition Criteria for
Upward Two-Phase Flow in Vertical
Tubes"
Int. J. of Heat and Mass Transfer, Vol.
27, No 5
May 1984

14. T. SIIKONEN
Comparison of Flashing Heat Transfer Correlations
Second International Topical Meeting on Nuclear
Reactor Thermal-Hydraulics, Santa Barbara, Jan.
11-14, 1983.

15. E. G. BAUER, G. R. HOUDAYER, H. M. SMEAN
A Non-equilibrium Axial Flow Model and Application
to Loss-of-Coolant Accident Analysis: The CLYSTERE
System Code
CSNI Specialist Meeting on Transient Two-Phase Flow,
Toronto 1976.

16. R. C. GOTTULA, R. A. NELSON, J. C. CHEN, S. NETI
R. K. SUNDARAM.
Forced Convective Nonequilibrium Post-CHF Heat
Transfer Experiments in a Vertical Tube
ASME-JSME Thermal Engineering Joint Conference,
Honolulu, March 20-24, 1983.

17. S. W. WEBB, J. C. CHEN
A Two-Region Vapor Generation Rate Model for
Convective Film Boiling
International Workshop on Fundamental Aspects of
Post-Dryout Heat Transfer, Salt Lake City,
April 1-4, 1984.

18. P. CAMPOLUNGHI et al.
Subcooled and Bulk Boiling Correlations for Thermal Design of Steam Generators.
Advances in Heat Transfer CNEN-RT/ING (80)22.

19. K. STEPHAN, H. AURACHER
Correlations for Nucleate Boiling Heat Transfer in Forced Covection.
Int. J. of Heat and Mass Transfer,
Jan. 1981.

20. J. G. COLLIER
Convective Boiling and Condensation
McGraw-Hill, London, 1972.

21. G. F. HEWITT
Critical Heat Flux in Flow Boiling
6th Intern. Heat Transfer Conf. Toronto,
1978.

22. J. C. LEUNG
Transient Critical Heat Flux and Blowdown Heat Transfer Studies.
ANL-80-53, Argonne, Illinois.

23. M. CUMO et al
On the Limiting Critical Quality and the "deposition controlled" Burn-Out.
CNEN-RT/ING(80)22.

24. A. ERA, G. P. GASPARI
Heat Transfer Data in the Liquid Deficient Region for Steam-Water Mixtures at 70 kg/cm^2 in Tubular and Annular Conduits.
CISE-R 184, 1966.

25. K. M. BECKER, D. H. LING
Burnout Measurements in a Round Tube of 7.1 m Heated Length
KTH, Stockholm, 1970

26. H. ABEL-LARSEN.
Comparison between 5 Transistion Boiling Heat Transfer Correlations and some Temperature Controlled Test-Data at 1-4 bar
(EPRI) SAK-5-D(84)-2

27. H. ABEL-LARSEN.
Heat Transfer in the Transition Boiling Region
SAK-5-D(81)-2.

28. D. C. GROENVELD.
Heat Transfer Phenomena
Related to the Boiling Crisis
AECL-7239, March 1981

29. J. C. CHEN et al.
A Phenomenological Correlation for
Post-CHF Heat Transfer.
NUREG-0237, June 1977

30. O. C. ILOEJE et al.
Three-Step Model of Dispersed Flow Heat Transfer
(Post-CHF Vertical Flow).
ASME Winter Annual Meeting 1975, 75-WA/HT-1.

31. L. S. TONG and J. D. YOUNG.
A Phenomenological Transition and Film Boiling Heat
Transfer Correlation
5.Int.Heat Transfer Conf., Sept. 1974. (Paper B3.9)

32. Y.Y. HSU
Tentative Correlations of Reflood Heat Transfer.
LOCA Research Highlights, 1975, (NCR).

33. TROND A. BJORNARD and PETER GRIFFITH.
PWR Blow-Down Heat Transfer.
ASME Winter Annual Meeting, Vol.1, 1977.

34. KIRCHNER, WALTER and PETER GRIFFITH
Reflood Heat Transfer in a Light Water Reactor.
AICHE-Symp. Series 1977: 73 NO. 164.

35. J. MIETTINEN.
The Modelling of the Transition Boiling During Rewetting
of a Hot Surface With an Analytical Correlation.
SÄK-5-F(82)2

36. J.G.M. ANDERSEN.
Low-Flow Film Boiling Heat Transfer on Vertical Surfaces.
PART I.
16. Nat. Heat Transfer Conf., AICHE-52, St. Louis, 1976.

37. J.E. LEONHARD, K.H. SUN and G.E. DIX
Low-Flow Film Boiling Heat Transfer on Vertical Surfaces.
PART II.
Same Conf.

38. M.K. DENHAM
Inverted Annular Film Boiling and the Bromley Model
AEEW-R 1590
AEE, Winfrith, Dorchester
Jan, 1983.

39. S.M. NIJHAWAN
Experimental Investigation of Thermal Nonequilibrium in Post-Dryout Steam-water Flow
Ph.D. Dissertation, Lehigh University, 1980

40. S. M. NIJHAWAN et al
Measurement of Vapour Superheat in Post-Critical Heat-Flux Boiling
Journal of Heat Transfer Vol 102
Aug 1980

41. D. G. EVANS, S. W. WEBB, J. C. CHEN
Measurement of Axially Varying Nonequilibrium in Post-Critical-Heat-Flux Boiling in a Vertical Tube
NUREG/CR-3363, Vols 1 and 2
June 1983

42. R. C. GOTTULA et al
Forced Convective, Nonequilibrium Post-CHF Heat Transfer Experiment Data and Correlation Comparision Report
NUREG/CR-3193, EGG-2245 DRAFT
Jan 1984

43. J. C. CHEN
Review of Post-Dryout Heat Transfer in Dispersed Two-Phase Flow
Lehigh University, PA
Presented at the International Workshop on Fundamentals Aspects of Post-Dryout Heat Transfer
Salt Lake City, April 1984

44. V. H. RANSOM et al
RELAP5/MOD1 Code Manual Volume 1
System Models and Numerical Methods
NUREG/CR-1826. EGG-2070
March 1982

45. A. SJÖBERG
RELAP5/MOD1 Calculations on Five Steady State Post-Dryout Heat Transfer Experiments
STUDSVIK Technical Report NR-83/338
SÄK-5-S(83)2
Dec 1983

46. J. RASMUSSEN
Simulation of Non-Equilibrium Effects
State Post-Dryout Heat Transfer
IFE Report IFE/KR/F-84/069
SÄK-5-N(84)1
June 1984

47. A. SJÖBERG
"RELAP5/MOD1 Simulation of
Non-Equilibrium Effects in the
Post-Dryout Regime
STUDSVIK Technical Report NR-84/452
SÄK-5-S(84)1
Aug 1984

48. K. G. CONDIE et al
Forced Convective, Nonequilibrium
Post-CHF Heat Transfer Experiment:
Description, Data Analysis
and Correlation Comparison
Presented at the International
Workshop on Fundamental Aspects of
Post-Dryout Heat Transfer
Salt Lake City April 1984

49. T. SIIKONEN
Calculations on some Steady-State
Heat Transfer Experiments.
(to be published)

50. T. SIIKONEN
Comparison of Flashing Heat Transfer Correlations
Second International Topical Meeting on Nuclear
Reactor Thermal-Hydraulics,
Santa Barbara
Jan. 11-14, 1983

51. A. R. EDWARDS, T. P. O'BRIAN
Studies of Phenomena Connected with the
Depressurization of Water Reactors
J. of the British Nuclear Society
Vol. 9, No. 2, 1970

52. The Marviken Full Scale Critical Flow Tests
Results from Test 15
MXC-215, Sept. 1979

53. L. R. KEVORKOV, S. Z. LUTONINOV, L. K. TIKHONENKO
Influence of the Scale Factors on the Critical
Disharge of Saturated Water from Straight Tubes with
Sharp Inlet Edge.
Teploenergetika 24(7), 1977.

54. Ph. VERNIER, Ph. BERNE
An Appraisal of Interfacial Vapor Generation Laws Used in Thermalhydraulics Analysis,
Second International Topical Meeting on Nuclear Reactor Thermalhydraulics,
Santa Barbara
Jan. 11-14, 1983.

55. P. SAHA, B. S. SHIRALKAR, G. E. DIX
A Post-Dryout Heat Transfer Model based on Actual Vapour Generation Rate in Dispersed Droplet Regime
ASME Paper 77-HT-80, 1977.

56. R. ROUMY
Burn out in Transient Conditions on Circular Tubes Presented at European Two Phase Flow Meeting
Harwell, June 1974

57. T. SIIKONEN, H. OLLIKKALA
RELAP5 Calculations for a Nucleate Boiling and CHF Test Case
VTT Technical Report SÄK-5-F(82)4

58. R. A. SMITH, P. GRIFFITH
A Simple Model for Estimating Time to CHF in a PWR LOCA
ASME paper No 76-HT-9, 1976

59. H. N. GUERRERO et al
Single Tube and Rod Bundle Blowdown Heat Transfer Experiments Simulating Pessurized Water Reactor LOCA Conditions
ASME-76-HT-11

60. J. MIETTINEN, T. SIIKONEN
Analysis of Steady Dryout Experiments (Becker) with RELAP5
VTT Technical Report OAP-22/83
SÄK-5-F(83)2, Sep 1983

61. A. SJÖBERG
Analysis of Three Steady State DO Experiments with RELAP5/MOD1
Studsvik Technical Report NR-83/276
SÄK-5-S(83)1, June 1983

62. H. ABEL-LARSEN, P. ASTRUP
Analysis of 4 Steady State Critical Heat Flux Experiments (Becker) with TRAC-PF1,
SÄK-5-D(83)1
May 1983

63. J. RASMUSSEN
NORAS Calculations on some Steady-State
Heat Transfer
Experiments with B O
IFE Report IFE/KR/F-83/031
SÄK-5-N(83)1
June 1983

64. K. M. BECKER
An Analytical and Experimental Study of
Burnout Conditions in Vertical Round
Ducts, Nucleonik 9, pp 257-270, 1967

65. T. VANTTOLA
Testing of Wall Heat Transfer Package
of RELAP5 Draft
VTT Technical Report SÄK-5-F(84)- ?
Sept 1984

66. J. MIETTINEN
Comparisons of Heat Transfer Models in
RELAP5/MOD1, DRUPAN and FLUT
Draft
VTT Technical Report SÄK-5-F(84)
Sept 1984

67. A. SJÖBERG
RELAP5/MOD1 Calculations on Five Steady
State Post Dry-out Heat Transfer
Experiments
Studsvik Technical Report NR-83/338
SÄK-5-S(83)2, Dec 1983

68. H. ABEL-LARSEN
Analysis of 5 Steady State Critical Heat Flux
Experiments (Becker) with Frozen CHF-Location
using TRAC(PF1)
SÄK-5-D(83)-5
September 1983

69. A. SJÖBERG
RELAP5/MOD1 Simulation of
Non-Equilibrium Effects in the
Post-Dryout Regime
Studsvik Technical Report NR-84/452
SÄK-5-S(84)1. Aug 1984

70. J. RASMUSSEN
NORAS- Calculations on Some Steady State
Heat Transfer Experiments with BO
Using a New Correlation for Vapour -
Droplet Heat Transfer
IFE Report IFE/KR/F-83/052
SÄK-5-N(83)2, Aug 1983

71. J. RASMUSSEN
Simulation of Non-Equilibrium Effects in Post-Dryout Heat Transfer
IFE Report IFE/KR/F-84/069
SAR-5-N(84)1, June 1984

72. G. L. YODER et al
Dispersed Flow Film Boiling in Rod Bundle Geometry - Steady State Heat Transfer Data and Correlation Comparisons, NUREG/CR-2435
ORNL-5822, March 1982

73. L. SARDH, K. M. BECKER
Assessment of CHF Correlations Based on Full-Scale Rod Bundle Experiments
Royal Institute of Technology, Nuclear Reactor Engineering
KTH-NEL-36
Stockholm Oct. 1984

74. P.G. BARNETT
A Correlation of Burn Data for Uniformly Heated Annuli and its Use for Predicting Burnout in Uniformly Heated Rod Bundles
AEEW-E463
1966

75. K.M. BECKER
A Burnout Correlation for Flow of Boiling Water in Vertical Rod Bundles
AE-276, April 1967

76. G.P. GASPARI et al.
A Rod Centered Subchannel Analysis with Turbulent Mixing for Critical Heat Flux Predictions in Rod Clusters Cooled by Boiling Water
Proc of the 5th International Heat Transfer Conference Tokyo, Sept. 1974

77. DESIRELLO et al.
Critical Power and Mass Content in a 8x8 Bundle
Paper Presented at the European Two-Phase Flow Group Meeting in Eindhover, June, 1981

78. S. PIMPUTKAR M. GROSS
The Thermal Hydraulic Performance of a 81-Rod Bundle under Boiling Water Reactor Conditions
Paper Presented at the European Two-Phase Flow Group Meeting in Ispra, June, 1979.

79. L. NILSSON
FIX-II Loca Blowdown and Pump Trip Heat Transfer Experiments
STUDSVIK REPORT NR-83/274, 1983

80. O. NYLUND et al.
Hydrodynamic and Heat Transfer Measurements on a Full-Scale Simulated 36-Rod Marviken Fuel Element with Non-uniform Radial Heat Flux Distribution. FRIGG-3, 1970

81. O. NYLUND et
Hydrodynamic and Heat Transfer Measurements on a Full-Scale Simulated 36-Rod Bundle BHWR Fuel Element with Non-Uniform Axial and Radial Heat Flux Distribution.
FRIGG-4, 1970

82. F. H BOWDITCH, R. T. SMYTH
Dryout and Pressure Drop Experiments on a Simulated SGHWR Channel with Five Unheated Rods
AEEW-M757, 1967

83. K. M. BECKER et al
Measurements of Burnout Conditions in Vertical Round Tubes with Non-Uniform Axial Heat Flux
AE-RL-1153, Nov 1969

84. K. M. BECKER
Personal Communication
Oct. 1984

85. O. NYLUND et al
OF-64. Results of BURNOUT Measurements
ASEA-ATOM
FRIGG PM-64 (ASEA-ATOM Proprietary)
Jan 1970

86. A. SJÖBERG, K. TANGEN
Comparison between OF-64 Burnout-Data
and Dryout-Locations Calculated from
RELAP5 Fluid Conditions using Becker's
CHF Correlation
STUDSVIK Technical Report NR-84/473
Restricted Distribution
SÄK-5-S(84)2, 1984

87. J. WEISMAN et al
Studies of Transition Boiling Heat Transfer
with Saturated Water at 1-4 bar.
EPRI-NP-1899, June, 1981.

88. M. ISHII, M.A. GROLMES
Inception Criteria for Droplet Entrainment
in Two-Phase Concurrent Film Flow.
AIChE Journal, Vol.21, No. 2, March 1975.

89. G. B. WALLIS
One-dimensional Two-Phase Flow.
McGraw-Hill Book Co., Inc., New York, 1969.

90. R. LEE et al
Size and Number Density
Change of Droplet Populations
above a Quench Front during Reflood
Int. Journ. Heat Mass Transfer
Vol. 27, No., 4, pp. 573-585, 1984.

91. N. LEE et al
PWR FLECHT SEASET
Unblocked Bundle, Forced and
Gravity Reflood Task Data
Evaluation and Analysis Report.
NUREG/CR-2256, EPRI NP-2013, WCAP-9891
Nov. 1981.

92. R.S. BRODKEY
The Phenomena of Fluid Motions
Addison-Wesley Publishing Co.
Reading, Mass., USA.

93. M. ISHII
"Thermo-Fluid Dynamic Theory of Two-Phase Flow".
Eyrolles, Paris 1975.

94. S. BANERJEE, A. M. CHAN
"Separatet Flow Models - I. Analysis of the Average
and Local Instantaneous Formulations"
Int. Journal of Multiphase Flow, Vol. 6
1980

95. G. YADIGARAGLU, T. T. LAHEY Jr.
"On the Various Forms of the
Conservation Equations in
Two-Phase Flow"
Int. Journal of Multiphase Flow, Vol. 2
1976.

96. N. ZUBER, J.A. FINDLAY
"Average Volumetric Concentration in
Two-Phase Flow Systems"
Journal of Heat Transfer, Vol. 87
1965.

97. T. SAITO
"Multi-Fluid Modeling of Two-Phase Flow
and Heat Transfer:
Application to Critical Heat Flux
Prediction for BWR Conditions"
Ph. D. THESIS, Nuclear Engineering
University of Wisconsin - Madison
1977

98. M. ISHII, K. MISHIMA
"Two-Fluid Model and Hydrodynamic
Constitutive Relations"
Nuclear Engineering and Design, 82
Dec. 1984

99. M. ISHII, K. MISHIMA
"Study of Two-Fluid Model and Interfacial Area"
ANL. NUREG/CR - 1873
Dec. 1980

100. M. ISHII, N. ZUBER
"Drag Coefficient and Relative Velocity
in Bubbly, Droplet or Particulate Flows"
AIChE Journal, Vol. 25, No. 5
Sept. 1979

101. M. ISHII, T. C. CHAWLA
"Local Drag Laws in Dispersed Two-Phase Flow"
ANL-79-105, NUREG/CR-1230
Dec. 1979

102. R. T. LAHEY Jr. et al
"The effect of Virtual Mass on the
Numerical Stability of Accelerating Two-Phase Flows"
Int. Journal of Multiphase Flow, Vol. 6
1980

103. H. LAMB
"Hydrodynamics"
Sixth Edition, pp. 123-124
Dover Publications
New York 1932

104. N. ZUBER
"On the Dispersed Two-Phase Flow in the Laminar Flow Regime"
Chemical Engineering Science, Vol. 19.
1964

105. H. LAMB
"Hydrodynamics"
Sixth Edition, pp. 124-125
Dover Publications
New York 1932

106. O. RATHMANN
The Added Mass Force Dependence on Concentration by Numerical Solution"
Risø Report NORHAV-D-80
May 1981

107. E. N. GANIĆ, W. M. ROHSENOW
"On the Mechanism of Liquid Drop Deposition in Two-Phase Flow"
ASME Meeting, New York City, Dec. 1976

108. A.J. CLARE, S.A. FAIRBAIN
Droplet Dynamic and Heat Transfer in Dispersed Two-Phase Flow, Int. Workshop on Fundamental Aspects of Post-Dryout Heat Transfer, Salt Lake City, 1984.

109. K.H. SUN, J.M. CONZALES
Calculations of Combined Radiation and Convection Heat Transfer in Ros Bundles under Emergency Cooling Conditions, ASME, 75-HT-64.

110. A.F. VARONE, W.M. ROHSENOW
Post-Dryout Heat Transfer Predictions, Int. Workshop on Fundamental Aspects of Post-Dryout Heat Transfer, Salt Lake City, 1984.

DK8600013

Nord
JUNE 1986

Heat Transfer Correlations in Nuclear Reactor Safety Calculations

Vol. II

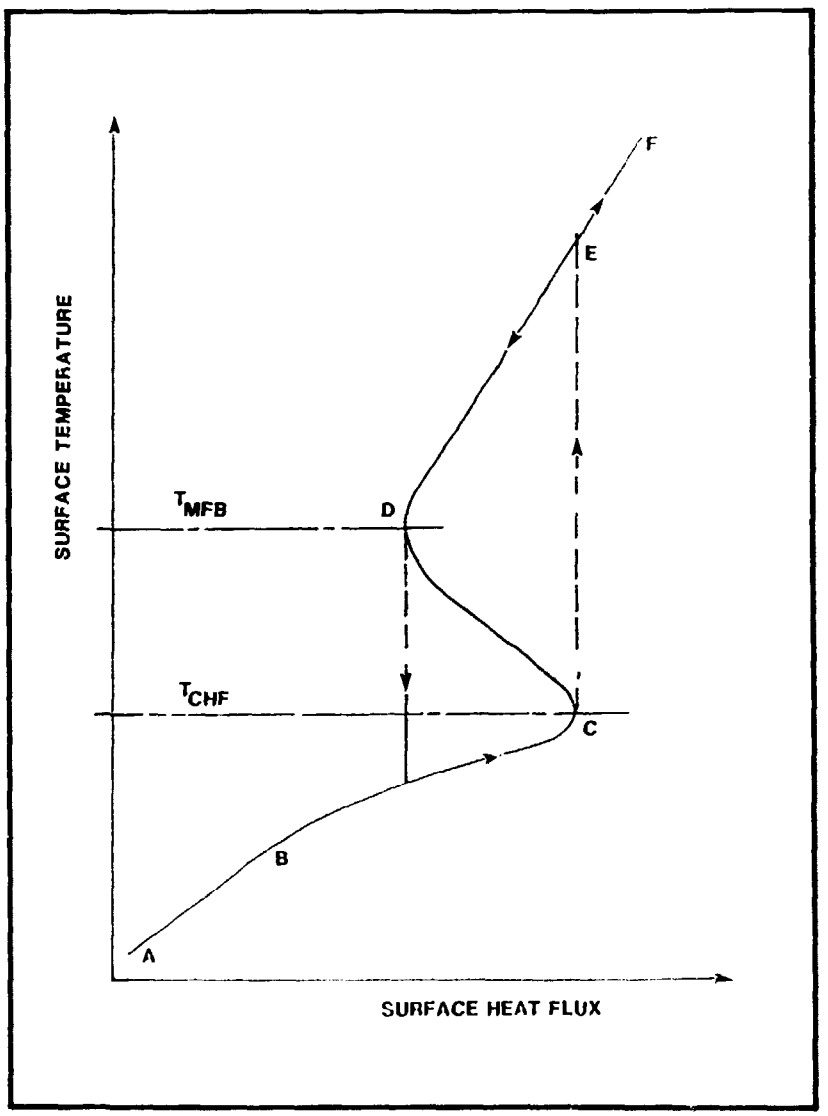

nka
Nordic
liaison committee for
atomic energy

nka

Nordisk kontaktorgan for atomenergispørgsmål | Nordiska kontaktorganet för atomenergifrågor | Pohjoismainen atomienergia-yhdyselin | Nordic liaison committee for atomic energy

RISØ-M-2504

(Vol. 2).

HEAT TRANSFER CORRELATIONS IN NUCLEAR REACTOR SAFETY CALCULATIONS SÄK-5

H. Abel-Larsen, Risø
A. Olsen, Risø
J. Miettinen, VTT
T. Siikonen, VTT
J. Rasmussen, IFE
A. Sjöberg, Studsvik
K. Becker, KTH

June 1985

Risø: Risø National Laboratory, Denmark
VTT: Technical Research Centre of Finland
IFE: Institute for Energy Technology, Norway
Studsvik: Studsvik Energiteknik AB, Sweden
KTH: Royal Institute of Technology, Stockholm, Sweden

LIST OF CONTENTS

VOLUME II : Page

FIGURES. Page

VOLUME I:

VOLUME II:

Page

Page

TABLES

APPENDIX A. PRESENT KNOWLEDGE

A1. Nucleate boiling and forced convective boiling

A literature search is reported in (7). Table A1.I taken from (18) contains four of the best known correlations for nucleate boiling and forced convective flow. Both experimental data and comparisons with different correlations are reported. The comcomparisons are of correlations with experimental data typical for steam generator conditions.

Correlations by Levy and Borishansky gave the best results with an RMS-error of 22-23%.

Two new correlations for bulk boiling and subcooled boiling are also presented in (18). They gave RMS-errors of 16 and 12%, respectively, for their own experimental data. The correlations are given in Table A1.II.

Stephan and Auracher (19) have presented new correlations for nucleate boiling and forced convective boiling heat transfer. The correlations are developed from a large set of data points (5000) using regression analysis. The correlations are given in Table A1.II.

It should be noted that these new correlations in Table A1.II can be written in the form:

$$h_{NcB} = F(B) \cdot q^{n^A}$$

with A ~ 0.65 - 0.7.

This is also the case for the correlations by Levy and Borishansky.

TABLE A1.I.

Authors	Correlations	RMS with CNEN data %
Thom	$T_w - T_{SAT} = 22.52 \cdot \left(\frac{q''}{10^6}\right)^{1/2} \cdot \exp(-0.0115 \cdot P)$ P in bar	59.6
Levy	$T_w - T_{SAT} = 0.9128 \cdot q''^{1/3} \cdot P^{-4/9}$ P in bar	22.4
Chen	$h_b = h_{mac} + h_{mic}$ $h_{mac} = h_f \cdot F$ $h_{mic} = 0.00122 \cdot \left(\frac{k_f^{0.49} \cdot C_{pf}^{0.45} \cdot \rho_f^{0.49}}{\sigma^{0.5} \cdot \mu_f^{0.29} \cdot H_{fg}^{0.24} \cdot \rho_g^{0.24}}\right) \cdot \left(\frac{H_{fg}}{T_{SAT}(v_g - v_f)}\right)^{0.75} \cdot \Delta T_{SAT} \cdot S$ $F = f\left(\frac{1}{X_{tt}}\right)$; $S = f(Re_{TP})$; $Re_{TP} = Re_f \cdot F^{1.25}$	35.0
Borishansky	$h_b = h_{pk} \cdot \left(1 + 7 \cdot 10^{-9} \cdot \left(\frac{w_m \cdot H_{fg} \cdot \rho_f}{q''}\right)^{3/2}\right)^{1/2}$ $w_m = \frac{G}{\rho_f} \cdot \left(1 + \frac{\rho_f - \rho_g}{\rho_g} \cdot X\right)$ $h_{pk} = h_k \cdot \left(1 + \left(\frac{h_\infty}{h_k}\right)^2\right)^{1/2}$ $h_k = 0.023 \cdot \frac{k_f}{D} \cdot \left(\frac{G \cdot D}{\mu_f}\right)^{0.8} \cdot Pr_f^{0.4}$ $h_\infty = 0.1379 \cdot (P^{0.14} + 1.88 \cdot 10^4 \cdot P^2) \cdot \left(\frac{q''}{10^4}\right)^{0.7}$ P in bar	22.9

TABLE A1.II.

Origin	New correlations for boiling heat transfer	RMS %
CNEN (bulk boiling)	$h_b = 150 \cdot \frac{k_\ell}{D} \left(\frac{q'' \cdot \sqrt{\frac{\sigma}{g \cdot (\rho_\ell - \rho_g)}}}{H_{fg} \cdot \mu_\ell} \right)^{n.65} \cdot \left(1 + 10^{-4} \cdot \frac{H_{fg} \cdot G}{q''} \right) \cdot \left(1 + \frac{1}{X_{tt}} \right)^{0.13} \cdot Pr_g$	16
CNEN (subcooled boiling)	$h_{sb} = \frac{q''}{\Delta T_{CNEN} + (\Delta T_{DB} - \Delta T_{CNEN}) \cdot \left(\frac{H_{SAT} - H(z)}{H_{SAT} - H_o} \right)^{0.5}}$ $\Delta T_{CNEN} = q''/h_b$ and $\Delta T_{DB} = q''/h_{DB}$ (DB: Dittus-Boelter)	12
Stephan & Auracher (nucleate boiling)	$h_{NcB} = \frac{k_\ell}{D} \cdot 0.246 \cdot 10^7 \cdot \left(\frac{\kappa_\ell^2}{H_{fg} \cdot D^2} \right)^{1.58} \cdot \left(\frac{q'' \cdot D}{k_\ell \cdot T_{SAT}} \right)^{0.673} \cdot \left(\frac{c_{p\,\ell} \cdot T_{SAT} \cdot D^2}{\kappa_\ell^2} \right)^{1.26} \cdot \left(\frac{\rho_\ell - \rho_g}{\rho_\ell} \right)^{5.22}$	11.3
Stephan & Auracher (forced convective boiling	$h = h_{NcB} \cdot 29 \cdot (Re_\ell)^{-0.3} \cdot (Fr_\ell)^{0.2}$ $Re_\ell = \frac{G \cdot (1-X) \cdot D}{\mu_\ell}$; $Fr_\ell = \frac{G^2 \cdot (1-X)^2}{\rho_\ell^2 \cdot g \cdot D}$	10
J. Rasmussen	$h_{NcB} = B1(P) \cdot (T_W - T_{SAT})$ $B1(P) = 2000 + 80 \cdot P - 1548 \cdot \exp(-0.175 \cdot P)$ $+ 37.5 \cdot (\exp(0.04815 \cdot P - 1)$; P in bar	

The correlations by Stephan and Auracher seem to perform quite well. They should, however, also be tested against the data base in (18). If this test comes out well, the correlations may be recommended for steam generator calculations.

Chen's correlation is considered as one of the best candidates for nuclear reactor core calculations. It should be remembered, however, that Chen's correlation is based mainly on low-pressure data with only a few data at higher pressures ($P < 70$ bar). A correlation that interpolates between Chen and Thom is suggested in (7) for pressures from 70 to 140 bar. This correlation is a simplification of Chen and is much simpler to use in a computer programme.

A2. Critical heat flux

A literature search is reported in (7). There are two classes of CHF-situations; DNB (Departure from Nucleate Boiling) in liquid continuous flow and DO (Dry Out) or DFCB (Departure from Forced Convective Boiling) in vapour continuous flow.

Most of the CHF-corelations are based on the concept of equilibrium flow with one vapour and one liquid component. The determination of CHF follows, using an appropriate correlation. One of four methods are used:

1. Heat flux versus local quality (q''_c/X).
   ("Local conditions" hypothesis).

   It is assumed that there is an unique relationship between CHF and l o c a l vapour quality. The method has a tendency to fail when applied to data with strong non-uniformity in axial heat flux.

2. The "Overall power" hypothesis.

   This method suggests that the total power that can be fed into a non-uniformly heated channel will be the same

as for a uniformly heated channel with the same geometry and inlet conditions. No prediction of the location of CHF is carried out. This method is found (20) to be slightly more accurate than the above-mentioned method for axially symmetrical non-uniform heat flux.

3. Critical quality versus boiling length (X_c/L_b). ("Equivalent length" hypothesis).

   The method suggests that the CHF is not a local phenomenon but an integral one i.e. it is dependent on the history of what has occurred upstream. The equivalent length is defined as:

$$L_e = \frac{1}{q''} \cdot \int_0^L q''(z)\, dz$$

   The method tends to perform better for non-uniform heat flux situations.

4. The F-factor method by Tong.

   Similar to the equivalent length method, this is an integral method. The F-factor is defined as:

$$F = \frac{(q''_c)_U}{(q''_c)_{NU}}$$

   where $(q''_c)_U$ is the value of the critical heat flux at any given local enthalpy for the uniform heat flux case and $(q''_c)_{NU}$ is the value of the critical heat flux at the same local enthalpy for the particular non-uniform heat flux case.

Another class of correlations or models are the so-called phenomenological models, which actually attempt to model the physical effects. Hewitt states in (21) that analytical models on CHF produce results which are comparable in accuracy to empirical correlations and which can be extrapolated over

much wider ranges. At present, these models are developed and tested for only simple geometries and annuli. More development is also needed in improving these models and obtaining better confidence in the description of the different processes such as deposition and entrainment. These models would require computer programmes where the different flow components are actually modelled.

Computer programmes like RELAP, TRAC and NORA model only one liquid component, and the application of any phenomenological model for CHF would need considerable programming effort. In a LOCA situation one therefore usually relies on empirical correlations based on the local conditions hypothesis. Leung (22) has made a comparison of such correlations with experimental observations from transient experiments.

Table A2.I reviews the correlations tested by Leung. The Westinghouse correlation (W-3), which is still used for design, was developed for low-quality CHF (DNB) at or above 7 MPa. At qualities > 0.5 and pressures below 12 MPa, the correlation yields negative CHF values. The W-3 correlation was not used by Leung due to this abnormal behaviour.

The correlations mentioned in Table A2.I are all listed in (7). The data base used by Leung consisted of more recent data on CHF in transient conditions.

Leung concluded that an appropriate steady-state CHF correlation was adequate to use for the prediction of CHF onset during a wide range of flow transients. The local conditions hypothesis was demonstrated to predict the trend of CHF data better than the equivalent-length hypothesis. In one test, the incapability to predict a CHF was a result of a discrepancy found in correlating the steady-state CHF data.

Further, it was recommended to use Griffith-Zuber in the following mass flux range:

$$-240 < G < 100 \text{ kg/m}^2\text{/s}.$$

TABLE A2.I. CHF correlations tested by Leung

Correlations	Geometry	Pressure MPa	Mass flux $kg/m^2/s$	Quality	Remarks
Bowring	Round tube	0.2-19	136-18600	all X	3792 points
Biasi	Round tube	0.3-14	100- 6000	~ 0-1.0	4500 points
CISE	Round tube	4.5-15	~ 100- 4000	~ 0-1.0	Freon data
B & W-2	Rod bundle	14 -16.6	1017- 5430	-0.03 to 0.20	Only DNB data
CONDIE MOD7	Rod bundle	3.0-17	70- 4700	-0.1 to 1.0	5163 points
GE	Rod bundle	6.9	< 680	0-0.84	Low flow data
Hsu-Beckner	Rod bundle	6-15	All	~ 0-1.0	Blowdown data
Griffith	Short annulus	All range	Low G	0-1.0	Counter current

Outside this mass flux range Biasi and CISE are said to be equally good possibilities.

Some work on steady-state CHF for steam generator conditions is described in (23). Their own experimental data in addition to data from CISE (24) and Becker (25) were compared with some CHF correlations. The data were from vapour continuous region, i.e. in the deposition-controlled region, and the transition region between liquid continuous (DNB-region) and the vapour continuous region (DO-region). The results of the comparison are summarized in Table A2.II.

TABLE A2.II. Testing of CHF correlations

Correlation	Dep. contr. region 137 data points		Dep. contr. + trans. region 290 data points	
	RMS %	Av. error %	RMS %	Av. error %
Biasi	12.6	8.7	18.7	15.2
Becker	11.9	8.2	17.9	14.3
Bowring	23.7	19.6	17.9	13.3
CISE	9.7	8.6	7.9	6.5
Macbeth-Th.	8.7	6.9	10.2	7.9
ROKO	7.8	6.2	17.5	13.8
CNEN	4.5	3.9	4.6	3.6

Besides their own correlation developed to fit these data, the CISE correlation seems to give the best performance. These results may therefore be seen as a support for the general applicability of the CISE correlation. It is remarked that according to Becker (private communication), his correlation is here in part used outside the range of applicability.

A3. Transition boiling

The heat transfer in the transition boiling region (C-D in Fig. 1) is described in (26). A literature search is reported in (27).

Groeneveld gives in (28) an excellent review of post-CHF heat transfer up to ~ 1974. Table A3.I shows three newer transition boiling heat transfer correlations from his compilation (nos. 1 to 3).

A few correlations have been published since then. In Table A3.I two correlations are shown. Number 4 is the correlation by Chen et al. (29). The correlation is together with no. 1 an attempt to make a phenomenological correlation. The last correlation in the table (no. 5) is an example of a purely empirical one. It is proposed by Bjornard and Griffith and used in TRAC.

Iloeje et al. (30) proposed a 3-step model as indicated in the table and illustrated in Fig. A3.1. Iloeje has only one step covering the contact period, B, C and D in Fig. A3.1. Chen uses also a 3-step model with all 3 steps in the touching period: waiting period, bubble nucleation- and growth-period and a liquid film evaporation period. Convection to bulk vapour is calculated using the Reynold's momentum analogy modified by Colburn.

The fraction of wall hit and wetted by droplets is determined empirically from experimental data taken from 8 different references (4167 points) ranging in pressures from 4 to 195 bar, mass fluxes from 15 to 3000 kg/m^2/sec, heat fluxes from 3 to 165 watt/cm^2 and equilibrium qualities from 0.5 to 1.7.

The fraction is determined using the relation:

$$FL = \frac{q''_T - q''_{vc}}{q''_{Lc} - q''_{vc}}$$

where q''_T is the total heat flux, q''_{vc} the convective heat flux calculated, as mentioned above, and q''_{Lc} the liquid contact heat flux.

The liquid contact area fraction, or the decay factor as designated by Tong and Young (see below), FL could be correlated as:

TABLE A3.I.

Correlations	Range of applicability
$q''=C\left[\frac{R\cdot\sigma\cdot C_{p\ell}\cdot\rho_\ell\cdot T_{SAT}^2}{P_\ell\cdot H_{fg}}\right]\cdot\left[\frac{1-XE}{XE}\right]\cdot$ $\frac{U_g\sqrt{f}}{\delta}\cdot\exp\left[-\frac{\Delta T_{SAT}}{\Delta T_{max}}\right]+$	Heat transfer to a single drop touching the wall
$\lambda\cdot(1-\alpha)\cdot\left[1-\exp\left(-\frac{\Delta T_{SAT}}{\Delta T_{max}}\right)\right]\cdot\frac{4\cdot k_{vg}}{\delta}\cdot$ $\left[\left(1+\frac{2\cdot\lambda_{mw}}{\delta}\right)\cdot\ln\left(1+\frac{\delta}{2\cdot\lambda_{mw}}\right)-1\right]\cdot\Delta T_{SAT}$	Heat transfer to drops in thermal boundary layer, but not touching the wall
$+0.023\cdot\frac{k_g}{D}\left[\frac{G\cdot D}{\mu_g}(XE+(1-XE)\frac{\rho_g}{\rho_\ell}\right]^{0.8}\cdot$ $\left(\frac{\mu C_p}{k}\right)_g^{0.4}\cdot\Delta T_{SAT}$;	Heat transfer to bulk vapour
$\lambda_{mw}=\varepsilon\cdot\left[\frac{\Delta T_{SAT}}{\Delta T_{max}}\Big/\left[1-\exp\left(\frac{\Delta T_{SAT}}{\Delta T_{max}}\right)\cdot\left(1+\frac{\Delta T_{SAT}}{\Delta T_{max}}\right)\right]\right]^{1/3}$	P: 6.89 MPa G: 410-1700 $kg/m^2\cdot s$ X: 0.1-0.7 Geometry: tube
ΔT_{max} given by $\frac{k_g\cdot\Delta T_{max}}{G\cdot D\cdot H_{fg}}=3.27\cdot10^{-5}\ (2.93+$ $4.44\cdot XE+2.923\cdot10^{-6}\cdot(G\cdot XE)^2-$ $1.51\cdot10^{-6}\cdot(G\cdot XE)^3)/\left(\frac{G\cdot D}{\mu_g}\right)^{0.477}$ C: Correlation constant λ: Geometric parameter	
Iloeje et al. (30) 1.	

p.t.o.

TABLE A3.I. (cont.)

Correlations	Range of applicability
$q''_{TB}=q''_{NCB}\cdot FLT+q''_{VCT}\cdot(1-FLT)$ q''_{NCB} e.g. Chen $q''_{VCT}=\frac{k_v}{D}\cdot(Re)^{0.8}\cdot(Pr)^{0.4}\cdot 0.023\cdot$ (T_w-T_v) ; $Re=\frac{V_m\cdot\rho_v\cdot D}{\mu_v}$; $v_m=\frac{G}{\rho_\ell}\cdot\frac{S\cdot(1-XA)+XA\cdot\rho_\ell/\rho_g}{S\cdot(1-XA)+XA}$; $FLT=\exp\left[-3.937\cdot10^{-2}\cdot\frac{XE^{0.667}}{dXE/dL}\cdot\right.$ $\left.(1.8\cdot10^{-2}\cdot(T_w-T_{SAT}))^{(1+2.88\cdot10^{-3}\cdot(T_w-T_{SAT}))}\right]$ Tong & Young (31) 2.	P: 6.89 MPa G: 410-5160 kg/m^2·s XE: 0.2-1.45 Geometry: tube P: 3.45-9.65 MPa G: 680-4210 kg/m^2·s XE: 0.15-1.10 Geometry: annulus & rod bundle $5.6 < \Delta T_{SAT} < 560$ ρ_g: Density at saturation ρ_v: Density at superheating
$q''_{TB}=(h_{FB}+h_C)\cdot(T_w-T_{SAT})$; $h_{FB}=0.62\cdot\left[\frac{k_v^3\cdot g\cdot\rho_v(\rho_\ell-\rho_v)\cdot H'_{fg}\cdot LaP}{\mu_v\cdot\Delta T_{SAT}}\right]^{1/4}$; $LaP=\frac{1}{2\pi}\cdot\sqrt{\frac{g\cdot(\rho_\ell-\rho_v)}{\sigma}}$; $H'_{fg}=H_{fg}+0.55\cdot c_{p,v}\cdot\Delta T_{SAT}$ p.t.o.	P: 0.103-0.620 MPa G: 50-250 kg/m^2·s Geometry: 100 rod bundle (FLECHT)

TABLE A3.I. (cont.)

Correlations	Range of applicability
$h_c = A \cdot \exp(-B \cdot (T_w - T_{SAT}))$ $A = 59.68 \cdot (P)^{0.558}$ $B = 1.459 \cdot 10^{-3} \cdot (P)^{0.1733}$ Hsu (32) 3.	
$q''_{TB} = q''_{LC} \cdot PL + q''_{VC} \cdot (1-PL)$ $q''_{VC} = h_{VC} \cdot (T_w - T_v)$ $h_{VC} = f/2 \cdot G \cdot XA \cdot c_{pv} \cdot Pr^{-2/3}$ $1/\sqrt{f} = 3.48 - 4.LOG\left(\frac{\varepsilon}{D} + \frac{9.3^r}{(Re \cdot \sqrt{f})}\right)$ $Re = \frac{D \cdot \rho_v \cdot j}{\mu_v}$ $j = \frac{G \cdot XA}{\rho_v} + \frac{G \cdot (1-XA)}{\rho_\ell}$ $\frac{XA}{XE} = \frac{H_{fg}}{H_{fg} + c_{pv} \cdot (T_w - T_{SAT}) \cdot \left(\frac{TD}{1+TD}\right)}$ and $\frac{XA}{XE} = 1 - B(P) \cdot TD$ $T_D = \frac{T_v - T_{SAT}}{T_w - T_v}$ p.t.o.	P: 4-195 bar G: 16-3000 kg/m^2·s XE: 0.5-1.7 q": 3-;65 W,'cm^2 (4167 data points 8 refs.)

TABLE A3.I. (cont.)

Correlations	Range of applicability
$B(P) = \dfrac{0.26}{1.15-(P/P_c)^{0.65}}$ $q''_{LC} = \dfrac{q''_a+q''_b+q''_c}{t_1+t_2+t_3}$ Waiting period $q''_a = \dfrac{R\cdot\sigma\cdot\rho_\ell\cdot c_{p\ell}\cdot T^2_{SAT}}{0.213\cdot P\cdot H_{fg}}$ $t_1 = \dfrac{R\cdot\sigma\cdot T^2_{SAT}}{0.24\cdot P\cdot H_{fg}\cdot\sqrt{a_\ell}}\cdot\left(\dfrac{R_T+1}{R_T}\cdot\dfrac{1}{T_w-T_{SAT}}\right)^2$ $R_T = \left(\dfrac{k_w\cdot\rho_w\cdot c_{pw}}{k_\ell\cdot\rho_\ell\cdot c_{p\ell}}\right)^{0.5}$ Nucleation period $q''_b = 0$ $R^+ = 2/3\cdot\left[(t^+{+}1)^{2/3}-(t^+)^{2/3}-1\right]$ $R^+ = \dfrac{M1}{(M2)^2}\cdot R(t)$; R(t) input $t^+ = \dfrac{(M1)^2}{(M2)^2}\cdot t_2$ $M2 = \left(\dfrac{12\cdot a_\ell}{\pi}\right)^{0.5}\cdot\left(\dfrac{\rho_\ell}{\rho_v}\right)\cdot\left(\dfrac{c_{pf}}{H_{fg}}\right)\cdot(T_w-T_{SAT})$ $M1 = \left[2/3\cdot\left(\dfrac{\rho_v}{\rho_\ell}\right)\cdot\dfrac{T_w-T_{SAT}}{T_{SAT}}\cdot H_{fg}\right]^{0.5}$ p.t.o.	

TABLE A3.I. (cont.)

Correlations	Range of applicability
<u>Evaporation period</u> $q''_C = \frac{8 \cdot \sigma \cdot T_{SAT}}{T_w - T_{SAT}} \cdot \frac{\rho_l}{\rho_g}$ $t_3 = \frac{32 \cdot \rho_l \cdot \sigma^2}{k_l \cdot \rho g \cdot H_{fg}} \cdot \frac{T_{SAT}^2}{(T_w - T_{SAT})^3}$ $FL = \exp(-\lambda \cdot (T_w - T_{SAT})^{0.5})$ $C2 = \frac{5.0 \cdot 10^{-3}}{(1-\alpha)^{40} + 9.0 \cdot 10^{-3} \cdot \alpha}$ $C1 = 24 \cdot C2$ $C3 = 0.2 \cdot C2$ $C4 = 7.3733 \cdot 10^{-4}$ $(\lambda 1) = (C1 - C2 \cdot C4 \cdot G) \cdot 1.341$ $(\lambda 2) = C3 \cdot C4 \cdot G \cdot 1.341$ $\lambda 1$ or $\lambda 2$, whichever is greater Chen et al. (29) 4.	
$q''_{TB} = q''_{CHF} \cdot FLB + q''_{MFB} \cdot (1 - FLB)$ $FLB = \left(\frac{T_w - T_{MFB}}{T_{CHF} - T_{MFB}} \right)^2$ $T_{MFB} = T_{MS} + \frac{T_{MS} - T_{SAT}}{R_T}$ $T_{MS} = T_K \cdot \left(1 - 0.095 \cdot \left(1 - \frac{T_{SAT}}{T_K} \right)^8 \right)$ Bjornard & Griffith (33) 5.	

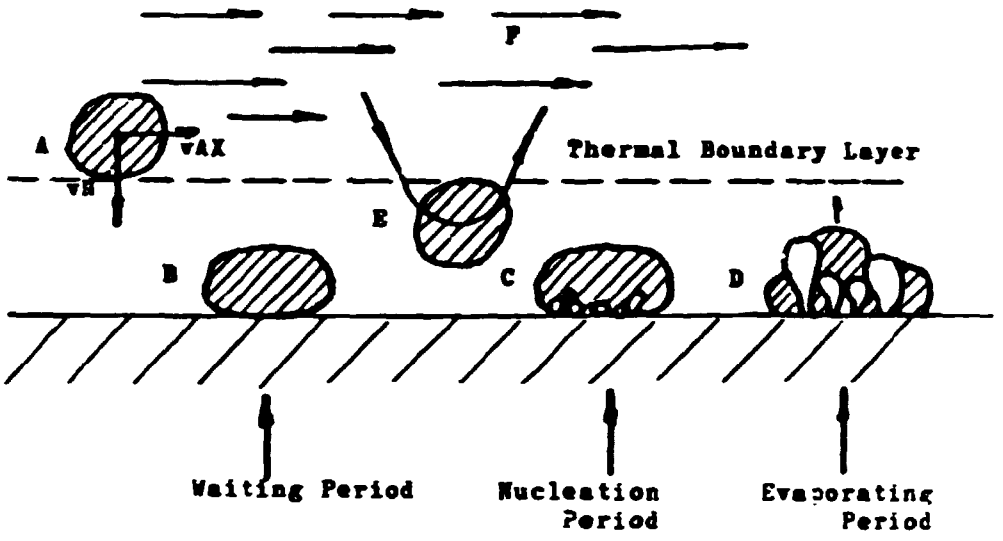

A. Liquid drop entering thermal boundary layer with velocity [v_N] normal to wall.
B. Liquid drop of higher kinetic energy based on [v_N] arriving on wall and beginning to absorb heat from wall via conduction.
C. Nucleation and bubble growth in liquid drop on wall.
D. End of bubble growth period. Part of liquid drop is ejected into the main stream by escaping vapour bubbles, part is left on wall to evaporate.
E. Liquid drop of lower kinetic energy in thermal boundary layer and being reversed into the main flow without touching the wall.
F. Bulk vapour flow.

FIGURE A3.1.

$$FL = \exp(-\lambda \cdot (T_w - T_{SAT})^n)$$

λ is a function of void and mass flux as shown in Table A3.I. The exponent n was determined to be 0.5.

The Chen correlation does take the thermodynamic nonequilibrium into account, i.e. part of the heat goes to superheat the vapour instead of evaporating the droplets and the actual vapour quality, XA, is less than the equilibrium quality, XE.

The Tong and Young correlation is also discussed in (26). It is a two-term correlation as the Chen correlation with a boiling term and a convective term. Tong and Young use the nucleate boiling heat flux at CHF as the boiling term and a modified single-phase heat tansfer correlation (Dittus-Boelter) as the convective term.

The decay factor has been empirically determined from some high-pressure experimental data (69 bar). It shows also an exponential decay and depends on the wall temperature and the quality.

The Chen- and Tong & Young-correlations are based on experimental data in vapour continuous flow and may be used only under such flow conditions.

The Hsu correlation, no. 3 in Table A3.I, is based on FLECHT data (subcooled data), and can be used in liquid continuous flow (inverse annular flow).

As a consequence of the scarcity of reliable and consistent data on transition boiling heat transfer,the simple interpolation between the CHF and the minimum film boiling heat flux is still used. The Bjornard and Griffith corelation, no. 5 in Table A3.I, is an example.

Kirchner and Griffith (34) have proposed another way of interpolating the boiling curve in the transition region:

$$h_{TB} = \frac{q''_{TB}}{\Delta T} = \frac{q''_{CHF}}{\Delta T} \cdot \left(\frac{T_w}{T_{CHF}} \right)^{XPNT}$$

where

$$XPNT = \frac{\ln(q''_{CHF}) - \ln(q''_{MFB})}{\ln(T_{CHF}) - \ln(T_{MFB})}$$

The correlation has been tested against FIECHT data with reasonable agreement.

The Bjornard & Griffith-, the Chen- and the Tong & Young-correlations are compared with experimental, temperature-controlled data. The results of this comparison are discussed in Appendix B4.2.

The following phenomenological decomposition of the heat transfer not only in the transition boiling region, but in all post-CHF regions, where droplets may be of importance in the total transport of energy from a heated surface to a two-phase mixture, is generally accepted:

1. Heat transfer from the surface to liquid droplets, which impinge on the wall ("wet" collisions)

2. Heat transfer from the surface to liquid droplets, which enter the thermal boundary layer without wetting the surface ("dry" collisions)

3. Convective heat transfer from the surface to the vapour

4. Convective heat transfer from the vapour to the dispersed droplets in the vapour (interfacial heat transfer)

5. Heat transfer by thermal radiation from the surface to the liquid

6. Heat transfer by thermal radiation from the surface to the vapour.

A4. Rewetting

Introduction and recommendation

In the middle of 1970 the experimental and modelling work around the rewetting mechanism by bottom reflooding and by top spray cooling was comprehensive, but very dispersed without any well-defined goal. The studies produced several mathematical models and many empirical proposals for the fitting factors in the models. In bottom reflooding and falling film cooling of the overheated fuel rod the length of the transition boiling region is short compared with other flow regions. This transition boiling region is in fact normally considered as a rewetting front. Due to the sharp temperature gradient over the front the heat from the hot, unwetted part is moved to the cold, wetted part by an axial conduction in the fuel rod cladding.

Because most of the computer programmes don't divide the heat structure into mesh intervals on the order of few millimeters, the usual heat structure models are unable to calculate properly the axial conduction effect, although the two dimensional heat conduction was solved for the rod structure. That is the reason why there are good arguments for a special handling of the rewetting mechanism in emergency core cooling programmes.

RELAP-4/MOD-6 includes a model describing the rewetting mechanism with the moving-mesh techniques. The axial conduction is not modelled in the programme and the axial conduction effect was replaced by an increment in the transition boiling coefficient. The result, e.g. from the CSNI standard problem 7 for reflooding indicated that no universally good user dials may be proposed for RELAP-4/Mod-6 users, when the transition boiling approach has been used.

RELAP5/Mod2 includes a rewetting model that uses the two-dimensional heat conduction equation for the core heat slabs. In the rewetting front the programme doubles or halves the structure nodes, depending on the temperature gradient in the rewetting front. The recommendation for fixed-core heat slab

dimensions is on the order of 0.10 m. For the fine-mesh division a minimum mesh length of 0.001 m is recommended. According to earlier calculations as well as the numerical study with the PHOENICS programme, numerical modelling of the two-dimensional heat conduction equations for the rewetting is close to the analytical solution if the mesh length in the front is less than 0.001 m. Thus in the rewetting calculation the recommended minimum 0.001 m may be seen as the maximum. There has been no known experience with the RELAP5/MOD2 rewetting model to date. It may may be expected that the use of a very fine mesh division increases the computation time.

The German programme for emergency core cooling (FLUT), having six field equations has been developed in the last 7 years and results obtained for the reflooding process show a good agreement with experimental results. The programme applies the old techniques where the axial conduction is modelled with a mathematical correlation and usually with two fitting factors.

Work reported in (35) showed that the experimental data published in the 1970's and expressed as correlations with fitting factors gave a large scatter between different proposals for the fitting factors in the correlations. The correlations are asymptotic solutions of the original differential equations. The advantage with this kind of correlations is that in the temperature solution only one halving procedure is needed for the axial heat structure around the rewetting front and thus no extra computing time is needed for the fine mesh.

Due to these experiences two possibilities may by seen with respect to the rewetting modelling. The classical method describing the rewetting mechanism as a mathematical formula and as fitting factors in it may be recommended as one possibility. The method may be recommended especially when large computational times for the fine mesh structure have to be avoided.

The other possibility is the method using the fine-mesh techniques, i.e. the coarse mesh interval around the rewetting front is divided into a fine mesh ranging from 0.0002 to 0.001 m.

The method may be recommended if the computing time is available. If meshes are used that are too coarse for the rewetting front, the rewetting speed resulting from the calculation deviates totally from the exact solution. Thus the method is recommended only if a sufficiently fine mesh is possible to use. In many applications the exact modelling of temperatures close to the rewetting front is not as interesting as the maximum wall temperatures.

Due to these experiences it may be recommended that the rewetting mechanism should be described by using the classical method: a correlation with two fitting parameters. This classical approach is considered more closely below.

Mathematical rewetting models

For reasons of simplicity the fuel rod cladding is considered as a slab. The unstationary heat conduction may be written as

$$\rho \cdot c \cdot \frac{\partial T}{\partial t} = k \left(\frac{\partial^2 T}{\partial y^2} + \frac{\partial^2 T}{\partial z^2} \right) \qquad (1$$

In the moving mesh method this equation is solved numerically. For the space derivatives the space-centred differencing may be used. For the time derivative only the backward differencing is possible, i.e. the implicit solution and thus the solution needs a matrix inversion technique. The solution of the two-dimensional, time-dependent heat conduction equation is included into RELAP5/MOD2 and TRAC and the equation is solved for core fuel rods. Around the rewetting front the heat structure is halved in the axial and radial directions if the temperature difference between two adjacent mesh cells becomes too high.

In the formulation of the mathematical correlation for the rewetting front the time-dependent heat conduction equation (1) is transformed by assuming moving coordinates that move with the velocity of the rewetting front. The rewetting velocity is assumed to be constant. The transformation applies the relationship:

$$\frac{\partial T}{\partial t} = \frac{\partial T}{\partial z} \cdot \frac{\partial z}{\partial t} = u \cdot \frac{\partial T}{\partial z} \qquad (2$$

Further, via relationships:

$$\theta = \frac{T - T_{SAT}}{T_O - T_{SAT}}, \qquad T_O = \text{quenching temperature} \qquad (3$$

$$\eta = z/\delta , \qquad \delta = \text{wall thickness} \qquad (4$$

$$\zeta = y/\delta \qquad (5$$

$$Bi = \frac{h \cdot \delta}{k_w} \qquad h = \text{heat transfer coefficient} \qquad (6$$

$$Pe = \frac{\delta \cdot \rho w \cdot c \cdot u}{k_w} \qquad (7$$

The nondimensional form of the equation may be written:

$$\theta_{\eta\eta} + \theta_{\zeta\zeta} + Pe \cdot \theta_{\eta} = 0 \qquad (8$$

The boundary conditions are:

$$\theta = 0 \quad \text{at} \quad \eta = -\infty , \quad \theta = \theta_w \text{ at } \eta = +\infty \qquad (9$$

$$\theta_{\zeta} = -0 \quad \text{at} \quad \zeta = 0 , \quad \theta_{\zeta} = -Bi \cdot \theta \quad \text{at} \quad \zeta = 1 \qquad (10$$

Equation (8 cannot be solved analytically only the asymptotes may be calculated. If the wall is assumed thin and the rewetting velocity low, the radial derivative $\theta_{\zeta\zeta}$ may be dropped. Further, by assuming $\theta_w >> 1$, $\theta_w = \theta(T_w)$, the solution for the equation is a widely used formula of Yamanouchi:

$$Pe = Bi^{0.5}/(\theta_w - 1) \qquad (11$$

The two-dimensional approximation may be formulated as the asymptotic solution for the original equation, by assuming a large rewetting velocity (Pe large) and Pe > Bi. The asymptote of the pure two-dimensional formulation is not very practical because it strongly overpredicts the rewetting velocity at low rewetting velocities. The use of the Yamanouchi model for the rapid rewetting regime underpredicts the velocity, but this can be accepted more easily than the overprediction (conservative).

Dua and Tien have made a useful proposal, however, which fits the fast rewetting and slow rewetting region as well. The calculations with the correlation have shown a good fit to the exact solution. The work is based on the original work of J.G.M. Andersen of Risø, and the following correlation is recommended as a correlation for the rewetting front propagation:

$$Pe = (Bi^* \cdot (1 + 0.40 \cdot Bi^*))^{0.5} \qquad (12$$

where

$$Bi^* = \frac{Bi}{\theta_w \cdot (\theta_w - 1)} \qquad (13$$

Heat transfer correlations for the moving mesh methods

Since reflooding cases have not been included in the test matrix in the SÄK-5 project and because RELAP5/MOD2 was unavailable before the end of 1984, no recommedations may be presented based on computer runs for the heat transfer correlations around the rewetting front. The heat transfer logic of RELAP5/MOD2 is listed, however:

- Nucleate boiling: Jens & Lottes subcooled boiling or Chen correlation.
- Critical heat flux: Zuber correlation multiplied by the correction proposed by Griffith $(1-\alpha)$ and multiplied by the large flow correction $(G/67.82)^{0.33}$, if the mass flux $G > 67.82$ kg/m^2·s.
- Transition boiling: Weissman correlation.

Fitting parameters for the correlation

The fitting parameters in the correlation are the heat transfer coefficient h in the Biot number Bi and the nondimensional rewetting temperature θ_o.

Previous work (35) showed that the proposal based on the experimental work of the 1970's is not directly useful due to large scatter. The German FLUT programme, using the rewetting velocity correlation, and RELAP5/MOD2 have similar proposals for the critical heat flux. The proposed critical heat flux may therefore be used as a basis of the heat transfer correlation. It is recommended that the heat transfer coefficient in Biot's number be determined from the Zuber critical heat flux correlation multiplied by the Griffith's correction factor $(1-\alpha)$. The Weisman correction $(G/67.82)^{0.33}$ may be used as well. The heat transfer coefficient is calculated by dividing the critical heat flux by the temperature difference $\Delta T_{CHF}=T_{w,CHF}-T_{SAT}$, which results from the heat transfer calculation in the nucleate boiling region, where e.g. Chen's correlation is used. The heat transfer coefficient h in Biot's number is then:

$$h = q_{CHF,Zuber} \cdot (1-\alpha)/(\Delta T_{SAT,\ Chen\ NB}) \qquad (14$$

(For $G>67.82$ $h = h \cdot (67.82)^{0.33}$ may be used)

The minimum film boiling temperature may be defined as the rewetting temperature T_o. One possibility is therefore to use a correlation for this. Another possibility is mentioned, viz. the choice in FLUT:

$$T_o = T_{SAT} + 160 + 6 \cdot \Delta T_{sub} \qquad (15$$

The third term on the right side takes the subcooling effect into consideration.

The recommended values should be considered as a first guess. The functioning of the rewetting model should be tested together with the whole heat transfer package.

A5. Film Boiling

In order to determine the wall fluid heat transfer when the CHF has been exceeded, it is important to identify the flow regions appearing at different conditions. The different types of post-CHF flow regions are described in Chapter 1.3.

The post-CHF flow regions are generally categorized according to the distribution of the vapour and liquid phases, vapour continuous or liquid continuous (see Fig. 2). The distribution is strongly dependent on the prevailing pre-CHF flow regions and the type of CHF that has occurred. At low quality-CHF the bubbly pre-CHF region will experience a transition to inverted annular flow and further downstream a new transition to inverted slug and finally dispersed droplet flow (Fig. A5.1). At moderate quality CHF the slug or churn-turbulent pre-CHF region will undergo a transition to inverted slug flow with a subsequent transition to dispersed droplet flow. At high quality-CHF the annular or annular mist pre-CHF region will change to dispersed droplet flow (Fig. A5.1).

The transition criteria may be evaluated from (10):
Liquid continuous (Inverted annular flow), when

$$\alpha < \alpha_{tran} - 0.1$$

Transition flow (churn/slug flow), when

$$\alpha_{tran} - 0.1 < \alpha < \alpha_{tran}$$

Vapour continuous (dispersed flow), when

$$\alpha > \alpha_{tran}$$

where

$$\alpha_{tran} = \left(1 + \frac{4}{(\rho_\ell/\rho_g)}\right) \cdot \frac{1}{C_o} - \frac{4}{(\rho_\ell/\rho_g)}$$

and

$$C_o = C_\infty - (C_\infty - 1) \cdot (\rho_g/\rho_\ell)^{0.5}$$

$$C_\infty = 1.393 - 0.015 \cdot \ln(Re)$$

$$Re = \frac{\rho_\ell \cdot j \cdot D}{\mu_\ell}$$

The dispersed flow film boiling region has been subjected to quite intense research efforts, especially in recent years.

Inverted Annular Film Boiling

Figure A5.2 shows three possible types of inverted annular flow. The continuous liquid core is separated from the wall by a low viscosity vapour film which can accomodate steep velocity gradients. The velocity in the liquid core is usually fairly uniform. At low velocities the vapour film is laminar with a rather smooth vapour - liquid interface (Fig. A5.2a). If the velocity is increased the vapour film becomes turbulent and the interface will be wavy and unstable (Fig. A5.2b). If the velocity is further increased liquid droplets will be torn away from the wavy interface thus giving rise to entrainment in the vapour film (Fig. A5.2c).

As long as the wall temperature is greater than the minimum film boiling temperature the heat is transferred from the wall to the vapour film and subsequently from the vapour to the vapour-liquid interface. If the liquid core is subcooled a significant fraction of the heat flux will be used for heating the liquid; if the liquid is saturated the heat transferred from the interface will be used for evaporation thus increasing the vapour velocity. The increased velocity differential across the interface will lead to an increased entrainment in the vapour film and also to a higher turbulence level in the vapour annulus. This will increase the wall-vapour and the vapour-liquid core heat

transfer which in turn will lower the wall temperature. If the wall temperature drops below the minimum film boiling temperature rewetting of the wall may occur.

Different types of correlations have been developed for calculating the heat transfer coefficient in the inverted annular flow region (see (12)). The correlations can be divided into the following categories:

* Correlations applicable to pool boiling conditions and heat transfer at low mass fluxes. A well-known example of these is the Bromley correlation. Most of the correlations of this type have the form

$$h = a \cdot \left[\frac{k_v^3 \cdot \rho_v \cdot (\rho_l - \rho_v) H'_{fg} g}{\mu_v \cdot \Delta T_{SAT}}\right]^{1/4} f(V,\lambda)$$

The latent heat H'_{fg} is usually modified to include the vapour superheat while the velocity effect is included through the function $f(V,\lambda)$ where λ is equal either to the hydraulic diameter, the critical wavelength, or the most unstable wavelength.

* Correlations of the modified McAdams type. These correlations basically have the form

$$Nu = a \cdot Re^b \cdot Pr^c \cdot P$$

where P usually is a function of quality or vapour film temperature.

* Phenomenological correlations based on the different mechanisms governing this type of heat transfer.

The literature search reported in (12) resulted in a recommedation to use a modified Bromley correlation when evaluating the heat transfer for the inverted annular flow. This correlation can be written as

$$q'' = h \cdot (T_W - T_{SAT})$$

$$h = 0.62 \cdot \left[\frac{k_v^3 \cdot \rho_v \cdot (\rho_\ell - \rho_v) H'_{fg} \cdot g}{\lambda_c \cdot \mu_v \cdot \Delta T_{SAT}}\right]^{1/4}$$

where

$$\lambda_c = 2\pi \cdot \left[\frac{\sigma}{g(\rho_\ell - \rho_v)}\right]^{1/2}$$

λ_c is the critical wavelength of Taylor instability. This correlation seems to fit the data reasonably well within the parameter range

Pressure	0.1 - 0.7 MPa
Wall Heat Flux	30 - 130 kW/m^2
Subcooling	< 78 K
Velocity	< 0.3 m/s
Void	< 0.4

An interesting study of the low flow film boiling heat transfer coeffiecient of Bromley was carried out by GE, USA (36,37). In a recent study (38) some deficiencies of the modified Bromley models were pointed out. Specifically mentioned were the lack of influence of the distance from the CHF location and the exclusion of flowrate and subcooling effects. In that context a new model was also developed, based on the Bromley type of analysis but including the above mentioned effects. The analysis terminated in a differential equation that was integrated numerically with adequate boundary conditions. The result was compared to some new data from a single tube reflooding experiment and the comparison was quite satisfactory (Fig. A5.3). The result using the modified Bromley model was much less successful, as shown in Fig. A5.4. However one major drawback with this new model is the difficulty of implementing it in the numerical scheme of an already existing computer code like RELAP5 and TRAC due to the differential form of the model.

Breakdown of Inverted Annular Flow

The breakdown of the liquid core into slugs and further down-

stream to droplets has also been related by some authors to a critical Weber number based on the diameter of the liquid core (approximately equal to the channel hydraulic diameter) and the relative velocity between the phases at this point:

$$We_{tr} = \frac{\rho_g \cdot (v_g - v_l)^2 \cdot D}{\sigma}$$

According to (12) a We-number of approximately 10 seems to fairly well correlate the data obtained in reflooding experiments. However in (38) We ~ 20 is obtained. This We-number was based on the vapour velocity only, but as the liquid velocity was rather small in that study the result would be only slighty lower if the relative velocity definition was used. Thus when a We-number of 10 to 20 is exceeded the liquid core can be assumed to break down.

Dispersed Droplet Film Boiling Region

In the dispersed droplet flow region the liquid phase exists as droplets of different sizes carried along in the vapour flow. Several investigations have shown that the vapour phase in general is superheated (12) with respect to the local saturation temperature while the liquid phase normally is found to be close to saturated conditions. These nonequilibrium effects have been found to be of major importance when describing the pertinent heat transfer mechanisms and the development of this region.

Due to the difficulty of measuring the vapour superheat when liquid droplets are present, the exact mechanisms for the heat transfer are poorly understood despite the intense research efforts made during the last years. In most of the experiments only the wall temperatures were measured and the nonequilibrium vapour conditions had to be inferred from these temperatures by use of a single-phase convective heat transfer correlation and the assumption that the wall-to-droplet heat transfer was negligible.

However, a leap forward was taken when a technique was developed to measure the vapour temperature by means of a specially designed aspiration thermocouple probe (39,40). In those studies the vapour superheat was measured at only one location downstream of the CHF-front though, so the axial behaviour of the nonequilibrium effect was unknown. Quite recently two experimental test series were conducted (41,42) in which the axial variation of the nonequilibrium conditions downstream of the CHF-front was also measured. From the results of these experiments it was evident that the vapour generation was quite high near the CHF location and decreased further downstream. The increased vapour generation near the CHF location was hypothesized to be caused by some sputtering effects when the wall liquid film was violently driven off the wall at the CHF location (17).

This indicates that the vapour generation has to be separated into a near field region where the vapour generation rate is relatively high, and a far-field region with a lower vapour generation rate. Thus, different mechanisms can be assumed to be dominant in each region.

Prediction Methods

Basically, two main groups of models can be identified when analyzing the approaches utilized for calculating the heat transfer in the dispersed droplet film boiling region (12,43): equilibrium correlations and nonequilibrium models.

Equilibrium Correlations

This approach is based on two assumptions:

* Thermodynamic equilibrium exists between the two phases

* Heat transfer at the heated walls occur primarily by turbulent vapour convection.

This can be expressed mathematically as

$$q'' = h_c \cdot (T_w - T_{SAT})$$

The heat transfer coefficient h_c is calculated from an equilibrium correlation, for instance, Groeneveld and Dougall-Rohsenow correlations (12). Also the Condie-Bengston correlation is of this type and is currently utilized in the RELAP5/ MOD1 computer code (44).

When compared with experimental data these types of correlations seem to predict reasonable trends, the quantitative disagreements can be substantial though (43). It is also questionable whether these types of correlations in nonequilibrium computer programmes like, eg. RELAP5, should be utilized (45).

Nonequilibrium Models

The nonequilibrium models recognize the importance of vapour superheating when calculating the heat transfer. The models can be grouped into two categories (12): a) local correlations, b) separate phase models.

a) Local Correlations

This type of correlation calculates the local vapour superheat and heat transfer coefficient from local thermal hydraulic parameters. Examples are the Groeneveld-Delorme correlations and the CSO correlation of Chen, Sundaram and Ozkaynak. Both of these correlations are given in (12). They relate either the actual quality or the vapour superheat and the wall heat transfer coefficient to such parameters as the vapour Reynolds number and equilibrium quality. They are easy to implement into existing thermohydraulic codes but due to their highly empirical nature the prediction results usually reveal quite substantial scatter although the average result from a large number of calculations can be rather good.

b) Separate Phases Models

In these models the degree of nonequilibrium at any axial location is dependent on the upstream development of different competitive heat transfer mechanisms. The models can be brought to different levels of sophistication where the highest level includes the full set of conservation equations for each phase. Inherent in this approach is the need to specify the interfacial transport phenomena as well as the partition of the wall heat transfer between the phases.

In the dispersed droplet flow the nonequilibrium effects are basically determined by a balance between the wall to vapour heat transfer and the evaporation of entrained liquid droplets. The wall-to-vapour heat transfer can be evaluated by means of an ordinary single phase heat transfer correlation or more preferably by a specially developed correlation (e.g. the heat transfer equation in the CSO correlation). The evaporation is determined by a volumetric vapour source term giving the rate of vaporization per unit mixture volume. Various models have been proposed for estimating the vapour source function but no final conclusion can be made yet (see A6). One example is the correlation of Webb and Chen (6):

$$\Gamma = 1.32 \left[\frac{P}{P_c}\right]^{-1.1} \left[\frac{G \cdot XA}{\alpha_h}\right]^2 \frac{(1-\alpha_h)^{2/3} \cdot (T_v - T_{SAT}) \cdot k_v}{\rho_v \cdot \sigma \cdot H_{fg} \cdot D}$$

This correlation was implemented in NORAS and RELAP5 computer codes and some-steady state post-dryout experiments were analysed assuming a two-step heat transfer process, e.g. the heat was transferred from the wall to the vapour phase and from the vapour to the liquid droplets (46, 47). As only the wall temperature was measured it could only be concluded that the complete model was fairly accurate in the prediction of the wall surface temperature, but no assessment of the calculated vapour superheat could be given. A comparison of different correlation predictions with measured nonequilibrium conditions revealed that the above equation correctly predicted some of the experimental data, showing a large scatter though (48).

As can be seen from the above equation the vapour generation rate is directly proportional to the local vapour superheat $T_V - T_{SAT}$. Near the CHF-front where the vapour superheat is very minor a small vapour generation rate will thus be predicted. This is in direct conflict with the new findings that the vapour generation is dependent on the distance from the CFH-front with a high vaporization in the region near the CHF location.

In order to improve the predictions and take these new observations into account a new model for the vapour source term was recently developed (17). In the near-field region of CHF the vapour generation rate was postulated to vary with:

1. Wall superheat $T_W - T_{SAT}$
   Due to the repulsive evaporative forces on the liquid the vapour generation rate is expected to decrease when the wall superheat increases.

2. Distance from the CHF-front L/D
   The near-field vapour generation rate should decrease when the distance increases.

3. Liquid mass $G \cdot (1-XA)$
   The vapour generation rate should be directly proportional to the liquid mass flux.

The near-field vapour generation was then suggested to be

$$\Gamma_{NF} = \frac{4 \cdot q''}{D \cdot H_{fg}} \cdot \exp\left[-C \frac{T_W - T_{SAT}) \cdot L/D}{G \cdot (1-XA)} \right]$$

where the empirical constant was found to be independent of pressure having the value

$$C = 0.0016 \text{ kg}/(\text{m}^2 \text{ s K})$$

In the far-field region, the vapour generation rate was determined by a revised form of the Webb and Chen correlation (6):

$$\Gamma_{FF} = 2.0 \cdot 10^3 \cdot j_v^2 \cdot \frac{(1-\alpha_h)^{2/3} \cdot (T_v - T_{SAT})}{H_{fg} \cdot D}$$

The total vapour generation rate was then simply the sum of the near-field and the far-field contributions:

$$\Gamma = \Gamma_{NF} + \Gamma_{FF}$$

This model was compared to experimental data obtained at Lehigh University (41) and at INEL (42). The model was able to predict the experimental values for both sets of data with reasonable agreement.

The parameter range of the model is

Pressure	0.2 - 7.0 MPa
Mass Flux	12 - 100 kg/m^2 s
CHF Quality	0.0 - 0.99
Wall Heat Flux	8 - 225 kW/m^2

The above given model for vapour generation rate was also used along with a new heat transfer correlation to predict the vapour superheat (17). The heat transfer correlation was a revised version of the modified CSO correlation and can be written as

$$h = h_{mod\ CSO}\ (1+F_s)(1+0.8/(L/D))$$

$$F_s = 250\left(\frac{P}{P_c}\right)^{0.69}\left(\frac{1-XA}{XA}\right)^{0.49} Re_v^{-0.55}$$

$$h_{mod\ CSO} = \frac{f}{2} \cdot C_{pv\ell} \cdot G \cdot XA \cdot Pr_{v\ell}^{-2/3}$$

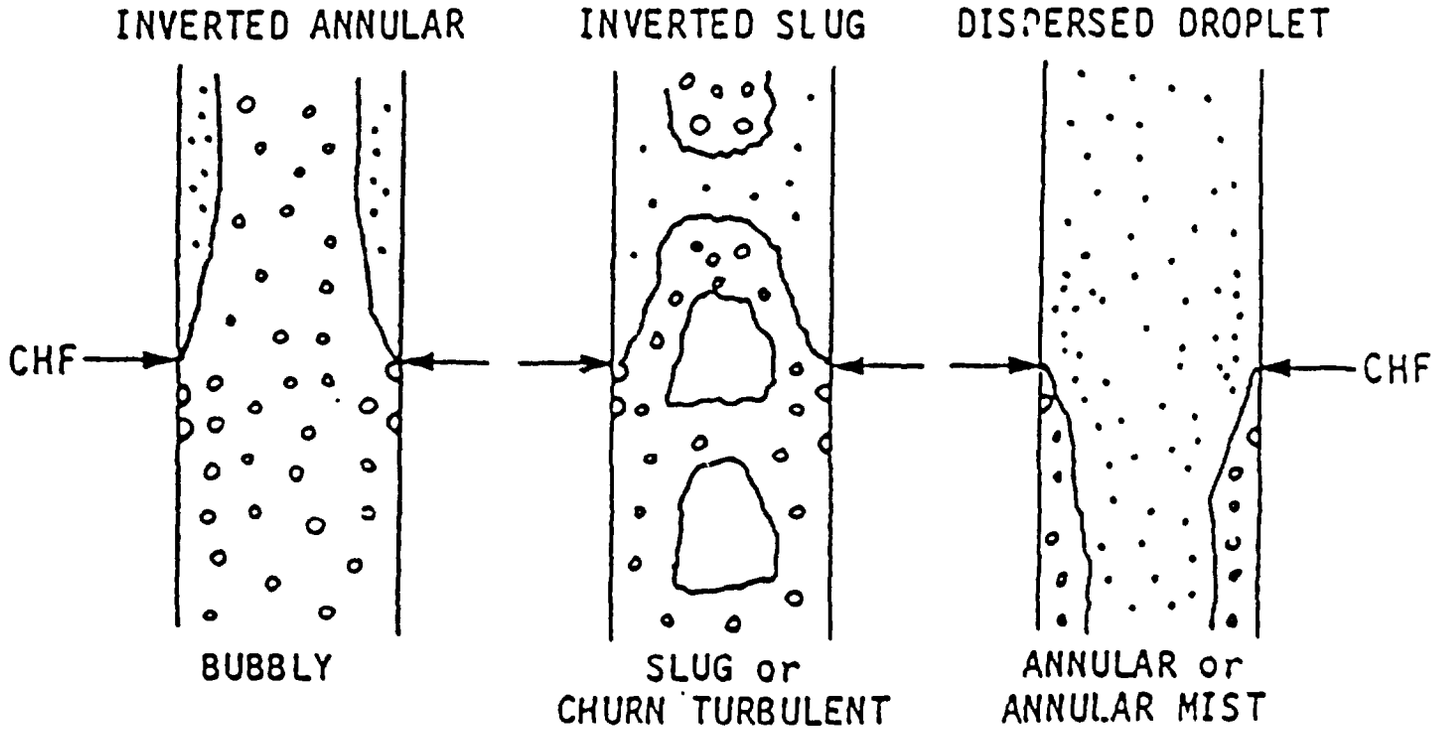

FIGURE A5.1 FLOW REGIONS, TRANSITIONS, AT CHF

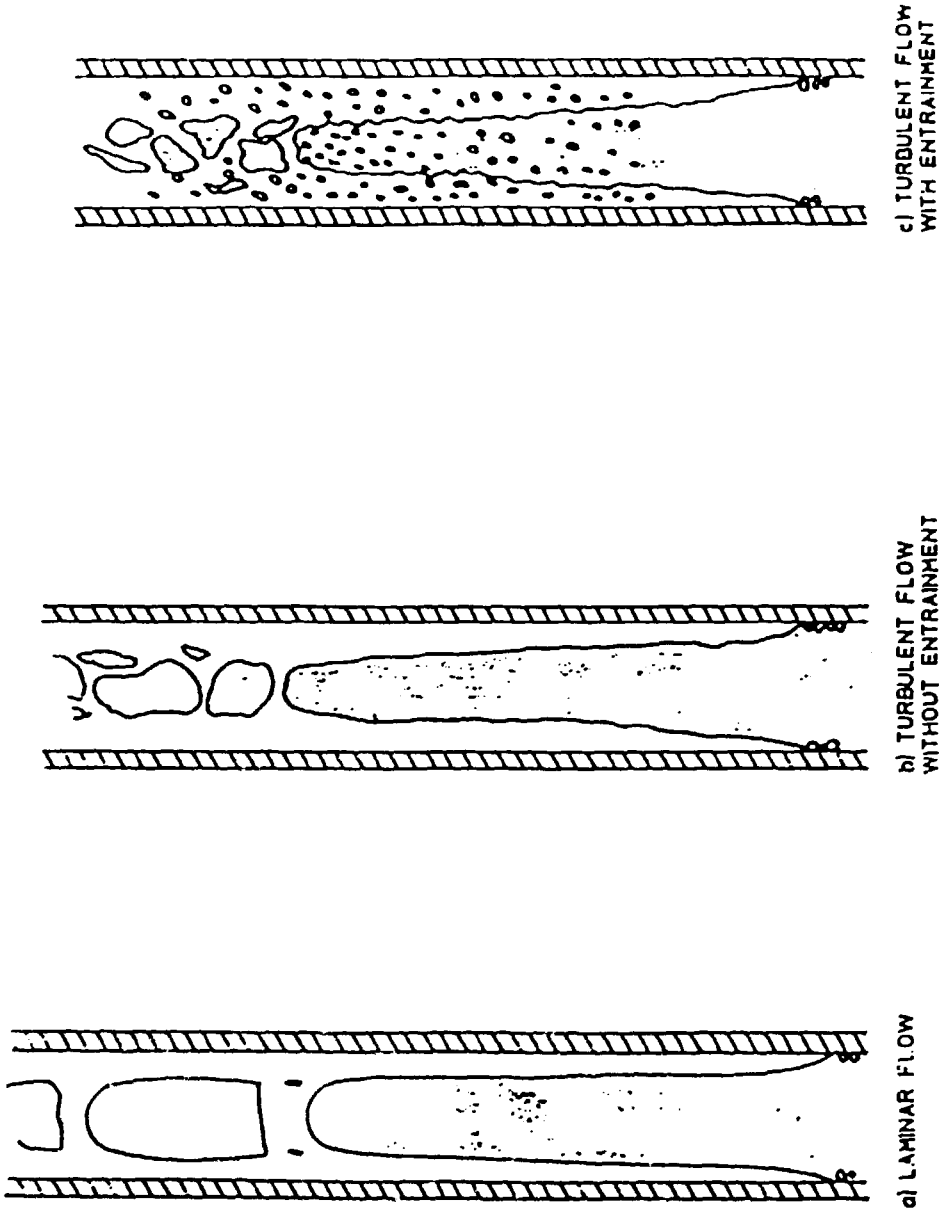

FIGURE A5.2
TYPES OF INVERTED ANNULAR FILM BOILING

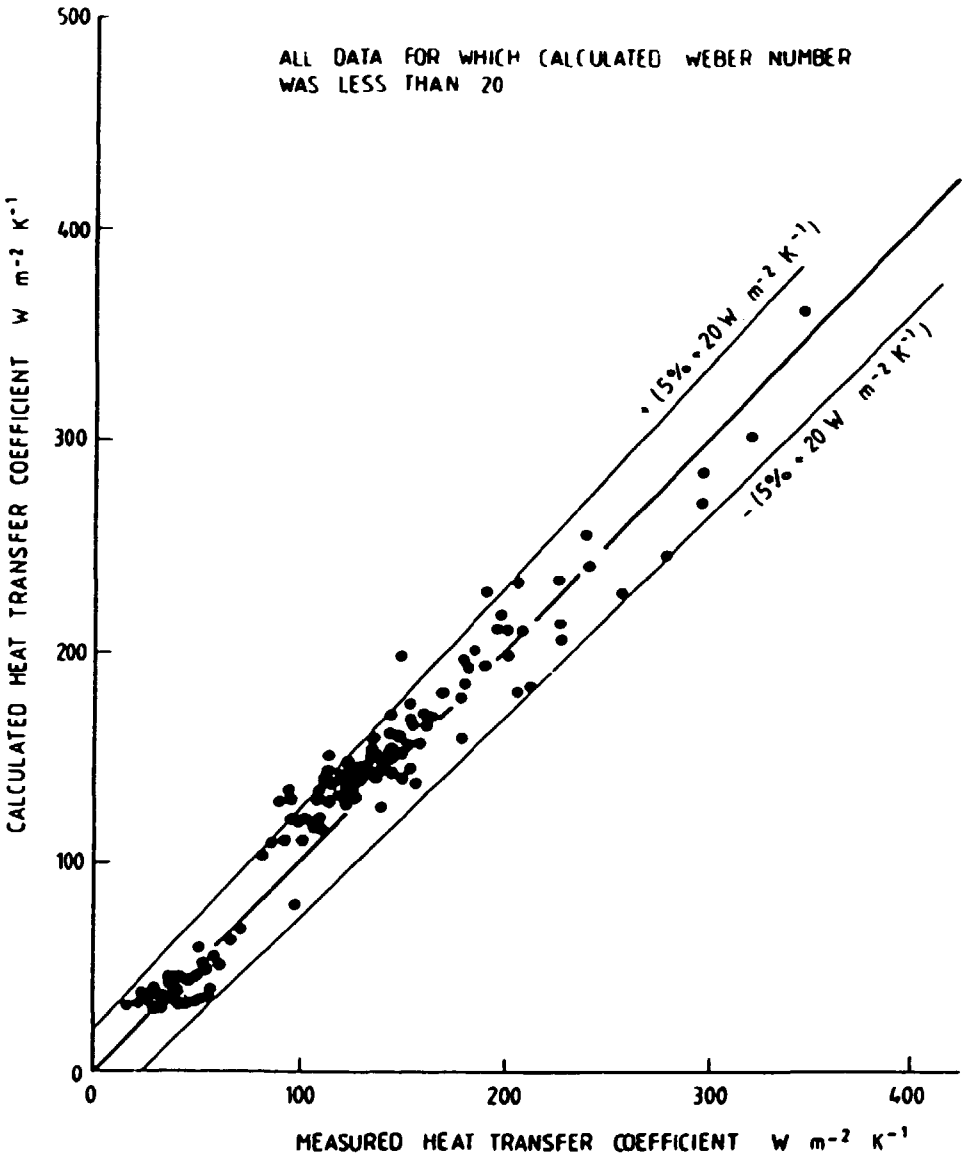

FIGURE A5.3
COMPARISON OF MEASURED AND CALCULATED HEAT TRANSFER COEFFICIENTS - PRESENT WORK (FROM REF. 38)

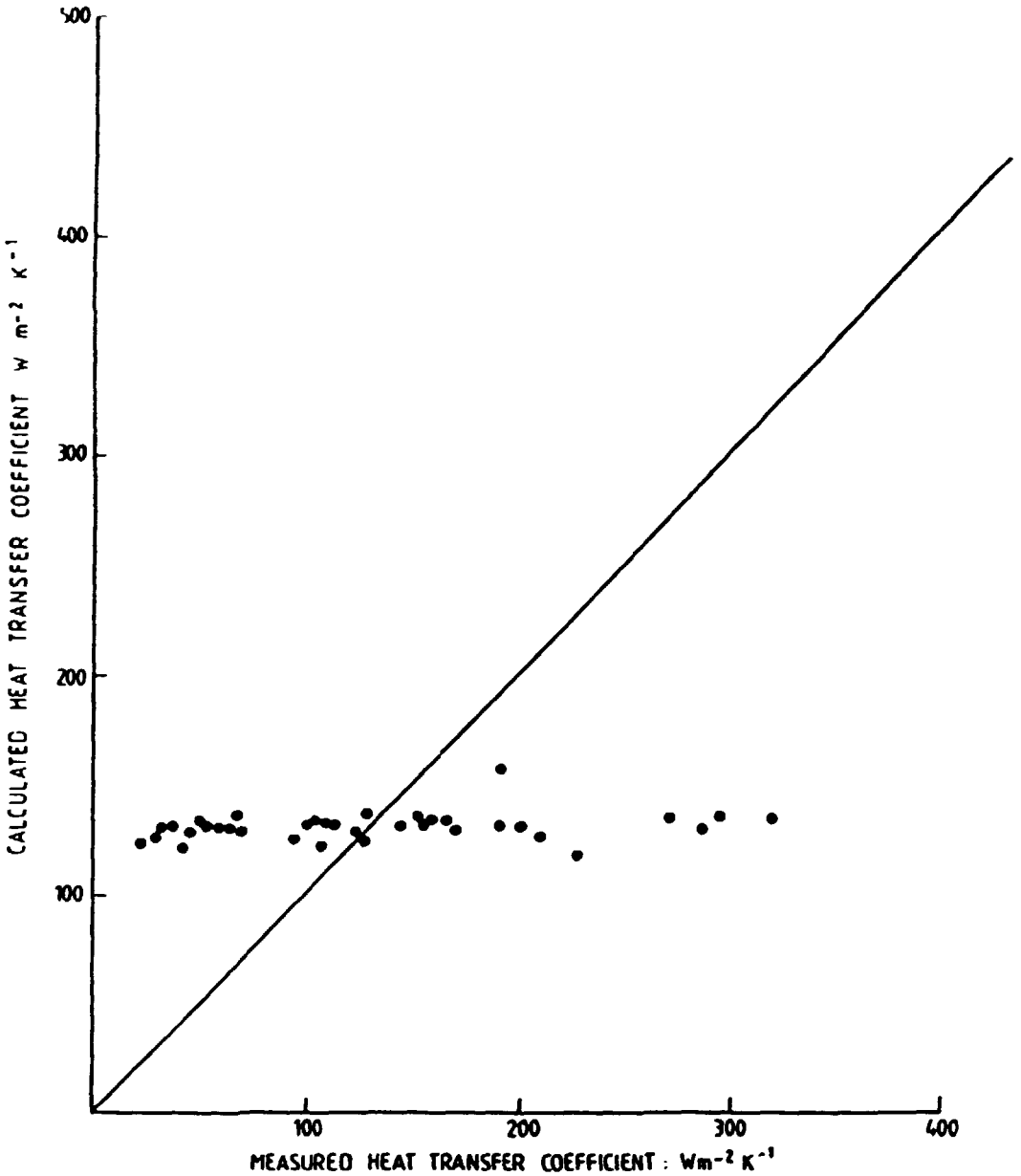

FIGURE A5.4

COMPARISON OF MEASURED HEAT TRANSFER COEFFICIENTS WITH "MODIFIED BROMLEY" MODEL (FROM REF. 38)

$$f = f_o \cdot \left(\frac{T_w}{T_v}\right)^{-0.1}$$

$$\frac{1}{\sqrt{f_o}} = 3.48 - 4 \cdot \log_{10}\left[\frac{2\varepsilon}{D} + \frac{9.35}{Re_v \sqrt{f_o}}\right]$$

The predicted vapour superheat from this film boiling model was compared with nonequilibrium experimental data. There was still some scatter but the model was an improvement compared to earlier models.

A6. Interfacial Heat Transfer

When a two-fluid model is used, interfacial mass-transfer rate Γ is calculated from

$$\Gamma = -\frac{Q_{i\ell} + Q_{ig}}{H_{fg}}$$

where $Q_{i\ell}$ is the heat transferred from the interface to the liquid phase, Q_{ig} is the heat transferred from the interface to the vapour phase and H_{fg} is latent heat of evaporation. The interfacial heat transfer rates are calculated from

$$Q_{ik} = h_{ik} \cdot (T_k - T_{SAT})$$

where T is the temperature, h_{ik} is the volumetric heat transfer coefficient, and the subscript k is either ℓ or v. Some correlations are expressed in terms of enthalphy or quality. From a computational point of view the use of enthalphy instead of temperature is more convenient, because usually enthalphy (or enthalpies) is one of the dependent variables to be evaluated. All the correlations can be transformed to a suitable form, for example

$$Q_{ik} = \frac{h_{ik}}{c_{pk}} (H_k - H_{kSAT})$$

where c_{pk} is specific heat.

Often the correlations are expressed in a form giving the mass transfer rate Γ. From a computional point of view it is however, convenient to have correlations for h_{ig} and $h_{i\ell}$ and to calculate Q_{ig} and $Q_{i\ell}$. Then Γ can be calculated from the first equation. If the original correlation is for the mass transfer rate, it can be transformed to a more suitable form by taking into account the fact that usually either

$$Q_{i\ell} >> Q_{ig}$$

or

$$Q_{ig} >> Q_{i\ell}$$

The first condition is valid when the mass fraction of liquid is larger than the mass fraction of vapour and the second condition holds in the opposite case. The conditions imply also that usually only one correlation for either h_{ig} or for $h_{i\ell}$ is needed. The other coefficient can be replaced with a sufficiently large value, which keeps the least massive phase near the saturated state.

There are four different interfacial heat transfer regions where either h_{ig} or $h_{i\ell}$ must be specified. These are summarized in the following:

1. $T_l > T_{\ell SAT}$ i.e. liquid is superheated. In this case liquid evaporates to vapour (flashing phenomemon).

2. $T_l < T_{\ell SAT}$. Vapour is condensed by the subcooled liquid

3. $T_g > T_{gSAT}$. Liquid is evaporated by the superheated vapour

4. $T_g < T_{gSAT}$. Subcooled vapour is condensed to liquid.

The first regions may occur in liquid-continuous flow and the two last regions in vapour-continuous flow. In vapour-continuous flow the different temperature conditions in the liquid phase do not lead to evaporation or condensation as

described in items 1 and 2, because the flashing rate is controlled by Q_{ig}. The same concerns the vapour phase in the low quality region. Four different correlations for interfacial heat transfer are therefore needed, two for $h_{i\,\ell}$ and two for h_{ig}. Furthermore, the correlations used for evaporation or condensation must be continuous at the point $T_k = T_{kSAT}$, because discontinuity may trigger an instability, where mass transfer rate and pressure are oscillating.

In addition to the flow boiling, a wall boiling (or condensation) model must be specified. In that case the total mass transfer rate Γ_{tot} is

$$\Gamma_{tot} = \Gamma + \Gamma_g$$

where Γ is calculated from the first equation and the mass transfer rate at the wall Γ_w is calculated using a separate model. This kind of model is needed for suncooled boiling, because in that case no evaporation is predicted using the two first equations. Another case is condensatipon of vapour at the cold wall. In these cases both Γ_w and Γ must be tailored so that the total mass transfer rate is correct.

Although the interfacial heat transfer is of great inportance in all two-phase flow calculations, very few empirical correlations exist at present. Very often the lack of a correlation must be compensated for by using a suitable large value for the interfacial heat transfer coefficient. This approach has also been used in the large system programmes like RELAP5 (see for example Appendix B3). Furthermore, in many cases the correlation developed are "semi-empirical", which means that a correlation is based on an analytical approach and it is tuned using some experimental data. Very often this tuning is based on a limited number of tests and consequently the correlation is not a reliable one for general purposes.

In SÄK-5 work interfacial heat transfer correlations have been tested for flashing and for post-dryout heat transfer (50, 46). In the case of flashing the correlations were tested by

calculating blowdown-experiments where the pressure undershoot below the saturated value is significant (51, 52), and by calculating critical flow experiments (52, 53). Five different correlations were tested and only the correlation of Bauer et al. was satisfactory. This correlation is a simple relaxation type model

$$\frac{\Gamma}{\rho} = \frac{XE-XA}{\tau}$$

where XA is the actual quality, XE is equilibrium quality, ρ is density and τ is time constant. In the case of flashing the condition $Q_{i\ell} >> Q_{ig}$ holds and the following heat transfer coefficient is obtained

$$h_{i\ell} = \frac{(1-\alpha)\cdot\rho_\ell\cdot C_{p\ell}}{\tau}$$

the time constant τ has been correlated using Moby Dick test as

$$\tau = \frac{660}{(\alpha+\alpha_o)(u+u_o)^2\sqrt{P}}$$

where α is void fraction, u is velocity in m/s and P is pressure in N/m^2. In the original model $\alpha_o = u_o = 0$, but in that case the above equation for τ cannot be used for initial flashing. The correlation is valid in the range of $0.01 < \alpha < 0.96$ and $5\ m/s < u < 54\ m/s$. In the present work the correlation has been extrapolated to cover also the early flashing process. For that purpose the constants were determined to be

$$\alpha_o = 0.003$$
$$u_o = 4\ m/s$$

These values are so small that they do not significantly change the correlation within its validity range, but they predict reasonable values for $h_{i\ell}$ when $\alpha = 0$ or $u = 0$. An alternative for this approach is presented in (54), where the time constant is the minimum of τ calculated from the above equation and the following

$$\tau = \frac{2.7 \cdot 10^{-5} H_{fg}^2}{(H_\ell - H_{\ell SAT})^2}$$

This approach has not been tested in the present work. When the first approach is used to predict the pressure recovery during the blowdown, the result seems to depend on the flow area. When medium-size pipes (D ~ 0.5 m) are simulated the calculated result is close to the experimental one (see Fig. A6.1). When the diameter is smaller, as in Edwards' pipe test, the predicted pressure recovery is too slow.In the case of a large vessel the predicted pressure recovery is too fast (50). This kind of deviation from the experimental data is not so harmful because the error is significant during only a very short period. Furthermore, it is difficult to obtain better results, because the initial flashing is a complicated phenomenon depending on soluble gases, surface roughness etc. It is obvious that in many cases the flashing correlation must be tuned in order to take into account these effects properly.

Better results were obtained from critical flow calculations. When the pipe length was 0.14 m and the diameter 0.014 m, the calculated results were close to the experimental ones on pressure range from 0.3 MPa to 9 MPa (Fig. A6 2). When the pressure was fixed, the correlation was able to predict the increase in mass flux when the pipe length was decreased (Fig. A6.3).

Because at present it seems that there are no better correlations for flashing, Bauer's correlation is recommended. In the test cases calculated it gave moderately good results.

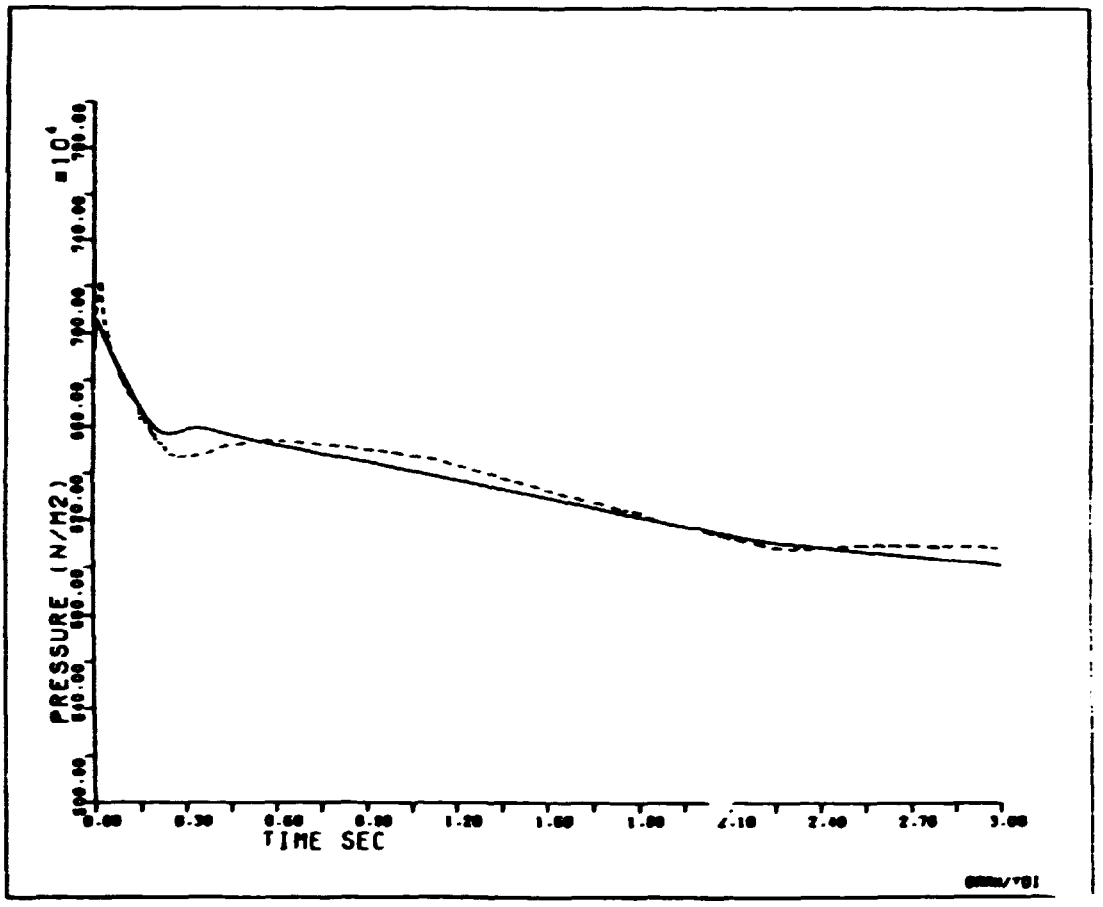

Fig.A6.1 OECD Standard Problem No. 6. Measured (-----) and calculated (——) pressures at the exit node. The correlation of Bauer et al. is used for interfacial heat transfer.

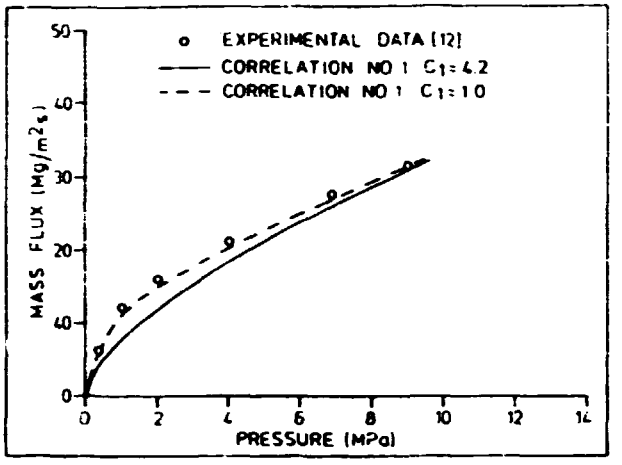

Fig.A6.2 Critical mass flux of saturated water as a function of pressure. Pipe diameter is 0.014 m and length is 0.14 m. A factor Cl is used to see the sensitivity of critical flow rate on flashing.

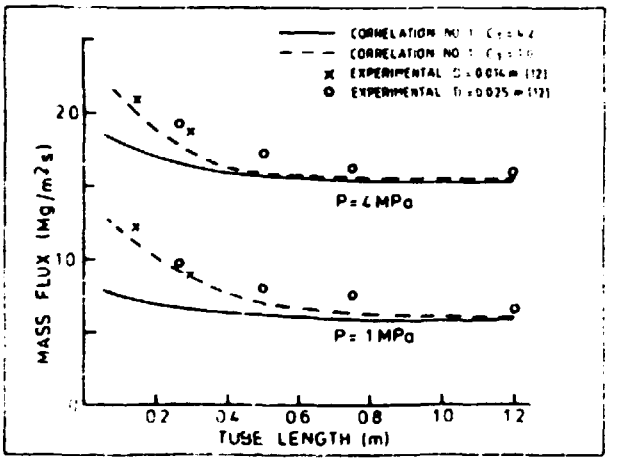

Fig.A6.3 Critical mass flux of saturated water as a function of pipe length. Pipe diameter is 0.014 m.

APPENDIX B COMPARISON WITH DATA

B1 Heat Transfer Package.

B1.1 RELAP-5

The heat transfer package of RELAP5/MOD1 was originally developed for the RELAP4-programme. In RELAP4 thermal equilibrium between the phases was assumed. RELAP5/MOD1 is a nonequilibrium programme, which utilizes only one energy equation for the thermal energy mixture . It is therefore possible to use the same heat transfer package as in RELAP4. However, certain modifications have to be made, because several heat transfer correlations are based on variables used in equilibrium calculations. When the calculation is based on a nonequilibrium assumption these variables must be calculated using the dependent variables of the nonequilibrium programme. An example is the equilibrium flow quality used in several critical heat flux correlations. The equilibrium quality is not directly solved in computer programmes, that allow thermal nonequilibrium.

The RELAP5/MOD1 heat transfer package (HTRC1) consists of a forced convection (flow related) group of correlation adopted from RELAP4/MOD6 and a pool boiling/natural convection (independent of flow) group of correlations. The low flow region is defined for mass fluxes lower than 200 kg/m^2s.

The heat transfer selection logic is based on wall temperature, saturation temperature, equilibrium quality and void fraction. The single-phase heat transfer to liquid is selected if equilibrium quality is lower than zero and wall temperature is lower than saturation temperature. The single-phase heat transfer to vapour is selected if wall temperature exceeds saturation temperature and void fraction exceeds 0.999. The condensation heat

transfer is selected if wall temperature is lowere than saturation temperature and the two-phase mixture temperature is greater than the wall temperature. The nucleate boiling heat transfer is selected if equilibrium quality is lower than the critical and wall superheat is lower than the critical wall superheat as calculated from the critical heat flux correlation. In other cases the post CHF heat transfer correlations are used. The film boiling correlations are changed to the transition boiling correlation if the wall temperature is lower than the minimum film boiling temperature,

During the SÄK-5 project the heat transfer package of RELAP5/MOD1 has been modified in order to use it independently. This modification follows the original as closely as possible, but is altered slightly for a two-fluid (six-equation) mode. For this purpose the heat transfer coefficient has been shared between liquid and vapour phases. In general, the separated heat transfer part has worked well in the test calculations. Some remarks should be made, however, especially concerning the original RELAP5-programme. In RELAP5 the heat transfer is calculated directly as heat flux. The heat transfer coefficient is interpreted as the derivative of heat flux with respect to wall temperature and is used for the implicit integration of wall temperatures. According to the RELAP5 manual, the heat transfer coefficient of transition boiling should be negative. The programme, however, omits the negative values, perhaps for reasons of stability.

Another remark concerns the definition of quality in the heat transfer part. Although the static equilibrium quality may be more reasonable from a calculational point of view, most of the correlations have been developed using flow quality. In vertical channels, the vapour velocity close to the crisis point may be larger than the liquid velocity, and consequently the flow quality is larger than the static quality. Therefore, the original correlation that uses flow quality, predicts smaller critical heat flux than the same correlation in the RELAP5 package.

There are other problems that appear when heat transfer coefficient surfaces are plotted (Figs. B1.1 and B1.2). The crest of the two-dimensional surfaces in the figures correspond to CHF conditions. Above a cutoff void fraction (0.96) post-CHF heat transfer is automatically assumed. If calculations are made above the cutoff value and the wall temperature is close to the saturation line, the heat transfer coefficient may change discontinously from turbulent film condensation to film boiling (see Figures B1.1 and B1.2). The abrupt change may be avoided by removing the void limit, thus activating the transition boiling mode in RELAP5. This modification has been added to the separate RELAP5 package, when others than the default CHF correlations of RELAP5 are used (Figure B1.2).

Another discontinuity appears when there is change from turbulent film condensation to convection from subcooled water to the wall. In fact, the subroutine of RELAP5 that calculates condensation deviates from the description of the manual. In the same subroutine there is also a discontinuous change in laminar film condensation, when a horizontal part is slightly inclined.

The problems concerning the vapour quality and the discontinuities are not important in blowdown analyses. They may be the reasons for unstable oscillations, when the heat transfer package is applied to milder transient or steady-state calculations. It is probably impossible to remove all troubles from such a large package, because there are too many input variables involved for heat transfer correlations. Before starting a new case the graphical study of the heat coefficient surface could therefore be useful in order to avoid instability problems.

B1.2 TRAC (PF1)

The wall-to-fluid heat transfer selection and calculation is concentrated to one major subroutine HTCOR. Some of the heat transfer coefficients and critical heat flux are calculated in subroutines called from HTCOR.

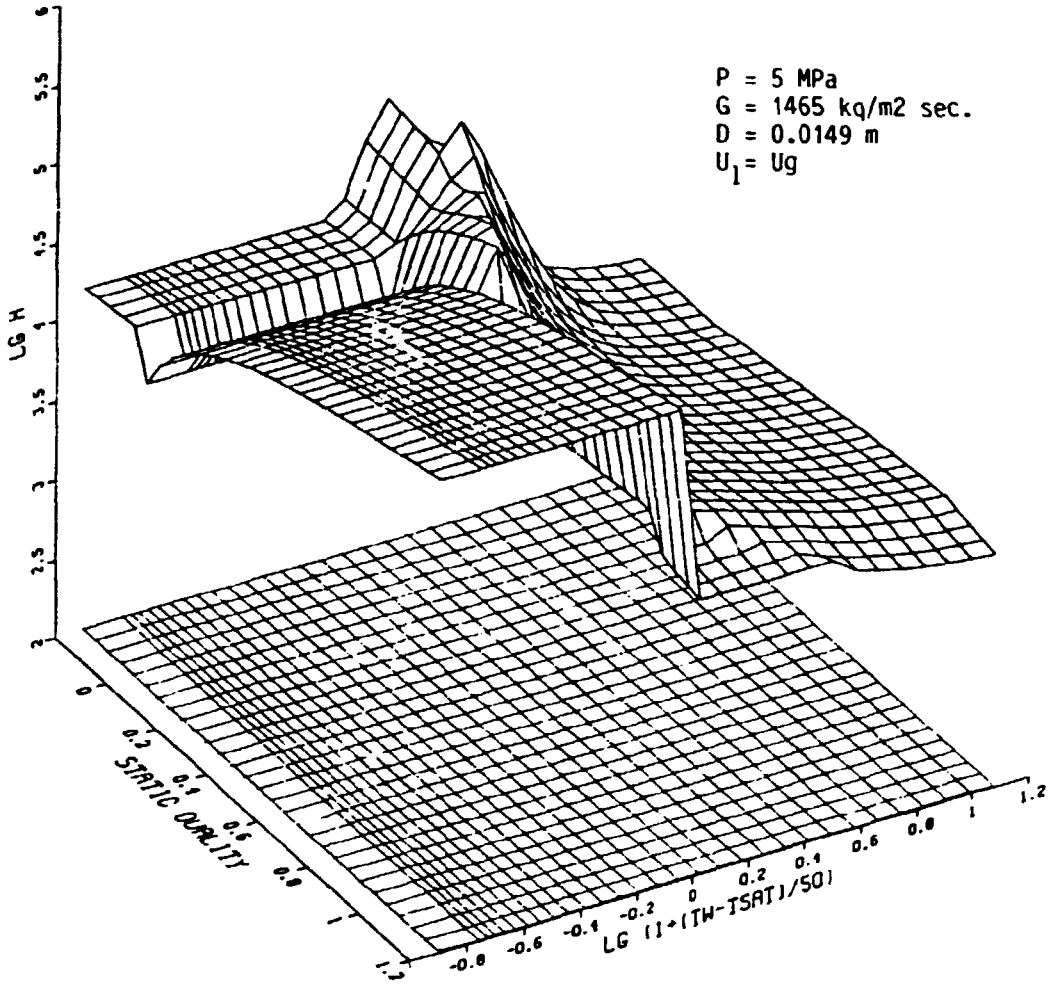

FIG. B1.1 HEAT TRANSFER COEFFICIENT SURFACE USING THE HEAT TRANSFER PACKAGE OF RELAP 5 WITH DEFAULT CHF-CORRELATION.

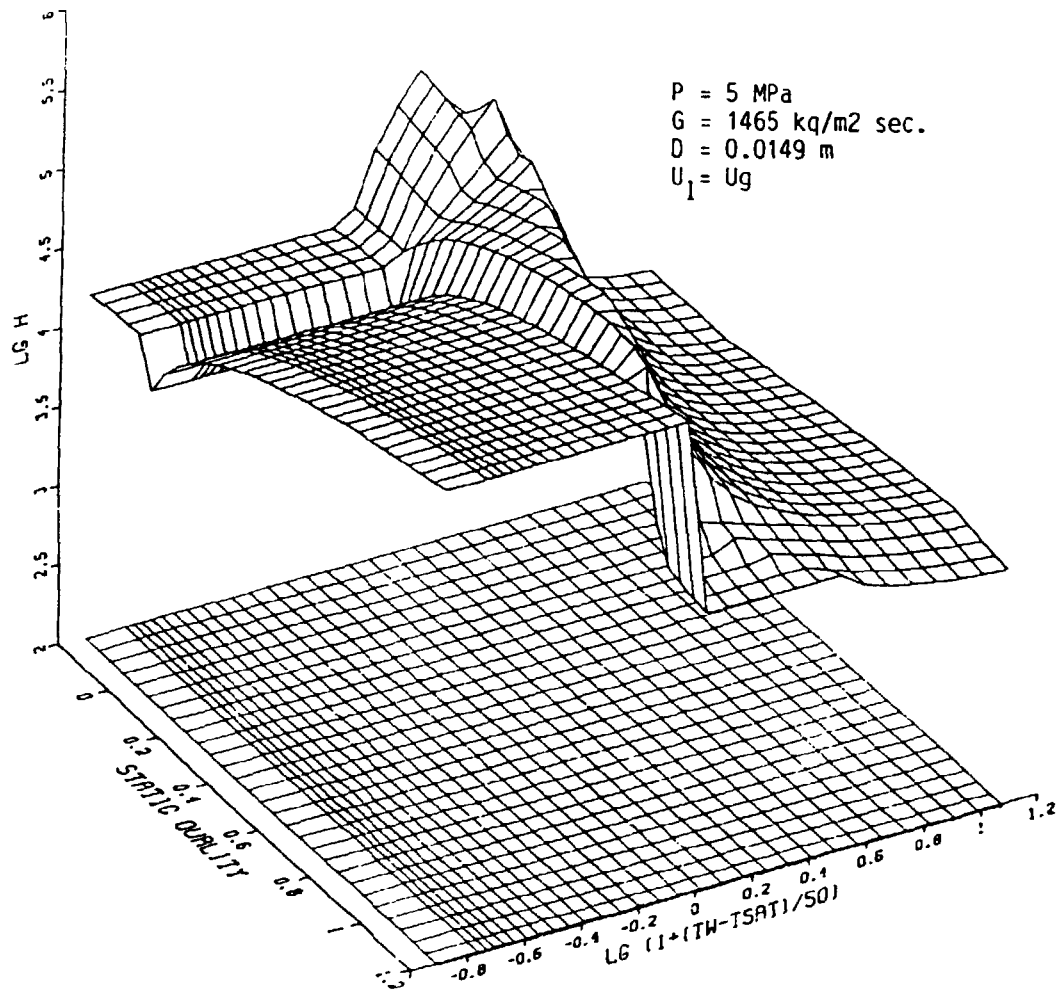

FIG. B1.2 HEAT TRANSFER COEFFICIENT SURFACE USING THE HEAT TRANSFER PACKAGE OF RELAP 5 WITH BECKERS CHF-CORRELATION AND THE VOID LIMIT EXCLUDED'

The programming in HTCOR is rather straightforward and the exchanging of correlations should not be too difficult. To do it, however, requires a good understanding of the selection and interpolation logic. The exchanging of correlations has not been tried but the fixing of the locus of CHF has been used and was easily made.

The selection is based on the calculated wall temperature, critical temperature, minimum film boiling temperature, bulk temperature, void fraction (vapour quality) and the boiling curve.

Eight modes of heat transfer are considered:

1. Forced convection to single-phase liquid.
2. Nucleate boiling.
3. Transition boiling.
4. Film boiling.
5. Convection to single-phase vapour.
6. Convection to two-phase mixture.
7. Condensation.
8. Liquid natural convection.

The selection of the first five modes are directly attached to the boiling curve.

The modes 6, 7, and 8 are separate modes of heat transfer.

The selection of mode 6, convection to two-phase mixture, is the result of an input option in TRAC. CHF can not occur in this case. The liquid heat transfer coefficient is determined as the maximum of the laminar and the turbulent flow values:

$$h_{\ell} = \max. (h_{\ell,\ lam.},\ h_{\ell \cdot turb})$$

$$h_{\ell,\ lam} = 4k_{\ell}/D \qquad \text{(McAdams)}$$

and Dittus-Boelter for turbulent flow:

$$h_{l,turb} = k_l/D \cdot 0.023 \cdot (Re_m)^{0.8} \cdot (Pr)^{0.4}$$

$$Re_m = G \cdot D/\mu_m$$

A two-phase viscosity based on actual quality is calculated and used in the calculation of the Reynold's number:

$$\mu_m = 1/\left(\frac{XA}{\mu_g} + \frac{(1-XA)}{\mu_l}\right)$$

If the void fraction is less than a cutoff value, h_l is chosen as the heat transfer coefficient.

If the void is greater than the cutoff value, the vapour heat transfer coefficient is determined as the maximum of the Dittus-Boelter value for vapour and the turbulent natural convection value:

$$h_g = \max.\ (h_{vnc},\ h_{vturb})$$

where

$$h_{vnc} = 0.13 \cdot k_g/D \cdot (Gr \cdot Pr)^{1/3}$$

The mixture heat transfer coefficient is determined from linear interpolation between these values of h_l and h_g and the single-phase values.

Mode 7 is the condensation mode. Condensation heat transfer has not been considered in this project. TRAC uses the Chen-correlation for nucleate boiling (Table A1.I) with the suppression factor S set equal to zero. If the equilibrium vapour quality XE is greater than 0.71, the limit of Chen's data base, then the correlation is evaluated at XE=0.71. Condensation is selected if $T_W < T_l$, $T_W < T_{SAT}$ and $\alpha > 0.05$.

Mode 8 is the liquid natural convection mode and is selected if:

$$Gr/Re^2 > 1.0$$

The Grashofs number is defined as:

$$Gr = \frac{\rho_\ell^2 \cdot \beta \cdot g \cdot \Delta T \cdot L_C^3}{\mu_\ell^2} = \frac{\rho_\ell \cdot \beta \cdot g \cdot \Delta T \cdot L_C}{\rho_\ell \cdot u^2} \cdot \left(\frac{\rho_\ell \cdot u \cdot L_C}{\mu_\ell}\right)^2$$

i.e. product of the Reynold number squared and a factor that is the ratio between the buoyancy and the velocity head. This ratio is greater than 1.0 when the buoyancy will prevail and natural convection exists.

The natural convection heat transfer coefficient is then determined from

$$Nu = C \cdot (Gr \cdot Pr)^n$$

where

$C = 0.59$ and $n = 0.25$ in laminar flow ($10^4 < (Gr.\ Pr) < 10^9$)

and $C = 0.13$ and $n = 0.3333$ in turbulent flow ($10^9 < (Gr.\ Pr) < 10^{12}$)

The other modes follow the boiling curve.

The single phase liquid heat transfer coefficient is calculated using McAdams correlation (see above) for laminar flow and Dittus-Boelter for turbulent flow, unless natural convection prevails.

Chen's correlation (Table A1.I) is used both in the nucleate and forced convective boiling region.

The Bjornard and Griffith's empirical correlation (Table A3. I) is used in the transition boiling region. The transition boiling is calculated when the surface temperature is above CHF temperature and below the minimum film-boiling temperature i.e. $T_{CHF} < T_W < T_{MFB}$. T_{CHF} is determined from the Biasi CHF correlation. The minimum film-boiling heat-flux correlation has not been studied in this project.

In the film-boiling region thermal radiation and dispersed flow heat transfer occur between the surface and the liquid.

The dispersed flow heat transfer coefficient is calculated using The Forslund and Rohsenow correlation:

$$h_{df} = 0.2552 \cdot ((1-\alpha) \cdot E)^{0.6667} \cdot \left(\frac{k_\ell}{D}\right) \left(\frac{\rho_\ell \cdot \rho_g \cdot g \cdot H'_{fg} D^3}{(T_w - T_{SAT}) \cdot \mu_g \cdot d \cdot k_\ell}\right)^{0.25}$$

where E is the entrained liquid fraction.

The vapour heat transfer coefficient is the maximum of the Bromley (Table A3. I, h_{PB} in No. 3), natural convection and Dougall and Rohsenow's modification to Dittus-Boelter

$$h_g = 0.223 \cdot \frac{k_g}{D} \cdot [Re_g \cdot (XE + \frac{\rho_g}{\rho_\ell}(1-XE)]^{0.8} \cdot Pr_g^{0.4}$$

In the single phase vapour region the maximum of turbulent natural convection and Dittus-Boelter are used. The selection is determined by XE>1.0, $T_w > T_\ell$ and $T_w > T_{SAT}$.

The interfacial heat transfer correlations are mixed within the programming and it may not be a simple task to change the correlations used.

B1. 3 NORA

The wall-to-fluid heat transfer selection and calculation is concentrated upon one major subroutine, WALLS. The critical heat flux is calculated by calling CHFCOR. The programming in WALLS is straightforward and the exchange of correlations is simple.

The logic for selecting the heat transfer mode is not complicated. First, a set of limiting values on void fraction and quality are calculated in subroutine LIMIT. If equilibrium quality is above a certain value, ALIM(1), a dry wall is always assumed. The heat transfer mode is the forced convection to steam or surface condensation, depending on wall surface temperature.

In all situations heat transfer coefficients based on convection to liquid and boiling are first calculated and a heat transfer mode is chosen such that it gives the highest heat flux. This heat flux is next compared with the critical heat flux. If the heat flux is less than CHF the calculation stops.

If the heat flux is greater than CHF, the minimum film boiling temperature, T_{MFB}, and the heat flux at this temperature are calculated. If the wall temperature is less than T_{MFB} an interpolation is made between heat the fluxes at CHF and T_{MFB} (transition boiling). If the wall temperature is larger than T_{MFB} film boiling or single-phase vapour heat transfer is chosen. The selection logic chooses the highest heat transfer coefficient calculated for the region.

The interface heat transfer calculation is done in two subroutines, FLASH and HPHASE. FLASH calculates the energy transfer due to mass transfer and HPHASE calculates heat transfer that is not directly related to mass transfer.

B2. Comparison with Data.

The different experiments utilized as test cases are summarized in Table 4.2.I. As can be seen from the table the experiments can be divided into four groups assigned as the Roumy experiments, the CE/EPRI experiment, the Becker experiments, and the ORNL experiments. A brief description of each group of experiments will be given in what follows together with some results from the calculations with the computer codes RELAP5/MOD1, TRAC(PF1) and NORA.

The Roumy Experiments

The Roumy experiments (56) utilized a vertical tubular test section with 0.010 m inside diameter. The heated length was 1.0 m and the initial conditions were to some extent comparable to those in a PWR core (see Table 4.2.I). Two experiments were selected from the experimental series, one with only a flow transient and the other with a flow transient combined with a power transient. All the remaining operating parameters were kept unchanged. In both cases the inlet mass flow and the exit wall surface temperature of the test section were measured. These parameters are plotted in Figs. B2.1 and B2.2. The wall temperature plots indicate that the exit in both of the cases experienced a departure from nucleate boiling (DNB) when the flow was decreasing (ascending temperature) with a following return to nucleate boiling (RNB) when the flow was increasing (descending temperature). Thus these cases could be used to test the capabilities of the computer programme to deal with transient low-quality CHF, inverted annular flow heat transfer and rewetting of a hot surface.

The two cases were calculated with RELAP5/MOD1, TRAC(PF1) and NORA. The boundary conditions were the outlet pressure, the inlet water properties, the inlet water flow, and power in the tube wall. Figures B2.3 to B2.8 exemplify typical RELAP5/MOD1 results with 20 axial nodes of equal length. As can be seen from the temperature plots (Figs. B2.5 and B2.8) no CHF was experienced, although the CHF-ratio was about unity (Figs. B2.4 and B2.7). The CHF-correlations used in RELAP5 in these calculations were the W-3 correlation (4) in the high-flow region (mass flux G >1356 kg/m^2 s) and modified Zuber correlation (58) in the low-flow region (G<271 kg/m^2 s). For intermediate flows the maximum CHF-value of W-3 correlation and modified Zuber correlation was used. This selection logic was the reason for the somewhat odd behaviour of the CHF-curve in Fig. B2.4 between 0.65 and 1.12 s. At 0.65 s a switch was made from the W-3 correlation to modified Zuber correlation because at that time the latter correlation began providing the largest CHF-value (G was between 271 and 1365 kg/m^2 s). At 1.12 s a switch back to the W-3 correlation

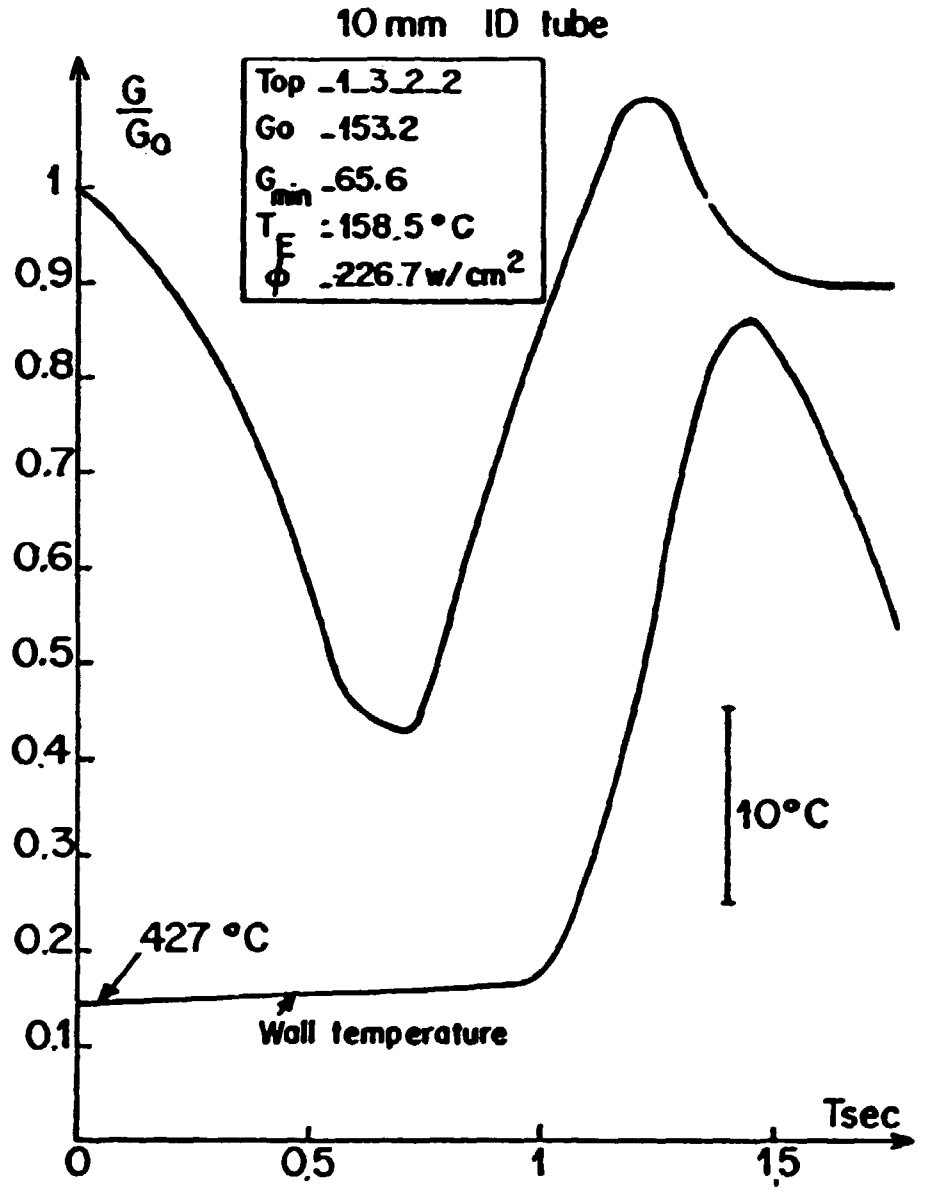

FIG. B2.1 ROUMY CASE 1. FLOW TRANSIENT (FROM REF. 56)

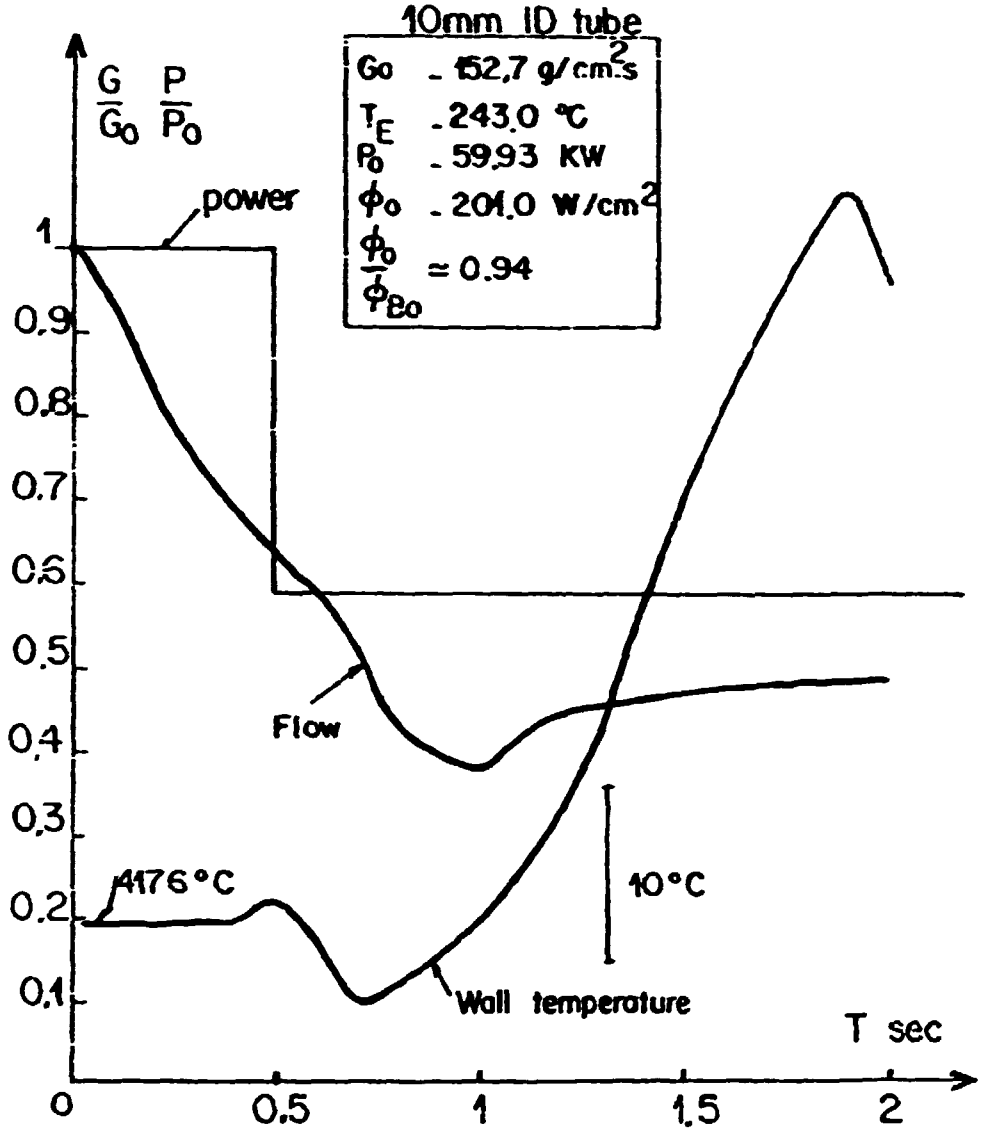

FIG. B2.2 ROUMY CASE 2. FLOW AND POWER TRANSIENT (FROM REF. 56)

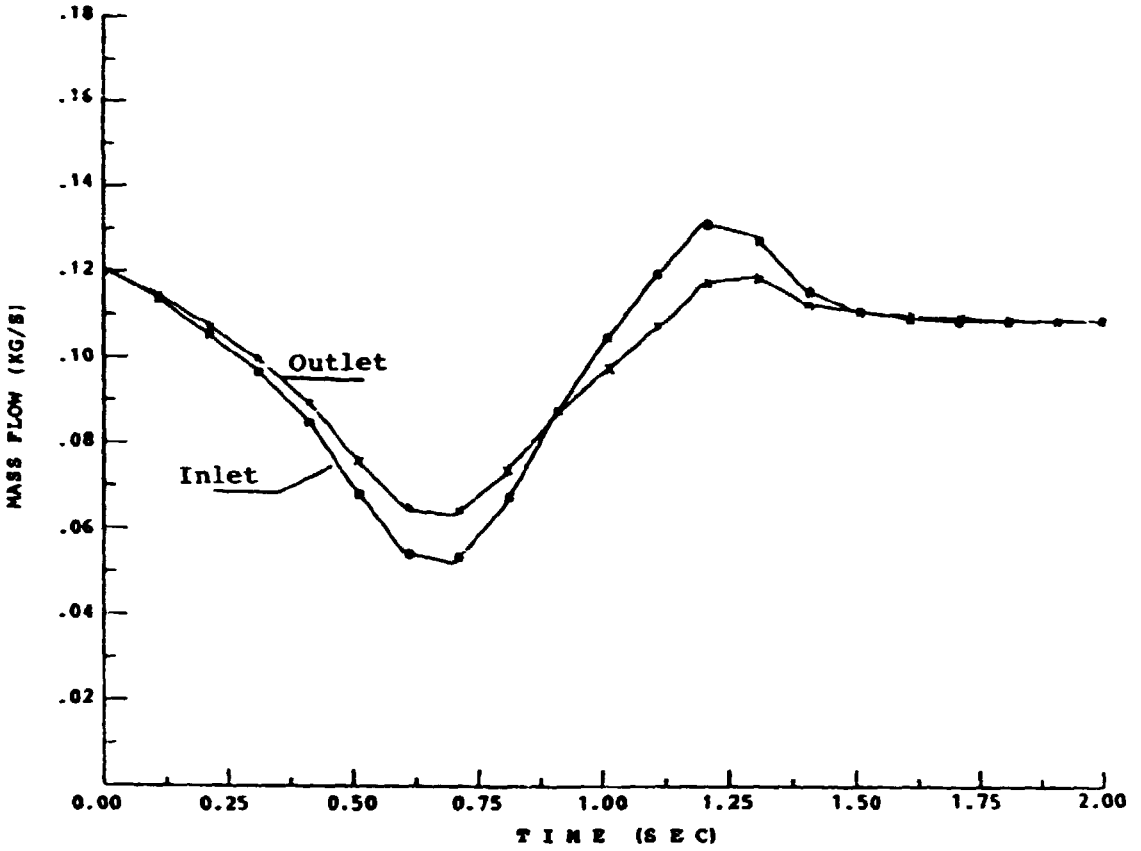

Fig. B2.3 RELAP5/MOD1/018 Roumy Case 1

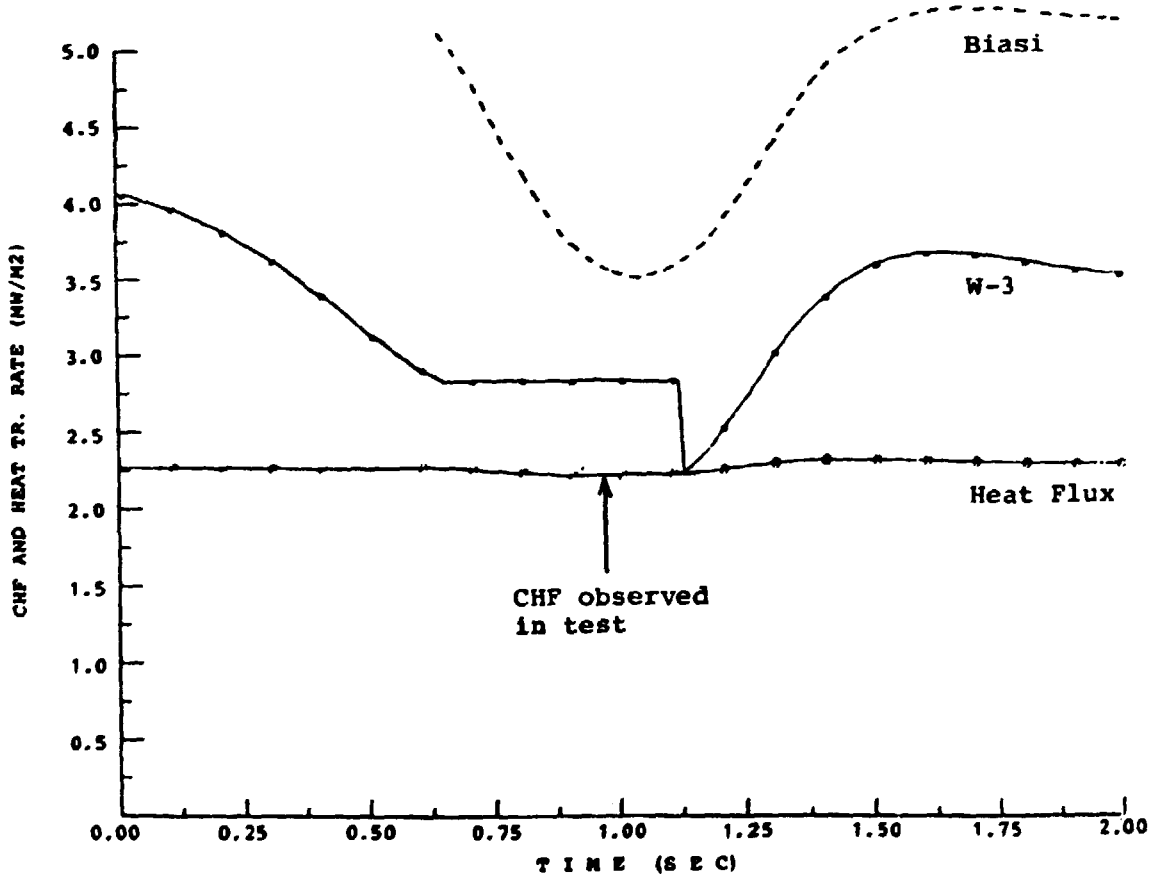

Fig. B2.4 RELAP5/MOD1/018 Roumy Case 1

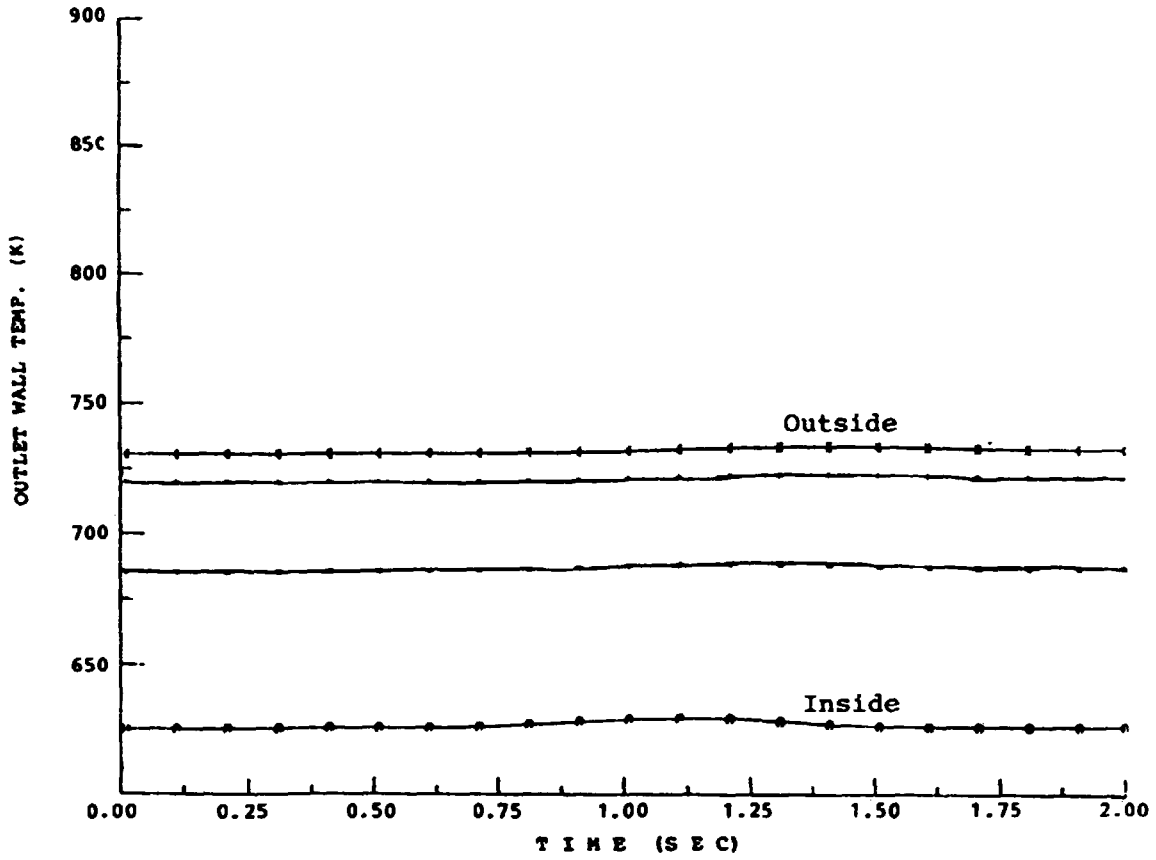

Fig. B2.5 RELAP5/MOD1/018 Roumy Case 1

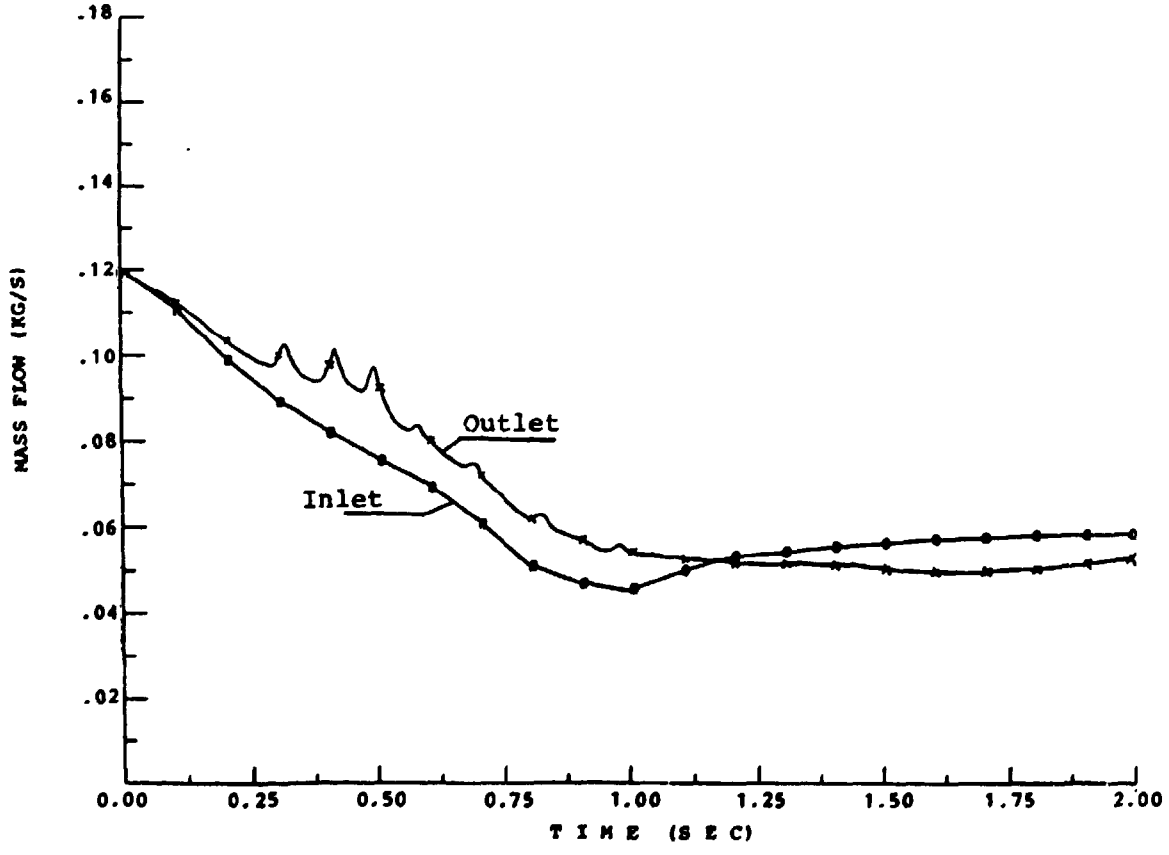

Fig. B2.6 RELAP5/MOD1/018 Roumy Case 2

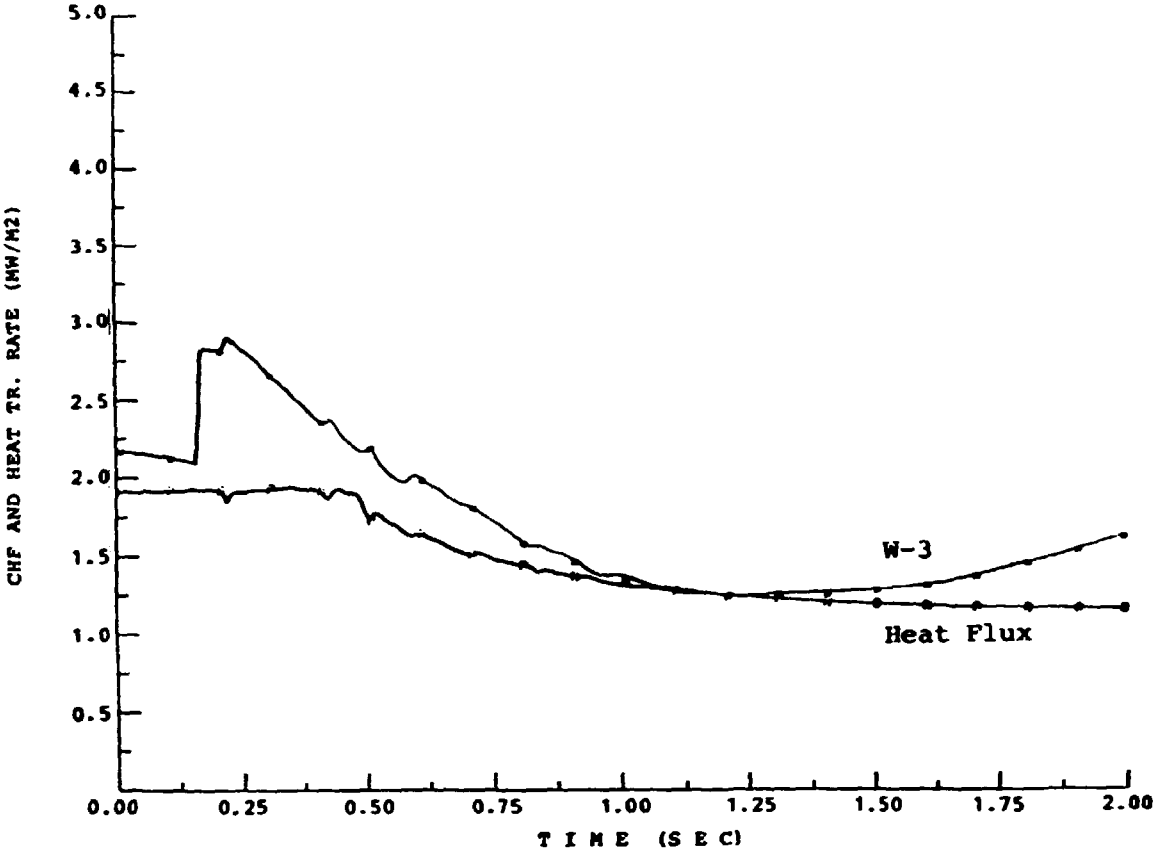

Fig. B2.7 RELAP5/MOD1/018 Roumy Case 2

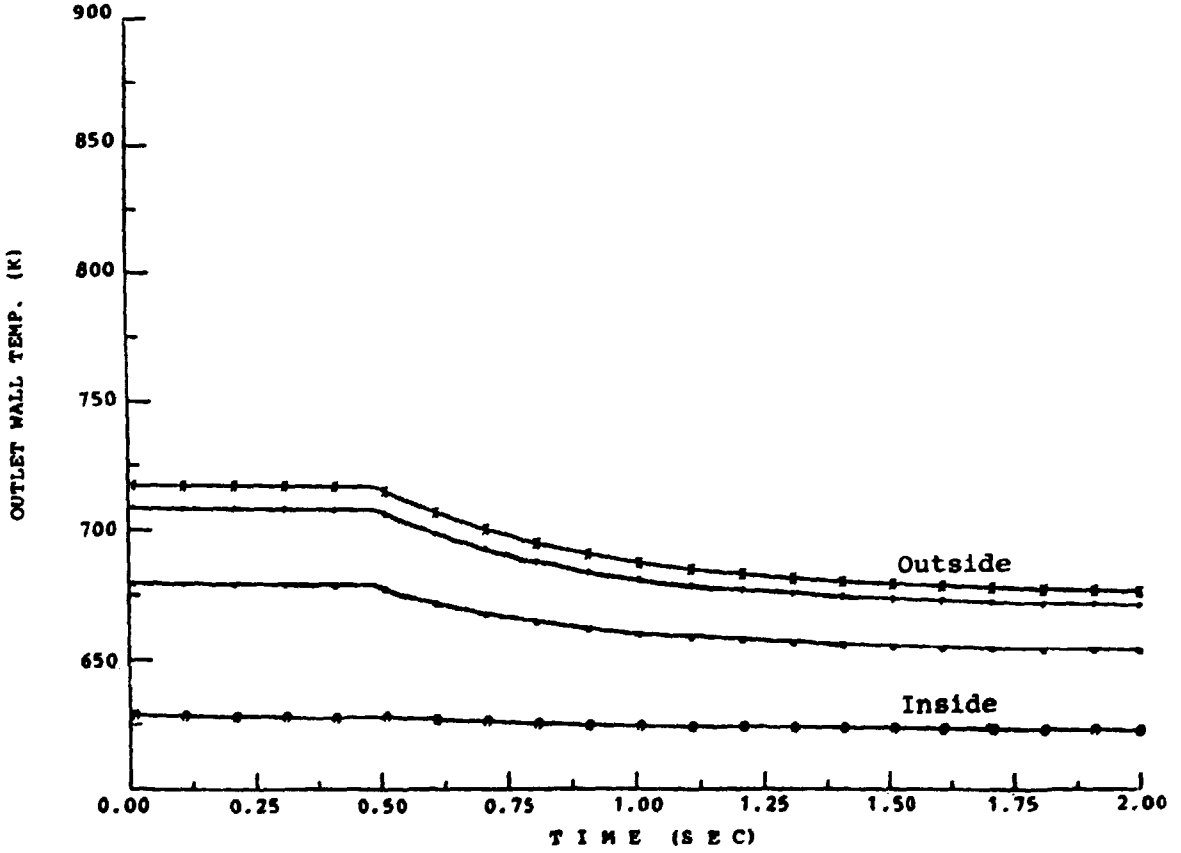

Fig. B2.8 RELAP5/MOD1/018 Roumy Case 2

was made as G exceeded the limit 1356 kg/m^2 s. The utilization of only the W-3 correlation would probably have given about the measured time to CHF. In Fig. B2.4 the CHF-value is also plotted according to the Biasi correlation (5). This correlation provided larger CHF-values than the combination W-3-modified Zuber correlation.

Similar results were obtained with TRAC(PF1) (Biasi correlation) and with NORA (modified Zuber correlation). The utilization of the modified Zuber correlation and the Biasi correlation in this case requires the calculation of subcooled void or subcooled actual quality. Since both RELAP5 and TRAC are not yet capable of calculating subcooled void formation it is not surprising that they failed in the CHF-predictions when these correlations are used.

The CE/EPRI Experiment

The CE/EPRI experiment was selected from a series of blowdown experiments (59) conducted using a loop containing a vertical single tube as the test section (Fig. B2.9). The heated length was 3.81 m and the initial conditions were typical for a PWR (see Table 4.2.I). The test section was a 0.0127 m outside diameter Incoloy-800 tube having a 0.00125 m wall thickness. It was instrumented with wall thermocouples and differential pressure transducers. The twenty wall thermocouples were distributed along 12 axial locations as can be seen in Fig. B2.9. The transient two-phase mass flow rate at the test section inlet and outlet was measured by two groups of instruments each consisting of a turbine meter, drag screen meter and gamma densitometer. The mass flow rate was determined by combining the turbine and densitometer readings assuming homogenous flow*. The test section inlet and outlet fluid temperatures were also measured. The measurements of void fractions, fluid temperatures and wall surface temperatures during the selected blowdown experiment are shown in Figs. B2.10 to B2.12. The time to CHF was about 1.0 sec.

---

* This assumption is justified for higher mass flows, however at low mass flow rates its validity is questionable.

In the calculations with the three computer programmes only the test section was modelled. Thus some adequate boundary conditions had to be given. The boundary conditions used in these calculations were the outlet pressure (Fig. B2.13), the inlet massflow (Fig. B2.14) and the test section power (Fig. B2.15). As the programmes required the phasic massflows the total massflux in Fig. B2.14 had to be divided on each phase. This was accomplished by means of Figs. B2.10 and B2.11 with the assumption of saturated homogeneous flow.

The results of the RELAP5/MOD1 calculations are shown in Figs. B2.16 to B2.19. Similar results were obtained with TRAC(PF1) and NORA. The exit void fraction in Fig. B2.16 showed about the same trend as the measured exit void fraction in Fig. B2.10, being on a somewhat higher level though. The measured exit temperature peak shown in Fig. B2.11 was also obtained in the calculations (Fig. B2.17). The temperature peak occurred somewhat earlier in the calculations and, significantly, it was predicted to have a shorter duration, about 1 sec or half of the measured 2-sec duration. In Figs. B2.18 and B2.19 some calculated wall surface temperatures are shown.

A comparison with the measured temperatures in Fig. B2.12 reveals an almost correct calculated time to CHF while the rewetting was predicted to occur too early. A more notable discrepancy was the prediction of fairly uniform CHF and rewetting throughout the test section while the measurements indicated an axial propagation of the CHF and also of the rewetting.

There could apparently be two reasons for these discrepancies: first, of course, some inadequacies of the models used in the programmes, and secondly the utilization of inadequate boundary conditions. One of these is certainly the assumption of saturated homogeneous flow when evaluating the phasic flow components from the measurements.

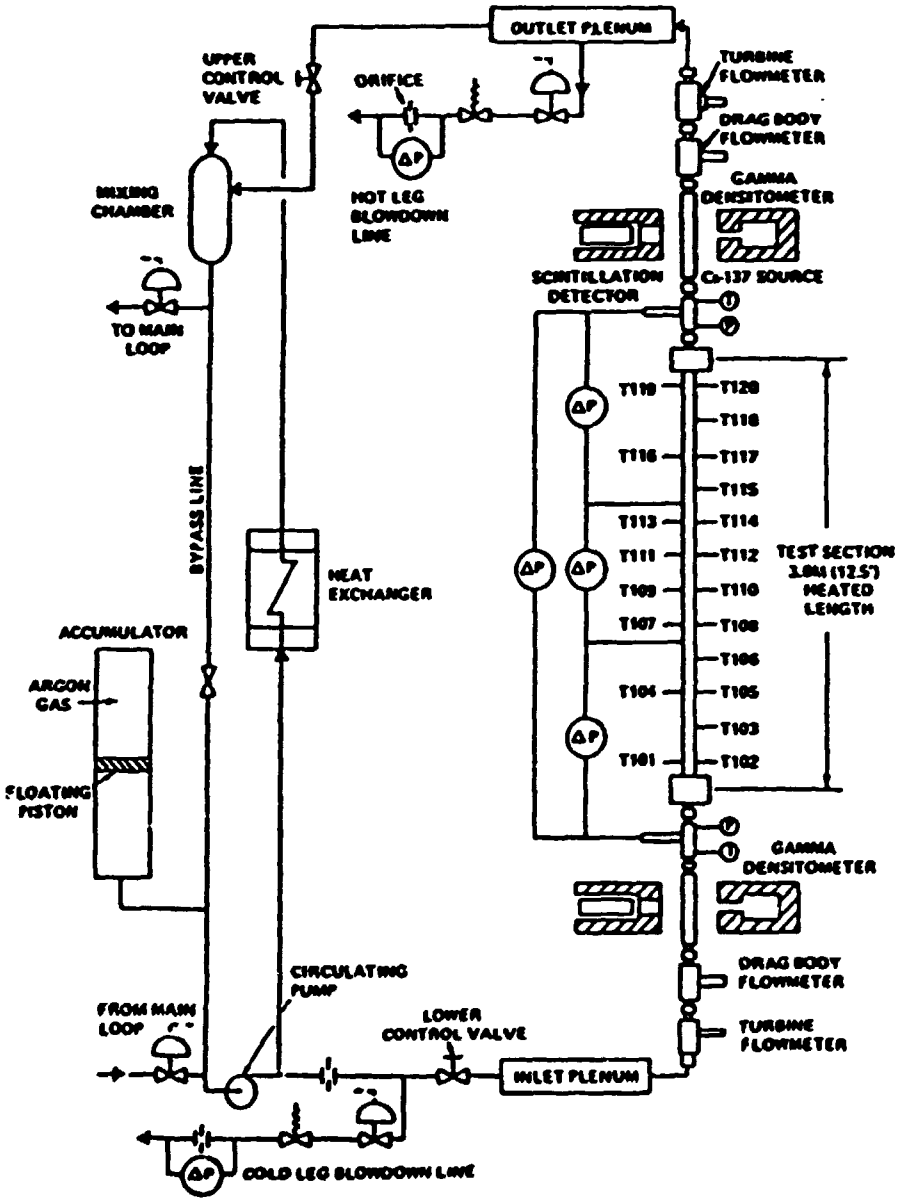

FIG. B2.9 CE/EPRI SINGLE TUBE BLOWDOWN LOOP (FROM REF. 59)

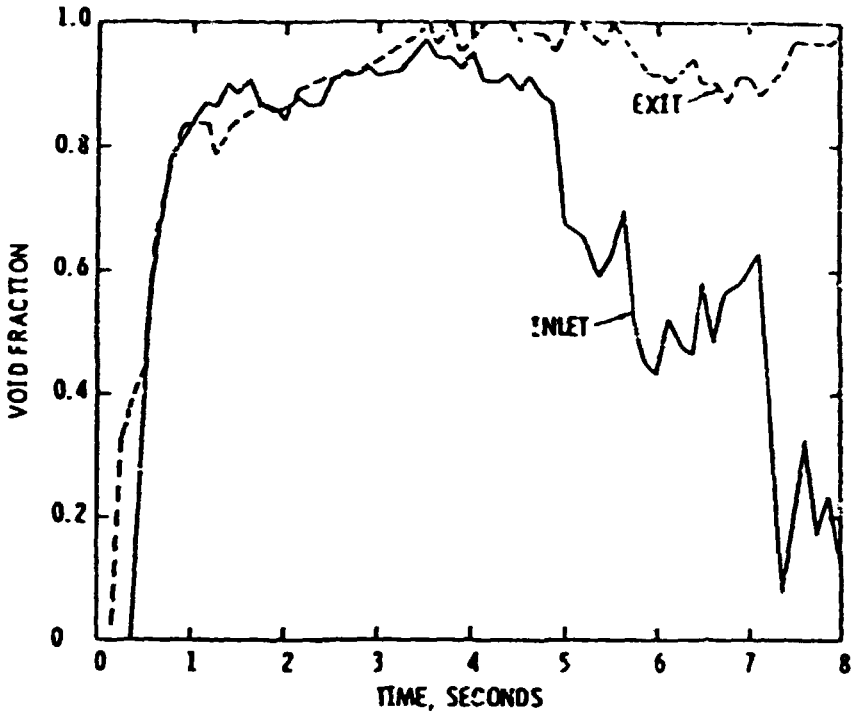

FIG. B2.10 Single tube transient void fractions
(FROM REF. 59)

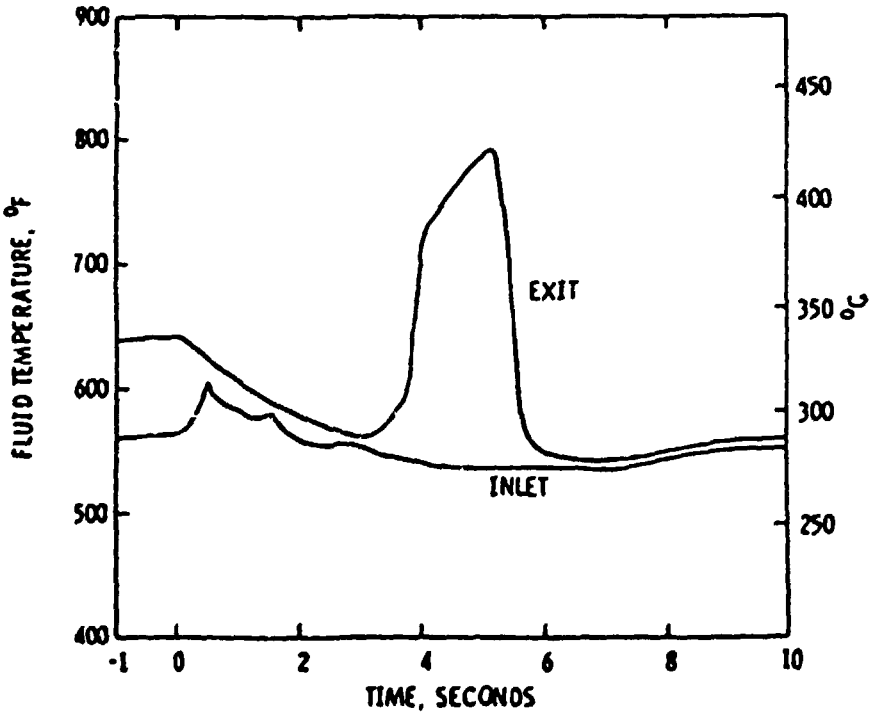

FIG. B2.11 Single tube transient fluid temperatures
(FROM REF. 59)

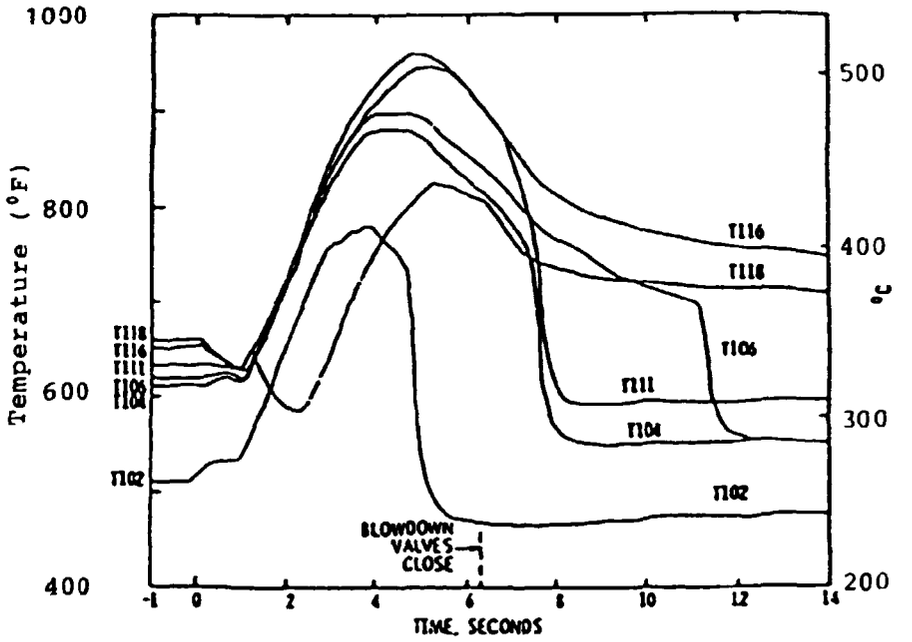

FIG. B2.12 TEST SECTION WALL SURFACE TEMPERATURES (FROM REF. 59)

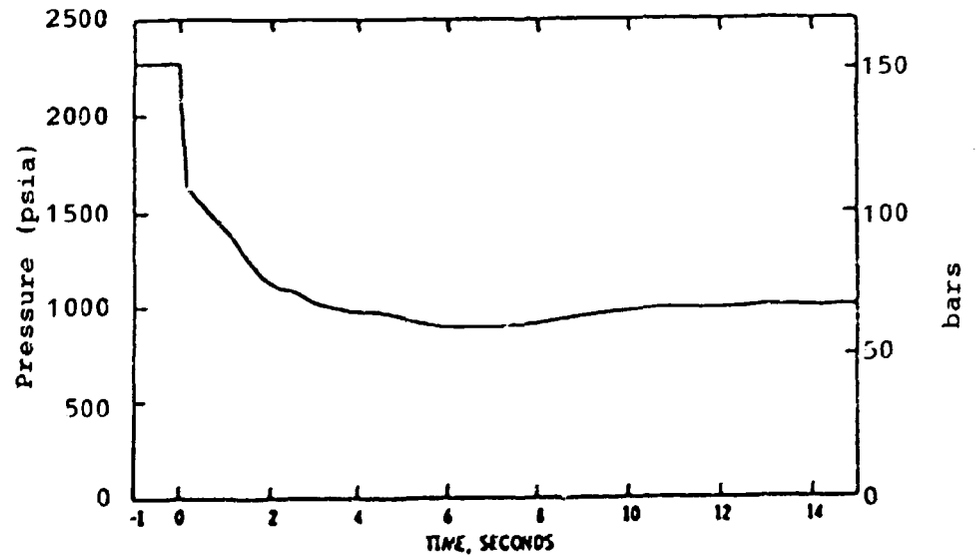

FIG. B2.13 TEST SECTION EXIT PRESSURE (FROM REF. 59)

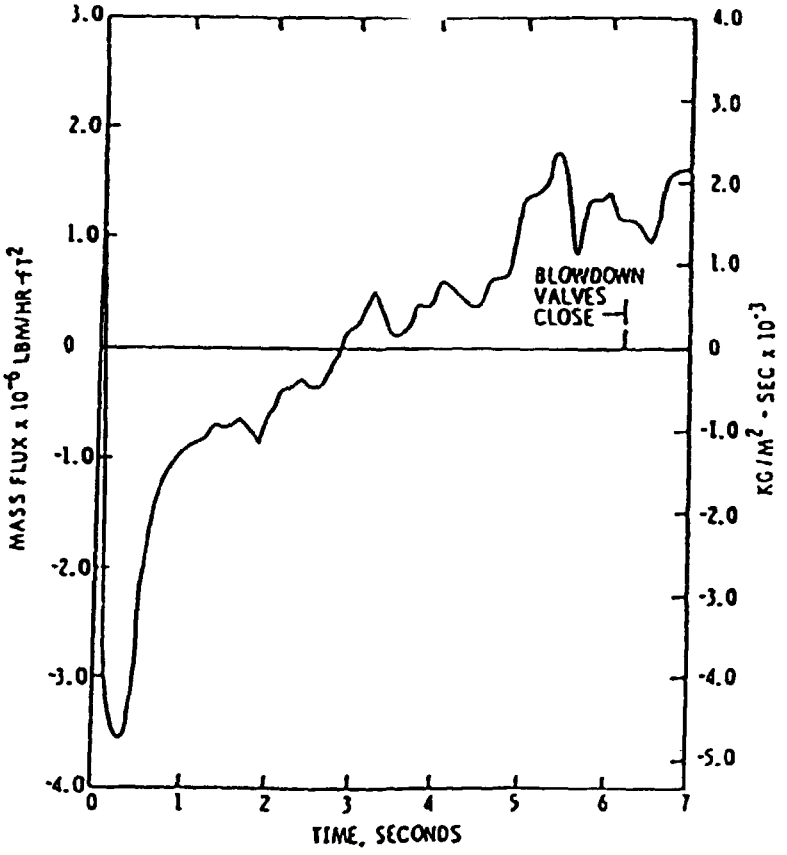

FIG. B2.14 TEST SECTION INLET MASS FLUX (FROM REF. 59)

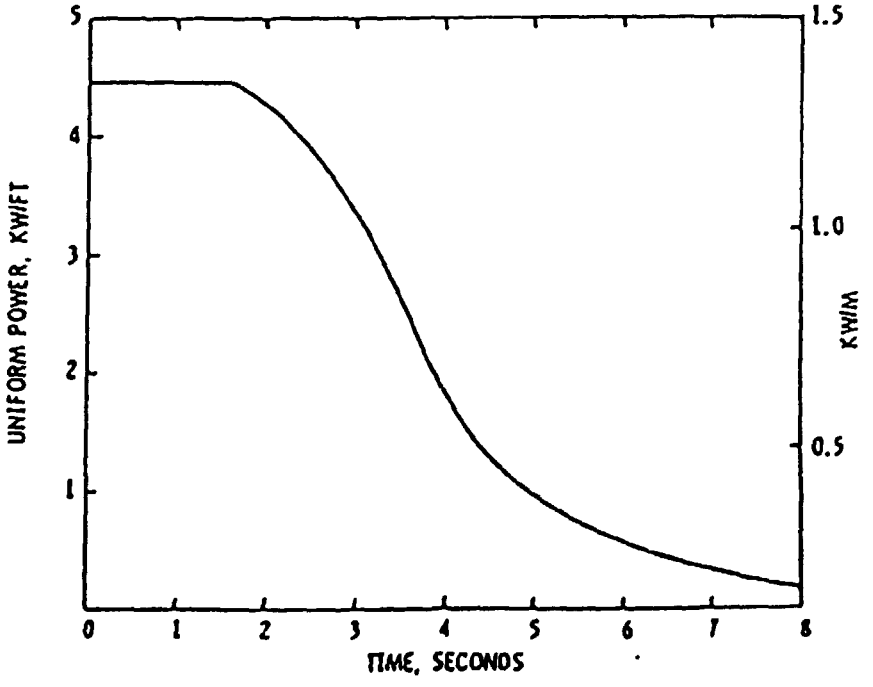

FIG. B2.15 TEST SECTION POWER (FROM REF. 59)

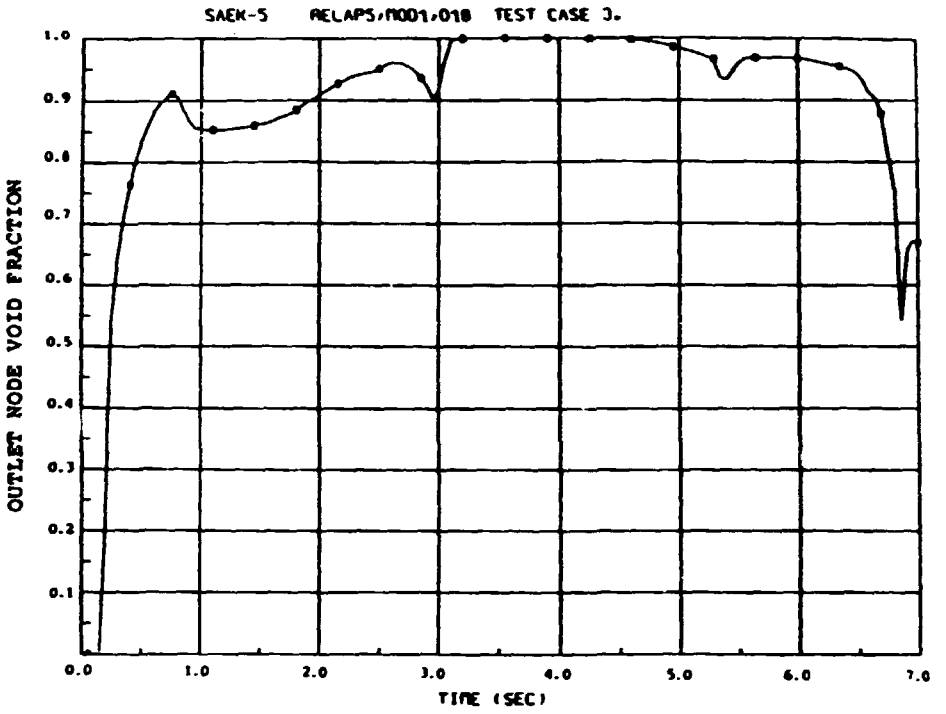

Fig. B2.16 CE/EPRI Case

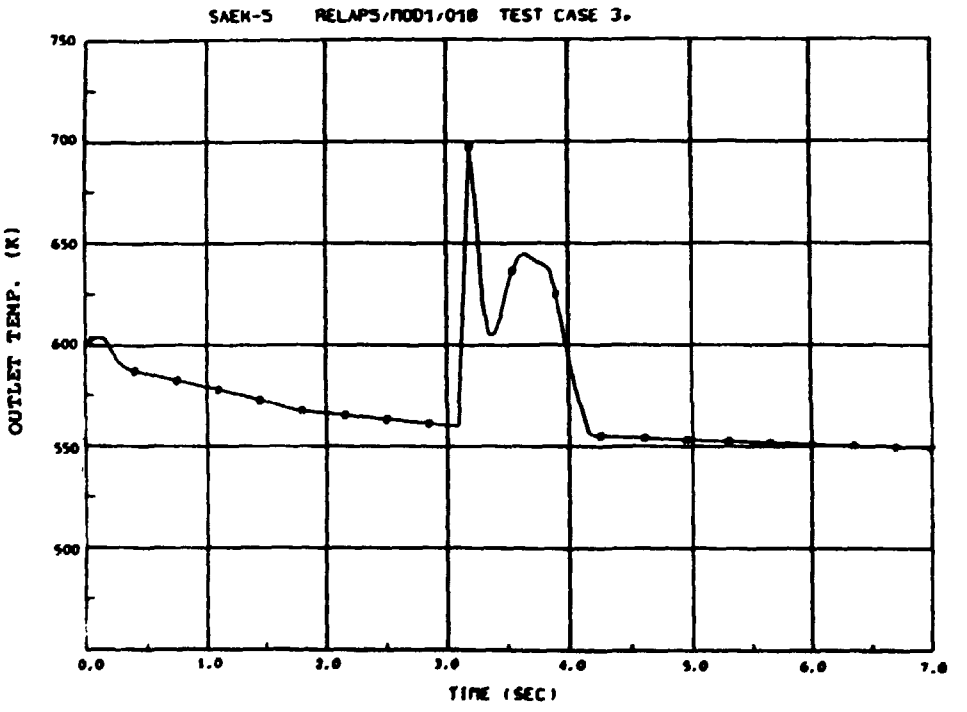

Fig. B2.17 CE/EPRI Case

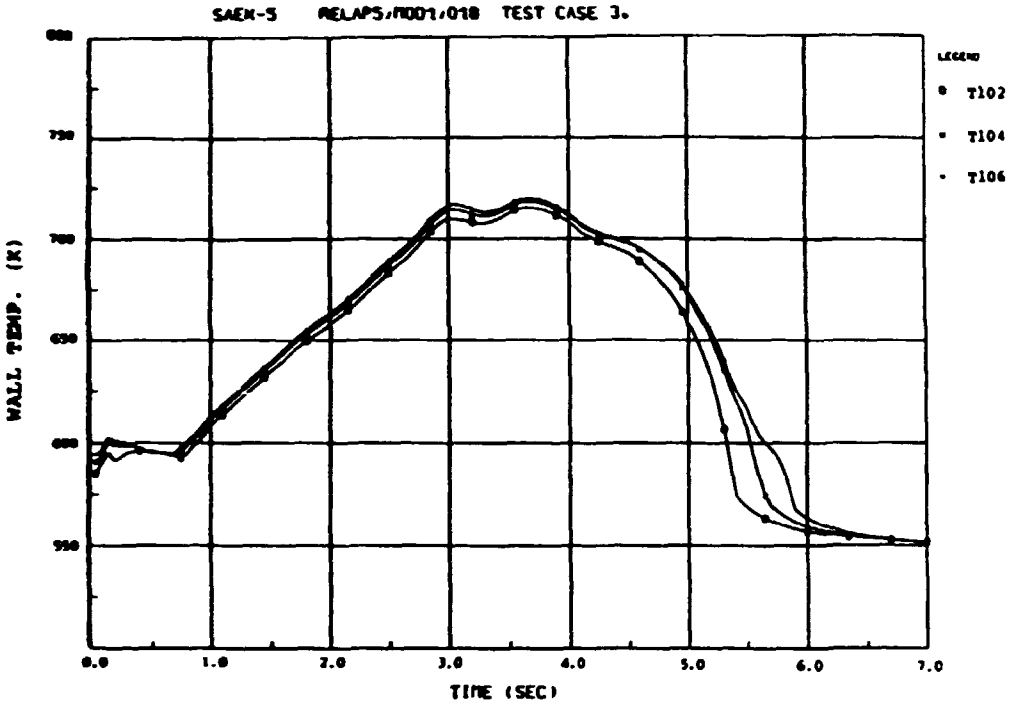

Fig B2.18 CE/EPRI Case

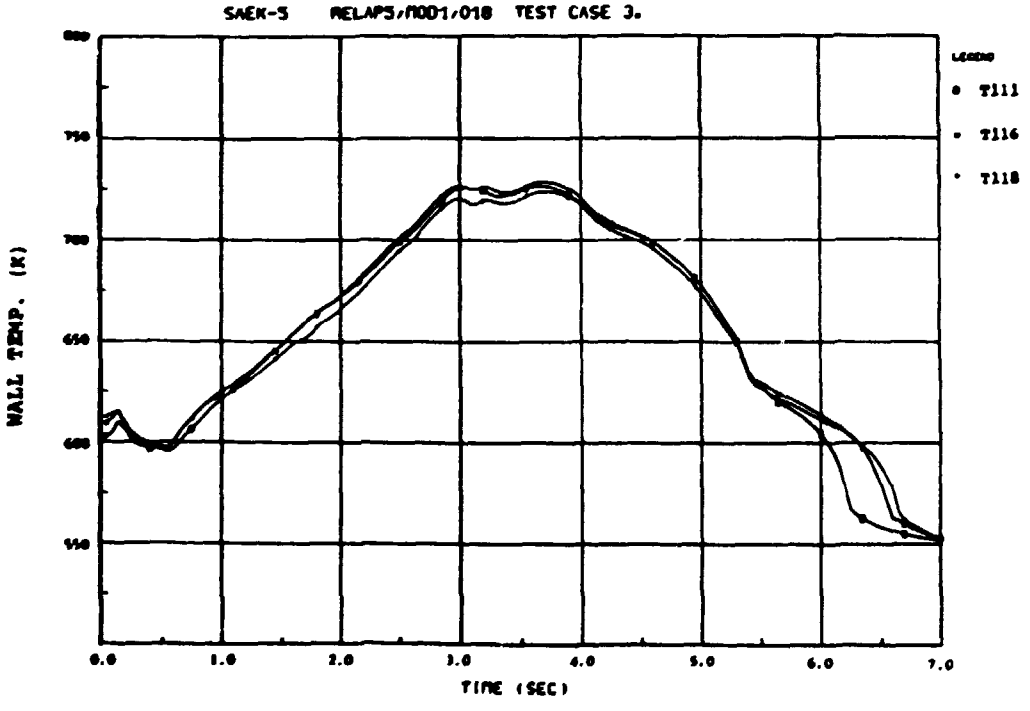

Fig B2.19 CE/EPRI Case

It soon became obvious from the results of the simulations of the three transient test cases described above that the calculations were influenced by a large number of utilized models and empirical correlations apart from the applied boundary conditions. Thus, it would be very difficult to assess the heat transfer correlations alone from these types of transient experiments. More simplified experiments were desirable, preferably steady-state experiments with well-defined boundary conditions. In order to cover the complete spectrum of heat transfer modes experiments in which it was desirable to exceed CHF. Two groups of experiments which met these new requirements were found, the Becker and ORNL experiments.

The Becker Experiments

The Becker experiments were selected from a series of CHF and post-CHF experiments reported in (2). As the CHF in these experiments all were of the annular liquid film dryout type, the term dryout (DO) will be used henceforth. The test section used in these experiments was a vertical tube, directly heated in the tube wall and insulated on the outer surface. The inside diameter was 0.0149 m and the heated length was 7 m with an uniform power distribution. The lower 3 m was instrumented with wall thermocouples at every 0.25 m and the upper 4 m at every 0.1 m (cf Fig. B2.20).

The steady-state conditions for the seven selected cases are shown in Table 4.2.I. The cases were calculated with the computer programmes RELAP5/MOD1, TRAC(PF1) and NORAS (the steady state version of NORA) and the steady state conditions in Table 4.2.I were used as boundary conditions, viz. exit pressure, inlet mass flow, inlet subcooling and heat flux.

The first calculations of these test cases (or some of the cases) are reported in (60) to (63). As there were no provisions in RELAP5 nor in TRAC to calculate the steady state this had to be done by analyzing a transient with time-invariant boundary conditions until the solution was stable. With 20 to 35 axial

nodes the CPU-time on a CDC CYBER 170-835 computer for obtaining the steady state in these cases ended up in the range 10 to 20 minutes while the NORAS programmes required only a few seconds. For that reason only some of the selected seven cases were calculated with RELAP5 and TRAC while all of them were calculated with NORAS.

The RELAP5/MOD1 calculations were carried out with two different CHF-correlations, the W-3 correlation (4) and the Biasi correlations (5). In all of the cases using the W-3 correlation the predicted locus of DO were too far upstream. In the calculations using the Biasi correlations the high flow DO was due to a cut-off void limit of 0.96. A more thorough examination of these results revealed that the value of DO too far upstream was caused by some flow oscillations during the course to steady state in combination with the incapability of RELAP5 to rewet an initially dry surface without decreasing the surface temperature, i.e. without decreasing the power.

The results from the TRAC(PF1) calculations revealed fairly accurate DO predictions. TRAC applies the Biasi correlation; however, in none of the cases did this correlation determine the locus of DO. Rather, an arbitrarily chosen cutoff void limit of 0.97 caused DO.

Both RELAP5 and TRAC calculations revealed significant discrepancies between predicted and measured wall surface post-DO temperatures. The post-DO conditions are known to be strongly dependent on the conditions at the locus of DO. It was therefore not possible to decide whether wall temperature discrepancies were due to an erroneous prediction of post-DO heat transfer.

The NORAS calculations (63) used three different CHF-correlations: Biasi, CISE4 and Becker (64). Biasi and Becker correlations predicted DO as lying too far downstream while, on the other hand, the CISE4 correlation predicted DO as too far upstream at high quality and too far downstream at low quality. Calculations were also performed with either Biasi or CISE4 correlation adjusted by a factor to obtain predicted DO locations as close as possible to

measured values. This was made in order to obtain a reasonable comparison between predicted and measured post-DO wall surface temperatures. The results from these calculations indicated that the post-DO interfacial heat transfer needed some improvements. For Becker case 1 the interfacial heat transfer was varied until a satisfactory agreement between predicted and measured post-DO temperatures was obtained (Fig. B2.21).

The major conclusions from these calculations were that the DO predictions in all of the codes needed substantial improvements and that the post-DO heat transfer calculations needed refinements.

Some examinations of the heat transfer package of RELAP5/MOD1 (65,66) revealed that the static equilibrium quality was used as an input to correlations even though the equilibrium flow quality was used in the development of the correlations. At the DO location the vapour velocity may be much higher than that of the liquid. Consequently, the flow quality will be higher than the static quality. This means that the use of static quality in a correlation will result in higher critical heat flux than if the flow quality was used.

It was also apparent that the interfacial heat transfer was too high in RELAP5 and TRAC(PF1) and too low in NORA.

In order to examine the post-DO heat transfer calculations in RELAP5/MOD1 and TRAC(PF1) five of the Becker test cases were recalculated with the experimental locus of DO given as input (67,68). To accommodate this new input the RELAP5 and TRAC computer programme had to be somewhat modified, especially the input routines and the routine performing the CHF calculations. When the DO locus was inserted, the uncertainties in the DO predictions were eliminated and the results from the post-DO heat transfer calculations could be used to examine the pertinent models and correlations more thoroughly. The results from the calculations with RELAP5 are shown in Figs. B2.22 to B2.26. The predicted post-DO wall temperatures were significantly lower than the measured ones. Moreover, it appeared that the calculations

of the nonequilibrium effects typical for the post-DO regime were inadequate in that no vapour superheat was calculated (the liquid and vapour post-DO temperatures we· about the same).

Four cases were recalculated with a test version of RELAP5/MOD 1 in which the post-DO interfacial mass transfer and the post-DO wall-to-fluid heat tranfer models were completely modified (69). The vapour phase was now allowed to be superheated when the quality exceeded the quality at DO rather than a fixed value*. In the post-DO region the vapour generation rate was calculated from a new correlation (6) and the wall heat transfer was assumed to take place from the wall surface to the superheated vapour phase only. The predicted wall temperature distributions in the post-DO region showed substantial improvements compared to the earlier calculations (Figs. B2.27 to B2.30).

The modifications outlined above had been adopted ealier in NORAS (70,71) and the Becker cases had been recalculated. The NORAS calculations then gave about the same temperature distributions in the post-DO region as the RELAP5 calculations described above. The modified NORAS was also used to simulate some rod bundle experiments conducted at ORNL. These are discussed below.

---

* Originally RELAP5 made use of a fixed static quality value to determine which phase was saturated. If the static quality was less than 0.5 the vapour phase was saturated; otherwise the liquid phase was saturated. The phase that was unsaturated was allowed to be either subcooled or superheated.

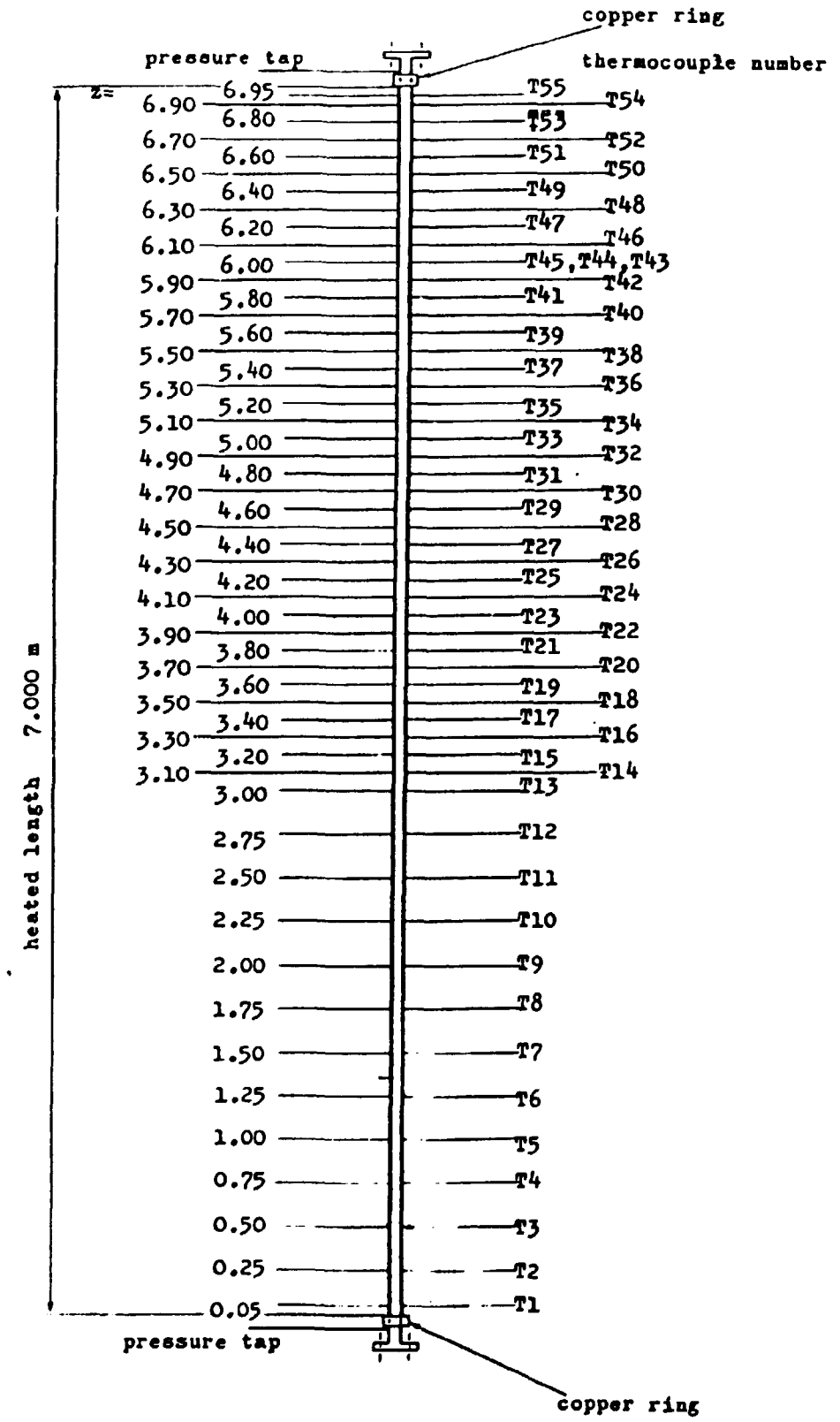

FIG. B2.20 BECKER TEST SECTION (FROM REF. 2)

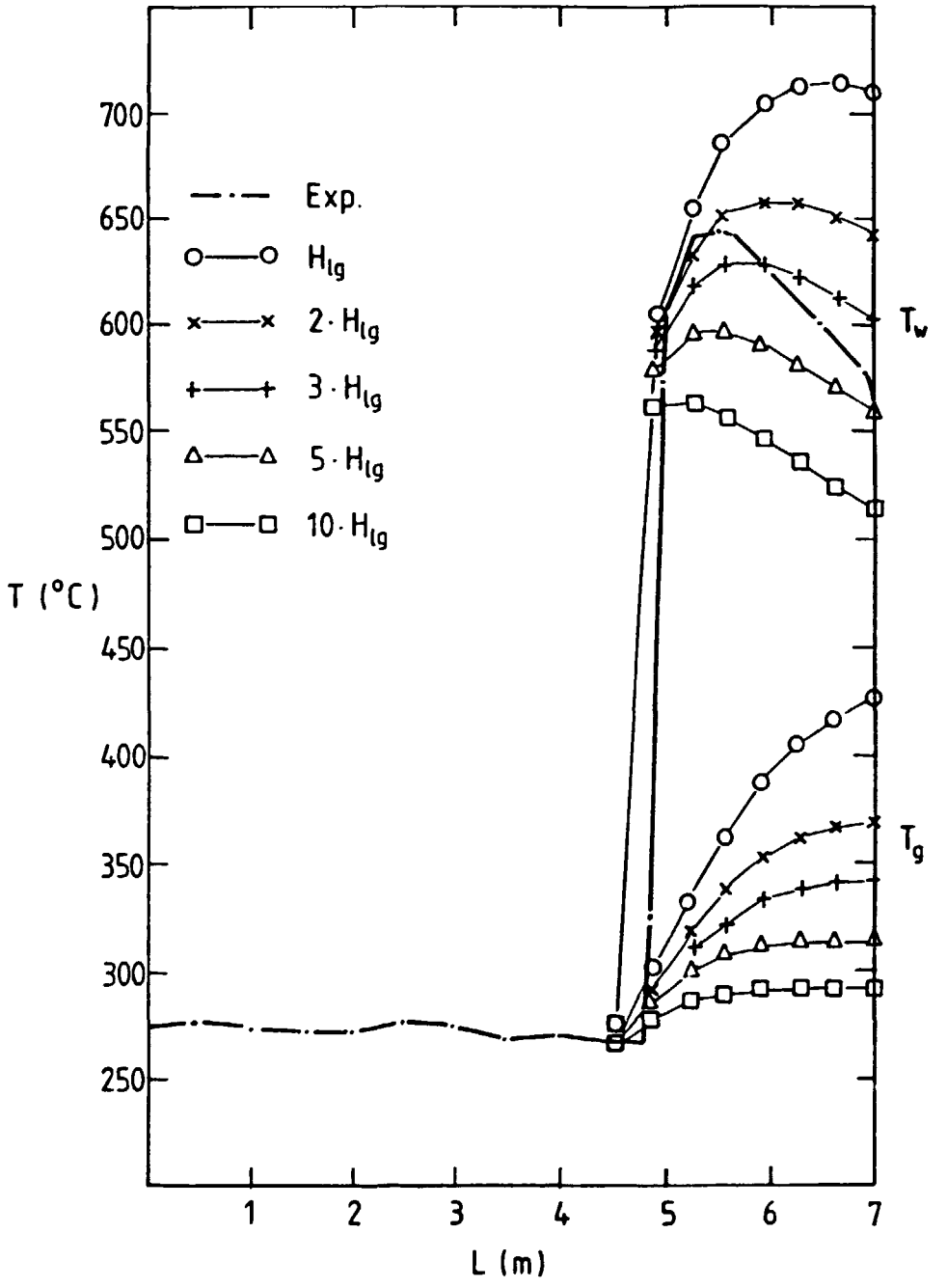

Fig. B2.21 BECKER CASE 1

NORA TEMPERATURES

P = 5.2 MPa G = 1476 kg/m^2 s

ΔT_{sub} = 9.8 K Q = 1.015 MW/m^2

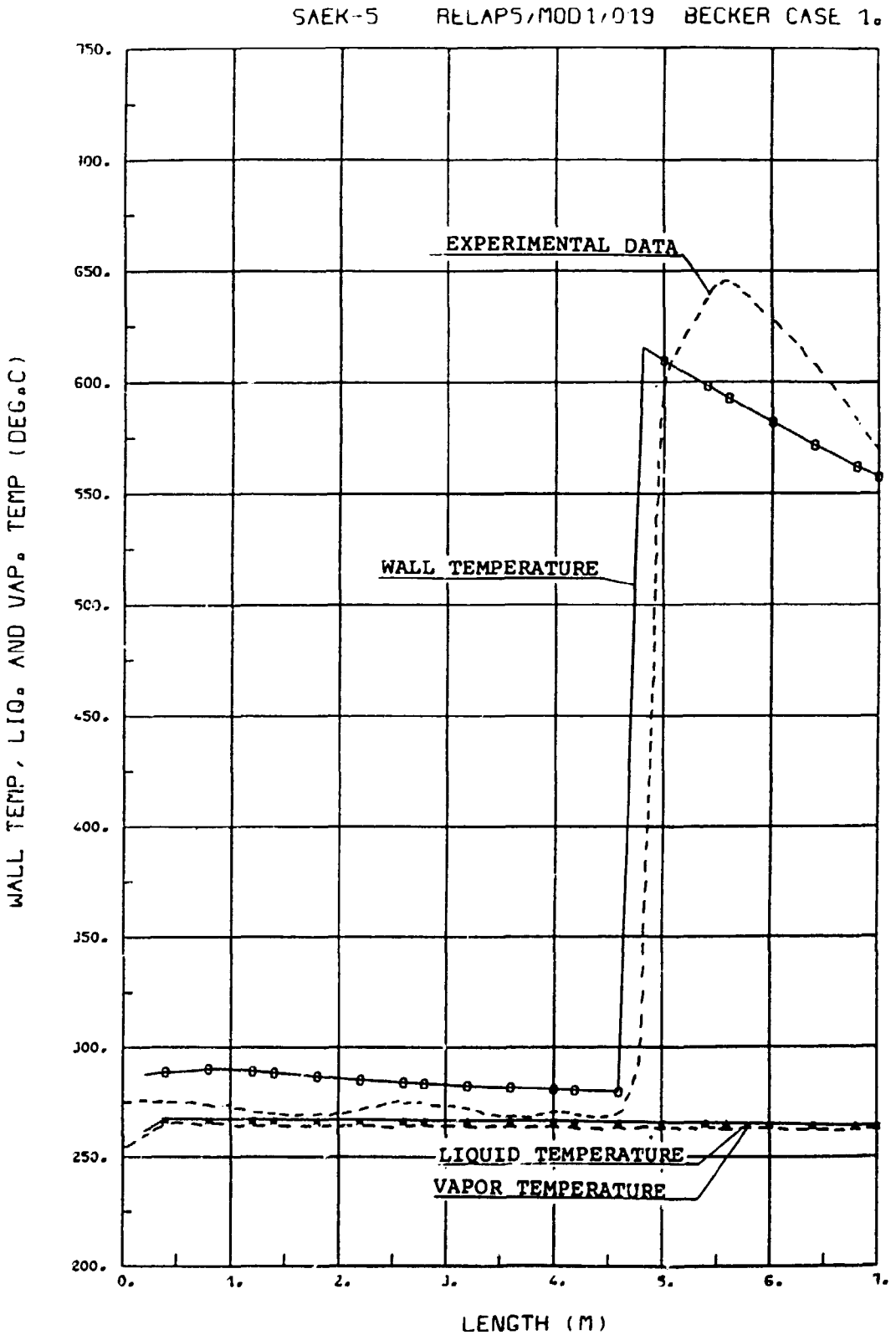
SAEK-5 RELAP5/MOD1/019 BECKER CASE 1.
WALL TEMP, LIQ. AND VAP. TEMP (DEG.C)
750.
700.
650.
600.
550.
500.
450.
400.
350.
300.
250.
200.
0.
1.
2.
3.
4.
5.
6.
7.
LENGTH (M)
EXPERIMENTAL DATA
WALL TEMPERATURE
LIQUID TEMPERATURE
VAPOR TEMPERATURE

FIGURE B2.22

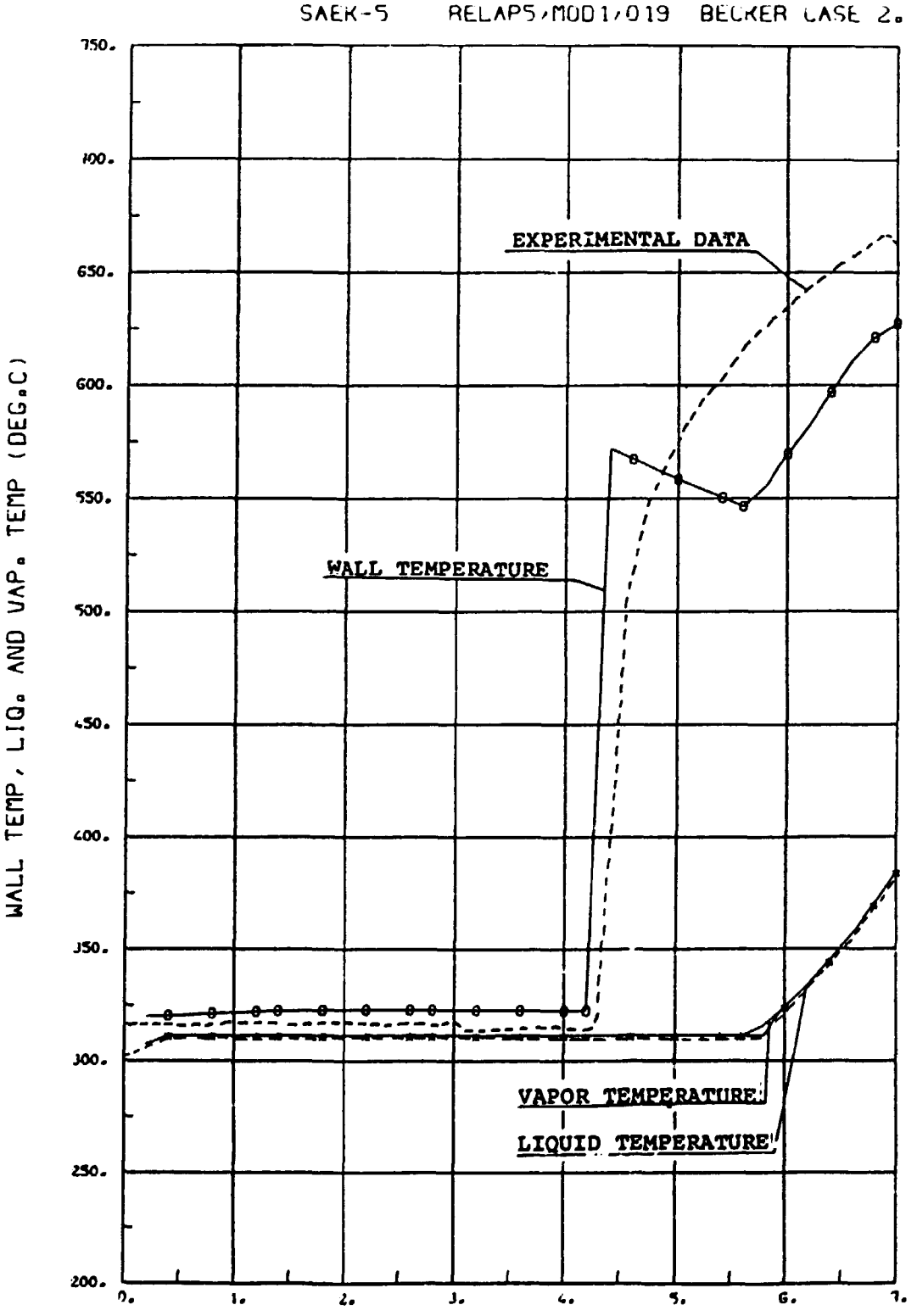
SAEK-5 RELAP5/MOD1/019 BECKER CASE 2.
WALL TEMP, LIQ. AND VAP. TEMP (DEG.C)
750.
700.
650.
600.
550.
500.
450.
400.
350.
300.
250.
200.
0.
1.
2.
3.
4.
5.
6.
7.
EXPERIMENTAL DATA
WALL TEMPERATURE
VAPOR TEMPERATURE
LIQUID TEMPERATURE
LENGTH (M)

FIGURE B2.23

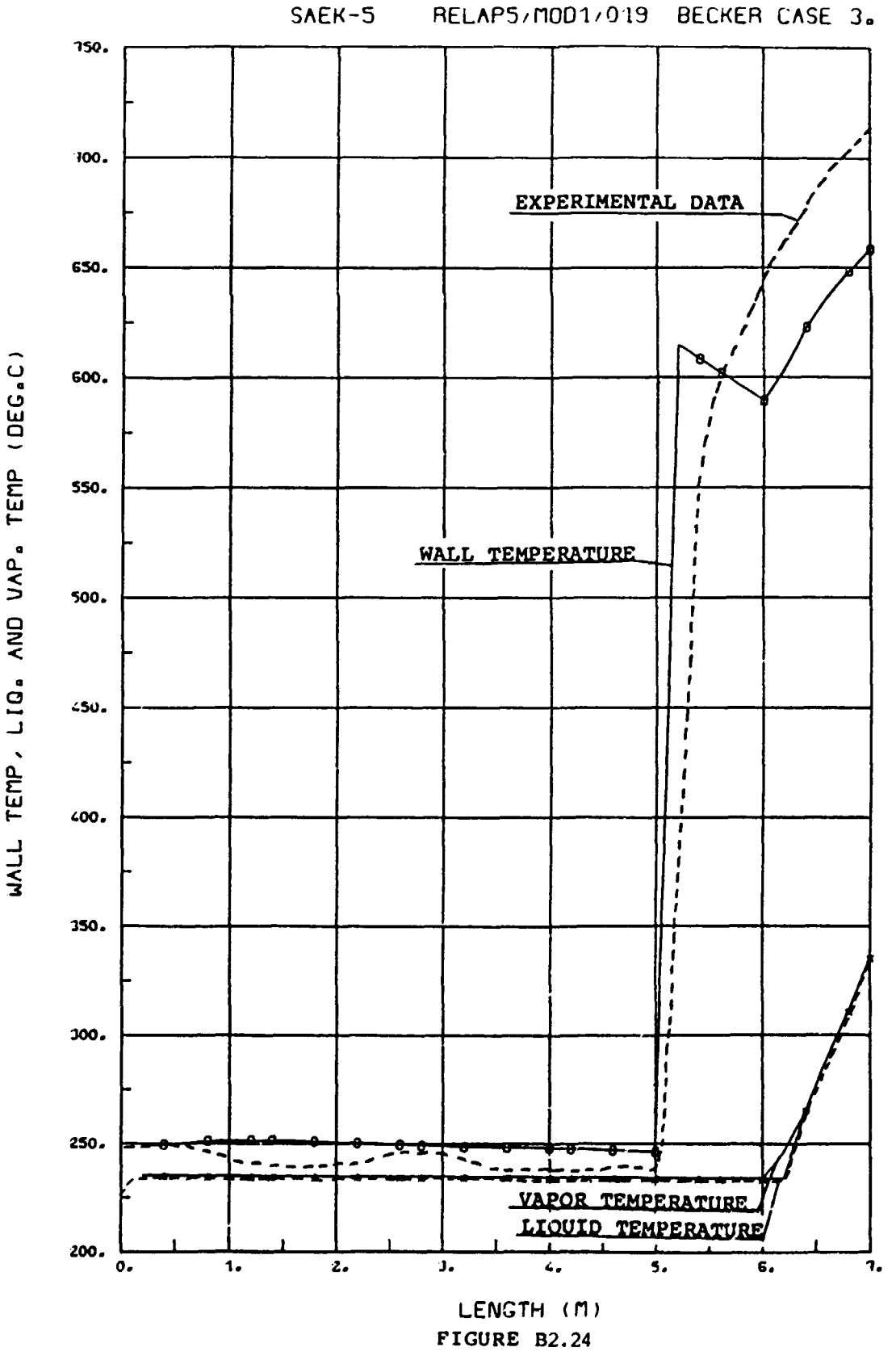
SAEK-5 RELAP5/MOD1/019 BECKER CASE 3.
EXPERIMENTAL DATA
WALL TEMPERATURE
VAPOR TEMPERATURE
LIQUID TEMPERATURE
WALL TEMP, LIQ. AND VAP. TEMP (DEG.C)
LENGTH (M)
750.
700.
650.
600.
550.
500.
450.
400.
350.
300.
250.
200.
0.
1.
2.
3.
4.
5.
6.
7.

FIGURE B2.24

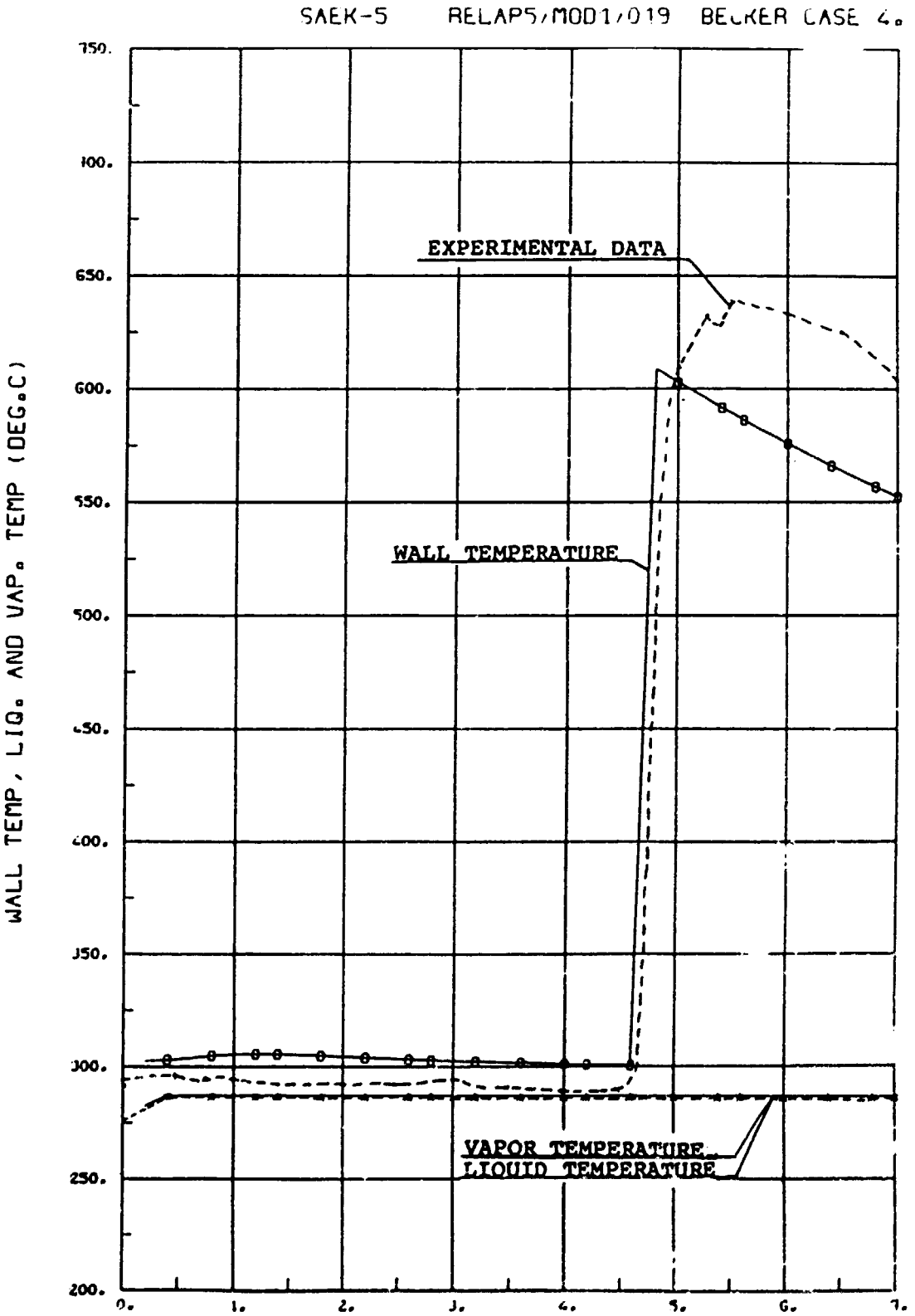
SAEK-5 RELAP5/MOD1/019 BECKER CASE 4.
WALL TEMP, LIQ. AND VAP. TEMP (DEG.C)
750.
700.
650.
600.
550.
500.
450.
400.
350.
300.
250.
200.
0.
1.
2.
3.
4.
5.
6.
7.
LENGTH (M)
EXPERIMENTAL DATA
WALL TEMPERATURE
VAPOR TEMPERATURE
LIQUID TEMPERATURE

FIGURE B2.25

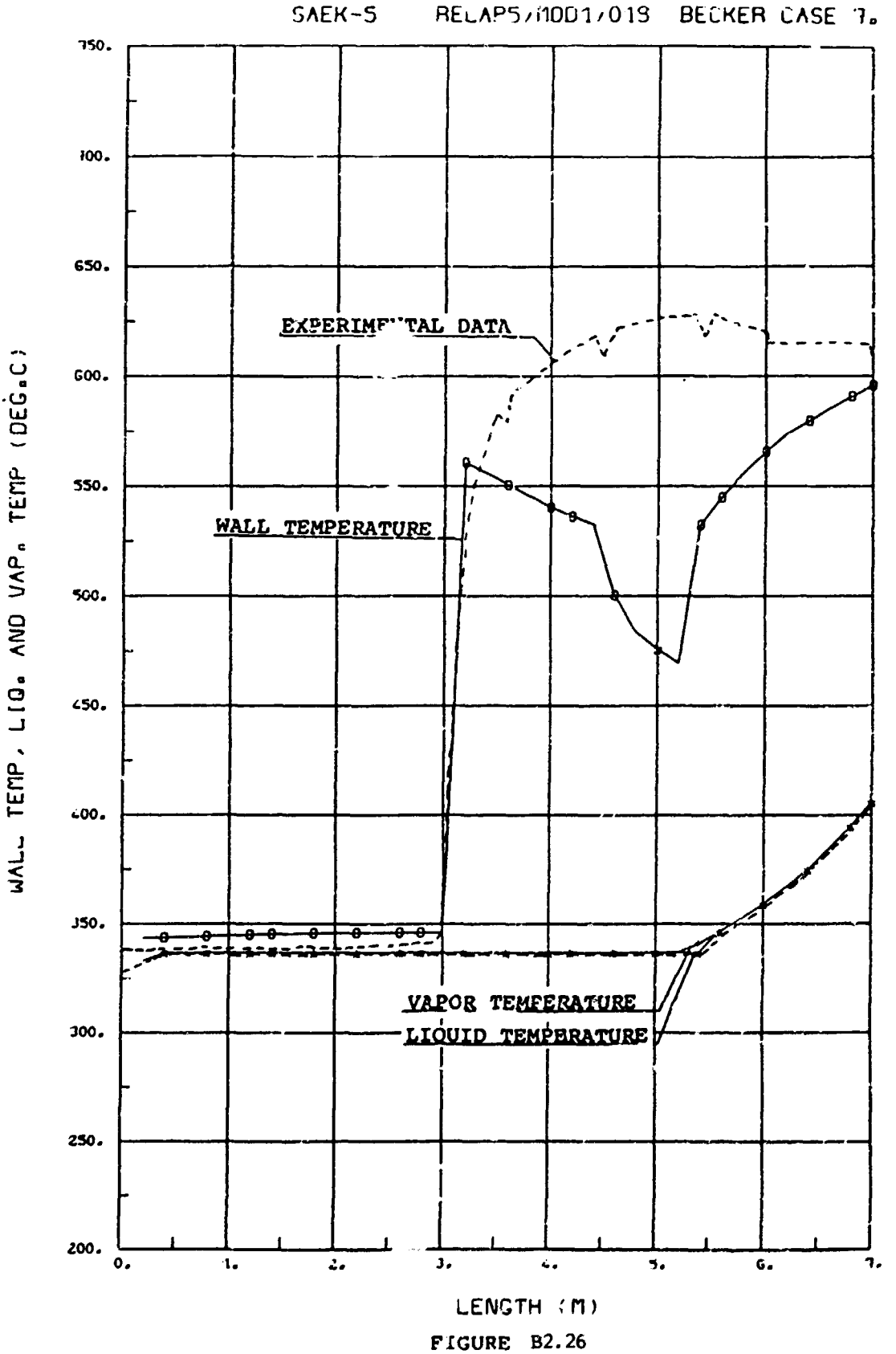
SAEK-S RELAP5/MOD1/018 BECKER CASE 7.
750.
700.
650.
600.
550.
500.
450.
400.
350.
300.
250.
200.
0.
1.
2.
3.
4.
5.
6.
7.
WALL TEMP, LIQ. AND VAP. TEMP (DEG.C)
LENGTH (M)
EXPERIMENTAL DATA
WALL TEMPERATURE
VAPOR TEMPERATURE
LIQUID TEMPERATURE

FIGURE B2.26

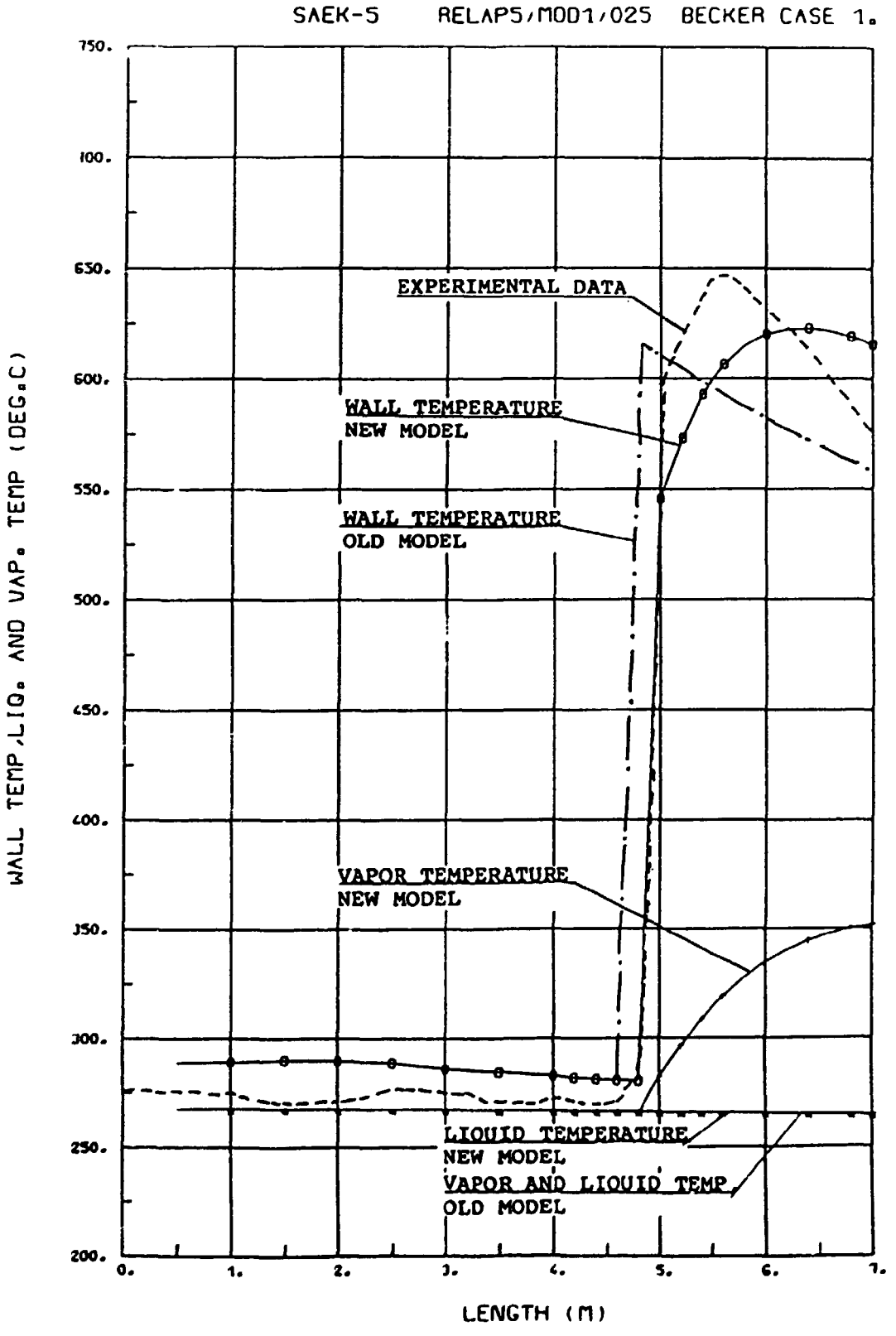
SAEK-S RELAP5/MOD1/025 BECKER CASE 1.
WALL TEMP/LIQ. AND VAP. TEMP (DEG.C)
LENGTH (M)
EXPERIMENTAL DATA
WALL TEMPERATURE
NEW MODEL
WALL TEMPERATURE
OLD MODEL
VAPOR TEMPERATURE
NEW MODEL
LIQUID TEMPERATURE
NEW MODEL
VAPOR AND LIQUID TEMP.
OLD MODEL
750.
700.
650.
600.
550.
500.
450.
400.
350.
300.
250.
200.
0.
1.
2.
3.
4.
5.
6.
7.

FIGURE B2.27

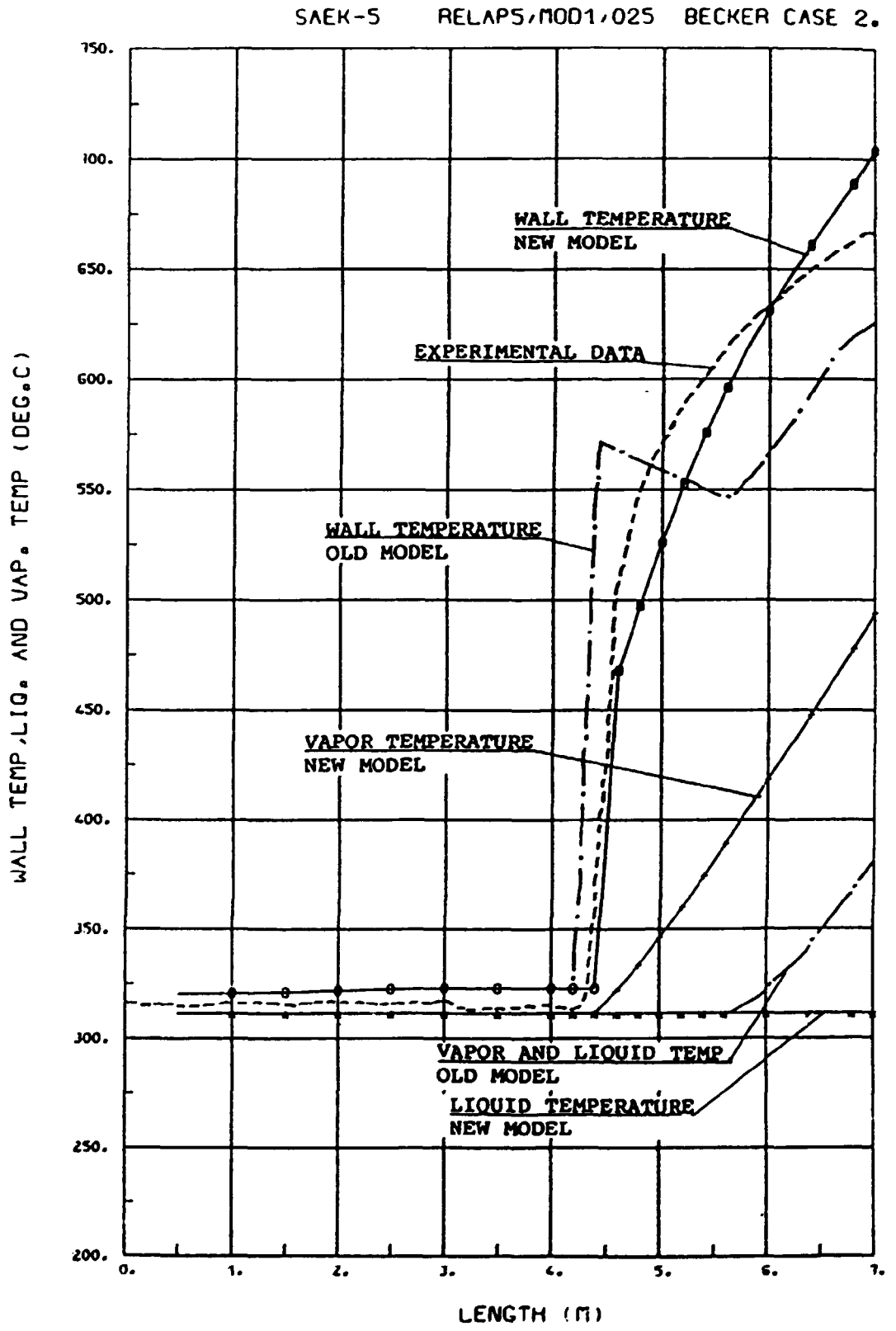
SAEK-S RELAP5/MOD1/025 BECKER CASE 2.
WALL TEMP,LIQ. AND VAP. TEMP (DEG.C)
750.
700.
650.
600.
550.
500.
450.
400.
350.
300.
250.
200.
0.
1.
2.
3.
4.
5.
6.
7.
LENGTH (M)
WALL TEMPERATURE
NEW MODEL
EXPERIMENTAL DATA
WALL TEMPERATURE
OLD MODEL
VAPOR TEMPERATURE
NEW MODEL
VAPOR AND LIQUID TEMP
OLD MODEL
LIQUID TEMPERATURE
NEW MODEL

FIGURE B2.28

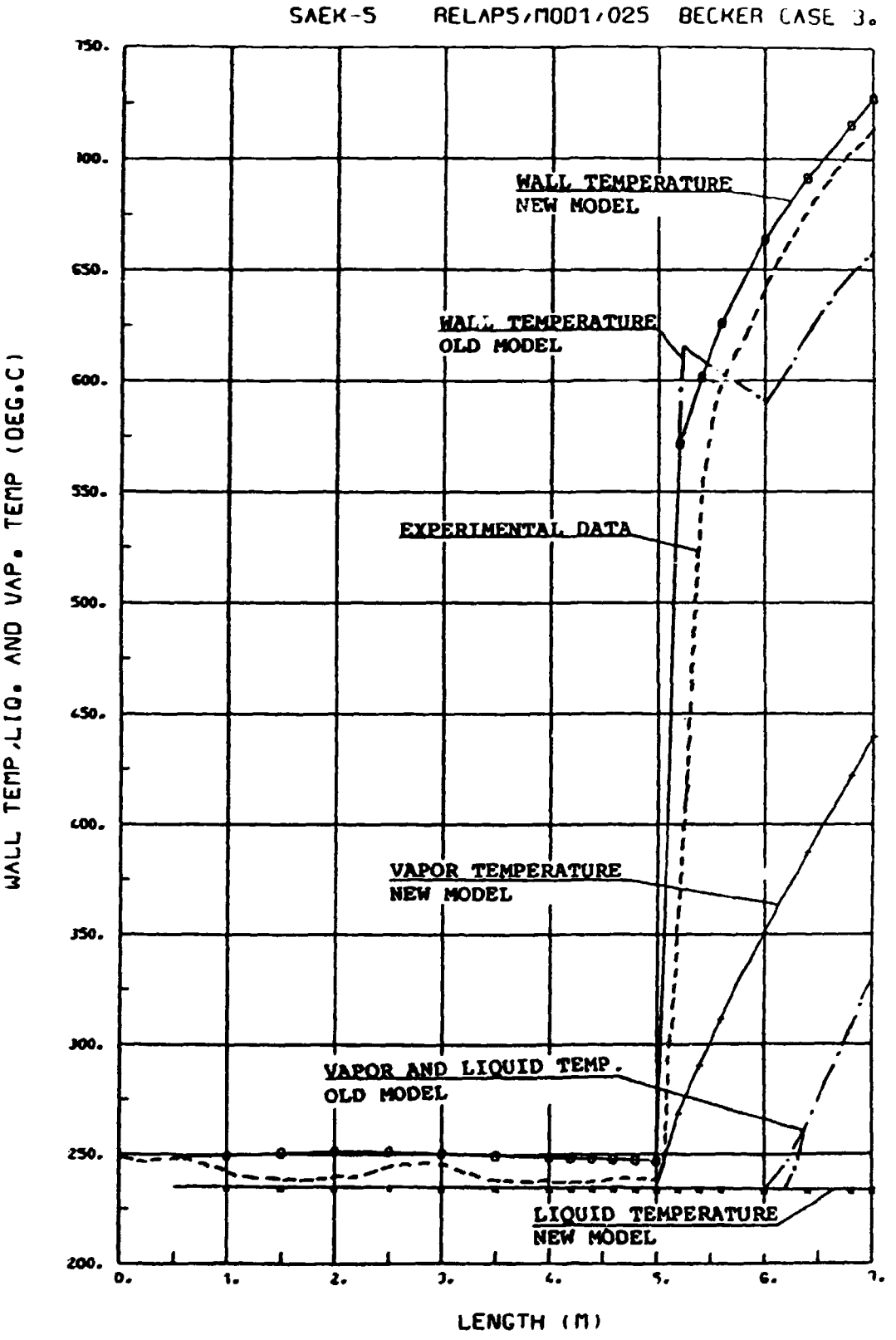
SAEK-S RELAP5/MOD1/025 BECKER CASE 3.
WALL TEMP./LIQ. AND VAP. TEMP (DEG.C)
750.
700.
650.
600.
550.
500.
450.
400.
350.
300.
250.
200.
0.
1.
2.
3.
4.
5.
6.
7.
LENGTH (M)
WALL TEMPERATURE NEW MODEL
WALL TEMPERATURE OLD MODEL
EXPERIMENTAL DATA
VAPOR TEMPERATURE NEW MODEL
VAPOR AND LIQUID TEMP. OLD MODEL
LIQUID TEMPERATURE NEW MODEL

FIGURE B2.29

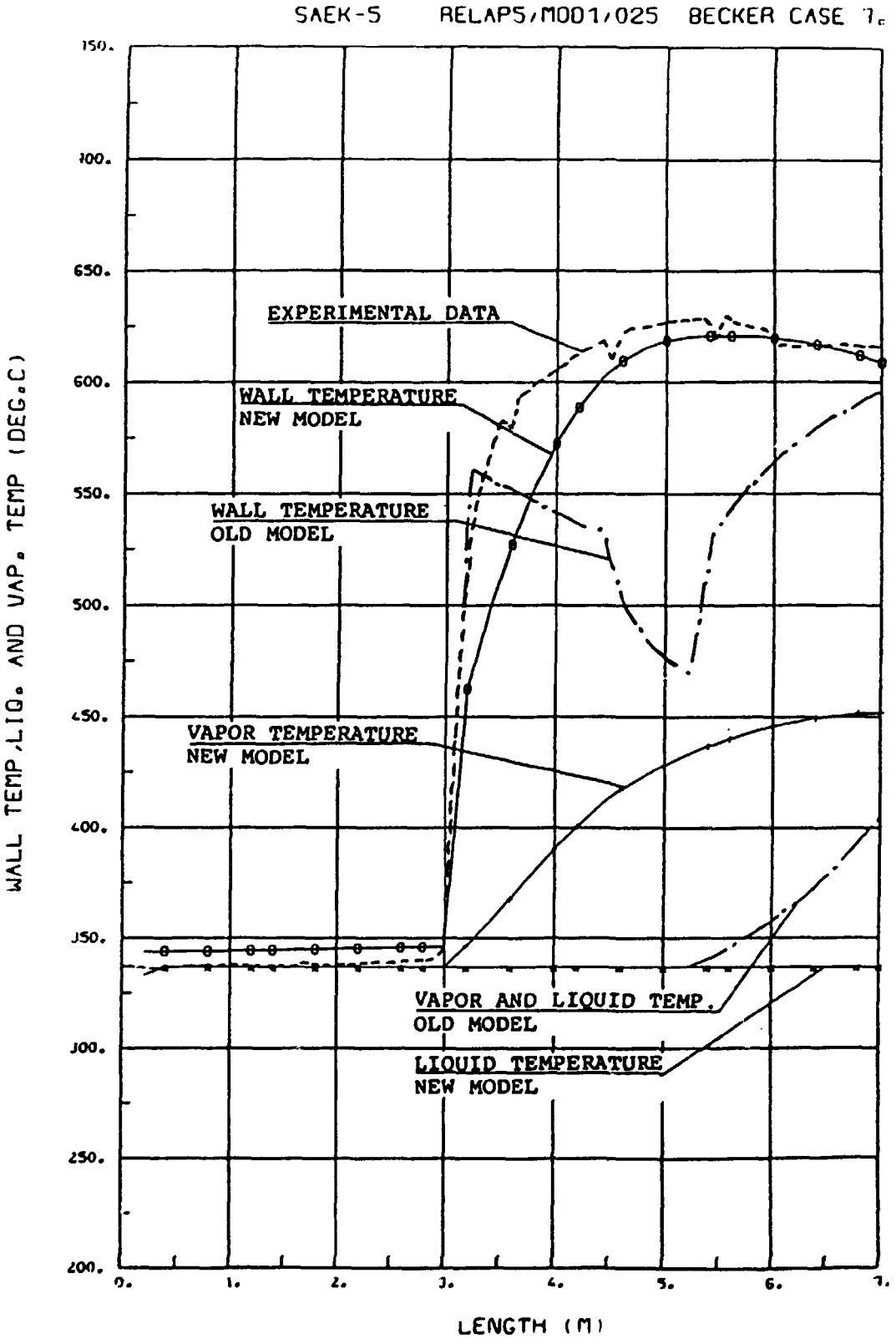
SAEK-5 RELAP5/MOD1/025 BECKER CASE 7
WALL TEMP,LIQ. AND VAP. TEMP (DEG.C)
LENGTH (M)
EXPERIMENTAL DATA
WALL TEMPERATURE
NEW MODEL
WALL TEMPERATURE
OLD MODEL
VAPOR TEMPERATURE
NEW MODEL
VAPOR AND LIQUID TEMP.
OLD MODEL
LIQUID TEMPERATURE
NEW MODEL
650.
600.
550.
500.
450.
400.
350.
300.
250.
200.
0.
1.
2.
3.
4.
5.
6.

FIGURE B2.30

The ORNL experiments

These experiments were conducted at Oak Ridge National Laboratory (ORNL) in the Thermal Hydraulic Test Facility (THTF) and are reported in (72). The test section was an electrically heated rod bundle comprising 64 rods in a square lattice. A cross section of the bundle is shown in Fig. B2.31 where a cross section of one of the heater rods is shown as well. The rod surface temperatures were estimated from measured internal temperatures and known heating power. The rod outside diameter was 0.0095 m and the rod pitch 0.0127 m.

The power distribution was uniform both axially and radially over the cross section. Figure B2.32 shows the axial locations of spacer grids and thermocouple levels. The heated length was 3.66 m.

Six experiments were selected as test cases from the complete series. The steady state conditions are given in Table 4.2.I. The bundle was modelled in NORAS as a 3.66 m long heated channel divided into 15 axial nodes of equal length (0.24 m). The 60 heated rods were represented by one single heated wall with heated perimeter equal to the sum of the heated perimeters of each heated rod. Hydraulically the bundle geometry was represented by a single channel with hydraulic diameter and flow area equal to those for the bundle.

The calculations were carried out with NORAS and the same models and correlations as in the Becker cases described above were used. Figures B2.33 to B2.38 show the calculated wall temperatures in comparison with the measured values. The measured values are given in terms of an average value for all rods at a particular level and the standard deviation. All rods where wetted are indicated on the top of the figures at the highest location in the channel. At the lowest location all rods were dry. The calculated vapour temperatures are shown as well.

The measured data clearly show the influence of the spacers. The spacer locations are indicated on the top of the figures.

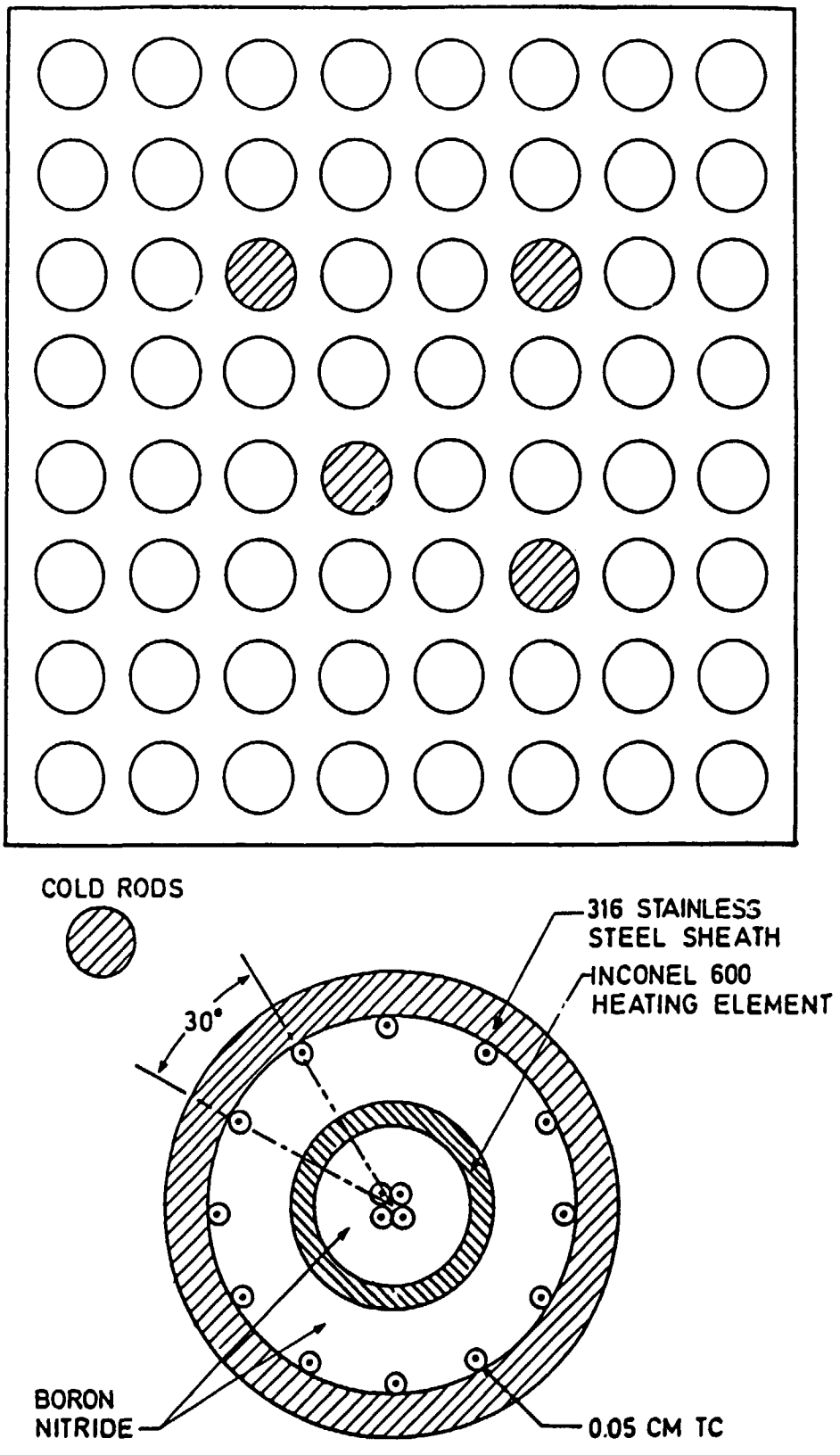

Fig. B2.31 ORNL - 64 rod test bundle. Cross section of bundle and single heater rod (FROM REF. 72)

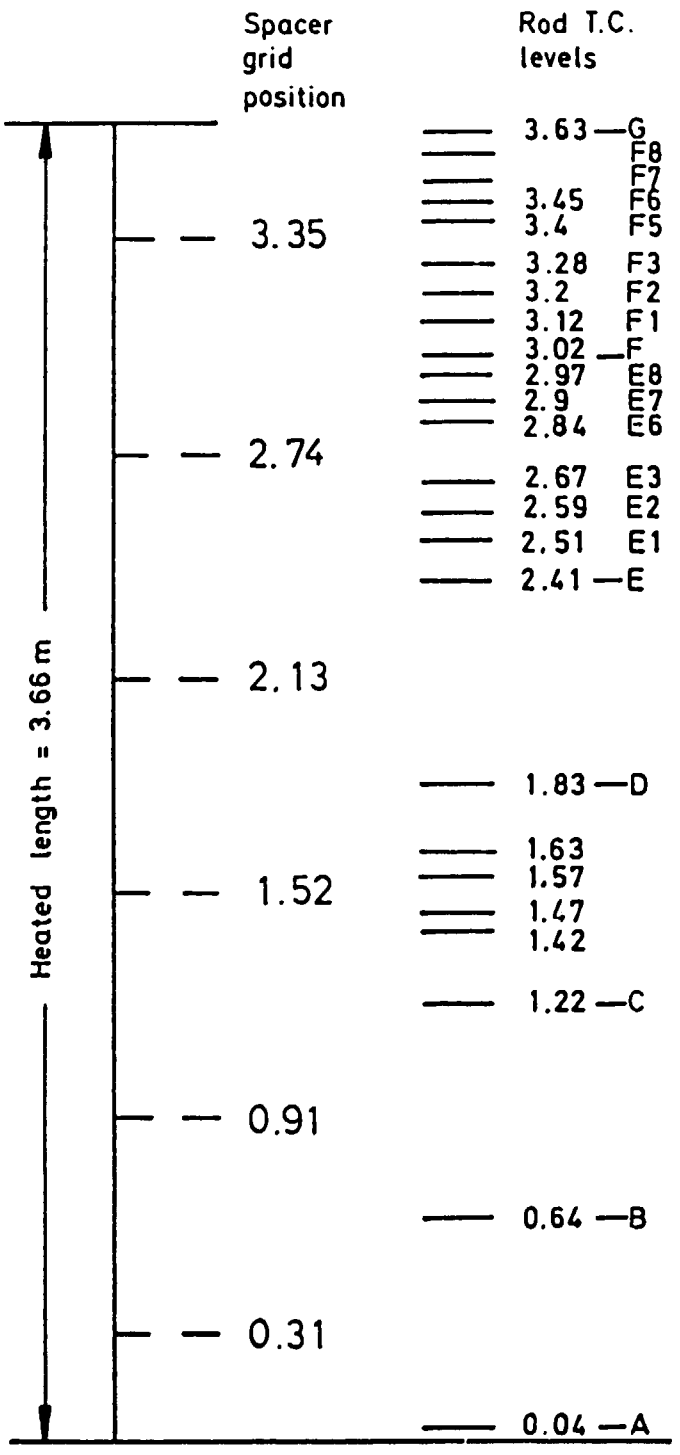

Fig. B2.32 Axial location of spacer grids and thermocouples for ORNL test bundle (FROM REF. 72)

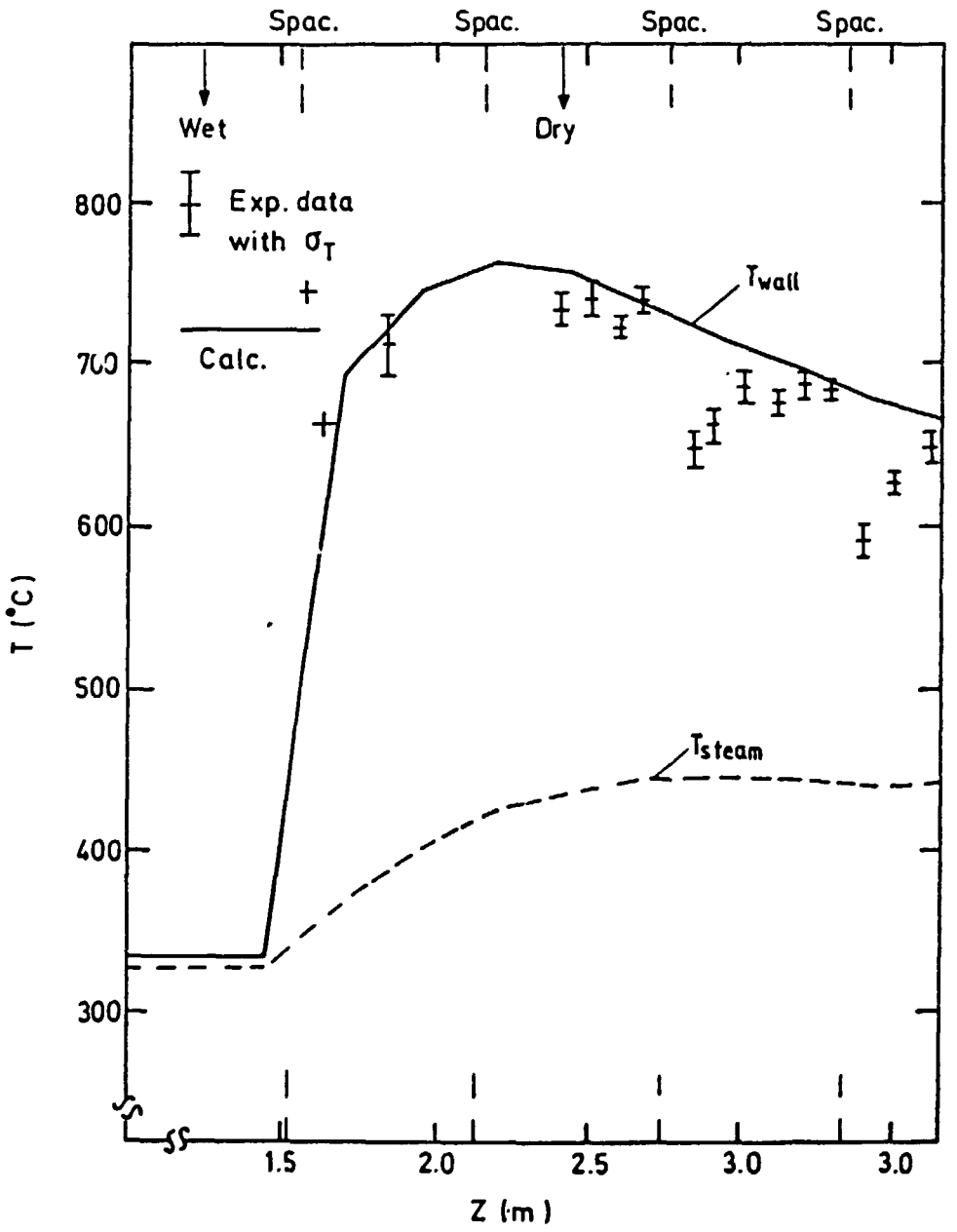

Fig. B2.33 ORNL Case B

P = 12.76 MPa $\quad \Delta T_{subc}$ = 19. °C

G = 712.9 kg/m^2 s $\quad T_{sat.}$ = 329.3 °C

Q = 0.91 MW/m^2

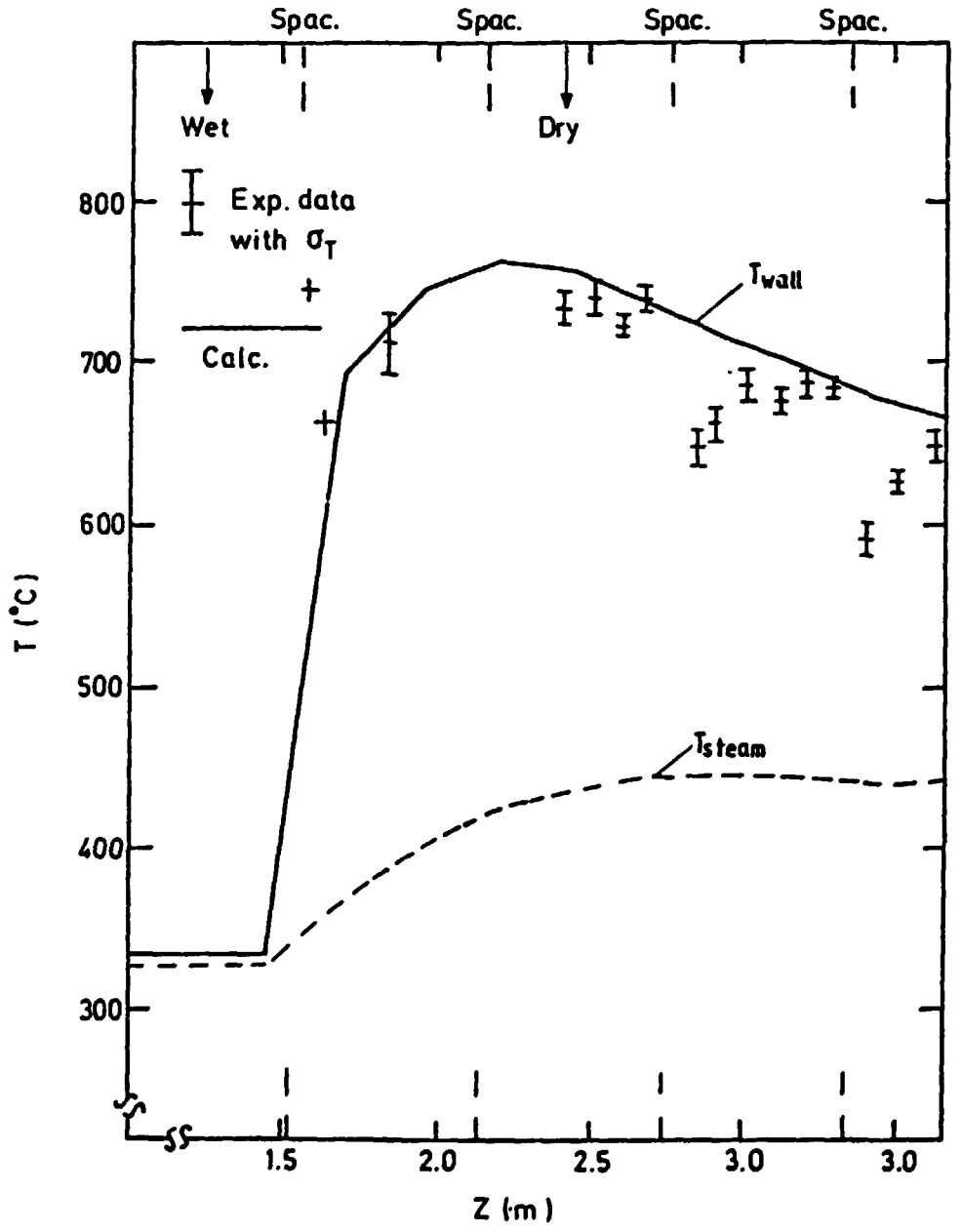

Fig. B2.33 ORNL Case B

P = 12.76 MPa $\quad \Delta T_{subc}$ = 19. °C

G = 712.9 kg/m^2 s $\quad T_{sat.}$ = 329.3 °C

Q = 0.91 MW/m^2

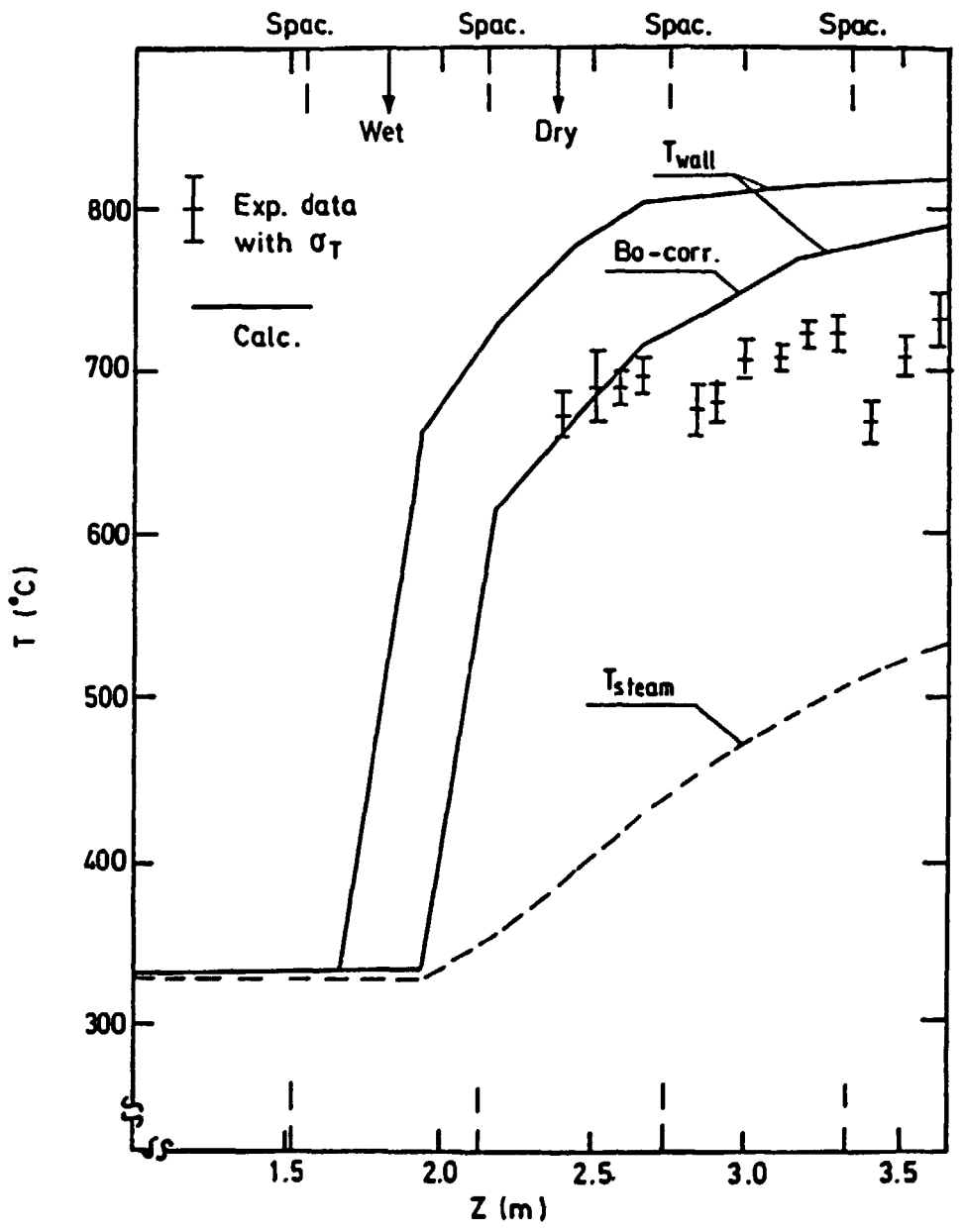

Fig. B2.34 ORNL Case C

P = 12.46 MPa $\quad \Delta T_{subc}$ = 3.5 °C

G = 334.2 kg/m²s $\quad T_{sat}$ = 327.5 °C

Q = 0.56 MW/m²

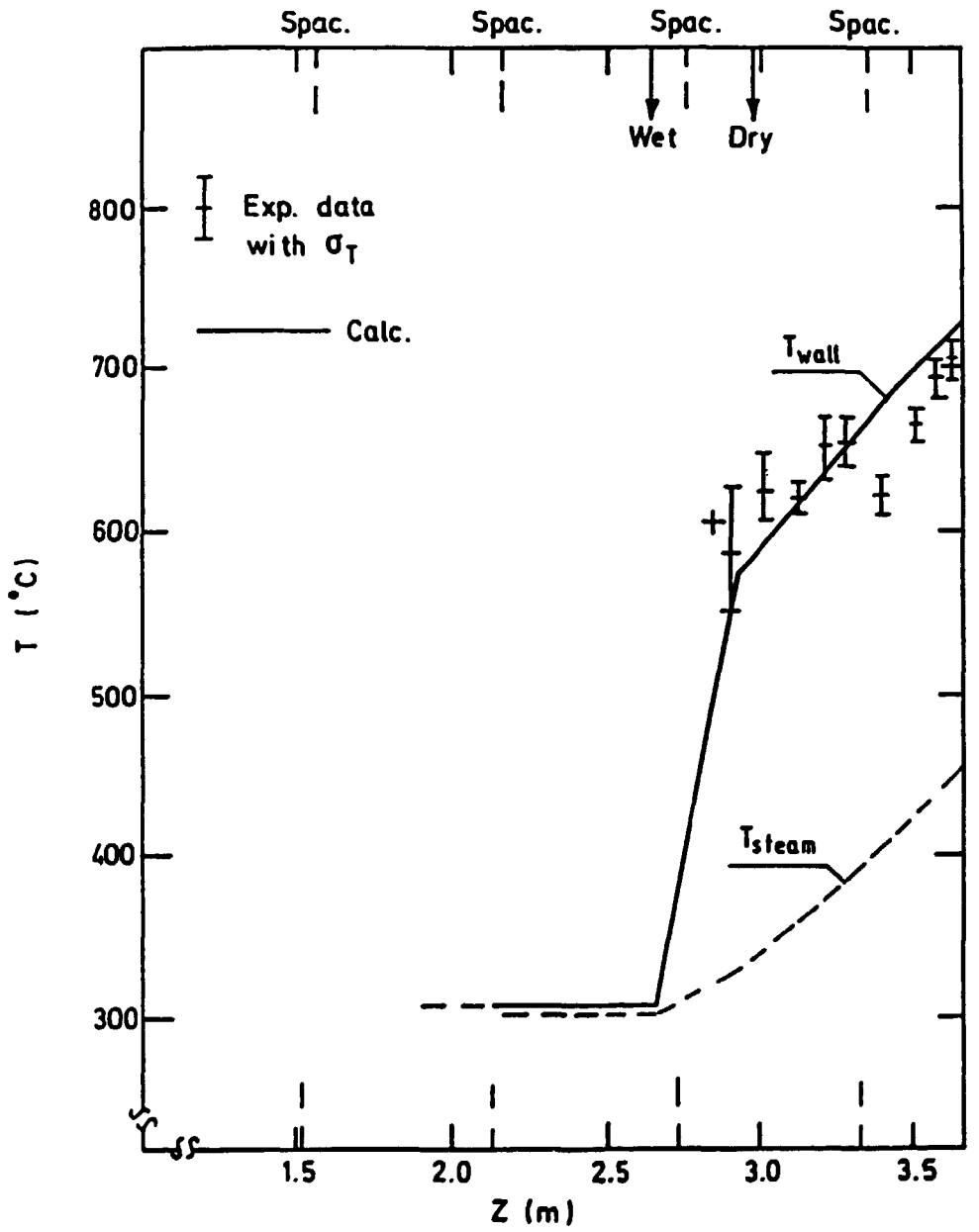

Fig. B2.35 ORNL Case H

P = 8.86 MPa $\quad \Delta T_{subc}$ = 38. °C

G = 256. kg/m^2 s $\quad T_{sat.}$ = 302.4 °C

Q = 0.417 MW/m^2

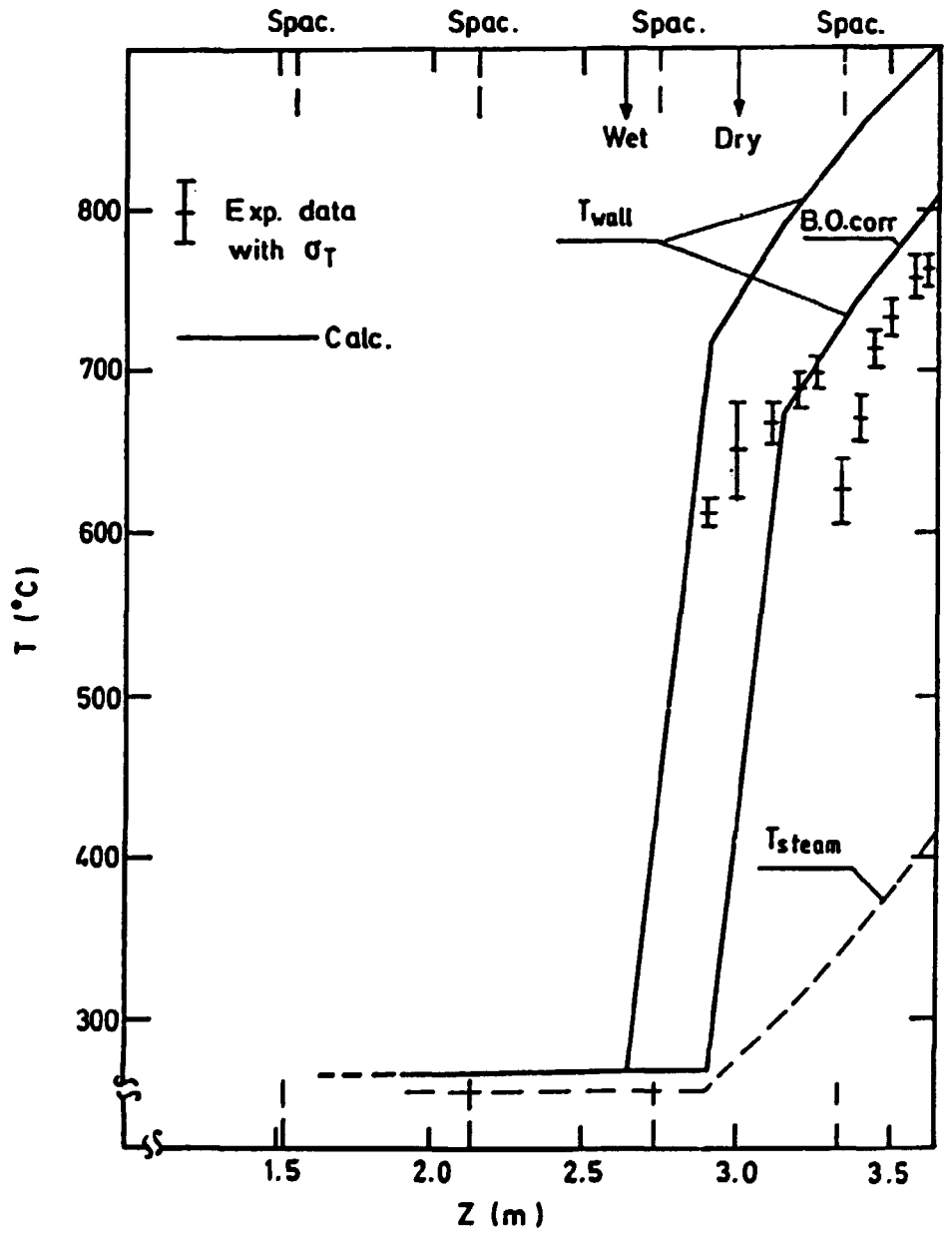

Fig. B2.36 ORNL Case K

P = 4.36 MPa $\quad \Delta T_{subc}$ = 45.8 °C

G = 226. kg/m^2 s $\quad T_{sat.}$ = 255.8 °C

Q = 0.44 MW/m^2

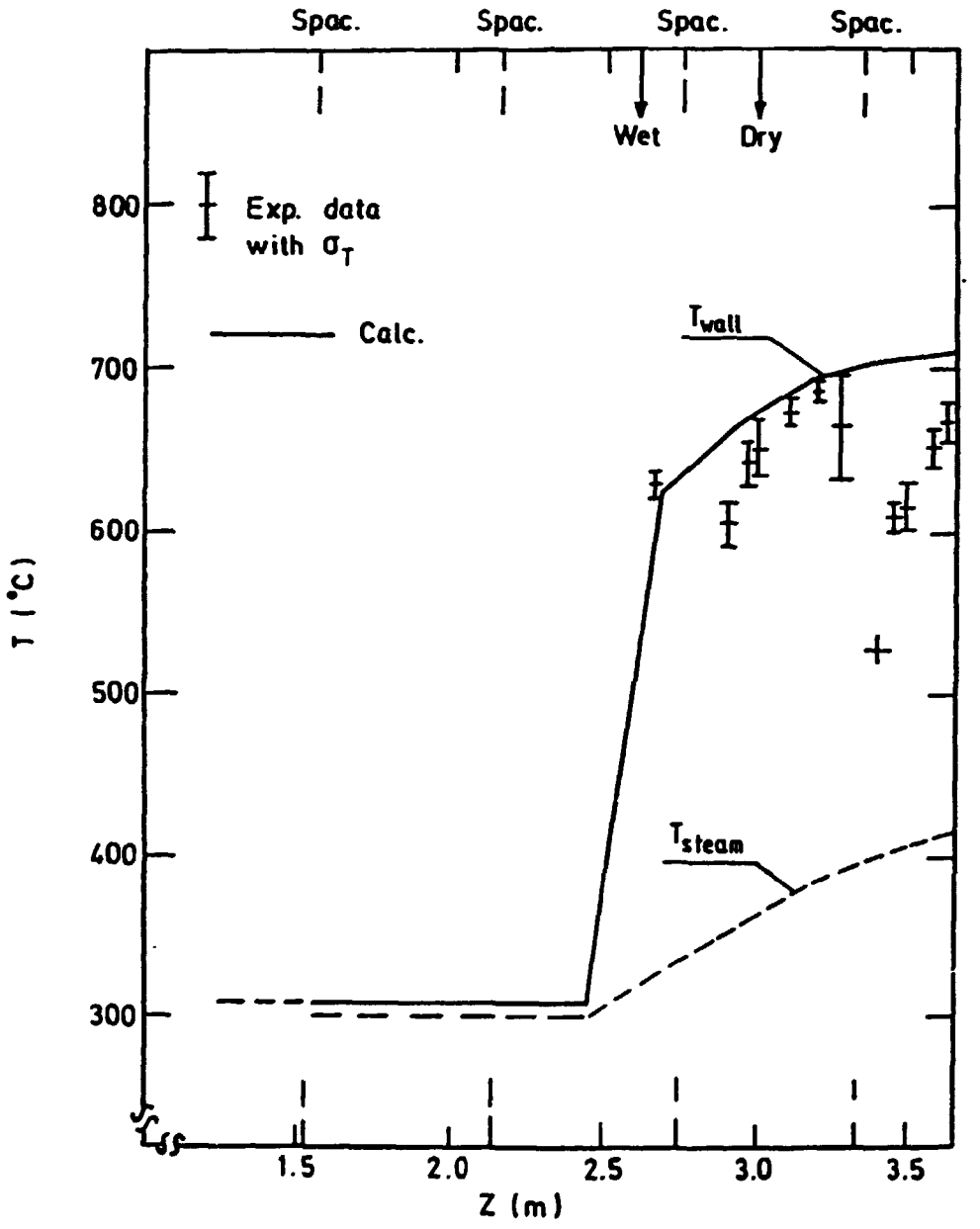

Fig. B2.37 ORNL Case N

P = 8.52 MPa $\quad \Delta T_{subc}$ = 15. °C

G = 806. kg/m^{2}s $\quad T_{sat.}$ = 300 °C

Q = 0.94 MW/m^2

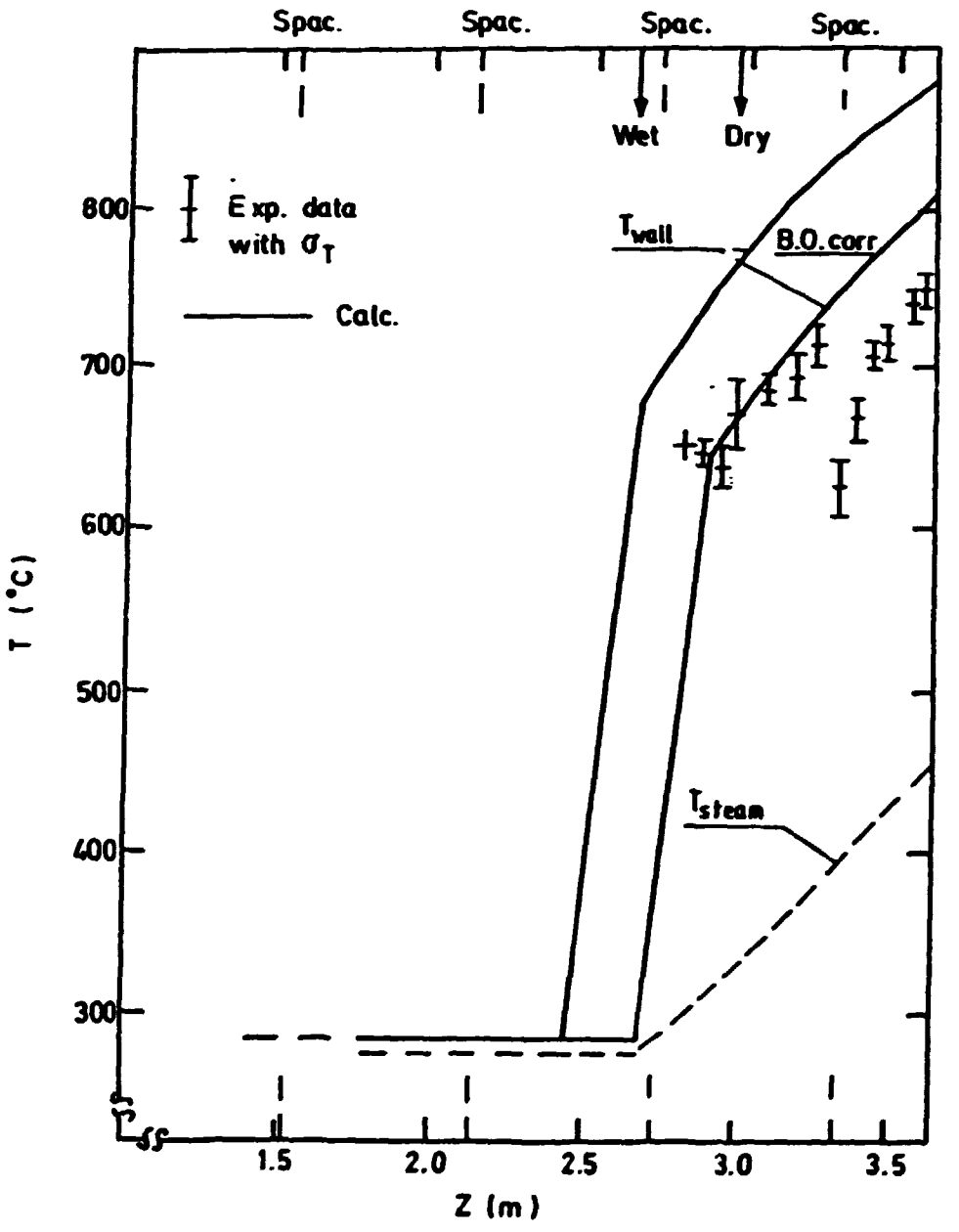

Fig. B2.38 ORNL Case 0

P = 5.98 MPa $\quad \Delta T_{subc}$ = 22.3 °C

G = 307. kg/m^2 s $\quad T_{sat.}$ = 275.3 °C

Q = 0.53 MW/m^2

Right downstream from a spacer the wall temperature drops due to flow perturbations induced by it. No spacer effects were accounted for in the calculations, however.

The locus of DO was predicted using the CISE4 CHF-correlation. For some of the cases it was considered that the locus of DC was too far upstream and these cases were recalculated with the locus of the DO moved one node length downstream. These new wall temperatures are indicated by "BO-corr" in the figures. The results clearly demonstrate the sensitivity of calculated wall temperatures to the calculated locus of DO.

B3. Experiences using the computer programmes.

Numerical methods

The work performed in SÄK-5 project has mainly been concentrated on the calculation of steady state tests. For this purpose the numerical method of RELAP5/MOD1 is a semi-implicit one, which has the maximum time step of

$$\Delta t_{max} < \Delta z/u$$

where Δz is the node length and u is the velocity. In SÄK-5 work the maximum time step according to this criteria has been in some cases less than 5 ms, which leads to excessive computing time (~ 1000-2000 s). If a fully implicit numerical method could be used, the steady state is obtained using a single infinitely long time step. In that case the solution method is iterative and the number of iteration cycles may be large, but in spite of that the total computation time can be two orders of magnitude less than it would be using RELAP5.

TRAC(PF1) utilizes a so-called two-step method, which avoids the stability criteria. A similar method is also used in RELAP5/MOD 2, which has not been used in this project. Although the two-step method has no stability criteria, the solution does not approach the steady state when the size of the time step is increased. Thus steady state solutions have to be

obtained by transient calculation, which is more time consuming than the use of a fully implicit method. In order to calculate the steady state in the test case, TRAC(PF1) required about 200-300 seconds computing time, while the fully implicit method used in Finland consumed only 20-30 seconds. A steady state version of NORA, called NORAS, consumed less than 10 seconds, but the number of volumes was smaller (20 instead of 35). Furthermore, a direct comparison of the execution times is not possible, because of different computers, but it seems that TRAC(PF1) consumed at least 10 times more computing time than a fully implicit method, and RELAP/MOD1 about ten times more than TRAC(PF1). The physical assumptions and spatial discretization methods have also been different in different computer programmes. RELAP5/MOD1 utilizes only one energy equations. However, this did not cause any trouble in comparing the calculated results.

All the computer programmes have a conservative discretization for mass and energy equations. TRAC and RELAP5 have a non-conservative form of momentum equations. The results depend somewhat on which form of the momentum equations is used, but in the calculated cases the error was not significant when the node size was 0.2 m. This is natural, because all consistent numerical methods should have the same solution when the node size approaches zero. With a larger node size, the difference between a conservative and non-conservative method may be more significant. In the present case there were also more significant differences in the momentum fluxes of the individual phases, but the difference in the total momentum flux was small.

Constitutive equations

Heat transfer correlations are evaluated in a separate Appendix; experiences with other constitutive models are shortly described here. During the work it appeared that many constitutive models were not only poorly tested, but they were also different in different versions of the same computer

programme. An example is the interfacial drag correlation of RELAP5/MOD1-Cycle 19, which has been applied for the calculations in Finland and Sweden. The programme version used in Finland has a drag smoothing model, which caused very peculiar velocity profiles (see Fig. B3.1).

Another important constitutive model is the one used for interfacial heat transfer. These models are at present very simple and crude. In all cases the RELAP-programme predicted almost equilibrium conditions between the phases. The maximum temperature difference between the phases was always less than 1K and usually less than 0.1K (see Fig. B3.2). It can be concluded that RELAP5 behaves like an equilibrium computer programme except in the very early stages of flashing, which usually occurs only in rapid transients.

There have also been some difficulties in the application of constitutive equations. Usually the difficulties are caused by discontinuities in the set of correlation. In RELAP5 these discontinuities have been discovered in interfacial friction, wall friction and critical heat flux. These are described in the next chapter.

Difficulties in the application of correlations

The main difficulties in the application of any constitutive model are caused by discontinuities, when a correlation used is changed during the calculation. The discontinuities may prevent convergence of the numerical method and the calculated result is oscillatory. These oscillations also strongly affect the mass and energy balance and consequently the calculated result is unreliable.

In the present work the main difficulties have been caused by the models of interfacial and wall friction of RELAP5. An example is the interfacial friction coefficient depicted in Fig. B3.3. It can be seen that there is a discontinuous change in the friction coefficient when the void fraction equals 0.65. During the solution, when the void fraction is greater

than 0.65, the friction coefficient has a low value resulting in a large velocity difference between the phases. This, in turn, may cause a decrease in void fraction so that on the next time step or iteration cycle the void fraction is less than 0.65, which results in a large friction coefficient. Hence, on the next cycle the velocity difference is again small and the void fraction is greater than 0.65. Unless a large amount of numerical damping is added, this oscillatory cycle goes on forever. When a non-iterative numerical method is used like the one of RELAP5, is used this damping can be obtained only by the use very small timer steps, which are not possible in practice.

Another example of numerical difficulties that arise is the discontinous way wall friction is shared among the phases in RELAP5.

It is obvious that a constitutive model should not include computational discontinuities described above, because in these cases the problem has either no solution at all, or the solution is obtained only by an ultimately large computational effort i.e. by using tiny time steps or a large number of iterations. Because of this a modified wall friction package has been developed, which has been used for the calculations of Becker's test cases. In this package the partition of the wall friction is performed so that the hysteresis phenomenon is not possible. The results using the new package are nearly the same as the results of the original package. The new package results were close to the average of the oscillatory results, when oscillations occurred in using the original package. In all cases the total frictional pressure drop in the channel was the same. Thus the smoothened wall friction model didnot change the absolute values, but improved the stability of the calculation.

B4. Comparison using separate programmes

B4.1 Critical heat flux

Due to the difficulties of making an assessment of different

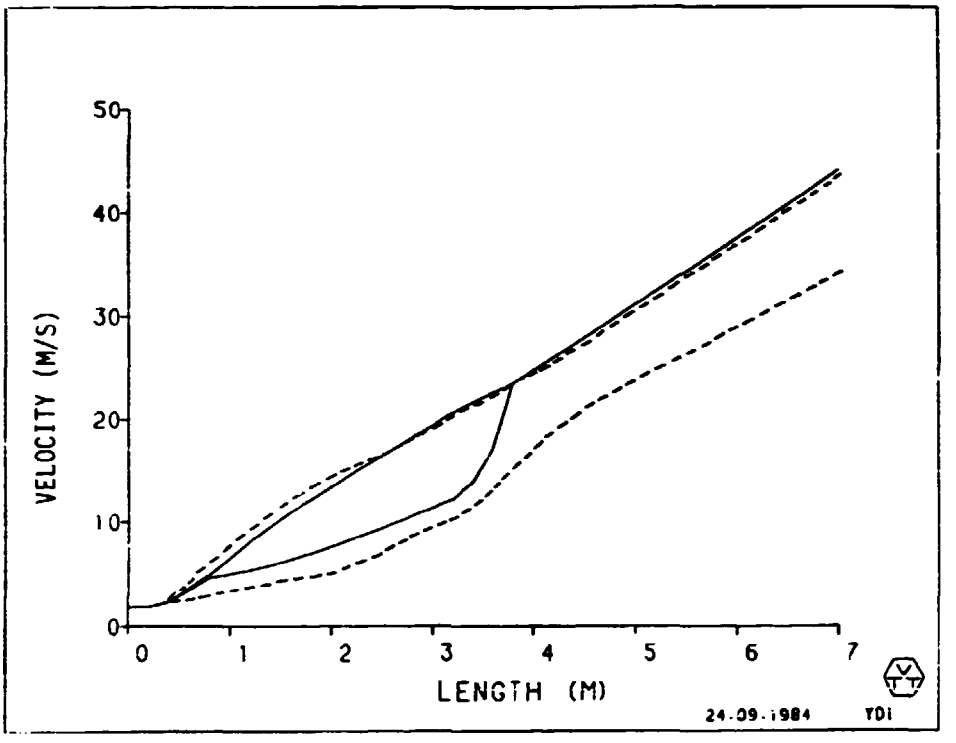

Fig.B3.1 Calculated velocity profiles in Becker's test case no.1. ____RELAP5/Mod1/CYCLE19 in Finland, -----RELAP5/Mod1/CYCLE19 in Sweden.

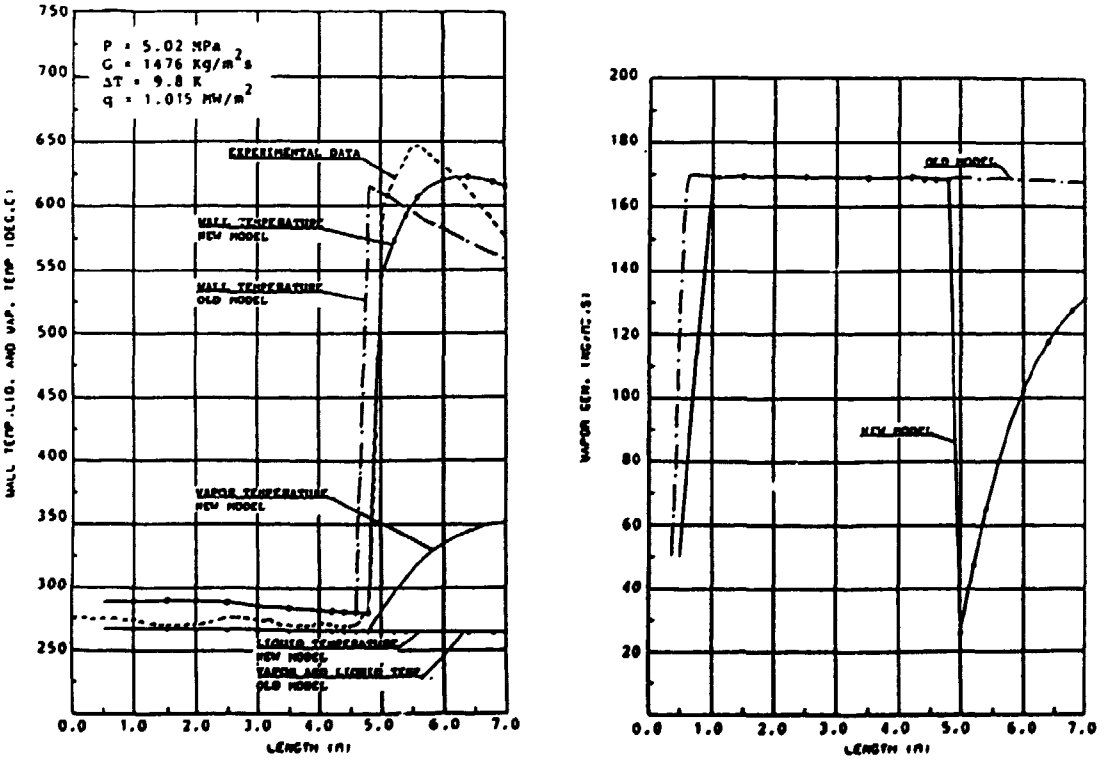

Fig. B3.2 Calculated temperatures and vapour generation rate in Becker's test case No. 1.

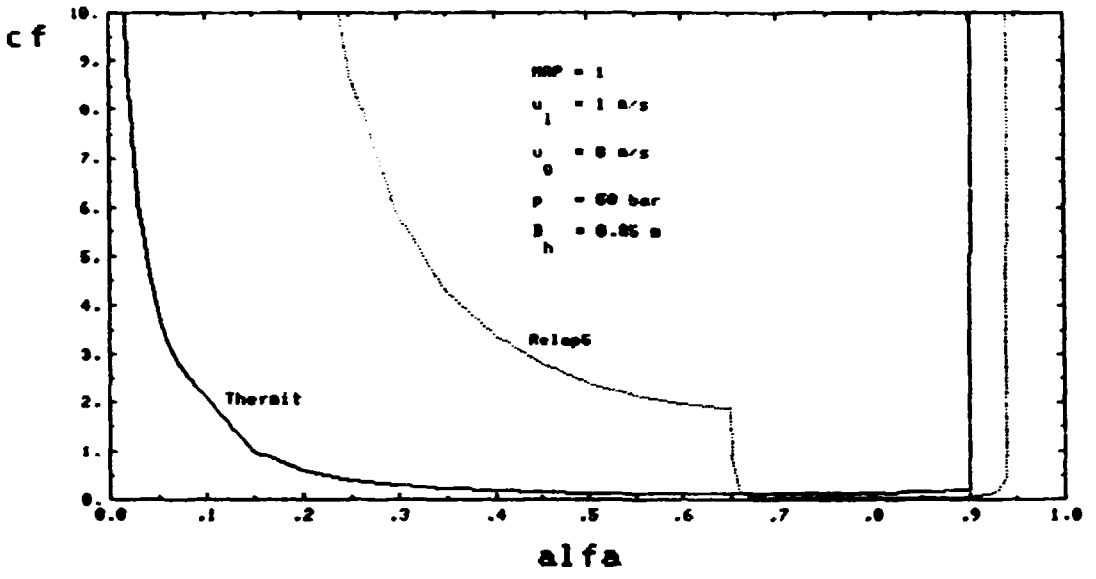

Fig.B3.3 Interfacial friction coefficient as a function of void fraction.

CHF-correlations employing the thermohydraulic system programmes like RELAP5 and TRAC, a separate examination of this issue was made. The assessment was performed as a separate part of the SÄK-5 project and was conducted at the Royal Institute of Technology in Stockholm. The result of this assessment is reported in (73) and in what follows a short summary of the work will be given. Also some additional efforts made during the late phase of the project will be reviewed.

The assessment was limited to four different CHF-correlations and was based on six full-scale steady-state rod bundle experiments. The correlations included in the assessment were:

Barnett	(74)
Becker	(75)
Biasi	(5)
CISE-4	(76)

The Biasi and CISE-4 correlations were originally developed for round tubes and thus the performance in rod bundle geometries could be questionable. However, as they are utilized in several of the commonly used transient computer programmes, for instance TRAC(PF1) and RELAP5/MOD1, it was decided also to include those correlations in the assessment. The experimental data used for this assessment were obtained in a 64-rod bundle (Desirello et al 77), 81-rod bundle (Pimputkar et al 78), 36-rod bundle (Nilsson 79 and Nylund 80, 81), and 37-rod bundle (Bowditch and Smyth 82). These experiments included axially uniform as well as axially variable heat flux distributions.

The dryout predictions were carried out employing either the total power hypothesis or the local conditions hypothesis. In the total power hypothesis the total channel dryout power was predicted assuming uniform axial heat flux distribution and compared to the measured power. Thus this method did not yield any information about the axial location of dryout. In the local conditions hypothesis, proposed by Becker in 1969 (83), the dryout is assumed to be dependent only on local flow parameters at the locus of dryout. The principle of this

method is demonstrated in Fig B4.1.1 where the experimental heat flux is plotted versus the quality along the channel. In the figure an arbitrary dryout correlation is also included and the heat balance is represented by a straight line. The locus of dryout is determined by drawing a family of heat balance lines for different axial locations and then selecting the line yielding the minimum value of the ratio $(q/A)_{BOPRE}/(q/A)_{BOEXP}$.

Because of the difficulty of defining a proper boiling length in transient and LOCA situations it is obvious that the method employing the local conditions hypothesis has to be adopted for the CHF predictions in these type of transients. Thus the following will deal only with the results obtained when using the local conditions hypothesis.

A total number of 269 runs were obtained in the utilized experimental studies mentioned above covering the following parameter ranges:

Pressure	3.0 - 9.0 MPa
Mass Flux	200 - 2400 kg/m^{2}s
Inlet Subcooling	12 - 286 kJ/kg
Dryout Heat Flux	0.23 - 1.49 MW/m^2
Dryout Steam Quality	0.18 - 0.805

143 of the measurements were obtained with axially non-uniformly heated test sections while the remaining 126 measurements had a uniform axial flux distribution.

Only the Becker and the Biasi correlations covered all the utilized experimetal data. Concerning the CISE-4 correlation the results at pressure 3.0 MPa were outside the range of the correlation. Finally the Barnett correlation was valid only for pressure 7.0 MPa.

The result of the comparison between measurements and predic-

tions can be illustrated by Figs. B4.1.2 to B4.1.5 showing the measured versus the predicted dryout power for the 64- and 81-rod bundles. The trends for all of the experiments were similar; the Biasi and CISE 4 correlations generally over-predicted the data considerably while the Barnett and the Becker correlations yielded rather good predictions especially for the square lattice 81, 64 and 36-rod bundles.

A summary of the results obtained with the local condition hypothesis is shown in Table B4.1.I. The best predictions were obtained with the Becker correlation yielding a RMS error of 9.7% including all the runs of the 6 experimental studies. The Biasi and CISE-4 correlations were in poor agreement with the experimental data; the reason for this is probably that these correlations were developed for predictions of dryout in circular tubes.

Also some selected experiments from the OF-64 experimental dryout series were analysed (84). This test series was conducted by ASEA-ATOM, Sweden, in 1969 and is reported in (85). The test section was designed as a full-scale simulation of an Oskarskamn I fuel assembly and consisted of 64 heated rods. The internal radial power distribution was symmetrical with a peaking factor of 1.24 while the axial power distribution was peaked towards the outlet with a peaking factor of 1.55. The tests were performed with pressures ranging from 4.8 to 8.7 MPa, mass fluxes from 400 to 2000 kg/m^{2}s, and bundle powers from 5.1 to 8.6 MW. Seven dryout tests were selected for separate examination and the conditions for these tests were:

Test No	Pressure (MPa)	Inlet Subcooling (K)	Mass Flux (kg/m^{2}s)	Power (kW)
703007	6.71	8.7	498	5957
703073	6.82	7.8	971	7683
703015	6.67	9.4	1168	7899
703075	6.72	9.5	1336	8192
703077	6.82	9.0	1535	8594
703087	8.64	9.2	1382	6843
703043	4.79	2.1	789	7693

In these analyses the Becker and for the 7 MPa cases also the Barnett correlations revealed the best agreement, while the Biasi and the CISE-4 correlations were in fairly poor agreement with data, i.e. the results were consistent with the findings in the assessment reported above. The results obtained with the Becker correlation is illustrated in Fig. B4.1.6, indicating a very good agreement although somewhat conservative.

Finally, some predictions of the locus of dryout for the above-mentioned OF-64 cases were carried out by means of Becker and Biasi correlations and compared with the measured ones (86). The conclusions from these calculations were that the Becker correlation revealed a very good correspondence between predicted and measured locus of dryout for mass fluxes above 1000 kg/m^2 s, the errors being within the measurement accuracy. For mass fluxes below 1000 kg/m^{2}s the correspondence in some cases was not quite that good, being on the conservative side though (the predicted locations were found to be upstream of the measured ones). It should also be mentioned that the Biasi CHF correlations did not predict dryout in any of the cases, thus being very non-conservative.

B4.2 Transition boiling.

The literature search resulted in the selection of 5 correlations:

1. Chen correlation (29),
2. Correlation by Tong & Young (31),
3. Correlation by Bjornard & Griffith (33),
4. EPRI correlation (87),
5. Correlation by Hsu (32).

The correlations 1, 2, 3 and 5 are shown in Table A3.I.

In 1 and partly also in 2 physical phenomena have been considered to a certain degree. The other correlations may be

	Barnett		Becker		Biasi		CISE-4	
	No. of Runs	RMS Error	No. of Runs	RMS Error	No. of Runs	RMS Error	No. of Runs	RMS Error
64-rod bundle, ref.77	18	6.5	18	11.5	18	30.7	18	21.5
81-rod bundle, ref.78	24	5.5	24	7.0	24	26.9	24	18.2
36-rod bundle, ref.79	11	15.3	18	3.3	18	20.9	16	7.9
36-rod bundle, ref.80	11	12.2	38	10.5	38	30.3	32	23.2
36-rod bundle, ref.81	26	8.4	83	12.5	83	31.3	71	22.6
37-rod bundle, ref.82	69	11.7	88	7.0	88	34.2	69	23.2
All Bundles	159	10.3	269	9.7	269	31.2	230	21.6

TABLE B4.1.I. RMS-ERRORS OBTAINED WITH THE LOCAL HYPOTHESIS

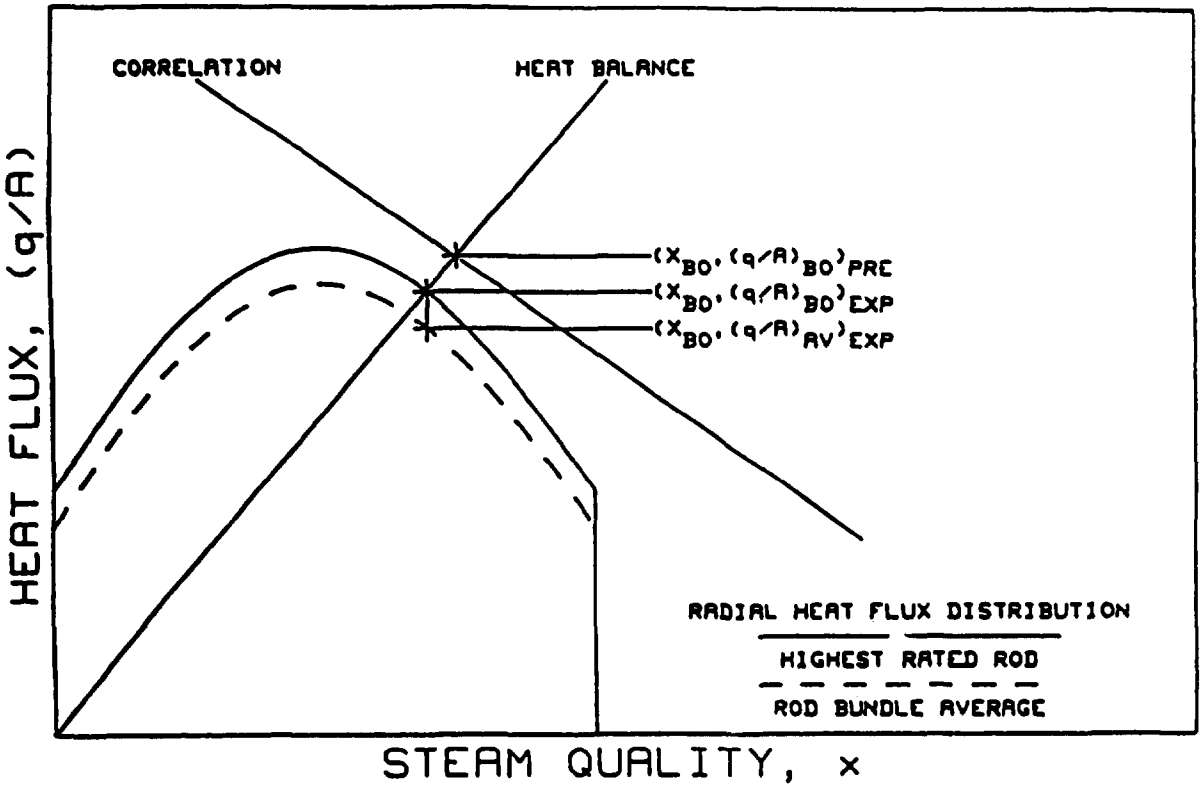

FIGURE B4.1.1 LOCAL CONDITION HYPOTHESIS

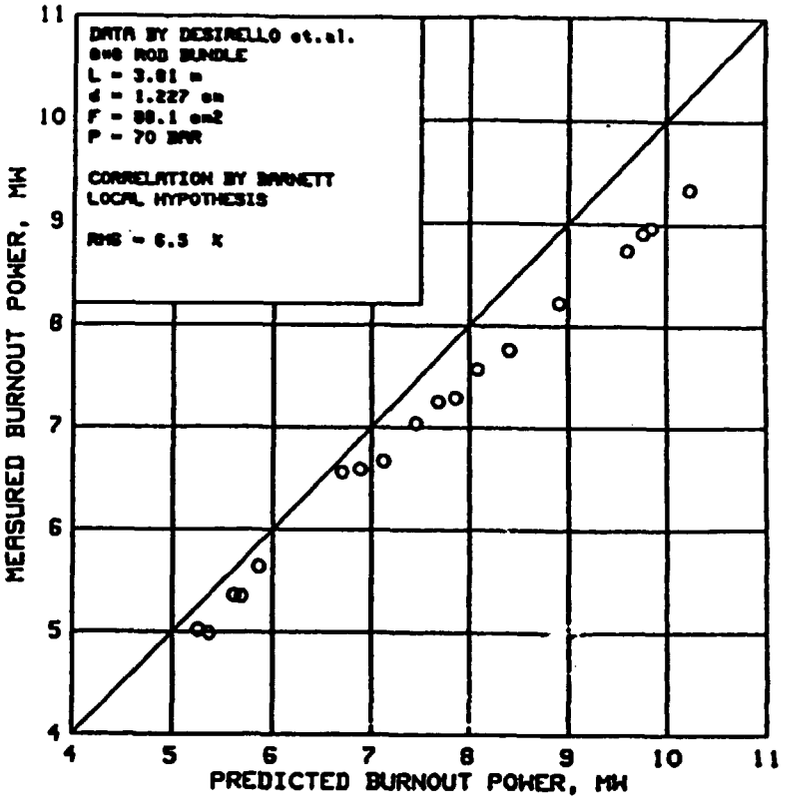

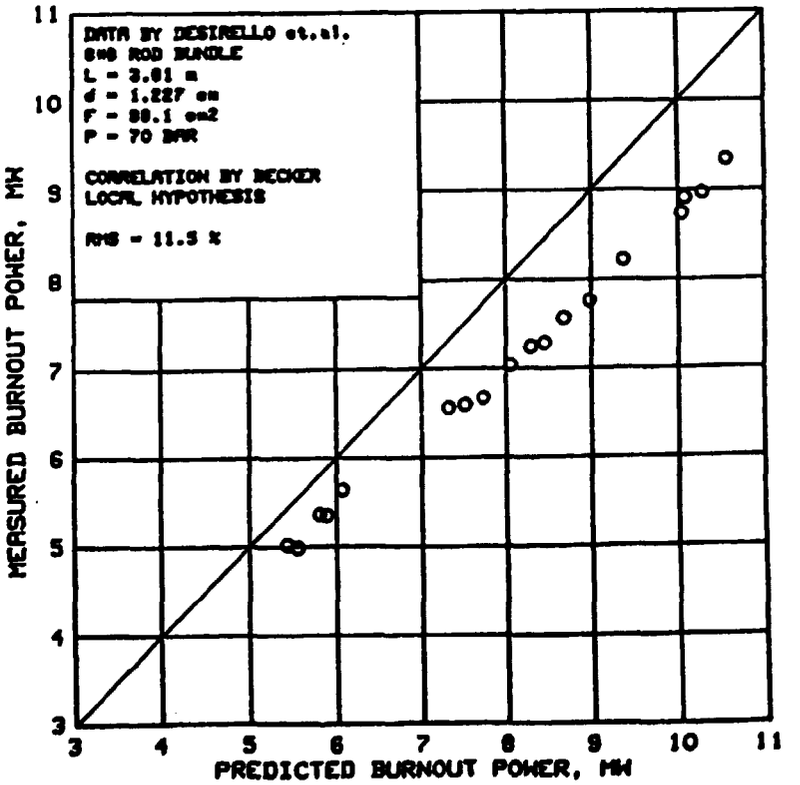

FIGURE B4.1.2 COMPARISON BETWEEN MEASURED AND PREDICTED BURNOUT POWER

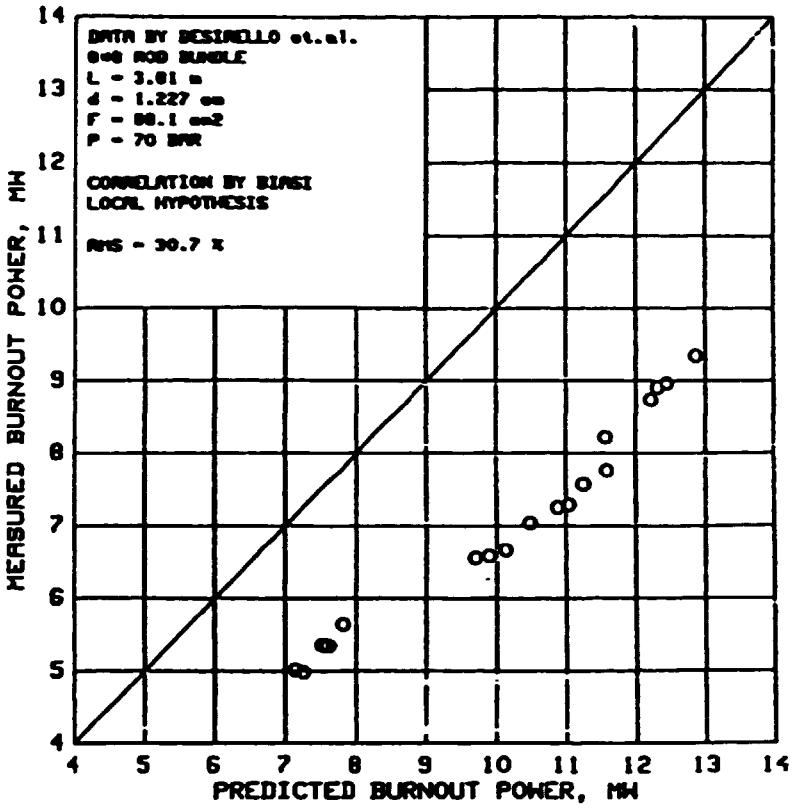

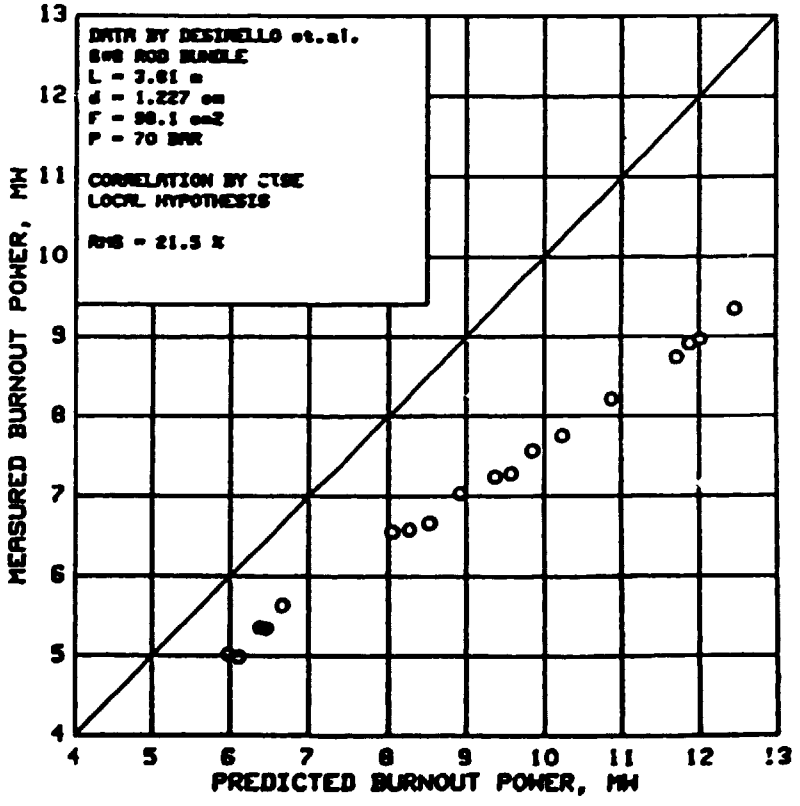

FIGURE B4.1.3 COMPARISON BETWEEN MEASURED AND PREDICTED BURNOUT POWER

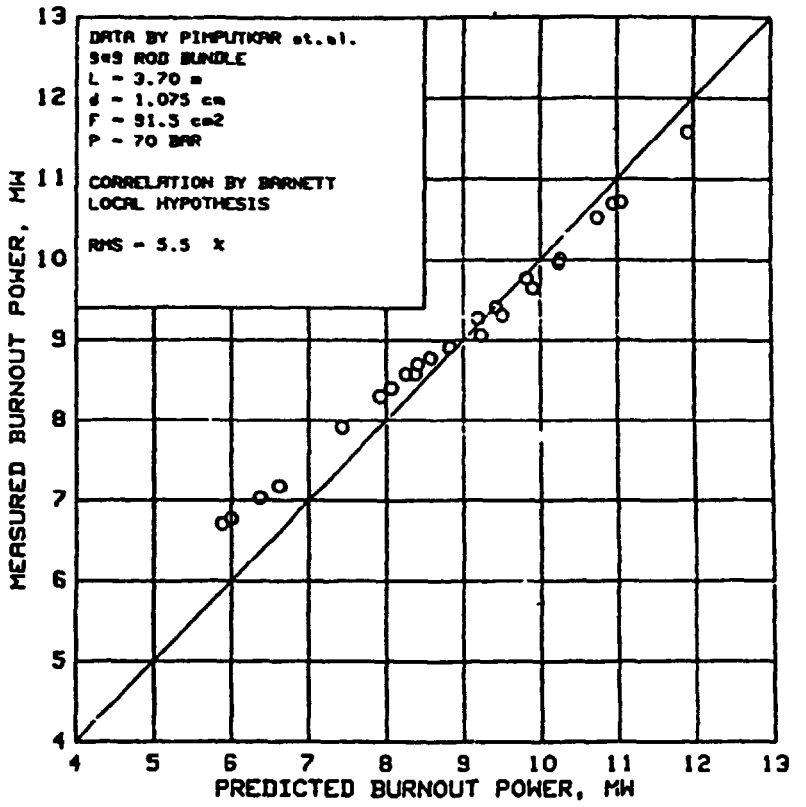

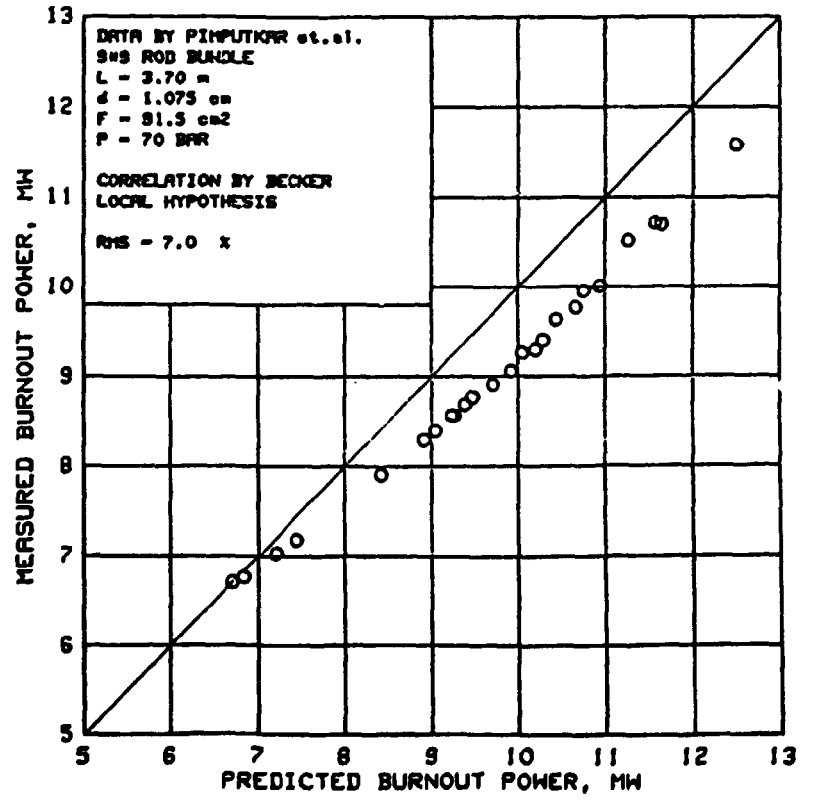

FIGURE B4.1.4 COMPARISON BETWEEN MEASURED AND PREDICTED BURNOUT POWER

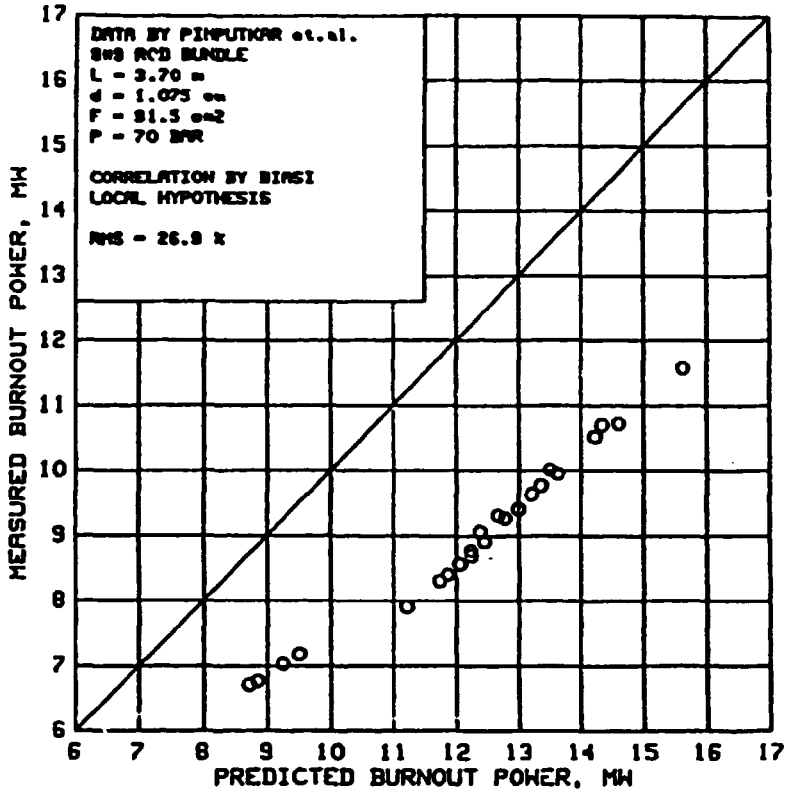

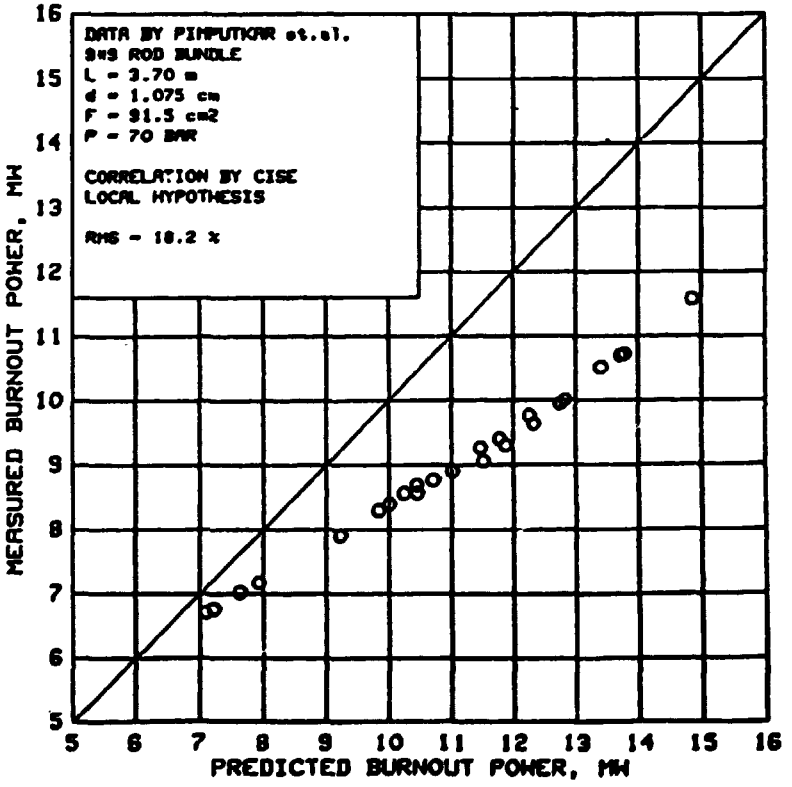

FIGURE B4.1.5 COMPARISON BETWEEN MEASURED AND PREDICTED BURNOUT POWER

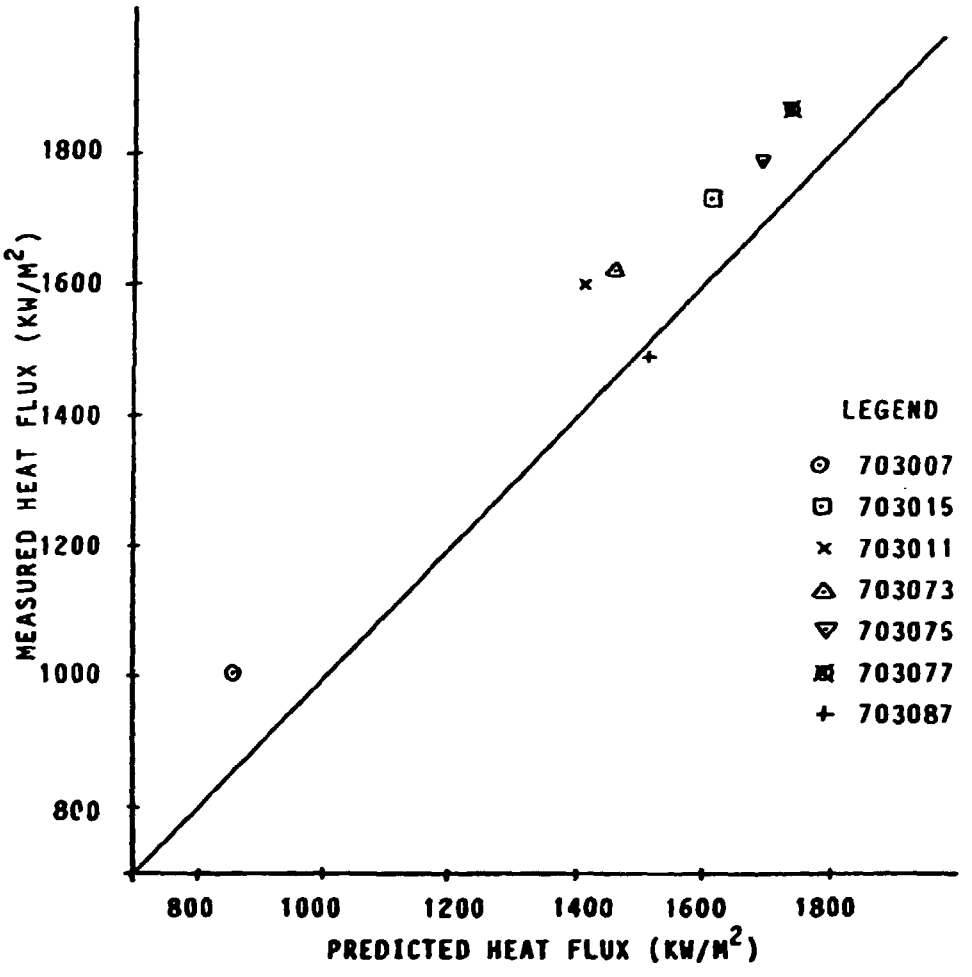

Figure B4.1.6 OF - 64. Comparison between measured and predicted dry-out heat flux.

described as empirical correlations. All correlations are of the two-term type.

A detailed description of the correlations is given in (26). A literature search was made in order to find relevant temperature controlled test data. Very few references were found. The best and most relevant experimental data were those conducted by Prof. J. Weisman at University of Cincinnati and published by Electric Power Research Institute (EPRI),(87).

The temperature controlled surface is ensured by heating the boiling water by hot flowing mercury. The water flows upward in an annulus and the mercury flowing downward in a center tube. Measurement of wall and mercury temperatures at several elevations allows the heat transfer to be determined.

The pressures are from 1 to 4 bar. Mass fluxes used in the evaluation are from 10 to 36 $kg/m^2/sec$ and steam qualities from 0.02 to 0.54.

A separate computer programme was written to evaluate the 5 correlations with the stated experimental data as input.

A listing of the computer programme is reproduced in Appendix B in ref. (26). The final results from the evaluation are reproduced in Appendix A of the same reference.

The Chen correlation is based on experimental data from 8 references with pressures ranging from 4 to 195 bar, mass fluxes from 16 to 3000 $kg/m^2/sec$, and equilibrium qualities from 0.5 to 1.7.

For some parameters the evaluation is the outside the previous range.

The first evaluations gave large deviations from the EPRI results. Two important parameters in the correlation have been examined: the thermodynamic nonequilibrium and the liquid contact area fraction (the decay factor).

Both are empirically determined and based on the experimental data mentioned above.

The vapour may be superheated, i.e. part of the heat from the surface has been used to superheat the vapour instead of evaporating the droplets. The actual vapour quality, XA, is less than the equilibrium quality, XE.

The heat balance gives the following relation between XA and XE:

$$\frac{XA}{XE} = \frac{H_{fg}}{H_{fg} + C_{pv}(T_v - T_{SAT})}$$

There are two unknowns in this equation XA and T_v, the superheated vapour temperature.

Chen defined a parameter B(P):

$$\frac{XA}{XE} = 1.0 - B(P) \cdot \frac{T_v - T_{SAT}}{T_w - T_v}$$

and determined B(P) from the experimental data:

$$B(P) = \frac{0.26}{1.15 - (P/P_c)^{0.65}}$$

P is the pressure and P_c is the critical pressure.

B(P) approaches 0.226 when P approaches 0.0, where B(P) should approach 0.0. Some of the experimental data on which B(P) is determined make it plausible to infer that B(P) is 0.0 when P is 0.0. Based only on these data B(P) may be correlated as:

$$B(P) = 8.1 \cdot 10^{-2} + 2.0 \cdot (P/P_c) - 4.0\ (P/PC)^2$$

for pressures less than 50 bar (Figure B4.2.1). The result of this correction is that there will be vapour at lower pressures as the EPRI data will be superheated earlier than after the Chen results, in agreement with EPRI data. The deviation has however, to be examined in more detail.

Chen used his data bank to determine the decay factor using the relation:

$$FL = \frac{q_T - q_{VC}}{q_{LC} - q_{VC}}$$

The decay factor was correlated with the equation:

$$FL = \exp(-\lambda \cdot (T_w - T_{SAT})^n),$$

where λ is a function of void and mass flux.

Chen determined the exponent n to 0.5. This gave too low values of the heat transfer compared with the EPRI result, however.

The results from the calculations based on the EPRI data were therefore substituted in the relation for the decay factor; FL and the exponent n were determined. The functional relationship for λ was retained. Plot of the exponent n is shown in Fig. B4.2.2. The data have been correlated by two straight lines. It cannot be excluded that the strong increase in the exponent near the critical point is due to an inaccurate determination of the experimental total heat flux near this point cf. Figs. B4.2.3-B4.2.7. Only data above about 40 degrees in the temperature difference, $T_w - T_{SAT}$, should have been taken into into account.

As mentioned above, all experimental data used by Chen et al. are above 4 bar and most of them are at high pressure. This may be one explanation of the small exponent.

Chen et al. do not take interfacial heat transfer into account. An explanation may be that the B(P)-values after Chen's equation imply that the vapour will not be superheated.

Tong & Young published their correlation in 1974. In contradiction to Chen et al. they use the nucleate boiling heat flux at CHF as the boiling term, and a modified single-phase heat transfer correlation (Dittus-Boelter) for the convection term (see Table A3.I no.2).

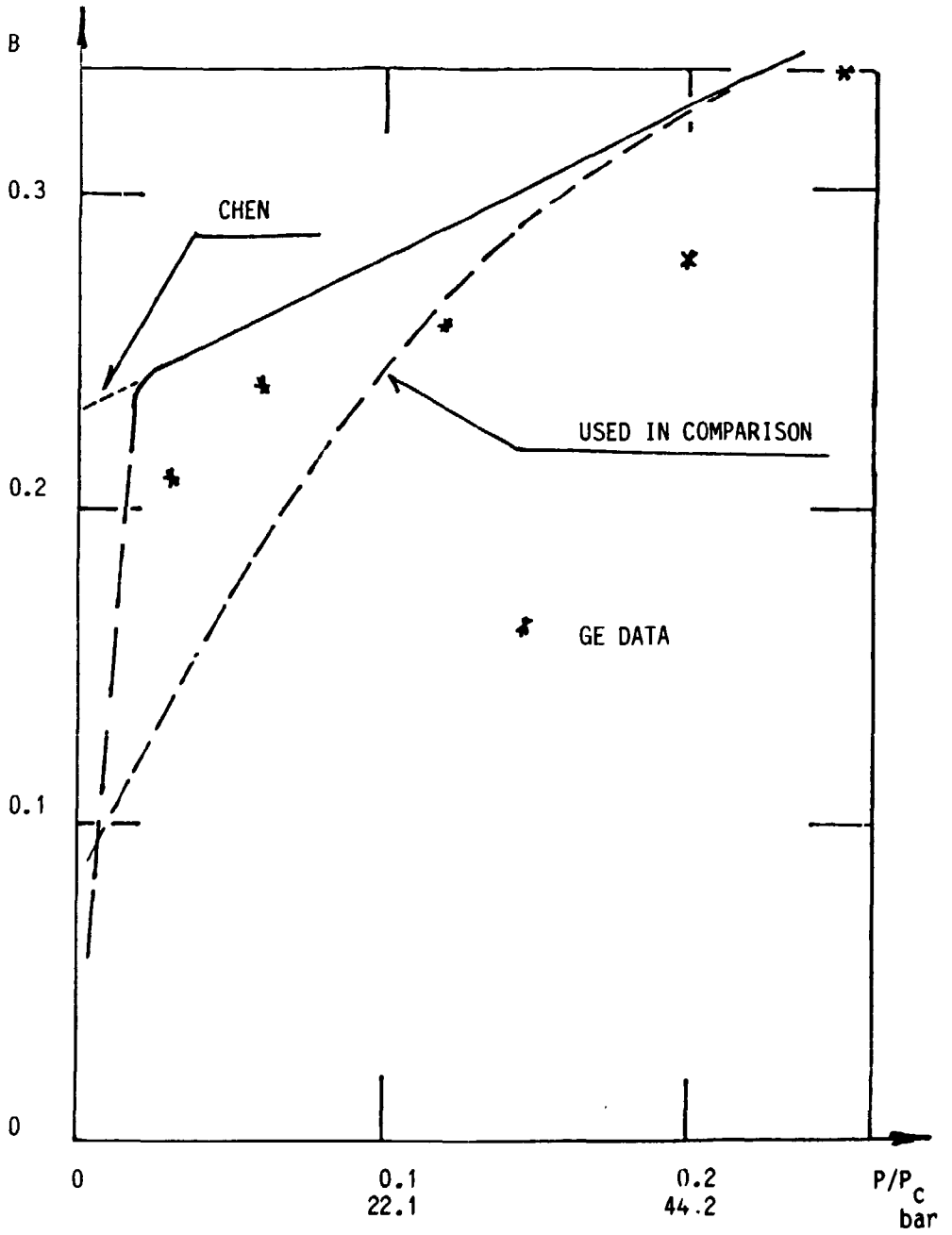
B
0.3
0.2
0.1
0
CHEN
USED IN COMPARISON
GE DATA
0
0.1
22.1
0.2
44.2
P/P_c
bar

FIGURE B4.2.1

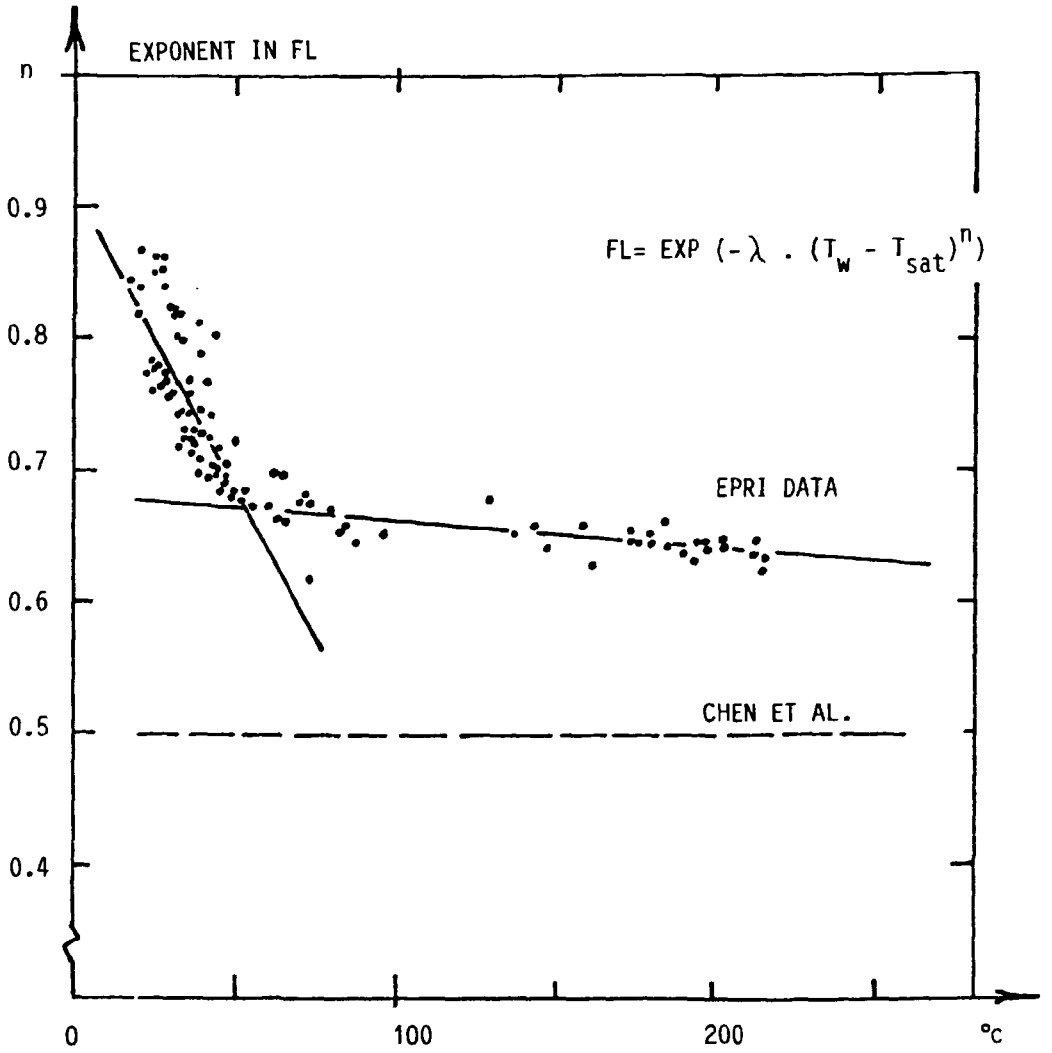
EXPONENT IN FL
n
0.9
0.8
0.7
0.6
0.5
0.4
FL= EXP (-λ . (T_w - T_sat)^n)
EPRI DATA
CHEN ET AL.
0
100
200
°c

FIGURE B4.2.2

Tong & Young have used high pressure data to determine the decay factor. The use of their equation for the decay factor on the EPRI data gives values that are too high i.e. it is the boiling term, which is dominant and the correlation will be in agreement only at low temperature differences near the CHF.

The Tong & Young results are not shown in the figures.

The correlation by Bjornard & Griffith (see Table A3. I no.5) is a purely empirical two-term correlation. The two terms are defined as the limits between which transition boiling heat transfer may exist i.e. the critical heat flux and corresponding critical temperature, T_{CHF}, and the minimum film boiling heat flux and corresponding temperature, T_{MFB}.

The results of the examination are plotted the Figs. B4.2.3 - B4.2.7.

The EPRI correlation is considered because it is developed from their own experimental results as basis and may therefore give a first indication of how good are the results.

The above-mentioned correlations are all primarily evaluated in the vapour-continuous flow region.

The Hsu correlation is developed from subcooled FLECHT data, i.e. in the liquid-continuous flow region. The results using EPRI data show a heat transfer that is too high, as may be expected.

The comparison shows that the description of dispersed flow with droplets discretely distributed through the continuous vapour phase and the deposition motion of the droplets toward the wall is of fundamental importance for the heat transfer not only in the transition-boiling region, but also partly in the film-boiling region.

The dividing points between the two regions is the minimum heat

flux, which just represents the point of prevailing droplet wet collision heat transfer, over heat transferred to the vapour by convection and droplets entering the thermal boundary layer withour wetting the surface ("dry" collisions), and represents the point of incipient rewetting in emergency core cooling.

The heat transfer using a droplet deposition model may be divided into, two main questions:

1. How much heat can be carried away every time a droplet of a certain size impinges and wet the wall?
2. How many droplets per unit time of what size will penetrate the thermal boundary layer and wet the wall?

Chen et al. inferred a droplet diameter and determined the heat carried away by "wet" collisions, but did not take "dry" collisions into account. Nor did they consider the phenomena under point 2, but determined their liquid contact area fraction, the decay factor from the data base they used.

Tong & Young determined their decay factor as covering both points 1 and 2.

None of the correlations are phenomenological in the real sense of the word.

It is obvious that even some effort has been made to describe some of the important phenomena, it may be concluded from these comparisons that the correlations examined in the vapour continuous flow are valid only within the data base from which they are developed, i.e. they must still be considered as statistical correlations.

TRANSITION BOILING HEAT TRANSFER

EPRI TEST DATA
SERIE 350
070284

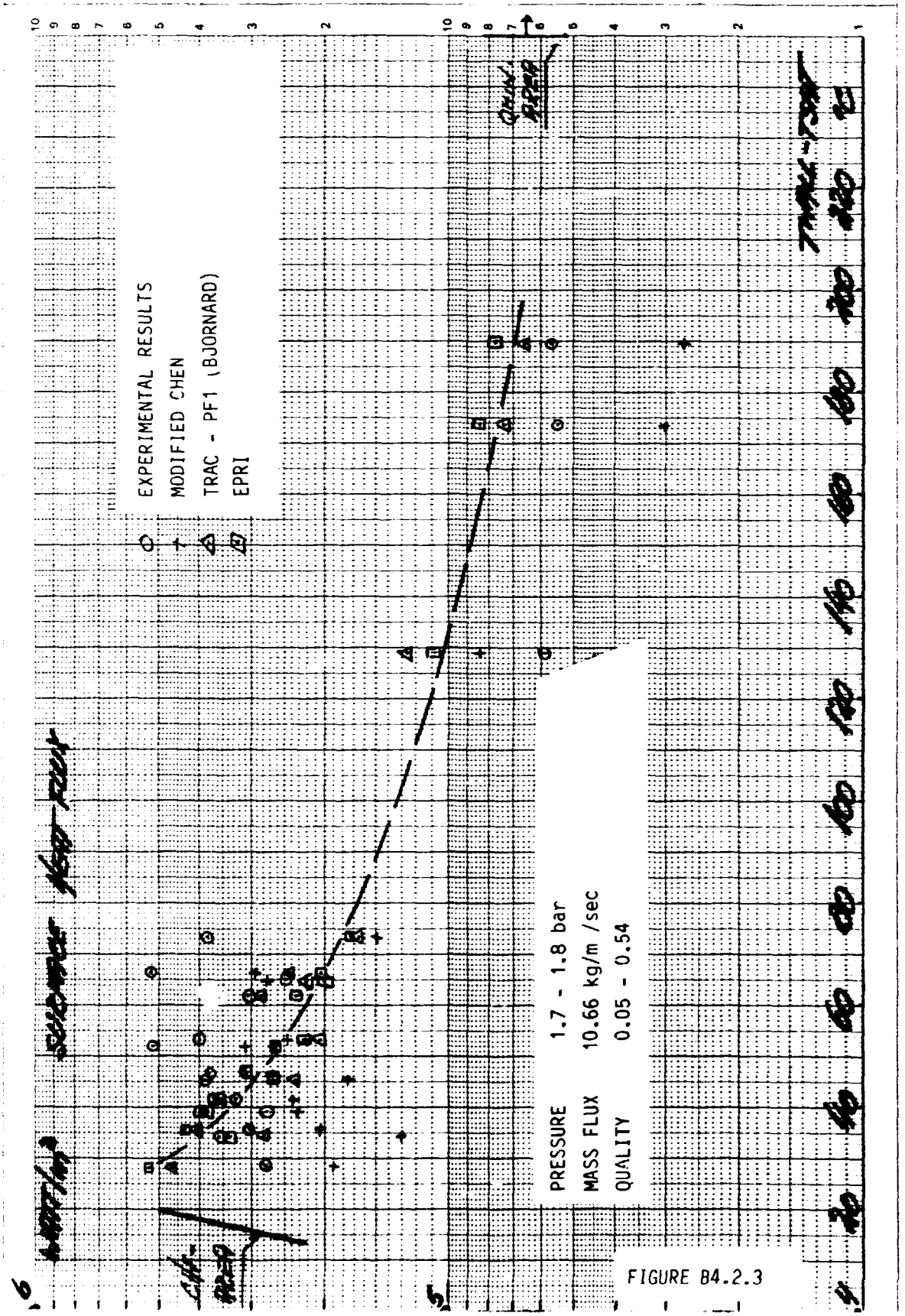

FIGURE B4.2.3

SAC-5

EPRI TEST DATA
SERIE 500
250184

TRANSITION BOILING HEAT TRANSFER

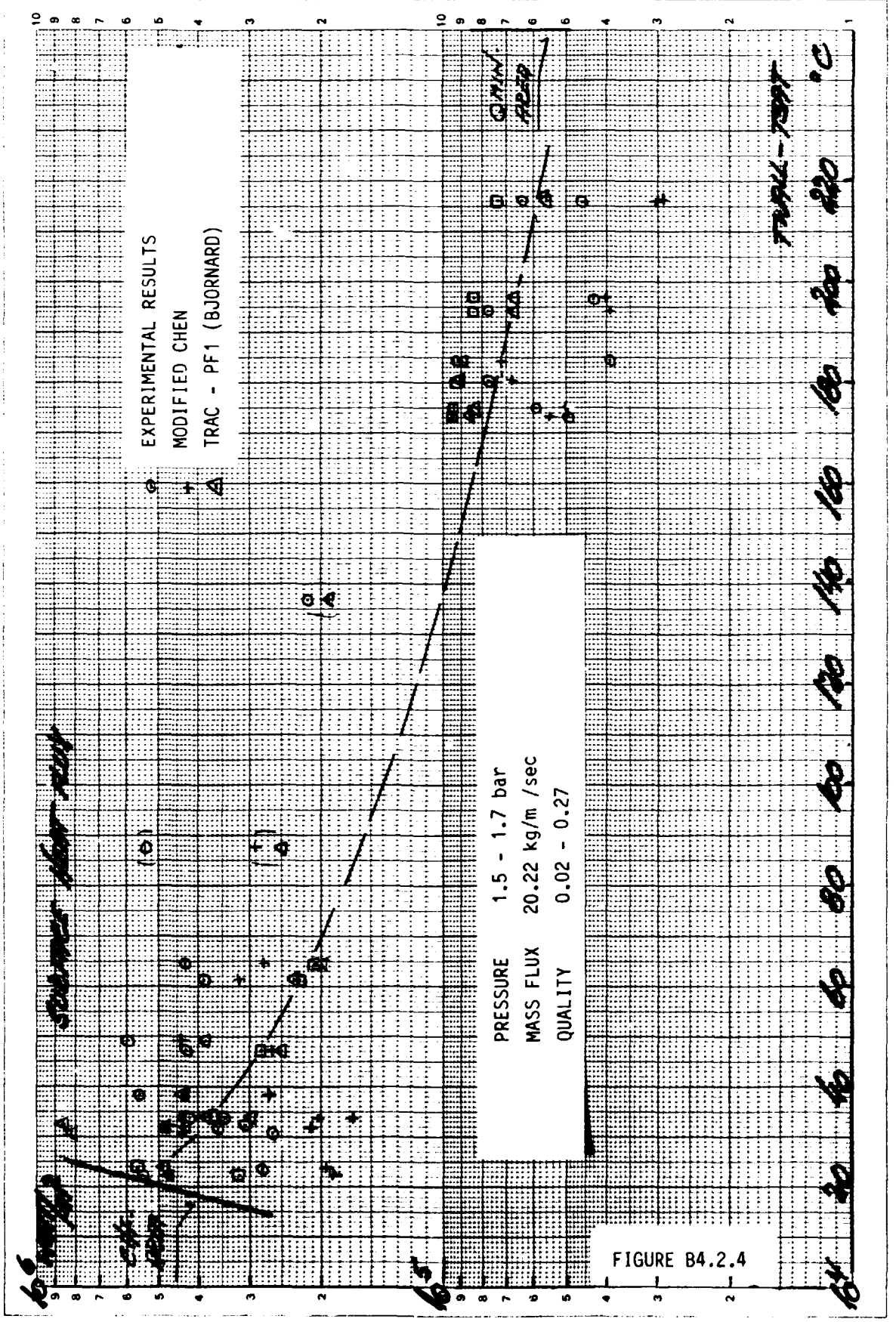

FIGURE B4.2.4

TRANSITION BOILING HEAT TRANSFER

EPRI TEST DATA
SERIE 600
060284

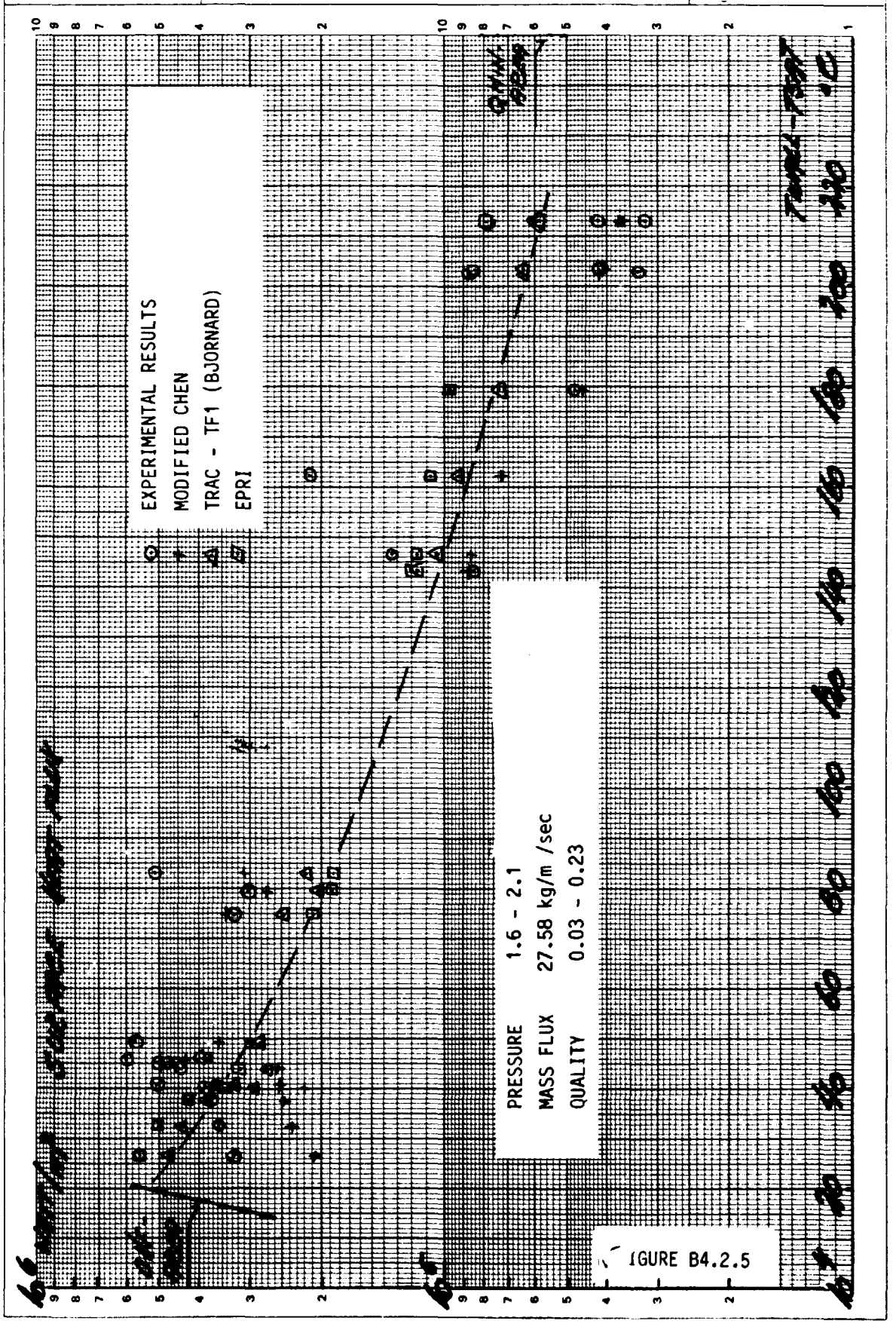

FIGURE B4.2.5

TRANSITION BOILING HEAT TRANSFER

EPRI TEST DATA
SERIE 700
060284

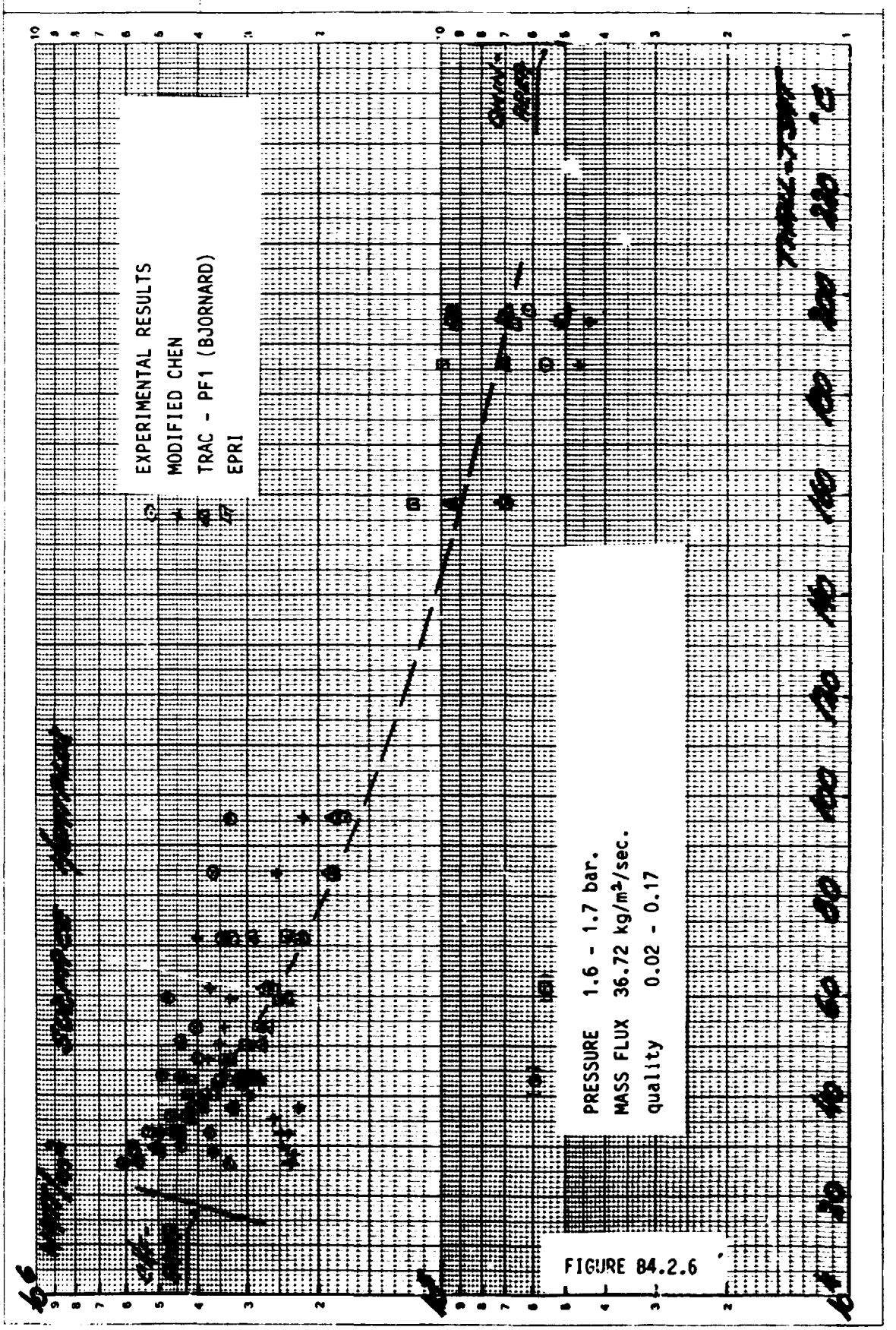

FIGURE 84.2.6

TRANSITION BOILING HEAT TRANSFER

EPRI TEST DATA
SERIE 900
070284

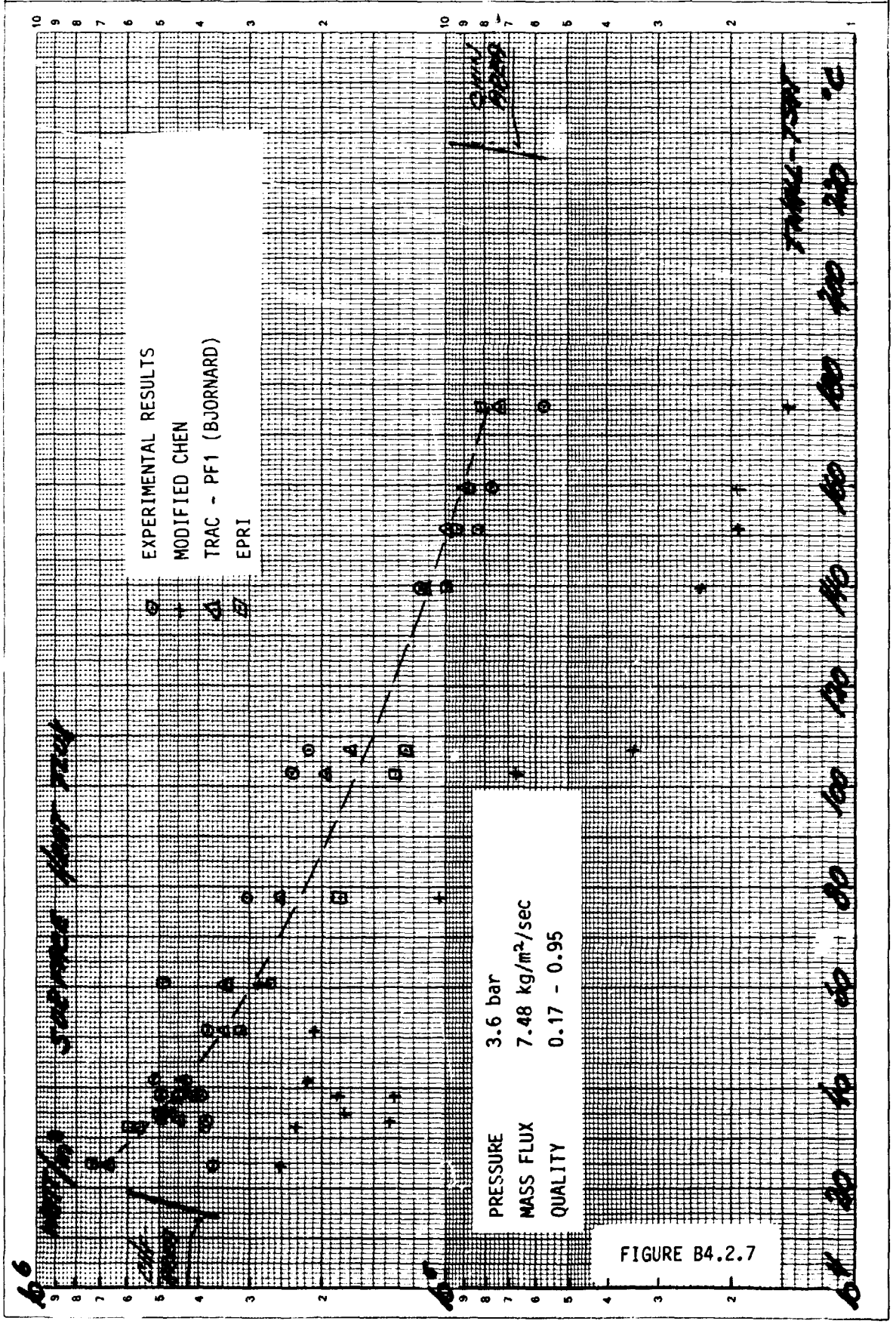

FIGURE B4.2.7

APPENDIX C. DISPERSED FLOW

C1. Droplet Generation

Droplets are generated partly at all points of the water-vapour interface in pre-CHF regions due to entrainment and partly by sputtering in transition boiling in the post-CHF region.

The droplet generation by entrainment may be postulated to take place in a number of different ways governed by hydrodynamic- and surface tension forces. (88,10)

Fig. C1.1 shows the various mechanisms.

In the first type the droplets are sheared off from the wave crests of large-amplitude roll waves. The interfacial friction deforms the interface against the retaining force of liquid surface tension.

In the second type the droplets are generated by undercutting the liquid flow.

In the third type the droplet generation is related to bubbles rising to a free surface of liquid and bursting. When the bubble reaches the interface, a thin liquid film forms at the top of the bubble (Fig. C1.1. type 3 at left). As the liquid is drained from the film it may rupture resulting in a large number of entrained small droplets. (Fig. C1.1, type 3 at center).

A less numerous population of large droplets may be formed by the surging flow of liquid into the depression left after the bubble has burst. A spike-like filament rises at the center of the crater which is then disintegrated into droplets. (Fig. C1.1, type 3 at right).

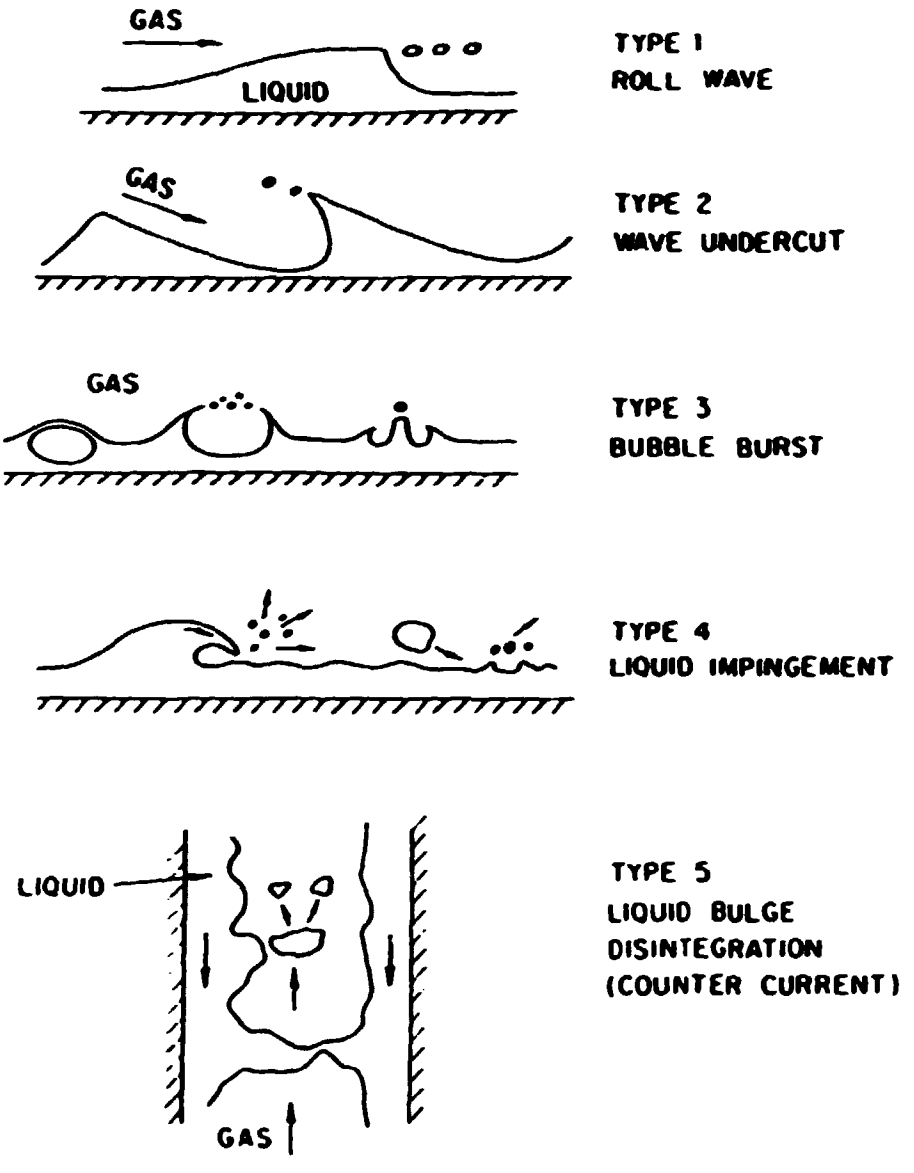

FIGURE C1.1 Droplet generation by entrainment (88).

In the fourth type the impingment of liquid mass or droplets may produce new droplets.

In counter-current flow the last type may occur as a result of flooding. Large amplitude waves may be separated from the liquid film to form a liquid bridge. This may disintegrate into several droplets.

Numerous small droplets are generated in convection with the quenching of the surface during the emergency cooling of the fuel rods. The quenching area is the region on the cladding surface where initial continuous contact between cladding surface and liquid is established i.e. the transition boiling region before the return to nucleate boiling.

In post-CHF regions and in vapour-continous flow further droplet generation can occur only through further breakup of larger droplets to smaller ones due to hydrodynamic forces or impingement of the droplets on a hot surface with high velocity and no rewetting.

Droplets Size.

The upper size limit of the droplet is given by the critical Weber number:

$$We_c = \frac{\rho_g \cdot d \cdot (u_g - u_\ell)^2}{\sigma}$$

A maximum stable droplet size is given by a critical Weber number of 12 - 13 (89). A value of 6.5 may be suggested to represent an average droplet size (10).

Droplet break up by impingment on a hot surface with a subsequently high velocity has been examined experimentally. The droplets will break up into a number of smaller droplets depending on the perpendicuar velocity of the droplet at the time of impingment.

The process is correlated in terms of Weber number:

$$We_p = \frac{\rho_\ell \cdot u_p^2 \cdot d}{\sigma}$$

with following classification

$We_p \leq 30$ no break up
$30 < We_p \leq 80$ break up into a few large fragments
$We_p > 80$ break up into smaller fragments.

It should be noted that most experiments have been carried out with flat plates with surfaces significantly larger than the incoming droplets.

Experiments show that droplet populations can be divided into two separate groups: a population of small droplets with diameters from 10 μ to 140 μ with a maximum number at 50 - 60 μ (90), and a population of large droplets with diameter from 300 μ to 2000 μ with a maximum number at about 800 μ (90,91).

The size and also the number distribution in the axial direction depends primarily on the evaporation, i.e. interfacial heat transfer. Coagulation and further break up due to grid spacers in the fuel element and other channel restriction may also play a role.

The small droplets have a larger surface-to-volume ratio than large droplets i.e. the lifetime history is shorter for small droplets, than for the larger droplets. The energy absorption rate from these small droplets is very high so long as the small droplets continues to exist.

The initial distribution of the two droplet populations is characterized by a large but rapidly diminishing number of small droplets and evolves into one relatively stable population of large droplets which are slowly diminishing in size.

These results may serve to explain qualitatively the observed heat transfer phenomena near the return to nucleate boiling, the near-field-theories (17).

Droplet Size Distribution.

Various theories on the formation of droplets usually predict a single uniform size, cf. e.g. the critical Weber number mentioned above.

As it is noted above, droplets are generated in populations of various sizes. The droplets in a population generated by the same mechanism, may be expected to be clustered around a characteristic mean in a distribution which reflects the randomness in the process of generation, in other words be stochastic in nature.

Droplet size distribution can be represented by a plot of the number of droplets versus the diameter of droplets. The function representing the plot has various names in the literature: in the density function, the distribution curve or frequency function.

The plot function is a number distribution function of the droplets f(x) of a given diameter x. The total number of droplets is then

$$n = \int_0^{\infty} dn = \int_{-\infty}^{\infty} f(x)dx.$$

The arithmetic mean of the diameter is defined as

$$\bar{x}_d = \int_{-\infty}^{\infty} xf(x)dx / \int_{-\infty}^{\infty} f(x)dx = \frac{\int_{-\infty}^{\infty} xf(x)dx}{n}$$

the geometric mean diameter as

$$\ln x_g = \int_{-\infty}^{+\infty} \ln x f(x)dx / \int_{-\infty}^{\infty} f(x)dx.$$

The denominator is still simply equal to the total number.

In general a mean can be defined as

$$\bar{x}_{ab} = \int_{-\infty}^{\infty} x^a f(x)dx / \int_{-\infty}^{\infty} x^b f(x)dx.$$

If a is 3 and b 2 the mean most commonly used among the many averages is the Sauter mean diameter.

When using a statistical mean diameter to correlate data, it should be noticed , that it is important to use one that is relevant to the problem. The field of application of the Sauter mean diameter is in mass transfer and kinetics. When mass distribution is in question the mean diameter based on volume may be relevant, i.e. a is 3 and b zero. With respect to evaporation the diameter alone or the volume-to-diameter ratio may be relevant i.e.either a = 1, b = 0, or a = 3, b = 1 (92).

Experimental examinations of droplet distributions on probability paper show that droplet populations can be considered as a distributed logarithmic normal (log-normal distribution) (91) i.e.

$$\frac{dn}{d(\ln x)} = x \cdot \frac{dn}{dx} = x \cdot f(x) =$$

$$\frac{1}{\sqrt{2\pi} \cdot \sigma_g} \cdot \exp\left[-\frac{(\ln x - \ln \bar{x}_{ng})^2}{2\sigma_g^2}\right],$$

where $\bar{x}_{ng}$ is the number geometric mean diameter as defined above and σ_g is the geometric standard deviation, $\sigma_g = \ln\sigma$.

If the distribution is based on the volume of the droplets i.e.

$$V = \int_0^n k \cdot x^3 dn$$

then

$$\frac{dV}{d(\ln x)} = x \cdot \frac{dV}{dx} = xf(x^3) =$$

$$\frac{1}{\sqrt{2\pi} \cdot \sigma_g} \cdot \exp\left[-\frac{(\ln x - \ln \bar{x}_{vg})^2}{2\sigma_g^2}\right],$$

and

$$\frac{dV}{d(\ln x)} = kx^3 \cdot \frac{dn}{d(\ln x)} = kx^4 \cdot \frac{dn}{dx} = kx^4 \cdot f(x).$$

Using this on the number distribution gives:

$$\frac{dV}{d(\ln x)} = \frac{k}{\sqrt{2\pi}\,\sigma_g} \cdot \exp\left[-\frac{(\ln x - \ln \bar{x}_{ng})^2}{2\sigma_g^2}\right] -$$

$$\exp(3 \ln x)$$

or

$$\frac{dV}{d(\ln x)} = \frac{k}{\sqrt{2\pi\,\sigma_g^2}} \cdot \exp\left[-\frac{(\ln x - (\ln \bar{x}_{ng} + 3\sigma_g^2))^2}{2\sigma_g^2}\right] \cdot$$

$$\exp\left(3 \ln \bar{x}_{ng} + \frac{9}{2}\sigma_g^2\right.$$

A comparison of equation with the volume distribution shows that

$$\ln \bar{x}_{vg} = \ln \bar{x}_{ng} + 3\sigma_g^2$$

if it can be shown that $k \cdot \exp(3\ln \bar{x}_{ng} + 9/2\ \sigma_g{}^2) \approx 1.0$.

If the distribution is based on surface the result would be:

$$\ln \bar{x}_{sg} \cong \ln \bar{x}_{ng} + 2\sigma_g^2$$

and for the Sauter mean, the relation is

$$\ln \bar{x}_{vsg} \cong \ln \bar{x}_{ng} + 2.5\sigma_g^2.$$

Other number distribution functions have also been used. The Nukiyama - Tanasawa distribution has the form (89):

$$f(x) = A \cdot x^m \exp(-b \cdot x^n).$$

A and b are normalization factors, whereas m and n are usually integers which sometimes can be given physical significance. This distribution function has been extensively used in pneumatic atomization.

C2. Droplet flow

In the following some discussion will be given on forces acting on droplets in the droplet-dispersed flow region. The discussion is by no means thought of as providing a thorough examination of the topic but will rather furnish a general overview of the phenomena with some deeper examinations of specific details.

In analyzing the forces acting on the droplets and the relative motion between the phases it is beneficial to start with an examination of the momentum equations for the two phases. In order to have a tractable set of equations these have to be derived from the general local instantaneous form of the momentum equations by applying some sort of averaging procedures, usually the Eulerian space and time averaging. In this way the microscopic local instant fluctuations of the fluid motion are eliminated resulting in equations describing the collective interactions of fluid particles. The averaging operations applied to the basic equations are commutative meaning that the order the averaging is carried out does not matter.

Space averaging could be done first followed by time averaging or vice versa without altering the result.

The derivation of the microscopic conservation equation can be found in different textbooks and reports, e.g. (93, 94,95). Here just one possible form of the obtained momentum equations will be given. If the space averaging is carried out for a slice with thickness Δz and cross-section equal to the constant channel area A (i.e. $\Delta V = A \cdot \Delta z$), the equation for conservation of z-direction (flow direction) momentum of phase k can be simplified to (93, 94):

$$\frac{\partial}{\partial t}(\alpha_k \langle \rho_k u_k \rangle) + \frac{\partial}{\partial z}(\alpha_k \langle \rho_k u^2_k \rangle) = - \alpha_k \cdot \frac{\partial \langle p_k \rangle}{\partial z} -$$

$$\frac{\partial}{\partial z}(\alpha_k \langle \tau_{zz,k} \rangle) + \alpha_k \langle \rho_k F_{z,k} \rangle + \langle u_k \Gamma_k \rangle_i +$$

$$+ \langle (\bar{n}_k \cdot \bar{\tau}_z) \rangle_i + \langle (\bar{n}_{kw} \cdot \bar{\tau}_z) \rangle_w + M_{ik} \qquad (1)$$

Here the angle brackets <> indicate quantites averaged over the volume ΔV. The two terms on the L.H.S. of eq. (1) are the temporal and spatial acceleration terms, respectively. The first term on the R.H.S. is the pressure force, the second represents the force due to viscous and turbulent stresses in the bulk of phase k, and the third term is the body force which in normal two-phase flow is limited to gravitational forces only. The fourth term on the R.H.S. represents the momentum transfer due to mass generation. The fifth term is the interfacial shear force. The sixth is the wall shear force and the seventh term represents the generalized drag force. Corresponding equations can be derived for the x- and y-directions.

For droplets in vapour surroundings it may be reasonable to assume that the term due to viscous and turbulent stresses inside the droplets are of minor magnitude in comparison with the remaining terms. Further, the interfacial shear force can be thought of as being inherently accounted for through the generalized droplet drag force M_{ik}.

Thus, the equation of motion in z-direction for the droplets (liquid phase ℓ) can be written as

$$\frac{\partial}{\partial t}\left[(1-\alpha)<\rho_\ell\ u_\ell>\right] + \frac{\partial}{\partial z}\left[(1-\alpha)<\rho_\ell u^2{}_\ell>\right] = -(1-\alpha)\frac{\partial p}{\partial z} +$$

$$+ (1-\alpha)<\rho_\ell \cdot F_{z,\ell}> + <u_\ell \cdot \Gamma_\ell>_i + <(\bar{\bar{n}}_{\ell w} \cdot \bar{\bar{\tau}}_z>_w + M_{i\ell} \quad (2)$$

where also the void fraction α has been introduced:

$$\begin{aligned} \alpha &= \alpha_v \\ 1-\alpha &= \alpha_\ell \end{aligned} \quad (3)$$

and the pressure has been assumed constant throughout the volume ΔV.

The interfacial transfer terms in eq. (2) can be related through the conservation equation across the interface, resulting in the jump conditions, whence

$$\begin{aligned} <\Gamma_\ell> + <\Gamma_v> &= 0 \\ M_{i\ell} + M_{iv} &= 0 \end{aligned} \quad (4)$$

As these terms appear as source terms in eq. (2) in its vapour phase counterpart it is necessary to provide constitutive equations for Γ_ℓ and $M_{i\ell}$. The equation for $M_{i\ell}$ will be elucidated later on.

Equation (2) is given in the instantaneous volume average form or area average form if the thickness Δz of the slice is taken sufficiently small. The different terms can now be time averaged due to the commutative property of the averaging operators. In that operation the form of the equation remains exactly the same. Terms like

$$\frac{\partial}{\partial t}\left[(1-\alpha)<\rho_\ell u_\ell>\right] \text{ become } \frac{\partial}{\partial t}\overline{\left[(1-\alpha)<\rho_\ell u_\ell>\right]}$$

where the overbar denotes time or statistical averaging. In order to make eq (2) tractable it is necessary to separate an average of a product into a product of averages. This can be obtained by defining distribution coefficients of the form

$$C \equiv \frac{\overline{(1-\alpha)\langle u^2_\ell \rangle}}{\overline{(1-\alpha)} \cdot \langle \overline{u_\ell} \rangle^2} \qquad (5)$$

The distribution coefficients depend on the flow and void fraction profiles. To illustrate the magnitude of the distribution effects the coefficient C has been calculated for the power law velocity and void fraction profiles shown in figure 1 (from ref. (94)). For af flat velocity profile ($m \to \infty$) the distribution coefficient equals unity and it deviates significantly from unity only for very peaked velocity profiles. Thus, for high velocity droplet flow where the velocity profile usually is flat it seems reasonable to assume C=1.0. For lower velocities the distribution effect becomes increasingly important and then it is also necessary to incorporate the droplet concentration evaluated at the wall which has been shown to have pronounced influence on the distribution coefficient (96). It is felt that this wall concentration of droplets can be closely related to the liquid film breakdown at the locus of dryout and thus be one parameter when explaining the near and far field post-CHF heat transfer regions found in experiments.

Another approach for dealing with the distribution effects is to set up conservation equations for each part of a phase in which the distribution can be assumed fairly uniform (distribution coefficient set equal to unity). A study of the CHF phenomena using this approach can be found in (97). Thus the problem of treating the distribution coefficient is shifted to one of regarding transfer relationships between the separated parts of the two phases. This seems to be a more appealing approach especially for film-type flow regions like annular flow and for regions with an extremly peaked concentration profile like the subcooled boiling region.

In what now follows there will be a discussion of the constitu-

tive relationships for the wall friction and for the generalized interfacial drag terms of eq. (2). It is necessary that these momentum interaction terms are properly modeled, otherwise the advantage of the two-fluid model over the mixture model disappears and, in certain cases, numerical instabilities may occur (98).

Wall friction

The term $\langle(\bar{n}_{\ell w} \cdot \bar{\tau}_z)\rangle_w$ in eq. (2) is the volume average wall shear stress component in the z-direction for the liquid phase. Thus this represents the portion of the wall friction caused by droplets penetrating the boundary layer at the wall. In the vapour phase momentum equation a corresponding term appears which in the same way represent the portion of the total wall friction caused by the vapour. Thus the problem arises of how to make a proper partition of the overall two-phase friction pressure drop between the two phases.

The normal way of expressing the overall two-phase friction pressure drop is by means of two-phase friction multipliers. Thus, the overall pressure drop can be expressed in terms of the liquid- and vapour-alone wall friction pressure drop:

$$\left(\frac{\Delta p}{\Delta z}\right)_{TP} = \phi_\ell^2 \cdot \left(\frac{\Delta p}{\Delta z}\right)_\ell \qquad (6)$$

$$\left(\frac{\Delta p}{\Delta z}\right)_{TP} = \phi_g^2 \cdot \left(\frac{\Delta p}{\Delta z}\right)_g \qquad (7)$$

where ϕ_ℓ^2 and ϕ_g^2 are the liquid- and vapour-alone two-phase friction multipliers, respectively, and

$$\left(\frac{\Delta p}{\Delta z}\right)_\ell = f_\ell' \cdot 1/2 \cdot \rho_\ell \cdot u_\ell^2 \cdot 1/D \qquad (8)$$

$$\left(\frac{\Delta p}{\Delta z}\right)_g = f_g' \cdot 1/2 \cdot \rho_g \cdot u_g'^2 \cdot 1/D \tag{9}$$

The prime quantities are evaluated when each phase is assumed to flow alone in the channel (superficial velocities) i.e.

$$u_l' = (1 - \alpha) \cdot u_l \tag{10}$$

$$u_g' = \alpha \cdot u_g \tag{11}$$

and f_l and f_g' are functions of Reynolds number at velocities u_l and u_g', respectively.

The term $\langle(\bar{n}_{lw} \cdot \bar{\tau}_z)\rangle_w$ is frequently approximated by the value obtained for steady flow with no evaporation. If eq (2) is applied to a volume $\Delta V = A \cdot \Delta z$ for those conditions it can be written as

$$-(1 - \alpha) \cdot \left(\frac{\Delta p}{\Delta z}\right)_{TP} + \langle(\pi_{lw} \cdot \tau_z)\rangle_w + M_{il}^* = 0 \tag{12}$$

where M_{il}^* is the static drag per unit volume

By means of eq. (6) and taking the limit as Δz approaches zero, it yields

$$\langle(\pi_{lw} \cdot \tau_z)\rangle_w = \phi_l^2 \left(\frac{\partial p}{\partial z}\right)_l (1 - \alpha) - M_{il}^* \tag{13}$$

A corresponding equation can be obtained for the vapour phase by means of eq. (7)

$$\langle(\pi_{vw} \cdot \tau_z)\rangle_w = \phi_g^2 \left(\frac{\partial p}{\partial z}\right)_g \alpha - M_{iv}^* \tag{14}$$

These two equations provide the rationale for partition the overall two-phase friction pressure drop between the phases. The multipliers ϕ_l^2, ϕ_g^2, may be interrelated through the Lockhart - Martinelli parameter, defined as

$$X^2 = \frac{\phi_g^2}{\phi_\ell^2} \tag{15}$$

For turbulent flow with the single phase friction factor as $f = C_o/Re^{0.2}$ this parameter can be expressed as

$$X_{tt}^2 = \left(\frac{1 - XE}{XE}\right)^{1.8} \cdot \left(\frac{\rho_g}{\rho_\ell}\right) \cdot \left(\frac{\mu_\ell}{\mu_g}\right)^{0.2} \tag{16}$$

The Generalized Drag Force

The generalized drag force in eq. (2) is expressed as a total force exchange per unit mixture volume. This can be related to af total drag force F_T per typical droplet by means of

$$M_{i\ell} = \frac{1 - \alpha}{V_d} \cdot F_T \tag{17}$$

where V_d is the volume of a typical droplet.

The force F_T can be divided into a number of forces some of which can be shown to have a pronounced influence on the numerical stability of the two-fluid model. Here the following forces will be dealt with: the skin and form drag force, virtual mass force, Basset force and forces due to asymmetrical evaporation. Additional forces may be taken into account if necessary for a specific analysis, e.g. diffusion forces due to concentration gradients may be important in slow flow if droplets are very nonuniformly distributed over the channel cross sectional area. It is assumed that the total drag force can be obtained simply by superposition of the included forces.

The Skin and Form Drag Force

This "standard" drag force acting on a droplet under steady state conditions can be given as

$$F_D = - C_D \cdot \frac{\rho_l \cdot u_r \cdot |u_r|}{2} \cdot A_d \qquad (18)$$

where

C_D is a drag coefficient

A_d is the projected area of the droplet facing the flow

u_r is the relative velocity given by

$$u_r = u_l - u_v \qquad (19)$$

The total skin and drag force per mixture volume can be expressed as

$$F_{TD} = - \frac{1 - \alpha}{V_d} \cdot C_D \cdot \frac{\rho_l u_r |u_r|}{2} \cdot A_d \qquad (20)$$

For a dispersed flow system it is common to define some important length scales (98, 99)

Sauter mean radius $r_{sm} \equiv \frac{3 \cdot V_d}{A_i}$ (21)

Drag radius $r_D \equiv \frac{3 \cdot V_d}{4 \cdot A_d}$ (22)

Equivalent radius $r_e \equiv \left(\frac{3}{4\pi} \cdot V_d\right)^{1/3}$ (23)

Surface radius $r_s \equiv \left(\frac{A_i}{4\pi}\right)^{1/2}$ (24)

Here A_i is the surface area of a typical droplet. For spherical droplets these defined radii are all equivalent.
By introducing the area concentration given by

$$a_i = \frac{1-\alpha}{V_d} \cdot A_i \qquad (25)$$

eq. (20) can be written by means of eqs. (21) and (23) as

$$F_{TD} = - a_i \cdot \frac{C_D}{4} \cdot \frac{r_{Sm}}{r_D} \cdot \frac{\rho_\ell \cdot u_r |u_r|}{2} \qquad (26)$$

Thus the total skin and drag force per mixture volume is proportional to the interfacial area concentration and the drag force for the droplets. The ratio of the Sauter mean radius to the drag radius can be thought of as a shape factor for the droplets. For spherical droplets this shape factor equals unity.

It is evident that in order to have an accurate evaluation of F_{TD}, proper knowledge of the interfacial area concentration as well as the drag coefficient is essential. The problems concerning the area concentration are closely related to the droplet number density and are discussed in chapter C1. Here only a few comments on the drag coefficient will be given.

The Drag Coefficient

A thorough examination of the drag coefficient in different flow regions can be found in ref. (100, 101).

For a liquid droplet dispersed system there are two regions that have to be separated: the viscous region or undistorted droplet regions and the distorded droplet region. In the former the viscosity has a pronounced influence on the droplet motion, i.e. the drag coefficient is strongly dependent on the Reynolds number of the droplets. In the latter region C_D is essentially independent of Reynolds number.

For the viscous region two similarity hypothesis were introduced (100). First it was assumed that the drag coefficient C_D can be given as a function of the droplet Reynolds number

$$C_D = C_D (Re_d) \qquad (27)$$

where the Reynolds number was defined in terms of the mixture viscosity μ_m as

$$Re_d \equiv \frac{2 \cdot \rho_v \cdot |u_r| \cdot r_d}{\mu_m} \tag{28}$$

The effect of other droplets results in additional deformation of the flow field. This deformation will give rise to additional stresses meaning that an original droplet sees an increase in the resistance to its motion which can be thought of as an increase of the viscosity. Thus, the mixture viscosity should be used when analyzing the motion of dispersed liquid droplets in vapour surroundings. The mixture viscosity can be calculated as (101):

$$\frac{\mu_m}{\mu_v} = \left(1 - \frac{\alpha_\ell}{\alpha_{\ell m}}\right)^{-2.5 \cdot \alpha_{\ell m} \cdot \mu^*} \tag{29}$$

$$\mu^* = \frac{\mu_\ell + 0.4 \cdot \mu_v}{\mu_\ell + \mu_v} \tag{30}$$

where $\alpha_\ell = 1 - \alpha$ and $\alpha_{\ell m}$ is the maximum packing liquid volume fraction.

For droplets in a vapour flow it is reasonable to approximate μ^* to unity and $\alpha_{\ell m} \sim 0.62$ to 1.0 (98). If $\alpha_{\ell m}$ is assumed to equal unity the result for liquid droplets in vapour flow will become

$$\frac{\mu_m}{\mu_v} = \alpha^{-2.5} \tag{31}$$

The second similarity hypotheses introduced in (101) was that a complete similarity exists between a single-droplet system and a multi-droplet system. Therfore the functional form of C_D for a multi-droplet system is exactly the same as for a single-droplet system. Thus

$$C_D = 24 \frac{1 + 0.1 \cdot Re_d^{0.75}}{Re_d} \tag{32}$$

This correlation indicates that C_D increases with a decreasing vapour void fraction. For very small Reynolds number ($Re_d < 1$) eq. (32) reduces to the well-known Stokes drag law

$$C_D = \frac{24}{Re_d} \tag{33}$$

In the distorted droplet region the single-droplet drag coefficient depends only om droplet radius and fluid properties (101)

$$C_{D\infty} = \frac{4}{3} \cdot r_d \cdot \sqrt{\frac{g \cdot \Delta\rho}{\sigma}} \tag{34}$$

It was assumed (101) that for a multi-droplet system the increased drag due to other droplets was caused by the turbulent eddies in the droplets wake region in a similar way as for a solid-particle system and a multiparticle system, an equation for the drag coefficient of the multiparticle system was obtained in (101). Thus this equation combined with eq. (34) was assumed to be valid also for a multi-droplet system. By means of the approximation given by eq. (31) the following was obtained for a multi-droplet system (101):

$$C_D = \frac{4}{3} r_d \sqrt{\frac{g \cdot \Delta\rho}{\sigma}} \cdot \left[\frac{1 + 17.67 \cdot \alpha^{2.6}}{18.67 \cdot \alpha^3}\right]^2 \tag{35}$$

This correlation indicates that the momentum coupling between the phases increases with increasing droplet concentration (decreasing void fraction α).

For a single droplet in an infinite medium the viscous region extends up to about $Re_\infty = 10$ where

$$Re_\infty \equiv \frac{2 r_d \cdot \rho_v |u_{r\infty}|}{\mu_v} \tag{36}$$

$$u_{r\infty} = u_l - u_{v\infty} \tag{37}$$

$u_{v\infty}$ is the undisturbed vapour velocity. For higher Reynolds number the drag coefficient is essentially constant, i.e. the distorted droplet region is prevailing. In this region the

drag coefficient is proportional to the droplet size. Thus, the upper limit of the drag coefficient is governed by the maximum size of the droplet. This droplet size can be determined from a critical Weber number:

$$We_{cr} \equiv \frac{2\,\rho_v \cdot u_r^2 \cdot r_d}{\sigma} = 12 \tag{38}$$

The terminal velocity corresponding to eq (34) is

$$u_{r\infty} = \sqrt{2} \cdot \left[\frac{g \cdot \sigma \cdot \Delta\rho}{\rho_v^2}\right]^{1/4} \tag{39}$$

Eqs. (38) and (39) thus yield

$$r_{dmax} = 3 \cdot \sqrt{\frac{\sigma}{g \cdot \Delta\rho}} \tag{40}$$

which with eq. (34) gives the maximum drag coefficient C_D=4.

There is no thorough treatise in ref. (101) of how to handle the region transition for a multi-droplet system. A suggestion is to assume that the transition occurs at Re ~ 10, where the Reynolds number is based on the mixture viscosity according to eq.(28).

The above model was compared with one described by a large number of experimental data where satisfactory agreements were obtained for wide ranges of droplet concentration and Reynolds number (98, 101). Thus, the similarity hypothesis discussed above were concluded to be reasonable approach when developing the multidroplet drag coefficient.

Virtual Mass Force and Basset Force

The virtual mass force and the Basset force are transient forces occurring when a particle (bubble, droplet) is accelerating relative to the surrounding phase (liquid, vapour). When a droplet is moving in vapour surroundings these forces are usually very small compared, for instance, to the drag force. However, despite of its magnitude it has been shown

that the virtual mass force in particular has a pronounced influence on the numerical stability of the two-fluid model (102).

The virtual mass force can be explained briefly as follows: when a particle is set in motion relative to the surrounding medium it is given kinetic energy. In addition, the fluid which it displaces by its movement also is given a certain amount of kinetic energy. The total work done in accelerating the particle is therefore greater than if only the particle itself were moved, and the result is the same as if the mass of the particle were increased by a specified amount. This extra amount of mass is known as the added mass or induced mass of the particle, and the sum of the actual mass and the added mass is known as the virtual mass. It can be shown by potential flow theory (103) that for a sphere in unrestricted three-dimensional flow the added mass is half the mass of the fluid displaced by the sphere.

The forms of the virtual mass force and the Basset force for a collection of droplets simultaneously accelerating in the vapour phase are not firmly established. Newer and more adequate formulations of these forces are continually reported.

Zuber (104) studied the effect of concentration on the virtual mass force. From potential theory outlined in (105) and assuming low droplet concentration Zuber obtained an expression for the virtual mass force acting on one representative droplet as

$$F_V = -\rho_v \cdot V_l^* \cdot \frac{3-2\alpha}{\alpha} \frac{du_r}{dt} \qquad (41)$$

where as before α is the vapour void fraction and u_r the relative velocity as in eq. (19). $\rho_v \cdot V_l^*$ is the added or induced mass for one droplet. For a spherical droplet V_l^* can be expressed as

$$V_l^* = \frac{1}{2} \cdot \frac{\pi}{6} \cdot (2 \cdot r_{sm}) \qquad (42)$$

Equation (41) is valid for accelerating a spherical droplet in the centre of a vapour-filled hollow fixed sphere. The radius of the hollow sphere is taken so that at this distance from the droplet the vapour is assumed to be undisturbed.

In ref. (106) a reinterpretation of Zuber's result is made where the induced vapour flow caused by the droplet motion was also taken into account. From this analysis the virtual mass force became

$$F_V = -\rho_v \cdot V_\ell^* \cdot \alpha \ \frac{du_r}{dt} \tag{43}$$

In ref. (101) a new form of F_V is proposed based on Zuber's result and the work reported in (102). The resulting equation is

$$F_V = -\rho_v \cdot V_\ell^* \cdot \frac{3-2\alpha}{\alpha} \cdot \left(\frac{\partial u_r}{\partial t} - u_r \cdot \frac{\partial u_v}{\partial z}\right) \tag{44}$$

Equations (43) and (44) reveal quite a different trend when the void fraction decreases (droplet concentration increases). For decreasing void fraction the virtual mass force decreases accordingly to eq. (43) while it increases following eq. (44). Which one is most accurate is not readily pointed out. They represent both small terms compared to other forces and contribute only by a minor amount to the numerical result while their influence on the numerical stability is quite definite. In view of both their small magnitude for droplet dispersed flow and the overall uncertainty concerning the droplet shape and size distributions in full-scale systems it is not worthwhile to examine this issue more deeply here. Thus, the different formulations, eqs. (43) and (44), can be taken as evidence on the uncertainty in the present state of the art and it is expected that further research will shed more light on these phenomena.

The Basset force is the result of acceleration on the viscous drag and boundary layer development around the droplets. This

force can be expressed as (c.f. ref. (104))

$$F_B = -6 \cdot r^2 \sqrt{\pi \, \rho_v \cdot \mu_m} \int_t \frac{du_r}{d\xi} \cdot \frac{d\xi}{\sqrt{t-\xi}} \qquad (45)$$

where r is the droplet radius and μ_m the mixture viscosity according to eqs. (29) and (30). The integration is carried out for the acceleration time span.

In ref. (104) an analysis is carried out to find out under what conditions the Basset force can be neglected in comparison with the virtual mass force. By means of the mean value theorem of integral calculus the integral of eq. (45) can be related to the time function:

$$\int_o^t \frac{du_r}{d\xi} \frac{d\xi}{\sqrt{t-\xi}} \leq 2 \cdot \frac{du_r}{dt} \cdot \sqrt{t} \qquad (46)$$

By comparing the Basset force using eq. (46) with the virtual mass force, eq. (44), assuming that the spatial derivative is zero the following is obtained:

$$t \leq \frac{1}{216} \cdot \frac{\rho_v \cdot V_\ell^*}{\pi^2 \cdot r \cdot \mu_m} \left(\frac{\alpha}{3-2\alpha} \right)^2 \qquad (47)$$

As long as the acceleration time t obeys eq. (47) the Basset force can be neglected. Normally for fast transients in droplet-dispersed flow eq. (47) is fulfilled and thus the Basset force is of minor importance.

Evaporation Forces

The evaporation forces have transverse directions resulting in droplet movements in a plane normal to the flow direction away from the heat transfer surface. Because of the high temperature gradient inside the thermal boundary layer at the heat transfer surface a droplet residing within this layer will experience a nonuniform evaporation. The droplet side facing the heat transfer surface will have a higher vapour generation than the opposite

droplet side resulting in different vapour velocities normal to the droplet surface. This will create a force with a tendency to push the droplet away from the heat transfer surface. It can be expected that these evaporation forces give rise to substantial droplet transversal trajectories at the locus of CHF when the wall liquid film is boiled off and thus can be one major aspect to be taken into account when modelling the near- and far-field post-CFH heat transfer regions observed in experiments (17).

The derivation is quite straightforward. In (107) a linear temperature gradient within the thermal boundary is assumed:

$$T = T_{SAT} + (T_w - T_{SAT}) \cdot (1 - \frac{y}{\delta}) \tag{48}$$

and by assuming a constant heat transfer coefficient between the droplet surface and superheated vapour an integration of vapour generation for each half of the droplet yields the following average vapour velocities normal to the wall surface

$$u_h = \frac{h}{H_{fg} \cdot \rho_v} \cdot (T_w - T_{SAT}) \left[(1 - \frac{y}{\delta}) + \frac{d}{4\delta} \right] \tag{49}$$

$$u_c = \frac{h}{H_{fg} \cdot \rho_v} \cdot (T_w - T_{SAT}) \left[(1 - \frac{y}{\delta}) + \frac{d}{4\delta} \right] \tag{50}$$

for the hot and cold side of the droplet, respectively.

These velocities give rise to a resulting accelerating force according to

$$F_E = \rho_v \cdot \frac{\pi d^2}{4} (u_h^2 - u_c^2) \tag{51}$$

By means of eqs. (49) and (50) the force is obtained as

$$F_E = \frac{\pi d^2}{4} \cdot \frac{h^2}{H_{fg}^2 \cdot \rho_v} (T_w - T_{SAT})^2 \cdot \frac{d}{\delta} \cdot (1 - \frac{y}{\delta}) \tag{52}$$

This force is expressed for one droplet and is of course active only within the boundary layer.

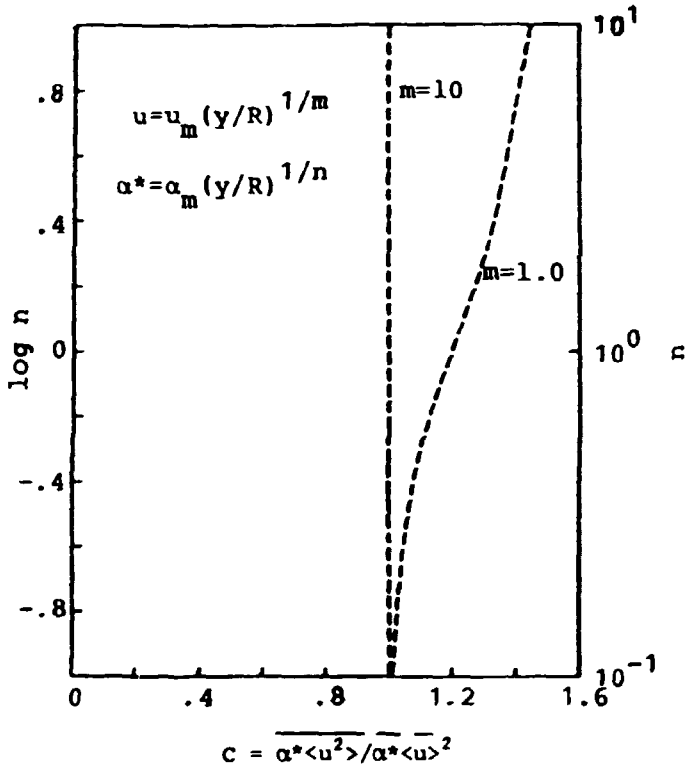

Distribution coefficient for various velocity and void fraction profiles.
From ref (2)

FIGURE C2.1

C3. Droplet flow heat transfer.

The problems of heat transfer will be considered here in general. Some correlations are proposed, but no evaluations with a computer programme including these correlations have been performed. In order to find the best fit correlation comparisons with experiments are needed using a computer programme including different proposed correlations. The correlations discussed are representative in such a way that they have been used in several two-fluid programmes or in simple mechanistical programmes for the modelling of droplet-dispersed flow heat transfer.

The examination of the modelling of heat transfer must start with the energy equation for two-phase flow. The equations are derived as local, instantaneous differential equations for three-dimensional flow. The equations are written in an Eulerian form, where the diffusion term is neglected. The real physics cannot be calculated using microscopic volumes in a class of few millimeters, which is the scale of basic subprocesses in two-phase flow. For microscopic volume used in calculating different kinds of averaging procedures must be used, including both averaging in space and time. In this chapter two averaging procedures for space will be defined. The volume averaging denoted with angle brackets (<>) means instantaneous averaged conditions in the volume. The time average denoted with an overbar ($\bar{}$) means the statistical average value for the volume average, e.g. that resulting from many repeated measurements with same experimental conditions. The time averaging is possible before volume averaging, too. The local temperature measurement with a single thermocouple is an example of this.

The thermocouple may give a good average for the local temperature, but the value may not be representative as a volume average. The generalized conservation equations for two-phase flow system may be written as (93)

$$\frac{\partial}{\partial t}\left(\alpha_k \langle \rho_k \Psi_k \rangle\right) + \frac{\partial}{\partial z}\left(\alpha_k \langle n_z \cdot (\rho_k \Psi_k v_k + j_k) \rangle\right) + \alpha_k \langle \rho_k S_k \rangle$$

$$= -\frac{1}{V}\int_{a_i} (\dot{m}_k \Psi_k + \bar{j}_k \cdot \bar{n}_k) dS - \frac{1}{V}\int_{a_{kw}} \bar{n}_{kw} \cdot \bar{j}_k dS$$

The $\rho_k \Psi_k$ is a generalized phase quantity to be considered, α_k the phase volume fraction defined as a instantaneous volumetric fraction for the phase ($\equiv \langle \alpha_k \rangle$), n_z the direction vedtor in the axial direction, n_k the direction vector perpendicular to the interphase surface, j_k the flux of Ψ_k, and S_k the source of Ψ_k.

The interfacial mass transfer rate may be written as

$$\dot{m}_k = \rho_k n_k \cdot (v_k - v_i)$$

The generalized form may be used for the derivation of the conservation equations for each quantity, as mass, momentum in the z direction, and energy. The quantities Ψ_k, j_k and S_k have separate meanings for the mass conservation equation, momentum conservation equation, and energy conservation equation. Here only the energy conservation equation will be considered.

For the energy equation the generalized terms are:

$$\Psi_k = E_k = (e_k + u_k^2/2)$$

$$\bar{j}_k = \dot{q}_k + (p_k \bar{\bar{I}} - \bar{\bar{\tau}}_k) \cdot \bar{v}_k$$

$$S_k = \bar{F}_k \cdot \bar{v}_k + Q_k$$

Here e_k is internal energy ($e \equiv h - p/\rho$), q_k heat flux to phase k, p_k pressure of phase k, I identity tensor, τ_k stress tensor, Q_k heat source in the fluid, F_k external force like gravity potential in the fluid, v_k velocity field in the fluid, and u_k the velocity component in the z-direction.

In addition to the volume averaging, volume-averaged quantities have been defined in the equation over both the interfacial and wall contact areas. These integrals are included into the generalized equation. The volume averaging discussed earlier is defined by an integral

$$\langle\ \rangle = 1/V \int\ (\ \ )$$

Further, the interfacial jump conditions are needed for two phase flow. The generalized jump conditions may be expressed as:

$$\sum_{k=1}^{2} (\rho_k \gamma_k (\bar{v}_k - \bar{v}_i) + \bar{j}_k) \cdot \bar{n}_k = 0$$

The averaging procedure is needed as well for interfacial jump conditions as for the original conservation equations. A discussion is needed for further understanding of two-phase physics of what is vanishing from physical reality due to other simplifications during the averaging process.

The real two-phase flow includes a high degree of turbulence. Both volume- and time-averaging do not take this subprocess into account. This process may be significant for the mixing and is the origin for the crosswise movement of droplets causing the impingment on the wall and enchances the wall heat transfer.

The volume average describes only one velocity component for each phase in each coordinate direction and then the information on real velocities for different droplet sizes vanishes. If this information should be conserved, the conservation equations for a single liquid have to be split into equations for two droplet classes. The method based on distribution functions will be discussed later. If different field equations for one phase have been derived, a question may arise as to which interfacial jump conditions are valid between different droplet classes and between droplet. The impingment may be expected

to cause mass transfer and momentum transfer terms between fractions, but modelling problems for energy equation may be overstated due to small enthalpy differences.

In further simplifications the phase pressures are assumed to be the same, i.e. $p = p_1 = p_2$. Then in the interfacial jump condition, the differential terms for the phase pressures $\langle p_{1i} \rangle - \langle p_{2i} \rangle$ vanishes. This pressure difference between phases is significant in the energy equation during rapid blowdown conditions, when the initiation of flashing is delayed. The pressure inside microscopic vapour bubbles is higher than in the water, corresponding to the difference in saturation temperature of 3....10 K. If different phase pressure are not calculated, the delay has to be included into interfacial heat transfer correlations.

The water pressure inside droplets is slightly higher than in the vapour pressure around them, depending on the surface tension and droplet diameter. This is the reason, why a cloud of very small droplets may exist in superheated vapour for quite a long time without evaporation. The mass of these micro-size droplets is small, however, and they are not needed to be considered separately in the energy conservation equation.

After assuming same phase pressures the only pressure terms in the energy equation are

$$\frac{\partial}{\partial z}\left(\alpha_k \langle p_k u_k \rangle\right) \text{ and } \langle p_k \rangle \frac{\partial \alpha_k}{\partial t}$$

The kinetic energy conservation equation is usually used together with the momentum conservation equation for modelling pressure losses of the real structure. The pressure losses in venturis and area changes may be changed to reversible and irreversible pressure losses.

The generalized conservation equation cannot be used for comparison with experimentally measured parameters, because usual instruments measure only local parameters which may be time averaged e.g. a gamma beam void fraction measurement where the single beam signals may be considered as time averaged and the volume average has to be calculated as a combination of parallel time averages.

The time average for main parameters, velocity and enthalpy, are defined as

$$\overline{\langle u_k \rangle} = \frac{\overline{\alpha_k \langle u_k \rangle}}{\overline{\alpha_k}}$$

$$\overline{\langle h_k \rangle} = \frac{\overline{\alpha_k \langle h_k \rangle}}{\overline{\alpha_k}}$$

Because the main parameter can be directly chosen as time average in conservation equations, no further interpretation is needed between primitive and averaged parameters in equations. The problem is how to formulate time averages for terms consisting of products of several main parameters. It is well known from the combination rule, that the average of a product is not equal to the product of two averages. Theorists have proposed a solution to overcome the combination rule by the use of distribution parameters that take into account the different conditions over the cross section.

The distribution parameters may be used both in momentum and energy conservation equations. There is a disadvantage, however, that distribution parameters defined for different subprocesses differ unless the processes are analogous. The convective term in the differential equation needs the averaging of $\langle \alpha_k \rangle \langle h_k u_k \rangle$.

The distribution parameter for the energy equation requires e.g. the distribution parameter

$$C_k = \frac{\overline{\alpha_k \langle h_k u_k \rangle}}{\overline{\alpha_k} \langle h_k \rangle \langle u_k \rangle}$$

The corresponding distribution parameters are needed for the interfacial jump condition, as for the interfacial surface area. In practice very few data distribution parameters exists and the parameter in computer models is usually set to unity. The situation typically reflects disagreements between theorists and programme developers. Although a theorist recommends the use of distribution parameters for the complicated two-phase flow form including droplet and film fields, the programme developer may find it easier to use split field equations.

The use of distribution parameters is easier for a droplet field that consists of several droplet sizes. Then the log-normal distribution can be used as a basis in the calculation of distribution parameters.

The distribution parameter becomes significant for vapour enthalpy convection if a nonflat vapour temperature profile must be expected over the cross section. This is possible, e.g. in a rod bundle, where the periphery of the bundle is not so hot as the central part.

For the discussion of problems in modelling of interfacial heat transfer the interfacial area is very essential, because the heat flux is expressed as a product of heat transfer coefficient, interfacial surface area and temperature difference between superheated vapour and interfase. The interfacial area is related to void fraction and droplet diameter by:

$$A_i = n \pi d^2 = \frac{6 (1 - \alpha)}{d}$$

The question that arises is: How well is the droplet size distribution known for different void fraction regions? In many models the average droplet size is calculated from the Weber number criteria using phase velocity difference as a parameter, and further, the differential velocity is calculated from the drag gravity balance, as in TRAC using (10)

$$V_r = \frac{4(\rho_l - \rho_g)g\ d}{3\ \rho_g}$$

One possible problem may be mentioned, however. The Weber number criterion is perhaps some kind of time average in limited experimental conditions. The interfacial drag models are based typically on measurement with solid spheres in gas stream. The combination of these two criteria may work poorer in computer programmes than it is generally believed. The Weber criterion in particular is not easy to apply in computer programmes because the droplet size is a drastic function of the velocity difference. The phase separation model before the droplet entrainment must be well fitted to theWeber number criterion, in order to give the correct velocity difference between phases. Some experiments for reflooding indicate that the droplets typically have a size of 1...3 mm. Using Weber the number criterion only a narrow range of velocity differenses is then possible.

Because interfacial heat transfer depends on the interfacial area, the integration method should conserve the interfacial area in the convection term. The need is similar for the interfacial momentum conservation. The mass conservation equation does not directly give the droplet size as solution. Then an extra equation is needed for this, unless the distribution parameters solve the problem.

In the heat transfer coefficient between interfases, only the heat transfer resistance from vapour to droplet surface is significant and the heat transfer resistance from the droplet surface into liquid is negligible. Then it follows that practically liquid is saturated in dispersed flow. If cold liquid is injected to saturated or superheated vapour the subcooling may be assumed to vanish at once by condensation.

The correlations using droplet Reynolds number may be recommended for the interfasial heat transfer. As an example the correlation of Lee and Ryley may be mentioned (108)

$$Nu_d = 2 + 0.74\ Re_d^{0.5}\ Pr_g^{0.3}$$

The correlation is based on measurements with solid spheres in a gas stream. There is one advantage in this kind of correlation: The heat transfer rate is proportional to the square root of the velocity difference. This dependency makes the iteration process more stable than, e.g. the nucleate boiling heat transfer as it is proportional to the second power of temperature difference. The Reynolds number is defined as:

$$Re_d = \frac{d(u_g - u_d)\ \rho_g}{\mu_g}$$

In the wall heat transfer two components have to be separated, the heat flux to vapour and the heat flux directly to liquid. The first assumption is that the wall is superheated so much that droplets cannot wet the wall.

The heat transfer to vapour is a product of surface area heat transfer coefficient, and temperature difference. The first approach is to use Reynolds' analogy between wall friction and wall heat transfer. Reynolds' analogy is expressed by $St = 0.5\ f_w$. The modified Reynolds' analogy proposed by Blair is (108)

$$St = 0.5\ f_w\ (1.18 + 1.3\ T)$$

$$St = Nu/(Re\ Pr)$$

Here f_w means the Fanning friction and T turbulent intensity of free stream ($T = \sqrt{u'^2} / u$). The Dittus-Boelter correlation is one result of Reynolds' analogy. For wall to vapour heat transfer in dispersed flow the Dittus-Boelter correlation is not the best choice, but rather the modification of it. In (48) the Dougall-Rohsenow correlation is recommended:

$$Nu_g = 0.023\ Re^{0.8}\ Pr_g^{0.4}$$

$$Re = \frac{D\ G}{\mu_g}\ (XE + \frac{\rho_g}{\rho_l}\ (1 - XE))$$

There are some models like that of Chen & Webb and that of Hein, which tend to correlate the interfacial heat transfer without any specific droplet size. The models are empirical. In SAK-5 tests with NORA programme good results were obtained by using the Chen & Webb model. The explanation for the success without droplet diameters may be, that in reality the droplet size spectra in free flow is quite narrow, without the break-up caused by structures. Only in spray nozzles and close to restrictions (like spacers) may a wider droplet size spectrum be expected.

The heat transfer between wall and liquid consists partly of radiation and partly of direct contact with the wall. The calculation is simpler for radiation because the heat absorption to droplets is only a function of void fraction and temperature difference. The formulation of radiation heat transfer is well presented by Sun & Conzales (109).

The direct contact heat transfer to liquid would be correlated as a product of time-averaged contact area, heat transfer coefficient, and temperature difference. The heat transfer mode is quite difficult to handle. The time-averaged contact area is a function of droplet density and radial droplet velocity caused by turbulence. The turbulent velocity components for the liquid flow are not known as well as for the gas flow. Some experiments have been made for droplets impinging on a hot surface. From these experiments quite sophisticated models have been formulated. The formulation is perhaps too complicated to be used in computer models. If Reynolds' analogy is assumed for the dispersed flow (homogenous approximation), the Dougall-Rohsenow correlation predicts the heat flux to vapour-liquid mixture well.

The direct liquid contact heat transfer has been applied in many programmes. The model is very simple in the German reflooding programme FLUT. Varone (110) has used a complicated model proposed by Kendall & Rohsenow in his own programme.

ISBN 87-550-1109-8
ISSN 0418-6435
minab/gotab Stockholm 1985